Westfälische
Wilhelms-Universität
Münster

Institut für Angewandte Mathematik

A dimensional reduction approach based on the application of Reduced Basis Methods in the context of Hierarchical Model Reduction

Inaugural-Dissertation
zur Erlangung des Doktorgrades
der Naturwissenschaften im Fachbereich
Mathematik und Informatik
der Mathematisch-Naturwissenschaftlichen Fakultät
der Westfälischen Wilhelms-Universität Münster

vorgelegt von
Kathrin Smetana
aus Bietigheim-Bissingen
- April 2013 -

Dekan:	Prof. Dr. Martin Stein
Erster Gutachter:	Prof. Dr. Mario Ohlberger (Universität Münster)
Zweite Gutachterin:	Prof. Dr. Simona Perotto (Politecnico di Milano)
Tag der mündlichen Prüfung:	28.05.2013
Tag der Promotion:	28.05.2013

To my parents.

Abstract

In this thesis we introduce a new dimensional reduction approach which is based on the application of Reduced Basis (RB) techniques in the Hierarchical Model Reduction (HMR) framework. Considering problems that exhibit a dominant spatial direction, the idea of HMR is to perform a Galerkin projection onto a reduced space, which combines the full solution space in the dominant direction with a reduction space in the transverse direction. The latter is spanned by modal orthonormal basis functions. While so far the basis functions in the HMR approach have been chosen a priori, for instance as Legendre or trigonometric polynomials, in this work a highly nonlinear approximation is employed for the construction of the reduction space. To this end we first derive a parametrized problem in the transverse direction from the full problem where the parameters reflect the influence from the unknown solution in the dominant direction. Exploiting the good approximation properties of RB methods, we then construct a reduction space to approximate a suitable solution manifold of the parametrized transverse problem from snapshots and a subsequent proper orthogonal decomposition. For an efficient construction of the snapshots we apply adaptive refinement in parameter space based on an a posteriori error estimate that is also derived in this thesis.

To accomplish a dimensional reduction for nonlinear problems we propose to approximate also the nonlinear operator with an orthonormal expansion in an orthonormal, so-called collateral basis on the transverse direction. The collateral basis space is constructed in a highly nonlinear fashion analogously to the reduction space by first generating a manifold of parametrized lower dimensional operator evaluations and subsequently employing RB methods for the selection of the basis functions from snapshots of the former. The coefficients in the orthonormal expansion are efficiently computed by the newly introduced Empirical Projection Method, which is an adaptive integration algorithm based on the Empirical Interpolation Method. Rigorous a priori and a posteriori error bounds which do not require additional regularity of the nonlinear operator are proven for the Empirical Projection Method.

Having the application of our dimensional reduction approach to subsurface flow problems in mind, we finally propose an ansatz for the approximation of a possibly skewed water table (or similar interface) with tensor-based model reduction methods.

Numerical experiments for general advection-diffusion problems and the elliptic nonlinear diffusion equation demonstrate a fast convergence of the proposed dimensionally reduced approximation to the solution of the full-dimensional problem. Run-time experiments verify a linear scaling of the method in the number of degrees of freedom used for the computations in the dominant direction both in the linear and nonlinear setting.

Acknowledgements

First and foremost, I would like to express my deepest gratitude to my supervisor Professor Mario Ohlberger for inspiring this work and for letting me find my own way in dealing with it. I also sincerely thank him for his strong and kind support, his trust, and for having been a mentor for quite a long time. I am also very grateful to Professor Simona Perotto for her great hospitality during my visits in Milano, for her numerous comments and advice, and for her encouragement and patience.

I appreciate the open and pleasant atmosphere at the Institute for Applied Mathematics and I want to thank all my former and current colleagues. Special thanks goes to Martin Drohmann for proofreading this thesis.

I would like to thank my friends, particularly Patrick Henning, for their understanding and for always being there when I needed them. Last but not least, I would like to heartily thank my family, especially my parents Dagmar and Wolfgang Smetana, for their encouragement, for always standing behind me, and for their never-ending support.

Contents

1 Introduction **1**
- 1.1 Aim, scope and contributions of this work . . . 1
- 1.2 Overview on the literature . . . 3
- 1.3 Outline of this work . . . 4

2 The HMR-RB approach for linear elliptic problems **7**
- 2.1 Hierarchical model reduction for linear elliptic problems . . . 7
  - 2.1.1 Formulation of the reduced problem . . . 9
  - 2.1.2 Example: An advection-diffusion problem . . . 9
  - 2.1.3 Discretization of the reduced problem . . . 10
- 2.2 Basis generation with Reduced Basis Methods . . . 10
  - 2.2.1 Proper Orthogonal Decomposition . . . 11
  - 2.2.2 The Greedy Algorithm . . . 12
- 2.3 The Hierarchical Model Reduction-Reduced Basis approach . . . 15
  - 2.3.1 Derivation of a parametrized 1D problem in transverse direction . . . 15
  - 2.3.2 Example: An advection-diffusion problem . . . 16
  - 2.3.3 Discretization of the parametrized 1D problem in transverse direction . . . 17
  - 2.3.4 Basis generation with RB techniques: The Adaptive-HMR-POD algorithm 18
- 2.4 A posteriori error estimation . . . 20
  - 2.4.1 An a posteriori error estimator based on the Riesz representative of the residual 20
  - 2.4.2 A localized residual-type a posteriori error estimator . . . 21
- 2.5 Analysis of the computational costs of the HMR-RB approach . . . 26
- 2.6 Numerical experiments . . . 27

3 Application of the HMR-RB approach to nonlinear PDEs **45**
- 3.1 The HMR framework for nonlinear PDEs . . . 46
  - 3.1.1 Formulation of the reduced problem . . . 47
  - 3.1.2 Solution of the discrete reduced problem with Newton's method . . . 48
- 3.2 The Empirical Projection Method (EPM) . . . 51
  - 3.2.1 Rigorous a priori and a posteriori error analysis for the EPM . . . 55
- 3.3 The HMR-RB approach (using the EPM) . . . 58
  - 3.3.1 Formulation of the reduced problem in the HMR-RB framework employing the EPM . . . 58
  - 3.3.2 Derivation of a parametrized 1D problem in transverse direction . . . 59
  - 3.3.3 The generation of parametrized 1D operator evaluations . . . 61
  - 3.3.4 Example: The nonlinear diffusion equation . . . 61

3.3.5 Reduced and collateral basis generation with RB methods — the Adaptive-HMR-RB algorithm . . . 63
3.4 A posteriori error estimates . . . 66
3.4.1 An a posteriori error bound based on the Brezzi-Rapaz-Raviart Theory . . . 67
3.4.2 Computation of the inf-sup stability factor and the Lipschitz constant . . . 73
3.5 Analysis of the computational costs of the HMR-RB approach . . . 73
3.6 Numerical Experiments . . . 75

4 Approximation of skewed interfaces 89
4.1 An ansatz for approximating skewed interfaces . . . 90
4.1.1 Locating the interface . . . 90
4.1.2 Removing the interface from the model reduction procedure . . . 91
4.2 Exemplification for the HMR-RB approach . . . 92
4.2.1 Formulation of the reduced problem . . . 92
4.2.2 Derivation of a parametrized 1D problem in transverse direction . . . 93
4.2.3 Example: An advection-diffusion problem . . . 94
4.3 Numerical Experiments . . . 96

5 Conclusion and Perspectives 107

Appendices 111

A Appendix to Chapter 1 113
A.1 The HMR-RB approach for a domain with a curved boundary . . . 113
A.1.1 Formulation of the reduced problem in the Hierarchical Model Reduction framework . . . 114
A.1.2 Derivation of the parameter dependent one-dimensional problem in the HMR-RB approach . . . 115
A.2 Alternative derivation of the localized estimator . . . 116
A.3 Definition of the source term s of test case 2 . . . 118

B Appendix to Chapter 3 121
B.1 Convergence of the EPM in the discrete setting . . . 121

Bibliography 125

Chapter 1

Introduction

1.1 Aim, scope and contributions of this work

Many phenomena in nature have dominant spatial directions along which the essential dynamics occur. Examples are blood flow problems, fluid dynamics in pipes or river beds and subsurface flow. This property can be exploited to derive a dimensionally reduced model. However, the processes in the transverse directions are often too relevant for the whole problem to be neglected. This can be due to local features as the presence of a narrowing (stenosis) of an artery or the outlet of a river in a lake, but also to possibly nonlocal processes as infiltration of soil. To obtain a good approximation of the full dimensional problem, the dimensionally reduced model should therefore include information on the transverse dynamics.
The major goal of this thesis is the development of an efficient dimensional reduction approach which yields a fast convergence of the solution of the dimensionally reduced model to the solution of the full dimensional problem against the application background of saturated-unsaturated subsurface flow. The latter is of interest for instance in environmental applications or in the fields of reliable flood forecasting and construction of flood protection measures. This aim is achieved by the application of Reduced Basis (RB) Methods in the Hierarchical Model Reduction (HMR) framework and yields the Hierarchical Model Reduction-Reduced Basis (HMR-RB) approach. The key idea of HMR, originally introduced in [124–126] and studied in a more general geometric setting in [48, 100, 102, 103], is to perform a Galerkin projection of the original variational problem onto a reduced space of approximation order m of the form $V_m = \{v_m(x,y) = \sum_{l=1}^{m} \bar{v}_l(x)\phi_l(y), x \in \mathbb{R}^k, y \in \mathbb{R}^{d-k}\}$, where the coefficients $\bar{v}_l(x)$, $l = 1, ..., m$, are defined on the dominant direction and the orthonormal functions ϕ_l, $l = 1, ..., m$, on the so-called transverse direction. The projection is thus determined by the choice of the reduction space in the transverse direction $Y_m := \text{span}(\phi_1, \ldots, \phi_m)$. While in all previous papers the choice of the reduction space is based on an a priori chosen set of basis functions such as trigonometric or Legendre polynomials, one of the major contributions of the present work is to employ a double stage (and thus highly) nonlinear approximation in the sense of [38] to construct the reduction space. First, we derive a parametrized lower dimensional problem in the transverse direction from the full problem, where the parameters reflect the influence from the unknown solution in the dominant direction. For the selection of the basis $\{\phi_l\}_{l=1}^{m}$ from the solution manifold formed by the solutions of the parametrized dimensionally reduced problem, we apply RB methods, exploiting their good and in some cases even optimal approximation properties [17, 21, 40, 69, 104]. In particular we make use of an adaptive training set extension in the parameter space, which combines ideas from [61, 62] and [46] for an efficient generation of a snapshot set. One central ingredient of this construction process is a reliable and efficient a posteriori

error estimator for the discretized reduced model which is also derived. On the snapshot set a proper orthogonal decomposition (POD) is applied to construct the reduction space Y_m, where the approximation order m is determined automatically by the POD by prescribing a certain error tolerance. Thus, both in the construction of the solution manifold and the subsequent choice of the basis functions, information on the full solution is included to obtain a fast convergence of the reduced solution to the full one.

As mentioned above the motivating application and long-term goal of our ongoing research is the treatment of saturated-unsaturated subsurface flow, which can be modeled by Richards' equation if a constant air pressure is assumed. Richards' equation comes from the physical principle of mass conservation and Darcy's law and is a nonlinear parabolic partial differential equation (PDE) for the water saturation in the soil. As it unites many difficulties we address some of them, namely the nonlinearity and the formation of a possibly skewed interface at the water table, separately, and use the obtained results for future research. Although we mainly focus on the application to saturated-unsaturated subsurface flow, the HMR-RB approach is equally applicable to other phenomena exhibiting a dominant flow direction.
We begin with the introduction of the HMR-RB approach for general linear elliptic equations. Within this setting the HMR approach hierarchically reduces the full problem to a small dimensionally reduced system in the dominant direction, coupled by the transverse behavior. Numerical experiments show a fast convergence of the HMR-RB approximation to the full solution. Compared to the classical HMR approach with sine functions we obtain a faster convergence for all considered test cases. Run-time experiments verify a linear scaling of the proposed method in the number of degrees of freedom used for the computations in the dominant direction. The concept of the HMR-RB approach for linear problems and parts of the numerical results have been published in [92] and as a preprint in [91].
Next, we treat general nonlinear PDEs, where the nonlinear operator A is a mapping from $H_0^1(\Omega)$ to $H^{-1}(\Omega)$ and Ω denotes the computational domain. As the nonlinearity of A prevents a dimensional reduction, we propose to approximate A with $A_k = \sum_{j=1}^{k} \bar{A}_j(x)\kappa_j(y)$, $(x, y) \in \Omega$, where $\{\kappa_j\}_{j=1}^{k}$ are orthonormal basis functions, forming the so-called collateral basis. Also for the construction of the collateral basis $\{\kappa_j\}_{j=1}^{k}$, we employ a highly nonlinear approximation. To generate a manifold of parametrized lower dimensional operator evaluations we employ the solutions of the parametrized dimensionally reduced problem and the associated parametrization. During the adaptive training set extension procedure the sets of solution and operator snapshots are simultaneously generated. The collateral basis space W_k is constructed by applying a POD to the operator snapshots. For an efficient computation of the coefficients $\bar{A}_j(x)$, $j = 1, \ldots, k$, we introduce the Empirical Projection Method (EPM). The key idea is to approximate the integrals in the coefficients of the orthonormal expansion by an automatic numerical integration program, which is based on the Empirical Interpolation Method [12], and choose the $\bar{A}_j(x)$, $j = 1, \ldots, k$, as the outcome. Rigorous a priori and a posteriori error bounds for the EPM which do not require additional regularity of the nonlinear operator are proven. These bounds are employed for the derivation of a reliable and efficient a posteriori error estimator, which is used within the context of the adaptive snapshot generation procedure. Numerical experiments for the elliptic nonlinear diffusion equation demonstrate a fast convergence of the HMR-RB approach and a linear scaling in the number of degrees of freedom used for the computations in the dominant direction.
Finally, the approximation of the water table requires some additional efforts for the following reason. If the water table is skewed a bad convergence behavior of tensor-based model reduction approaches can be observed. This is due to the fact that for a full approximation of the water table the saturation profile in every point along the dominant direction has to be included. To prevent this effect we propose to first locate the water table by solving the lower dimensional problem in

the dominant direction, which is derived under a hydrostatic pressure assumption and describes the location of the water table. Then we prescribe the so obtained saturation profile as the lifting function of the Dirichlet boundary conditions. In this way we remove the part of the full solution which causes the bad convergence rate from the approximation process and therefore expect to significantly improve the convergence behavior of the employed tensor-based model reduction approach. For prescribed interfaces the latter is demonstrated in numerical experiments for linear elliptic equations and the HMR-RB approach.

1.2 Overview on the literature

There is a large variety of approaches in the fields of dimensional reduction and tensor based approximations. Thus, we only outline the ones most closely related to our method. An overview on the literature on Reduced Basis Methods is given in the parts of the thesis, where the respective techniques are employed.

One of the first dimensional reduced models for subsurface flow has been derived by Dupuit in 1863 assuming a hydrostatic pressure distribution, describing the height of the water table [44]. Using an *asymptotic expansion* it was shown in [37] that the solution of this reduced model is the first order approximation of the solution of the groundwater flow equation with a free surface. This technique has among others also been applied to derive lower-dimensional models for plates (see e.g. [36] and references therein) or water waves (see e.g. [57, 66, 116] and references therein). The method of *asymptotic partial domain decomposition* for thin domains (cf. [18,54,94–96]) generalizes the method of asymptotic expansion. Here, in the (small) part of the domain, where an asymptotically singular behavior of the solution is expected, the full problem is considered, while in the rest of the domain an asymptotic expansion is applied, which is also used to identify suitable coupling conditions at the interface. The main drawback of methods based on asymptotic expansion is, that they are only valid, if the considered domain is very thin, or equivalently, the solution is constant along the vertical direction, which is often not the case.
To overcome this difficulty in the work by Babuška and Vogelius [124] the *Hierarchical Model Reduction* (HMR) approach has been introduced in the context of heat conduction in plates and shells. For thin domains they proposed an optimal a priori choice of the reduction space which coincides with the Legendre polynomials if the coefficients of the considered PDE are constant. In [125] a polynomial convergence rate in m, which depends on the regularity of the full solution, is proven for domains of arbitrary size. Finally, in [126] an a posteriori error estimator is derived and used for an adaptive choice of m throughout the domain. A posteriori error estimation for this choice of the reduction space has been further studied in [2,11]. In a more general geometrical setting the application and applicability of the HMR approach for problems that exhibit a dominant flow direction has been studied and demonstrated by Perotto, Ern and Veneziani in [48, 102] and more recently by Perotto and coworkers in [100, 103]. Adaptive variants of HMR that allow for a local adaption of the approximation order m by a domain decomposition scheme [100, 102] or by associating the basis functions to the nodes of a finite element (FE) partition in the dominant direction [103] are introduced. The basis functions are chosen a priori either as sine functions or Legendre polynomials. Also for the former a polynomial convergence rate in the model order can be proved, which depends on the regularity of the full solution and the polynomial order of the finite element spaces used for the discretization in the dominant direction [26]. As the major part of reduced models obtained by asymptotic expansion or vertical averaging can be derived with a projection approach as presented above with approximation order $m = 1$, HMR constitutes in that sense a hierarchical approach to interpolate between such low dimensional models and their full dimensional counterparts.

A more restricted way of such interpolation is given by the so-called *geometrical multiscale approach*, where, based on a domain decomposition, the dimension of the model is adjusted locally. Both the coupling of full dimensional problems with one-dimensional problems (cf. for the application within hemodynamics e.g [55, 120] and for free-surface flow [86]) and with zero-dimensional, lumped models (cf. [56, 108]) are considered. The latter is particulary used in the context of blood flow simulation. While in all these articles the domain decomposition is chosen a priori, recently an adaptive geometrical multiscale approach has been introduced in [84]. Here, the domain is decomposed a posteriori, based on error indicators, allowing both for model refinement and model coarsening.
Another example for intermediate models are *multilayer shallow water systems* which have been proposed in [8–10, 52, 112] for the approximation of the free-surface Navier-Stokes or Euler equations. Here, the flow domain is discretized in the transverse direction by introducing intermediate water heights. Then, in each layer a classical shallow water equation is considered and a certain coupling between the layers is introduced. This results in general in a better description of the vertical profile of the horizontal velocity and an intermediate model between the classical shallow water equations and the full dimensional Navier-Stokes or Euler equations.

The *proper generalized decomposition approach (PGD)*, introduced in [6, 7, 88], also employs a truncated tensor product decomposition, but determines the tensor products of the expansion by iteratively solving the Euler-Lagrange equations associated with the considered problem. In contrast to RB methods and the HMR-RB approach proposed in this thesis, PGD aims at constructing an approximation based on the knowledge of the considered differential operator and not on a priori knowledge on the solution or an approximation of it [89]. Furthermore, in contrast to HMR, the PGD has been developed for the approximation of models defined in multidimensional spaces, such as problems in quantum chemistry or financial mathematics or parametrized models. Depending on the considered application the number of factors in the tensor products is therefore in general much larger than two. An error estimator for a quantity of interest has been derived in [5] where a PGD approximation of higher accuracy is employed to solve the dual problem. For the variational version of the PGD, where an energy functional is minimized, convergence has been proved for the Poisson problem in [77], for strongly convex nonlinear energy functionals in Hilbert spaces in [24] and in reflexive tensor Banach spaces in [51], and for high-dimensional Ornstein-Uhlenbeck operators with unbounded drift in [53]. For a review on the PGD method we refer to [33, 34].

1.3 Outline of this work

This thesis is organized as follows. In Chapter 2 we introduce the Hierarchical Model Reduction-Reduced Basis approach for general linear elliptic problems. First we recall in Section 2.1 the HMR framework introduced in [102] and give an overview on basis generation with RB methods in Section 2.2. The concept of the HMR-RB approach is developed in Section 2.3. In Section 2.4 we derive an a posteriori error estimator which is based on the Riesz representative of the residual and a localized residual-type estimator. Extensive numerical experiments have been conducted to validate the approximation properties and the computational efficiency of the proposed method. The results are presented in Section 2.6. In this section we also investigate the reliability and effectivity of the two estimators and compare their performance within the HMR-RB framework. In Chapter 3 we adapt the HMR-RB approach to nonlinear PDEs. For this purpose we introduce and analyze the Empirical Projection Method in Section 3.2. In Section 3.3 the formation of the solution and the

operator manifold and the subsequent construction of the reduction and collateral basis space is described. An a posteriori error estimator based on the Brezzi-Rappaz-Raviart theory [20, 23] is derived in Section 3.4. Here, the results in [27] for quadratically nonlinear PDEs and non-affine data functions are generalized to nonlinear PDEs with a nonlinear operator $A : H_0^1(\Omega) \to H^{-1}(\Omega)$. In the numerical experiments in Section 3.6 we investigate the approximation properties and the computational efficiency of the HMR-RB approach and test the applicability of the theoretical results for the elliptic nonlinear diffusion equation. The latter can be regarded as a simplified version of the nonlinear term in the Richards equation. As the coefficient functions in Richards' equation are degenerate in the sense that the relative permeability can become arbitrary small in the dry regions of the porous medium, we also study and demonstrate the applicability of the HMR-RB approach for small ellipticity constants. Chapter 4 is devoted to the approximation of the water table. An ansatz for the approximation of a skewed water table for tensor-based model reduction approaches is introduced in Section 4.1 and exemplified for the HMR-RB approach in Section 4.2. In Section 4.2 we also introduce an alternative ansatz for the derivation of the solution manifold. Numerical results are presented in Section 4.3. Finally, we draw some conclusions in Chapter 5 and give a short outlook. All computer programs used for the numerical experiments presented in this thesis can be found on the attached USB flash drive.

Chapter 2

The Hierarchical Model Reduction - Reduced Basis (HMR-RB) approach for linear elliptic problems

In this chapter we introduce the Hierarchical Model Reduction-Reduced Basis approach for general linear elliptic equations. The chapter is organized as follows. In Section 2.1 we introduce the problem setting and recall the Hierarchical Model Reduction approach following the framework presented in [102]. Afterwards, we describe the most popular procedures for basis generation in Reduced Basis methods, namely the proper orthogonal decomposition (POD) and the greedy algorithm. Important properties including results on their convergence behavior are cited from the literature. The main new contributions of this chapter are developed in Section 2.3 where we first derive a suitable parametrized equation in transverse direction and then detail the usage of Reduced Basis techniques to construct the reduction space. In Section 2.4 a reliable and efficient a posteriori error estimator based on the Riesz representative of the residual and a localized residual-type estimator are derived. Both can be used in the construction process of the reduction space. Subsequently, we thoroughly discuss the computational complexity of the resulting HMR-RB approach in Section 2.5. It is shown that the computional steps of the HMR-RB approach can be decomposed analogue to offline-online splitting in the RB method. However, different from classical RB methods, the HMR-RB scheme is designed to be more efficient than direct finite element methods also for single computations including the cpu-time spend for the offline-steps. Finally, we present several numerical experiments in Section 2.6 to validate the approximation properties and the computational efficiency of our approach including offline- and online phase. Furthermore, the reliability and effectivity of the two estimators is analyzed.

2.1 Hierarchical model reduction for linear elliptic problems

Let $\Omega \subset \mathbb{R}^2$ be a computational domain with Lipschitz boundary $\partial\Omega$ and outer normal ν. We define the solution space V such that $H_0^1(\Omega) \subseteq V \subseteq H^1(\Omega)$ and consider the following general elliptic problem:

$$\text{Find } p \in V: \quad a(p,v) = f(v) \quad \forall v \in V, \tag{2.1}$$

where $a(\cdot,\cdot)$ is a coercive and continuous bilinear form and $f \in V^*$, V^* being the dual space of V. For sake of clarity we assume that possible Dirichlet boundary conditions are homogeneous.

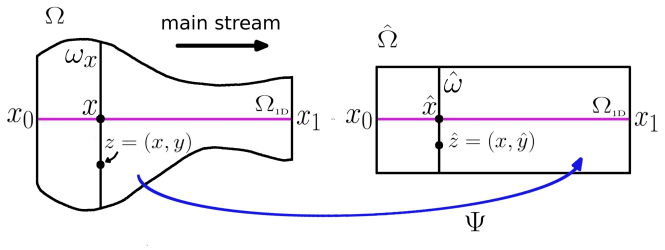

Figure 2.1: The mapping $\Psi : \Omega \to \widehat{\Omega}$, [102]

The extension to non-homogeneous Dirichlet boundary conditions is straightforward and treated in Chapter 4. Furthermore, we denote by $a_s(\cdot,\cdot)$ the symmetric part of $a(\cdot,\cdot)$, i.e. for all $v, w \in V$ there holds $a_s(v,w) = \frac{1}{2}(a(v,w) + a(w,v))$. We define a V-inner product and the induced V-norm as

$$(\cdot,\cdot)_V := a_s(\cdot,\cdot) \quad \text{and} \quad \|\cdot\|_V := \sqrt{(\cdot,\cdot)_V}. \tag{2.2}$$

Finally, we define the coercivity and the continuity constants of the bilinear form $a(\cdot,\cdot)$ with respect to the V-norm as

$$c_0 := \inf_{v\in V} \frac{a(v,v)}{\|v\|_V^2} \quad \text{and} \quad c_1 := \sup_{v\in V}\sup_{w\in V} \frac{a(v,w)}{\|v\|_V\|w\|_V}. \tag{2.3}$$

We adopt the hierarchical model reduction framework introduced by Perotto, Ern, and Veneziani [48, 102]. Thus, we refer to (2.1) as the full problem and assume that Ω can be considered as a two-dimensional fiber bundle

$$\Omega = \bigcup_{x\in\Omega_{1D}} \{x\} \times \omega_x,$$

where Ω_{1D} is the one-dimensional (1D) computational domain in the dominant direction and ω_x the transverse fiber associated with $x \in \Omega_{1D}$. For the sake of simplicity we assume Ω_{1D} to be a straight line, that is $\Omega_{1D} =]x_0, x_1[$. We denote

$$\Gamma_0 = \{x_0\} \times \omega_{x_0}, \qquad \Gamma_1 = \{x_1\} \times \omega_{x_1}, \qquad \Gamma_* = \bigcup_{x\in\Omega_{1D}} \{x\} \times \partial\omega_x. \tag{2.4}$$

Furthermore, we define for any $x \in \Omega_{1D}$ the mapping

$$\psi(\cdot; x) : \omega_x \to \widehat{\omega} \tag{2.5}$$

between the fiber ω_x associated with $x \in \Omega_{1D}$ and a reference fiber $\widehat{\omega}$ with $\widehat{\omega} =]y_0, y_1[$. We adopt the notation for $z = (x, y)$ being a generic point in Ω and $\hat{z} = (x, \hat{y})$ being the corresponding point in $\widehat{\Omega}$. The latter is constructed via the mapping $\Psi : \Omega \to \widehat{\Omega}$ depicted in Fig. 2.1 with $\hat{y} = \psi(y; x)$ for $y \in \omega_x$ and $\hat{x} = x$ for $x \in \Omega_{1D}$, which is why $\widehat{\Omega}_{1D} \equiv \Omega_{1D}$. We suppose that $\psi(\cdot; x)$ is a C^1-diffeomorphism and that the transformation Ψ is differentiable with respect to z. Finally, we denote

$$\mathcal{D}_1(z) = \partial_x\psi(\cdot; x), \qquad \text{and} \qquad \mathcal{D}_2(z) = \partial_y\psi(\cdot; x).$$

2.1.1 Formulation of the reduced problem

We exploit the fiber structure of Ω to define the spaces X and Y such that

$$H_0^1(\Omega_{1D}) \subseteq X \subseteq H^1(\Omega_{1D}) \text{ and } H_0^1(\widehat{\omega}) \subseteq Y \subseteq H^1(\widehat{\omega}).$$

In addition, both spaces have to be compatible with the prescribed boundary conditions on $\partial\Omega$. On $\widehat{\omega}$ we introduce a set of basis functions $\{\phi_k\}_{k\in\mathbb{N}} \in Y$, orthonormal with respect to the L^2-inner product on $\widehat{\omega}$, i.e.

$$\int_{\widehat{\omega}} \phi_k(\hat{y})\,\phi_l(\hat{y})\,d\hat{y} = \delta_{kl} \qquad \forall\, k,l \in \mathbb{N},$$

where δ_{kl} is the Kronecker symbol. In previous papers, possible choices for $\{\phi_k\}_{k\in\mathbb{N}}$ were suitable a priori chosen functions, like trigonometric [48, 102] or Legendre polynomials [102]. A major new contribution of this work is to replace the a priori chosen basis by a posteriori constructed basis functions that are tailored to the specific problem at hand (cf. §2.3). By combining the space X with the reduction space $Y_m = \text{span}(\phi_1, ..., \phi_m)$, we define the reduced space

$$V_m = \left\{ v_m(x,y) = \sum_{k=1}^{m} \overline{v}_k(x)\,\phi_k(\psi(y;x)), \text{ with } \overline{v}_k(x) \in X,\, x \in \Omega_{1D},\, y \in \omega_x \right\}, \tag{2.6}$$

where $m \in \mathbb{N}$ is the approximation order and the coefficients satisfy

$$\overline{v}_k(x) = \int_{\widehat{\omega}} v_m(x, \psi^{-1}(\hat{y};x))\,\phi_k(\hat{y})\,d\hat{y}, \qquad k = 1, ..., m.$$

A Galerkin projection onto V_m yields the reduced problem:

$$\text{Find } p_m \in V_m : \quad a(p_m, v_m) = f(v_m) \;\forall\, v_m \in V_m. \tag{2.7}$$

Rewriting p_m as $p_m(x,y) = \sum_{k=1}^{m} \overline{p}_k(x)\,\phi_k(\psi(y;x))$ leads to:

$$\text{Find } \overline{p}_k \in X, k = 1, ..., m : \quad \sum_{k=1}^{m} a(\overline{p}_k\phi_k, \xi\phi_l) = f(\xi\phi_l) \;\forall\, \xi \in X \text{ and } l = 1, ..., m. \tag{2.8}$$

Note that for a given set of basis functions $\{\phi_k\}_{k=1}^m$ the integrals in the transverse direction can be precomputed. The computation of $p_m(x,y)$ thus reduces to the solution of a one-dimensional coupled system, whose size depends on the model order m.

2.1.2 Example: An advection-diffusion problem

We exemplify the reduced problem (2.8) by an advection-diffusion problem with homogeneous Dirichlet boundary conditions. For the sake of clarity we restrict our exposition to a rectangular domain Ω, implicating $\Omega = \widehat{\Omega}$ and $y = \hat{y}$. We refer to the Appendix A.1 for the treatment of a domain with a curved boundary. The full space V coincides with $H_0^1(\Omega)$ and the spaces X and Y coincide with $H_0^1(\Omega_{1D})$ and $H_0^1(\widehat{\omega})$ respectively. We consider the following bilinear and linear form

$$a(p,v) := \int_\Omega k\nabla p \nabla v\,dxdy + \int_\Omega b\cdot\nabla p v\,dxdy \quad \text{and} \quad f(v) = \int_\Omega sv\,dxdy, \tag{2.9}$$

where $k \in L^\infty(\Omega)$ with $0 < c_3 \le k \le c_4$ for constants $c_3, c_4 \in \mathbb{R}^+$ and $b = (b_1, b_2)^t \in [W^{1,\infty}(\Omega)]^2$ with $\operatorname{div} b \le 0$ and $s \in L^2(\Omega)$. Under these assumptions $a(\cdot,\cdot)$ is a coercive and continuous bilinear

and $f(\cdot)$ a continuous linear form. Given a set of basis functions $\{\phi_l\}_{l=1}^m \in Y$, we obtain the reduced problem: Find $\overline{p}_l \in X$, $l = 1, ..., m$, such that for all $\xi \in X$ and $j = 1, ..., m$

$$\sum_{l=1}^{m} \int_{\Omega_{1D}} A_{lj}(x) \frac{d\overline{p}_l}{dx} \frac{d\xi}{dx} + B_{lj}(x) \frac{d\overline{p}_l}{dx} \xi + C_{lj}(x)\, \overline{p}_l\, \xi \, dx = \int_{\Omega_{1D}} F_j(x)\, \xi \, dx, \tag{2.10a}$$

where the coefficients $A_{lj}(x), B_{lj}(x), C_{lj}(x)$ and $F_j(x)$, $l = 1, ..., m$, $j = 1, ..., m$ are given by

$$\begin{aligned} A_{lj}(x) &= \int_{\widehat{\omega}} k(x,y)\, \phi_l\, \phi_j \, dy, \qquad B_{lj}(x) = \int_{\widehat{\omega}} b_1(x,y)\, \phi_l\, \phi_j \, dy, \\ C_{lj}(x) &= \int_{\widehat{\omega}} k(x,y)\, \phi_l'\, \phi_j' + b_2(x,y)\, \phi_l'\, \phi_j \, dy, \qquad F_j(x) = \int_{\widehat{\omega}} s(x,y)\, \phi_j \, dy. \end{aligned} \tag{2.10b}$$

We emphasize that although considering an advection-diffusion problem (2.9), the coupled system (2.10) also contains a reactive term due to the dimensional splitting.

2.1.3 Discretization of the reduced problem

For the computation of the coefficient functions $\overline{p}_l(x)$, $l = 1, ..., m$, we introduce a subdivision $\mathcal{T}_H$ of Ω_{1D} with elements $\mathcal{T}_i = (x_{i-1}, x_i)$ of width $H_i = x_i - x_{i-1}$ and maximal step size $H := \max_{\mathcal{T}_i} H_i$. We also introduce an associated conforming Finite Element space $X^H \subset X$ with $\dim(X^H) = N_H < \infty$ and basis ξ_i^H, $i = 1, ..., N_H$. X^H is then combined with Y_m to define the discrete reduced space

$$V_m^H = \left\{ v_m^H(x,y) = \sum_{k=1}^{m} \overline{v}_k^H(x)\, \phi_k(\psi(y;x)), \;\text{ with }\; \overline{v}_k^H(x) \in X^H,\, x \in \Omega_{1D},\, y \in \omega_x \right\}. \tag{2.11}$$

By rewriting the discrete reduced solution p_m^H as $p_m^H(x,y) = \sum_{k=1}^m \overline{p}_k^H(x)\, \phi_k(\psi(y;x))$ we obtain the discrete reduced problem: Find $\overline{p}_k^H \in X^H$, $k = 1, ..., m$, such that

$$\sum_{k=1}^{m} a(\overline{p}_k^H \phi_k, \xi_i^H \phi_l) = f(\xi_i^H \phi_l) \;\text{ for }\; i = 1, ..., N_H \;\text{ and }\; l = 1, ..., m. \tag{2.12}$$

We also introduce a coarse subdivision $\mathcal{T}_{H'}$ of Ω_{1D} and an associated low-dimensional conforming FE space $X^{H'} \subset X$ with $\dim(X^{H'}) = N_{H'} < N_H < \infty$. $V_m^{H'}$ and $p_m^{H'}$ shall be the respective coarse counterparts of V_m^H and p_m^H.

Before we describe the construction of the reduction space Y_m in Section 2.3 with Reduced Basis techniques, we give a short introduction to Reduced Basis methods with a particular focus on basis generation.

2.2 Basis generation with Reduced Basis Methods

Reduced Basis (RB) methods are especially designed for and applied within the *real-time* and *many-query* context. While in real-time applications we have constraints on the duration of the numerical simulation, in the many-query context simulations are conducted repeatedly for different inputs. By introducing an appropriate parametrization of the problem the solution space is restricted to a solution manifold, which contains the solutions that are relevant for the considered application. The key idea of RB methods is to perform a Galerkin projection on a suitably chosen low-dimensional reduced (basis) space which approximates this solution manifold. As the focus of real-time or

many-query applications lies on a fast input-output response, a possibly expensive so-called *offline phase* can be accepted. During this offline phase high-dimensional computations, i.e. solutions of a discretized PDE for certain parameter values, are performed to build the reduced basis space in such a way that for each admissible parameter value a small error between the high-dimensional and reduced approximation can be certified. Therefore, in the so-called *online phase* for a given parameter value only the reduced problem has to be solved. Note that RB methods aim at approximating the high-dimensional solution, assuming that the discretization error between the latter and the respective exact solution is negligible. The focus of this section lies on the generation of the reduced basis space. For other topics within the field of RB methods, such as offline-online decomposition, we refer to [42,97,106,110] and for an overview on the historical background of RB methods to [110].

We denote the solution manifold by

$$\mathcal{M}^h(\mu) = \{\mathcal{P}^h(\mu) \,:\, \mu \in \mathcal{D}\}, \tag{2.13}$$

where $\mathcal{P}^h(\mu) \in Y^h \subset Z$ is the solution of a discrete parametrized PDE, the parameter space $\mathcal{D}$ contains all admissible parameter values μ, and $Z \subset L^q(\widehat{\omega})$, $q \geq 1$. The linear n-dimensional subspace $Y_n \subset Y^h$, which yields the best approximation of $\mathcal{M}^h(\mu)$ among all other n-dimensional subspaces of Y^h, can then be characterized by the Kolmogorov n-width [104], which is given by

$$d_n(\mathcal{M}^h(\mu); Y^h) := \inf_{\substack{\tilde{Y} \subset Y^h \\ \dim(\tilde{Y})=n}} \sup_{\mathcal{P}^h(\mu) \in \mathcal{M}^h(\mu)} \inf_{\tilde{v} \in \tilde{Y}} \|\mathcal{P}^h(\mu) - \tilde{v}\|_Z. \tag{2.14}$$

For the computation of the reduced basis space, we introduce a finite dimensional train sample $\Xi_{train} \subset \mathcal{D}$ of size n_{train} and a corresponding discrete manifold

$$\mathcal{M}^h_{train}(\mu) = \{\mathcal{P}^h(\mu) \,:\, \mu \in \Xi_{train}\}. \tag{2.15}$$

As in [110] we further define for a given function $z : \mathcal{D} \to Y^h$ (or $z : \mathcal{D} \to Z$) the norms

$$\|z\|_{L^2(\Xi_{train};Z)} := \left(\frac{1}{n_{train}} \sum_{\mu \in \Xi_{train}} \|z(\mu)\|_Z^2 \right)^{1/2} \text{ and } \|z\|_{L^\infty(\Xi_{train};Z)} := \max_{\mu \in \Xi_{train}} \|z(\mu)\|_Z. \tag{2.16}$$

Next, we describe the most popular methods for the generation of the reduced basis space, namely the proper orthogonal decomposition (POD) and the greedy algorithm. The main difference between these two approaches is that the former yields the optimal space with respect to the $L^2(\Xi_{train}; Z)$-norm, while the latter constructs a reduced space which is suboptimal and in some cases even optimal with respect to the $L^\infty(\Xi_{train}; Z)$-norm.

2.2.1 Proper Orthogonal Decomposition

The POD, also known as the Karhunen-Loève expansion [70, 78] or Principal Component Analysis [67, 98] is very popular and has been used in different fields including fluid dynamics (see e.g. [60,64,115]). It has also been successfully applied in the parametric context for linear (see e.g. [69]) and nonlinear problems (see e.g. [31,75]). For a Hilbert space $Z \subset L^2(\widehat{\omega})$ the POD basis functions ϕ_i, $i = 1, ..., n$, are obtained by solving the optimization problem

$$\min \left(\frac{1}{n_{train}} \sum_{\mu \in \Xi_{train}} \|\mathcal{P}^h(\mu) - \sum_{i=1}^{n} (\mathcal{P}^h(\mu), \phi_i)_Z \phi_i\|_Z^2 \right) \text{ s.t. } (\phi_i, \phi_j)_Z = \delta_{ij}, 1 \leq i, j \leq n. \tag{2.17}$$

Here, $n \leq \dim(\Upsilon^h)$ is assumed, where $\Upsilon^h = \text{span}\{\mathcal{P}^h(\mu)\}$, $\mathcal{P}^h(\mu) \in \mathcal{M}^h_{train}(\mu)$, and $(\cdot,\cdot)_Z$ denotes the inner product associated with the space Z. The POD basis functions ϕ_i, $i = 1, ..., n$, then span the POD space Y_n^{POD}, which can be equivalently defined as

$$Y_n^{\text{POD}} := \arg \inf_{\substack{\tilde{Y} \subset \Upsilon^h \\ \dim(\tilde{Y})=n}} \left(\frac{1}{n_{train}} \sum_{\mu \in \Xi_{train}} \inf_{\tilde{v} \in \tilde{Y}} \|\mathcal{P}^h(\mu) - \tilde{v}\|_Z^2 \right). \tag{2.18}$$

The POD space Y_n^{POD} thus yields the best approximation of Υ^h among all other n-dimensional subspaces of Υ^h with respect to the $L^2(\Xi_{train}; Z)$-norm. In that sense Y_n^{POD} is optimal with respect to this norm. The POD basis $\{\phi_i\}_{i=1}^n$ can be determined by applying the method of snapshots [115]. First, we compute the Gramian matrix

$$\mathcal{K} := \left((\mathcal{P}^h(\mu_i), \mathcal{P}^h(\mu_j))_Z \right)_{1 \leq i,j \leq n_{train}} \in \mathbb{R}^{n_{train} \times n_{train}}. \tag{2.19}$$

Subsequently, we determine its first n eigenvalues $\lambda_1 \geq \lambda_2 \geq \cdots \geq \lambda_n > 0$ and associated eigenvectors $v_1, ..., v_n$, that are orthonormal with respect to the Euclidean inner product $(\cdot,\cdot)_2$, i.e. we solve

$$\mathcal{K} v_i = \lambda_i v_i, \;\; 1 \leq i \leq n \quad \text{and} \quad (v_i, v_j)_2 = \delta_{ij}, 1 \leq i, j \leq n. \tag{2.20}$$

The POD basis ϕ_i, $i = 1, ..., n$, is then given as

$$\phi_i = \frac{1}{\sqrt{n_{train}\lambda_i}} \sum_{j=1}^{n_{train}} (v_i)_j \mathcal{P}^h(\mu_j), \;\; 1 \leq i \leq n,$$

where $(v_i)_j$ denotes the jth component of the eigenvector v_i. The POD error e_n^{POD} defined as

$$e_n^{\text{POD}} := \left(\frac{1}{n_{train}} \sum_{\mu \in \Xi_{train}} \|\mathcal{P}^h(\mu) - \sum_{i=1}^{n} (\mathcal{P}^h(\mu), \phi_i)_Z \phi_i\|_Z^2 \right)^{1/2} \tag{2.21}$$

satisfies (cf. [69])

$$(e_n^{\text{POD}})^2 = \sum_{k=n+1}^{n_{train}} \lambda_k. \tag{2.22}$$

We finally remark that all stated results equally hold true for continuous functions $\mathcal{P}(\mu)$, $\mu \in \Xi_{train}$.

2.2.2 The Greedy Algorithm

As the construction of the POD basis requires the computation of $\mathcal{P}^h(\mu)$ for all $\mu \in \Xi_{train}$ and the subsequent solution of the eigenvalue problem, its computation can become very expensive for large train samples. Therefore, a *greedy* strategy has been proposed in [123] to overcome this difficulty. The objective of the greedy algorithm 2.2.1 (see e.g. [17, 21, 40, 81, 82, 110, 123]) is to construct a nested set of parameters $S_n = \{\mu_1, \ldots, \mu_n\}$ and a corresponding Lagrangian reduced basis space $Y_n := \text{span}\{\mathcal{P}^h(\mu_1), \ldots, \mathcal{P}^h(\mu_n)\}$. This is realized by choosing in each iteration the candidate snapshot $\mathcal{P}^h(\mu)$, which is (based on the prediction of an error estimator $\Delta_{n-1}(\mu)$) worst approximated by Y_{n-1}. Therefore, in contrast to the POD, only the snapshots associated with the set S_n have to be computed. To consider large train samples Ξ_{train} it is crucial that the error estimator is rapidly evaluable, i.e. with a complexity that does not depend on the dimension of the underlying high dimensional discretization. This can be realized if the error estimator allows for a

Algorithm 2.2.1: Greedy Algorithm

GREEDY(Ξ_{train},$N_{\max}$,tol)
Initialize: $S_0 = \emptyset$, $Y_0 = \emptyset$.
for $n = 1 : N_{max}$ **do**

$$\text{Find: } \mu_n = \arg\max_{\mu\in\Xi_{train}} \Delta_{n-1}(\mu).$$

$$\text{Extend: } S_n = S_{n-1} \cup \mu_n \text{ and } Y_n = Y_{n-1} \cup \text{span}\{\mathcal{P}^h(\mu_n)\}.$$

  Compute $\Delta_n(\mu)$ for all $\mu \in \Xi_{train}$.
  if $\arg\max_{\mu\in\Xi_{train}} \Delta_n(\mu) \leq tol$ **then**
    break
  end
end
return S_n, Y_n

so-called offline-online decomposition (cf. [110]). We remark that the greedy algorithm 2.2.1 aims at simultaneously approximating all functions $\mathcal{P}^h(\mu) \in \mathcal{M}^h_{train}(\mu)$ employing finite dimensional subspaces that are constructed using elements of $\mathcal{M}^h_{train}(\mu)$. Algorithm 2.2.1 thus differs from greedy algorithms with the objective to approximate a single function by a finite linear combination of functions from a given dictionary [17]. For a complete survey on the latter including convergence results see [117]. If the error estimator is rigorous and effective, i.e. it fulfills

$$\underline{c}\,\Delta_n(\mu) \leq \inf_{v^h\in Y_n} \|\mathcal{P}^h(\mu) - v^h\|_Z \leq \bar{C}\,\Delta_n(\mu), \tag{2.23}$$

for constants $0 < \underline{c} \leq \bar{C}$, convergence of the greedy algorithm 2.2.1 can be proven. First, we restrict to the case that Z is a Hilbert space. A first result for the convergence rate of the greedy algorithm has been proven in [21] for $\underline{c} = \bar{C} = 1$, assuming an exponential convergence of the Kolmogorov n-width. Various improvements have been proven in [17] for $0 < \underline{c}/\bar{C} \leq 1$, including the following. It was shown that if we have an polynomial convergence of the Kolmogorov n-width, the greedy algorithm converges with the same rate. If an exponential convergence of the Kolmogorov n-width is assumed, the greedy algorithm converges with a sub-optimal exponential rate. In contrast to the results in [17, 21] the very recent result in [40] does not require any assumption on the decay rate of the Kolmogorov n-width. If an exponential convergence of the Kolmogorov n-width is assumed, the result in [40] improves the rate in [17]. To simplify notations we set

$$\sigma_n(\mathcal{M}^h_{train}(\mu)) := \sup_{\mathcal{P}^h(\mu)\in\mathcal{M}^h_{train}(\mu)} \inf_{v^h\in Y_n} \|\mathcal{P}^h(\mu) - v^h\|_Z.$$

Theorem 2.1 (Convergence of the greedy algorithm 2.2.1 in Hilbert spaces, [40])**.** *Let us assume that Z is a Hilbert space, that $0 < \underline{c}/\bar{C} \leq 1$ and for notational convenience only that $\|\mathcal{P}^h(\mu)\|_Z \leq 1$ for $\mathcal{P}^h(\mu) \in \mathcal{M}^h_{train}(\mu)$. Then, for $n \geq 1$ we have*

(i)

$$\sigma_n(\mathcal{M}^h_{train}(\mu)) \leq \sqrt{2}\,\frac{\bar{C}}{\underline{c}} \min_{1\leq m<n} d_m(\mathcal{M}^h_{train}(\mu); Y^h)^{\frac{n-m}{n}}.$$

In particular this yields

$$\sigma_{2n}(\mathcal{M}^h_{train}(\mu)) \leq \sqrt{2}\,\frac{\bar{C}}{\underline{c}}\,\sqrt{d_n(\mathcal{M}^h_{train}(\mu);Y^h)}, \quad n=1,2,\dots.$$

(ii) If $d_n(\mathcal{M}^h_{train}(\mu);Y^h) \leq C_0 n^{-\alpha}$, $n=1,2,\dots$, *then* $\sigma_n(\mathcal{M}^h_{train}(\mu)) \leq C_1 n^{-\alpha}$, $n=1,2,\dots$, *with* $C_1 := 2^{5\alpha+1}\left(\frac{\bar{C}}{\underline{c}}\right)^2 C_0$.

(iii) If $d_n(\mathcal{M}^h_{train}(\mu);Y^h) \leq C_0 e^{-b_0 n^\alpha}$, $n=1,2,\dots$, *then* $\sigma_n(\mathcal{M}^h_{train}(\mu)) \leq \sqrt{2C_0}\frac{\bar{C}}{\underline{c}} e^{-b_1 n^\alpha}$, $n=1,2,\dots$, *where* $b_1 := 2^{-1-2\alpha} b_0$.

Proof. See [40]. □

Furthermore, in [40] the first result for the convergence of the greedy algorithm 2.2.1 in Banach spaces has been proven. Let therefore $Z \subset L^q(\widehat{\omega})$, $q \geq 1$.

Theorem 2.2 (Convergence of the greedy algorithm 2.2.1 in Banach spaces, [40])**.** *Let us assume that* Z *is a Banach space, that* $0 < \underline{c}/\bar{C} \leq 1$ *and that* $\|\mathcal{P}^h(\mu)\|_Z \leq 1$ *for* $\mathcal{P}^h(\mu) \in \mathcal{M}^h_{train}(\mu)$. *Then, for* $n \geq 1$ *we have*

(i)

$$\sigma_n(\mathcal{M}^h_{train}(\mu)) \leq \sqrt{2}\,\frac{\bar{C}}{\underline{c}} \min_{1\leq m<n} n^{\frac{n-m}{2n}} \left(\sum_{i=1}^{n} \sigma_i(\mathcal{M}^h_{train}(\mu))^2\right)^{\frac{m}{2n}} d_m(\mathcal{M}^h_{train}(\mu))^{\frac{n-m}{n}}.$$

In particular this yields

$$\sigma_{2n}(\mathcal{M}^h_{train}(\mu)) \leq 2\,\frac{\bar{C}}{\underline{c}}\,\sqrt{n d_n(\mathcal{M}^h_{train}(\mu);Y^h)}, \quad n=1,2,\dots.$$

(ii) If for $\alpha > 0$, *we have* $d_n(\mathcal{M}^h_{train}(\mu);Y^h) \leq C_0 n^{-\alpha}$, $n=1,2,\dots$, *then for any* $0 < \beta < \min\{\alpha, 1/2\}$, *we have* $\sigma_n(\mathcal{M}^h_{train}(\mu)) \leq C_1 n^{-\alpha+1/2+\beta}$, $n=1,2,\dots$, *with*

$$C_1 := \max\left\{ C_0 4^{4\alpha+1}\left(\frac{\bar{C}}{\underline{c}}\right)^4 \left(\frac{2\beta+1}{2\beta}\right)^\alpha, \max_{n=1,\dots,7}\{n^{\alpha-\beta-1/2}\}\right\}.$$

(iii) If for $\alpha > 0$, *we have* $d_n(\mathcal{M}^h_{train}(\mu);Y^h) \leq C_0 e^{-b_0 n^\alpha}$, $n=1,2,\dots$, *then* $\sigma_n(\mathcal{M}^h_{train}(\mu)) \leq \sqrt{2C_0}\frac{\bar{C}}{\underline{c}}\sqrt{n} e^{-b_1 n^\alpha}$, $n=1,2,\dots$, *where* $b_1 := 2^{-1-2\alpha} b_0$. *The factor* $\sqrt{n}$ *can be deleted by reducing the constant* b_1.

Proof. See [40]. □

For an extensive overview on examples, where the Kolmogorov n-width is actually known, we refer to [104]. Recently, it has been shown in [76] for linear PDEs that if the bilinear and linear form exhibit a affine parameter dependence and if the number of affine terms for the bilinear form is ≤ 2 and one of them is dominating, an exponential convergence of the Kolmogorov n-width can be obtained. Here, the rate depends on the number of terms in the affine decomposition of the linear form. Due to the results of Theorem 2.1 and 2.2 we can thus conclude that the greedy algorithm 2.2.1 constructs a reduced space which is suboptimal and in some cases even optimal with respect to the $L^\infty(\Xi_{train}; Z)$-norm.

2.3 The Hierarchical Model Reduction-Reduced Basis approach

The goal of this section is to construct a low-dimensional reduction space Y_m which approximates well the transverse behavior of the full problem (2.1), and can be used to set up the approximation spaces V_m (2.6) and V_m^H (2.11) in the HMR framework. Starting from the full problem we derive initially a 1D PDE in transverse direction in which the unknown behavior in the dominant direction enter as parameters (§2.3.1). The FE solutions of the corresponding parameter dependent discrete 1D problem (§2.3.3) form a solution manifold $\mathcal{M}^h$ (cf. (2.33) below), which can be approximated by RB methods with very few basis functions, at least if the manifold is smooth [17,21,40,104]. The key idea is to exploit the good approximation properties of RB methods (see §2.2) for the construction of a low-dimensional reduction space Y_m^h, where the index h indicates that Y_m^h contains discrete solutions. Precisely, we first use an adaptive training set extension similar to the one introduced in [61, 62] for an efficient generation of a snapshot set Y_M^h and subsequently apply a POD to find the principal components of Y_M^h, which then form the reduction space Y_m^h, where $m < M$ and $m = \dim(Y_m^h)$ (cf. §2.3.4).

2.3.1 Derivation of a parametrized 1D problem in transverse direction

One of the major challenges when deriving a lower dimensional PDE from a full problem is to realize a tensor product decomposition of the full solution. The approach we pursue in this chapter is to assume (only for the derivation of a suitable 1D PDE in transverse direction) that

$$p(x, \hat{y}) \approx U(x) \cdot \mathcal{P}(\hat{y}). \tag{2.24}$$

Here, the function $U(x)$ represents the behavior of the full solution in the dominant direction, which is unknown at this stage. By choosing the test functions as $v(x, y) = U(x) \cdot v(\hat{y})$ for any $v \in Y$ we obtain a reduced problem: Given any $U \in X$, find $\mathcal{P} \in Y$ such that

$$a(U\mathcal{P}, Uv) = f(Uv) \ \ \forall v \in Y. \tag{2.25}$$

As $U(x)$ is unknown, the integrals in the dominant direction cannot be precomputed as in (2.8). We therefore introduce for an arbitrary integrand $t \in L^1(\widehat{\Omega})$ of an integral $I(t) := \int_{\widehat{\omega}} \int_{\Omega_{1D}} t(x, \hat{y})\, dx d\hat{y}$ the quadrature formula

$$Q(t) := \sum_{l=1}^{Q} \alpha_l \int_{\widehat{\omega}} \tilde{t}(x_l^q, \hat{y})\ d\hat{y}, \quad \tilde{t}(x_l^q, \hat{y}) := \lim_{\varepsilon \to 0} \frac{1}{|B_\varepsilon(x_l^q)|} \int_{B_\varepsilon(x_l^q)} t(x, \hat{y})\, dx, \tag{2.26}$$

where α_l, $l = 1, ..., Q$ are the weights, and x_l^q, $l = 1, ..., Q$ are the quadrature points. Replacing $I(t)$ by $Q(t)$ in the bilinear form $a(\cdot, \cdot)$ and the linear form $f(\cdot)$, we obtain the approximations $a^q(\cdot, \cdot)$ and $f^q(\cdot)$. The reduced problem with quadrature then reads:

$$\text{Given any } U \in X, \text{ find } \mathcal{P} \in Y: \quad a^q(U\mathcal{P}, Uv) = f^q(Uv) \ \ \forall v \in Y. \tag{2.27}$$

Next we introduce a parametrization of (2.27) with the objective to apply RB methods (§2.3.4) to find optimal locations of the quadrature points and include information on the unknown behavior U of the solution in the dominant direction in the reduction space Y_m. For that purpose we define a parameter vector μ, which contains both the quadrature points x_l^q, $l = 1, ..., Q$, and the evaluations $U(x_l^q)$ and $\partial_x^k U(x_l^q)$, $k = 1, ..., n$, $l = 1, ..., Q$, occurring in (2.27). The parameter μ thus has the form $\mu = (x_l^q, U(x_l^q), \partial_x^k U(x_l^q), U(x_0), \partial_x^k U(x_0), U(x_1), \partial_x^k U(x_1))$, $l = 1, ..., Q$, $k = 1, ..., n$, where x_0 and x_1 have been defined in §2.1 as the interval boundaries of Ω_{1D}. The evaluations in x_0

and x_1 occur in μ if non-homogeneous Neumann or Robin boundary conditions are prescribed in the full problem (2.1) on Γ_0 or Γ_1, where Γ_i, $i = 0, 1$ are defined in (2.4). Moreover, if x_0 or $x_1 \in \{x_l^q\}_{l=1}^Q$, the respective quadrature point(s) and the evaluations $U(x_i)$ and $\partial_x^k U(x_i)$, $i = 0, 1$, which can be inferred from the prescribed boundary conditions drop out of μ. The parameter space $\mathcal{D}$ of dimension P, which contains all feasible parameter values of μ, is then defined as $\mathcal{D} := [\Omega_{1D} \times I_0 \times \cdots \times I_n]^Q \times I_0 \times \cdots \times I_n \times I_0 \times \cdots \times I_n \subset \mathbb{R}^P$, where the intervals $I_k \subset \mathbb{R}$, $k = 0, ..., n$ contain the ranges of $\partial_x^k U(x)$, $k = 0, ..., n$. To determine the latter no a priori information on the full solution is needed. The numerical tests in §2.6 show that the choice of the intervals $I_k \subset \mathbb{R}$, $k = 0, ..., n$ has little influence on the outcome. We obtain the following parametrized 1D partial differential equation in the transverse direction:

$$\text{Given any } \mu \in \mathcal{D}, \text{ find } \mathcal{P}(\mu) \in Y : a^q(\mathcal{P}(\mu), \upsilon\,; \mu) = f^q(\upsilon\,; \mu) \ \forall \upsilon \in Y. \tag{2.28}$$

Assuming that the quadrature points x_l^q, $l = 1, ..., Q$ are sorted in ascending order, the weights α_l, $l = 1, ..., Q$ in (2.26) we have used for the numerical tests in §2.6 are defined as

$$\alpha_1 := \frac{x_1^q + x_2^q}{2} - x_0, \quad \alpha_l := \frac{x_{l+1}^q - x_{l-1}^q}{2}, \ l = 2, ..., Q-1, \quad \alpha_Q := x_1 - \frac{x_{Q-2}^q + x_{Q-1}^q}{2}. \tag{2.29}$$

In §2.6 we compare the modified composite rectangle formula, obtained by choosing the weights as in (2.29), also with a standard composite trapezoidal rule (cf. [107]). Regarding reasonable values for Q the numerical test cases §2.6 show that for all purely diffusive problems in §2.6 one quadrature point is sufficient, whereas for problems with a dominant advection it is better to use two or three.

2.3.2 Example: An advection-diffusion problem

To exemplify the derivation of the parametrized 1D partial differential equation we revisit the example of the advection-diffusion problem defined in §2.1.2. By applying the quadrature formula defined in (2.26), we obtain the reduced problem with quadrature: Given any $U \in X$, find $\mathcal{P} \in Y$ such that:

$$\int_{\widehat{\omega}} \bar{\mathcal{A}}(y) \tfrac{d\mathcal{P}}{dy} \tfrac{d\upsilon}{dy} + \bar{\mathcal{B}}(y) \tfrac{d\mathcal{P}}{dy} \upsilon + \bar{\mathcal{C}}(y)\, \mathcal{P}\, \upsilon \, dy = \int_{\widehat{\omega}} \bar{\mathcal{F}}(y)\, \upsilon \, dy \quad \forall \upsilon \in Y, \tag{2.30a}$$

where the coefficients $\bar{\mathcal{A}}(y), \bar{\mathcal{B}}(y), \bar{\mathcal{C}}(y)$ and $\bar{\mathcal{F}}(y)$ are given by

$$\begin{aligned} \bar{\mathcal{A}}(y) &= \sum_{l=1}^{Q} \alpha_l k(x_l^q, y) U^2(x_l^q), \qquad \bar{\mathcal{B}}(y) = \sum_{l=1}^{Q} \alpha_l b_2(x_l^q, y) U^2(x_l^q), \\ \bar{\mathcal{C}}(y) &= \sum_{l=1}^{Q} \alpha_l k(x_l^q, y) (\partial_x U(x_l^q))^2 + b_1(x_l^q, y) \partial_x U(x_l^q) U(x_l^q) \qquad \bar{\mathcal{F}}(y) = \sum_{l=1}^{Q} \alpha_l s(x_l^q, y) U(x_l^q). \end{aligned} \tag{2.30b}$$

Here we have omitted the $\backsim$ on the integrands (cf. (2.26)) to simplify notation. We note that also the 1D problem in the transverse direction (2.30) additionally contains a reactive term due to the dimensional splitting. We assume that $x_0, x_1 \notin \{x_l^q\}_{l=1}^Q$. As we prescribe homogeneous Dirichlet boundary conditions (cf. §2.1.2) and (2.30) only contains first derivatives of U, the parameter μ and the parameter space $\mathcal{D}$ are defined as $\mu = (x_l^q, U(x_l^q), \partial_x U(x_l^q))$, $l = 1, ..., Q$, and $\mathcal{D} := [\Omega_{1D} \times I_0 \times I_1]^Q$, respectively. To shorten notations we set $\mu = [\mu_{l,1}, \mu_{l,2}, \mu_{l,3}]_{l=1}^Q$ where $\mu_{l,1}$ replaces x_l^q, $\mu_{l,2}$ replaces $U(x_l^q)$, and $\partial_x U(x_l^q)$ is replaced by $\mu_{l,3}$. The parametrized 1D PDE in transverse direction then reads: Given any $\mu \in \mathcal{D}$, find $\mathcal{P}(\mu) \in Y$ such that

$$\int_{\widehat{\omega}} \mathcal{A}(y;\mu) \frac{d\mathcal{P}(\mu)}{dy} \frac{d\upsilon}{dy} + \mathcal{B}(y;\mu) \frac{d\mathcal{P}(\mu)}{dy} \upsilon + \mathcal{C}(y;\mu)\, \mathcal{P}(\mu)\, \upsilon \, dy = \int_{\widehat{\omega}} \mathcal{F}(y;\mu)\, \upsilon \, dy \quad \forall \upsilon \in Y, \tag{2.31a}$$

Algorithm 2.3.1: Adaptive training set extension and snapshot generation

AdaptiveParameterRefinement$(G_0, \Xi_{G_0}, m_{\max}, i_{max}, n_\Xi, \theta, \sigma_{thres}, N_{H'})$
Initialize $G = G_0, \Xi_G = \Xi_{G_0}, \phi_0 = \emptyset, \rho_0(G) = 0$
for $m = 1, \ldots, m_{max}$ **do**
  Compute $\mathcal{P}_G^h$
  $[\eta(G), \sigma(G)] =$ ElementIndicators$(\{\phi_k\}_{k=1}^{m-1}, \mathcal{P}_G^h, G, \rho(G), N_{H'})$
  for $i = 1, \ldots, i_{max}$ **do**
    $\mathcal{G} :=$ Mark$(\eta(G), \sigma(G), \theta, \sigma_{thres})$
    $(G, \Xi_G) :=$ Refine$(\mathcal{G}, \Xi_\mathcal{G}, n_\Xi)$
    $\rho(G \setminus \mathcal{G}) = \rho(G \setminus \mathcal{G}) + 1$
    Compute $\mathcal{P}_\mathcal{G}^h$
    $[\eta(\mathcal{G}), \rho(\mathcal{G}), \sigma(\mathcal{G})] =$ ElementIndicators$(\{\phi_k\}_{k=1}^{m-1}, \mathcal{P}_\mathcal{G}^h, N_{H'})$
  end
  $\{\phi_k\}_{k=1}^m := \mathrm{POD}(\mathcal{P}_G^h, m)$
end
return $\mathcal{P}_G^h, \Xi_G$

where the coefficients $\mathcal{A}(y;\mu), \mathcal{B}(y;\mu), \mathcal{C}(y;\mu)$ and $\mathcal{F}(y;\mu)$ are given by

$$\begin{aligned} \mathcal{A}(y;\mu) &= \sum_{l=1}^{Q} \alpha_l k(\mu_{l,1}, y)\mu_{l,2}^2, \qquad \mathcal{B}(y;\mu) = \sum_{l=1}^{Q} \alpha_l b_2(\mu_{l,1}, y)\mu_{l,2}^2, \\ \mathcal{C}(y;\mu) &= \sum_{l=1}^{Q} \alpha_l k(\mu_{l,1}, y)\mu_{l,3}^2 + b_1(\mu_{l,1}, y)\mu_{l,3}\mu_{l,2} \qquad \mathcal{F}(y;\mu) = \sum_{l=1}^{Q} \alpha_l s(\mu_{l,1}, y)\mu_{l,2}. \end{aligned} \tag{2.31b}$$

For the sake of completeness, we remark that if $x_0, x_1 \in \{x_l^q\}_{l=1}^Q$, the parameter μ has the form $\mu = (x_l^q, U(x_l^q), \partial_x U(x_l^q), \partial_x U(x_0), \partial_x U(x_1))$, $l = 2, ..., Q-1$, assuming without loss of generality that $x_1^q = x_0$ and $x_Q^q = x_1$. Note that the prescribed homogeneous Dirichlet boundary conditions imply $U(x_0) = U(x_1) = 0$. The parameter space $\mathcal{D}$ can thus be defined as $\mathcal{D} := [\Omega_{1D} \times I_0 \times I_1]^{Q-2} \times I_1 \times I_1$.

2.3.3 Discretization of the parametrized 1D problem in transverse direction

For the computation of snapshots (i.e. solutions of (2.28) for a given parameter μ), we introduce a subdivision τ_h of $\widehat{\omega}$ with elements $\tau_j = (\hat{y}_{j-1}, \hat{y}_j)$ of width $h_j = \hat{y}_j - \hat{y}_{j-1}$ and maximal step size $h := \max_{\tau_j} h_j$. Furthermore, we introduce an associated conforming Finite Element space $Y^h \subset Y$ with $\dim(Y^h) = n_h < \infty$, and basis υ_j^h, $j = 1, ..., n_h$. The parameter dependent discrete 1D problem then reads:

$$\text{Given any } \mu \in \mathcal{D}, \text{ find } \mathcal{P}^h(\mu) \in Y^h : \quad a^q(\mathcal{P}^h, \upsilon_j^h; \mu) = f^q(\upsilon_j^h; \mu) \quad \text{for } j = 1, ..., n_h. \tag{2.32}$$

2.3.4 Basis generation with RB techniques: The Adaptive-HMR-POD algorithm

In this subsection we introduce the Adaptive-HMR-POD algorithm to construct the low dimensional reduction space $Y_m^h = \text{span}(\phi_1, \ldots, \phi_m) \subset Y^h$ based on sampling strategies from the RB framework. We first define the solution manifold $\mathcal{M}^h$ and a snapshot set Y_M^h, $M := dim(Y_M^h)$ through

$$\mathcal{M}^h := \{\mathcal{P}^h(\mu) | \mu \in \mathcal{D}\}, \qquad Y_M^h := \{\mathcal{P}^h(\mu) | \mu \in \Xi_{train}\}, \tag{2.33}$$

where $\mathcal{P}^h(\mu)$ solves (2.32), and $\Xi_{train} \subset \mathcal{D}$ of the size $n_{train} = |\Xi_{train}|$ denotes a finite training set. For an efficient snapshot generation and hence construction of Y_M^h, we use an adaptive training set extension resembling the one introduced in [61,62]. This adaptive refinement of the parameter space is performed by Algorithm 2.3.1 AdaptiveParameterRefinement, which is described in detail below. Algorithm 2.3.1 is a greedy algorithm of the same type as Algorithm 2.2.1, which enhances a preliminary basis in each iteration and additionally refines the parameter space. Note that different to Algorithm 2.2.1 we are interested in finding snapshots that yield a good approximation p_m^H of a certain 2D FE reference solution $p^{H\times h}$ with respect to an energy norm. Therefore, we refine the parameter space near the parameter value for which $p^{H\times h}$ is best approximated by p_m^H in order to find snapshots $\mathcal{P}^h(\mu)$ which may even yield a better approximation. Finally, we apply in Algorithm 2.3.2 a proper orthogonal decomposition (POD) (cf. 2.2.1) to determine the principal components of Y_M^h, which in turn span the reduction space Y_m^h with $m < M$.

Algorithm 2.3.1: AdaptiveParameterRefinement Let G denote a hyperrectangular, possibly non-conforming, adaptively refined grid in the parameter space $\mathcal{D}$, g a cell of G and N_G the number of cells in G. Different from the approach in [61,62], the training set Ξ_g consists of parameter values which are sampled from the uniform distribution over the cell g. n_Ξ denotes the sample size of Ξ_g and is chosen identical for all cells. Finally, we define the overall training set $\Xi_G = \cup_{g\in G}\Xi_g$. Inspired by [61, 62] we use a local mesh adaptation with a SOLVE $\rightarrow$ ESTIMATE $\rightarrow$ MARK $\rightarrow$ REFINE strategy to generate G and Ξ_G from a given coarse partition G_0 of the parameter space and an associated initial train sample Ξ_{G_0}. To estimate the error between p_m^H and $p^{H\times h}$ in the V-norm, we derive in §2.4 a reliable and efficient error estimator Δ_m. In order to detect the best approximating parameter values μ, we define a cell indicator

$$\eta(g) := \min_{\mu\in\Xi_g} \Delta_m(\mu). \tag{2.34}$$

Next, we fix $\theta \in (0, 1]$ and mark in each iteration the θN_G cells with the smallest indicators $\eta(g)$ for refinement. It is well known in the context of adaptive FEM that such an indicator may cause problems if the initial mesh is too coarse to resolve local structures of the data. Thus, we use as in [61, 62] an additional criterion to decide, if a cell is marked for refinement or not and define a second indicator

$$\sigma(g) := \text{diam}(g) \cdot \rho(g). \tag{2.35}$$

Here, $\rho(g)$ counts the number of iterations in which the cell g has not been refined, since its last refinement and diam(g) denotes the diameter of g. If $\sigma(g)$ lies above a certain threshold σ_{thres}, the cell g is marked for refinement as well. This leads asymptotically to a refinement of all cells. All cells marked for refinement are bisected in each direction, leading to $2^P - 1$ new cells per refined cell. To generate the training sets of the new cells, we first sort $\Xi_{g_{parent}}$ into the new cells $g_{children}$. Then, in each children $g_{children}$ we sample new parameter values from the uniform distribution over $g_{children}$ until the sample size of $\Xi_{g_{children}}$ reaches n_Ξ. The complete adaptive snapshot generation

Algorithm 2.3.2: Construction of the reduction space Y_m^h

ADAPTIVE-HMR-POD$(G_0, m_{\max}, i_{max}, n_\Xi, \theta, \sigma_{thres}, N_{H'}, \varepsilon_{\text{tol}})$
Initialize Ξ_{G_0}
$[\mathcal{P}_G^h, \Xi_G]$ = ADAPTIVEPARAMETERREFINEMENT$(G_0, \Xi_{G_0}, m_{\max}, i_{max}, n_\Xi, \theta, \sigma_{thres}, N_{H'})$
$Y_m^h := \text{POD}(\mathcal{P}_G^h, \varepsilon_{\text{tol}})$, such that $e_m^{\text{POD}} \leq \varepsilon_{\text{tol}}$.
return Y_m^h

procedure is described in Algorithm 2.3.1 in an abstract way. During each loop over the model order m, first the snapshots $\mathcal{P}_G^h$ and the cell indicators $\eta(G)$ and $\sigma(G)$ are computed for all cells in G. Then the parameter space is adaptively refined in order to find the best approximation using m basis functions. Finally, the m principal components $\{\phi_k\}_{k=1}^m$ of the set of snapshots $\mathcal{P}_G^h$ are identified by a POD. We highlight that throughout Algorithm 2.3.1 the computations dependent on the number of degrees of freedom in the dominant direction, namely the computation of the reduced solution and the error indicator $\eta(g)$, are not performed in the possibly high-dimensional space V_m^H but in the lower-dimensional space $V_m^{H'}$ of dimension $N_{H'} \cdot m$. This completes the description of Algorithm 2.3.1.

As G is a product-like hyper-rectangular grid, the applicability of Algorithm 2.3.1 is limited to small parameter dimensions P, where our numerical experiments showed a limit of $P = 8$. Furthermore, we mention that in contrast to [61,62] where the vertices of G generate the training set, we choose Ξ_g randomly in order to avoid repetitions, due to parameters lying on the same edge of an cell. We have borrowed the idea to choose the training sets of the cells randomly from [46]. Here, the two parameter values of the cell for which the highest value of the error estimator is attained are chosen as so-called anchor points and the cell is divided between these two points by using a Voronoi tessellation. In [83] an anisotropic refinement of the parameter space is proposed employing a distance function, which is based on the Hessian of the reduced basis approximation for each $\mu \in \Xi_{train}$. As neither of the two last-mentioned approaches relies on a product-like background grid, they could be feasible options to extend the HMR-RB approach to higher parameter dimensions. The generation of $\{\phi_k\}_{k=1}^m$ can also be done by a Greedy algorithm which adds in each iteration the basis function belonging to the parameter μ with the smallest value of Δ_m. However, numerical experiments showed much better performance for the POD approach, as more linear independent snapshots are found during the application of Algorithm 2.3.1.

Algorithm 2.3.2: ADAPTIVE-HMR-POD First, we initialize the train sample Ξ_{G_0} by sampling n_Ξ parameter values from the uniform distribution over each cell $g \in G_0$. Then Algorithm 2.3.1 is called for the efficient generation of the snapshots $\mathcal{P}_G^h$. Setting $\Xi_{train} = \Xi_G$, we identify the principal components of Y_M^h by a POD, where the POD spaces Y_k^{POD}, $k = 1, ..., m$, are defined as (cf. §2.2.1)

$$Y_k^{\text{POD}} = \arg \inf_{\substack{W_k \subset \text{span}\{Y_M^h\} \\ \dim(W_k)=k}} \left(\frac{1}{n_{train}} \sum_{\mu \in \Xi_{train}} \inf_{w_k \in W_k} \|\mathcal{P}^h(\mu) - w_k\|_{L^2(\widehat{\omega})}^2 \right). \tag{2.36}$$

Demanding that the POD-error e_m^{POD} (2.21) satisfies

$$e_m^{\mathrm{POD}} = \left(\frac{1}{n_{train}} \sum_{\mu \in \Xi_{train}} \inf_{w_k \in Y_m^{\mathrm{POD}}} \|\mathcal{P}^h(\mu) - w_k\|^2_{L^2(\widehat{\omega})} \right)^{1/2} \leq \varepsilon_{\mathrm{tol}}, \tag{2.37}$$

where ε_{tol} is a prescribed error tolerance, we set $Y_m^h := Y_m^{\mathrm{POD}}$. This completes the description of Algorithm 2.3.2 (ADAPTIVE-HMR-POD). The choice of the input parameters m_{max}, i_{max}, n_Ξ, σ_{thres} and $N_{H'}$ will be discussed in detail in §2.6.

Note that the $L^2(\widehat{\omega})$-norm could also be replaced by the $H^1(\widehat{\omega})$-norm in (2.36). However, as the POD based on the $L^2(\widehat{\omega})$-norm performed slightly better in our numerical experiments, we decided to use (2.36). We point out that by definition the POD space approximates Y_M^h (2.33). A validation if the selected basis functions approximate the solution $p(x, y)$ of the full problem 2.1 with the same approximation quality as Y_M^h will therefore be performed in §2.6.

2.4 A posteriori error estimation

2.4.1 An a posteriori error estimator based on the Riesz representative of the residual

In this subsection we derive a reliable and efficient error estimator. For this purpose we use as in the RB framework [97, 110] the error residual relationship to bound the error between the discrete reduced solution p_m^H, computed using basis functions $\{\phi_k\}_{k=1}^m$ constructed by Algorithm 2.3.2, and a reference solution. To define an appropriate reference solution in the HMR context, we initially introduce a partition $\widehat{T} := \mathcal{T}_H \times \tau_h$ of $\widehat{\Omega}$ induced by the subdivisions $\mathcal{T}_H$ of Ω_{1D} and τ_h of $\widehat{\omega}$ defined in §2.1.3 and §2.3.3, respectively. The elements of $\widehat{T}$ are defined as $T_{i,j} := \mathcal{T}_i \times \tau_j$, where $\mathcal{T}_i \in \mathcal{T}_H$ and $\tau_j \in \tau_h$. Following the notation of [19] we assume that X^H and Y^h, defined in §2.1.3 and §2.3.3, coincide with Lagrange FE spaces of k-th and l-th order and can therefore be defined as $X^H := \{w^H \in C^0(\Omega_{1D}) \,:\, w^H|_{\mathcal{T}_i} \in \mathbb{P}^1_k(\mathcal{T}_i), \mathcal{T}_i \in \mathcal{T}_H\}$ and $Y^h := \{w^h \in C^0(\widehat{\omega}) \,:\, w^h|_{\tau_j} \in \mathbb{P}^1_l(\tau_j), \tau_j \in \tau_h\}$, respectively. Here, $\mathbb{P}^1_k(\mathcal{T}_i)$ denotes the set of polynomials of order $\leq k$ over $\mathcal{T}_i$ in one variable. We further suppose that ξ_i^H, $i = 1, ..., N_H$ and υ_j^h, $j = 1, ..., n_h$ are the associated nodal bases.

Proposition 2.3. *The set of functions*

$$\{\varphi_{i,j}(x, \hat{y}) := \xi_i^H(x) \cdot \upsilon_j^h(\hat{y}), \quad i = 1, ..., N_H, j = 1, ..., n_h\} \tag{2.38}$$

forms a nodal basis of the conforming Tensor Product FE space

$$V^{H\times h} := \left\{ v^{H\times h} \in C^0(\widehat{\Omega}) \mid v^{H\times h}|_{T_{i,j}} \in \mathbb{Q}_{k,l}, T_{i,j} \in \widehat{T} \right\} \subset V, \tag{2.39}$$

where $\mathbb{Q}_{k,l}$ is defined as $\mathbb{Q}_{k,l} := \{\sum_j c_j v_j(x) w_j(\hat{y}) \;:\; v_j \in \mathbb{P}^1_k, w_j \in \mathbb{P}^1_l\}$.

Proof. We restrict our considerations to an element $T_{i,j} \in \widehat{T}$, assuming without loss of generality that $T_{i,j} = [0, 1]^2$. It is then sufficient to exploit the fact that for all $q \in \mathbb{Q}_{k,l}(T_{i,j})$ there holds

$$q \equiv \sum_{\substack{0\leq s\leq k \\ 0\leq t\leq l}} q_1\Big(\frac{s}{k}\Big) q_2\Big(\frac{t}{l}\Big) \prod_{\substack{i=0 \\ i\neq s}}^{k} \prod_{\substack{j=0 \\ j\neq t}}^{l} \frac{kx - i}{s - i} \, \frac{l\hat{y} - j}{t - j},$$

where $q_1 \in \mathbb{P}^1_k(\mathcal{T}_i)$, $\mathcal{T}_i \in \mathcal{T}_H$ and $q_2 \in \mathbb{P}^1_l(\tau_j)$, $\tau_j \in \tau_h$. □

We remark that since $Y_m^h \subset Y^h$ there holds $V_m^H \subset V^{H\times h}$. We denote $V^{H\times h}$ the reference FE space. The reference FE approximation of the full problem (2.1) then reads:

$$\text{Find } p^{H\times h} \in V^{H\times h}: \quad a(p^{H\times h}, v^{H\times h}) = f(v^{H\times h}) \quad \forall\, v^{H\times h} \in V^{H\times h}. \tag{2.40}$$

Due to the problem formulations for $p^{H\times h}$ (2.40) and p_m^H (2.12) the model error $e_m := p^{H\times h} - p_m^H$ satisfies

$$a(e_m, v^{H\times h}) = r_m^{H\times h}(v^{H\times h}) \quad \forall v^{H\times h} \in V^{H\times h}. \tag{2.41}$$

Here, the residual $r_m^{H\times h}(v^{H\times h}) \in (V^{H\times h})^*$, where $(V^{H\times h})^*$ denotes the dual space to $V^{H\times h}$, is defined as

$$r_m^{H\times h}(v^{H\times h}) := f(v^{H\times h}) - a(p_m^H, v^{H\times h}) \quad \forall v^{H\times h} \in V^{H\times h}. \tag{2.42}$$

The Riesz representation $\mathcal{R}_m^{H\times h}$ of the residual then satisfies the equation

$$(\mathcal{R}_m^{H\times h}, v^{H\times h})_V = r_m(v^{H\times h}) \quad \forall v^{H\times h} \in V^{H\times h}, \tag{2.43}$$

where the V-inner product has been defined in (2.2).

Proposition 2.4 (A posteriori error bound)**.** *The error estimator Δ_m defined as*

$$\Delta_m := \|\mathcal{R}_m^{H\times h}\|_V / c_0 \tag{2.44}$$

satisfies

$$\|p^{H\times h} - p_m^H\|_V \le \Delta_m \le \frac{c_1}{c_0}\|p^{H\times h} - p_m^H\|_V, \tag{2.45}$$

where the coercivity constant c_0 and the continuity constant c_1 of the bilinear form $a(\cdot,\cdot)$ have been defined in (2.3)*.*

Proof. The proof follows the ideas in [46, 97, 110]. To prove the lower bound in (2.45) we choose $v^{H\times h} = e_m$ in (2.41) and exploit (2.43), the Cauchy-Schwarz inequality, and coercivity to obtain

$$c_0\|e_m\|_V^2 \le a(e_m, e_m) = r_m(e_m) = (\mathcal{R}_m^{H\times h}, e_m)_V \le \|\mathcal{R}_m^{H\times h}\|_V \|e_m\|_V$$

and thus the lower bound in (2.45). To obtain the upper bound in (2.45) we choose $v^{H\times h} = \mathcal{R}_m^{H\times h}$ in (2.41) and exploit (2.43) and continuity to get

$$\|\mathcal{R}_m^{H\times h}\|_V^2 = r_m(\mathcal{R}_m^{H\times h}) = a(e_m, \mathcal{R}_m^{H\times h}) \le c_1\|e_m\|_V \|\mathcal{R}_m^{H\times h}\|_V.$$

Recalling the definition (2.44), this yields the upper bound in (2.45). □

Note that if the bilinear form $a(\cdot,\cdot)$ is symmetric there holds $\mathcal{R}_m^{H\times h} = e_m$ due to the definition of the V-inner product in (2.2). We remark that an error bound for the error between $p_m^{H'}$ and the corresponding reference solution $p^{H'\times h}$ in the V-norm can be analogously derived by replacing $\mathcal{T}_H$ and V_m^H by their coarse counterparts defined in §2.1.3.

2.4.2 A localized residual-type a posteriori error estimator

In this subsection we derive an a posteriori error bound for the error between the discrete reduced solution p_m^H of (2.12) and the exact solution p of the full problem (2.1). We suppose only in this subsection that the transformation $\psi(\cdot; x)$ defined in 2.5 is a C^2-diffeomorphism and that the transformation Ψ is twice differentiable with respect to z. In contrast to the previous subsection we do not suppose that the basis functions $\{\phi_k\}_{k=1}^m$ are generated by Algorithm 2.3.2 but allow all set of functions fulfilling the following assumption.

Assumption 2.5 (Assumptions on the basis functions)**.** *Let τ_h be a subdivision of $\widehat{\omega}$ with elements $\tau_j = (\hat{y}_{j-1}, \hat{y}_j)$ of width $h_j = \hat{y}_j - \hat{y}_{j-1}$, $j = 1, ..., \tilde{n}_h$, and maximal step size $h := \max_{\tau_j} h_j$. We assume that the set of linear independent functions $\{\phi_k\}_{k=1}^m$ is in $C^0(\widehat{\omega})$ and that $\phi_k'|_{\tau_j} \in H(\mathrm{div}; \tau_j) := \{v \in L^2(\tau_j) : \mathrm{div}(v) \in L^2(\tau_j)\}$, $j = 1, ..., \tilde{n}_h$.*

We remark that both, smooth basis functions ($\tilde{n}_h = 1$) like trigonometric or Legendre polynomials, and basis functions generated by Algorithm 2.3.2 fulfill Assumption 2.5. As the residual type error estimator of this subsection is only used for purely diffusive problems and moreover shows a relatively poor performance for advection-diffusion equations, we restrict ourselves in this subsection to the Poisson problem. We thus consider

$$a(w, v) := \int_\Omega k \nabla p_0 \nabla v \, dx \, dy \quad \text{and} \quad f(v) := \int_\Omega sv \, dx \, dy + \int_{\Sigma_N} g_N v \, d\sigma - \int_\Omega k \nabla g_D \nabla v \, dx \, dy, \tag{2.46}$$

where $k \in L^\infty(\Omega)$ with $0 < c_3 \leq k \leq c_4$ for constants $c_3, c_4 \in \mathbb{R}^+$ and $s \in L^2(\Omega)$. Furthermore, Σ_N denotes the Neumann boundary and $g_N \in L^2(\Sigma_N)$. $g_D \in H^1(\Omega)$ shall be the Dirichlet expansion of the Dirichlet boundary conditions. The solution p of the full problem is then defined as $p := p_0 + g_D$.

Proposition 2.6. *Let V^* denote the dual space of V. Defining the residual $r_m \in V^*$ as*

$$r_m(v) := f(v) - a(p_m^H, v) \quad \forall v \in V \tag{2.47}$$

we have

$$\|p - p_m^H\|_V \leq \frac{1}{\sqrt{c_3}} \sup_{\substack{w \in V \\ w \neq 0}} \frac{|r_m(w)|}{\|\nabla w\|_{L^2(\Omega)}}. \tag{2.48}$$

Proof. The error $e := p - p_m^H$ satisfies

$$a(e, v) = r_m(v) \quad \forall v \in V. \tag{2.49}$$

Coercivity of $a(\cdot, \cdot)$ — defined in (2.46) — with respect to the H^1-half norm and the V-norm and (2.49) then yields

$$\sup_{\substack{w \in V \\ w \neq 0}} \frac{|\, r_m(w) \,|}{\|\nabla w\|_{L^2(\Omega)}} \geq \frac{r_m(e)}{\|\nabla e\|_{L^2(\Omega)}} = \|e\|_V \frac{\|e\|_V}{\|\nabla e\|_{L^2(\Omega)}} \geq \sqrt{c_3} \|e\|_V.$$

□

An alternative proof of Proposition 2.6 using duality techniques is given in the Appendix A.2. Here, a slightly different constant in the estimate is obtained. To get a computable estimator, we further estimate the right hand side of (2.48). For this purpose we introduce a partition $\widehat{T} := \mathcal{T}_H \times \tau_h$ of $\widehat{\Omega}$ induced by the subdivisions $\mathcal{T}_H$ of Ω_{1D} and τ_h of $\widehat{\omega}$ defined in §2.1.3 and Assumption 2.5, respectively. As in the last subsection the elements of $\widehat{T}$ are defined as $T_{i,j} := \mathcal{T}_i \times \tau_j$, where $\mathcal{T}_i \in \mathcal{T}_H$ and $\tau_j \in \tau_h$. Using the FE expansion of the coefficients $\bar{p}_l^H$, $l = 1, ..., m$, (cf. §2.1.3) and Assumption 2.5 yields $\nabla p_m^H(\Psi^{-1}(\hat{x}, \hat{y}))|_{T_{i,j}} \in H(\mathrm{div}; T_{i,j})$ for all $T_{i,j} \in \widehat{T}$. This allows us to integrate by parts on the rectangles $T_{i,j} \in \widehat{T}$ in (2.48) and to deduce a computable, local error estimator. As we lack an interpolation estimate for the term $\|\nabla w - \nabla w_m^H\|_{L^2(\Psi^{-1}(T))}$, we expect that the residual-type error estimator we would get, neither has the right order in H nor in m. Therefore, we propose to reconstruct the discrete reduced solution p_m^H locally by polynomials of one order higher than the ones used in the computation of p_m^H with FE. By this means, we improve

the order of the estimator in H. This approach is inspired by the work of Akrivis, Makridakis and Nochetto [3], in which the numerical solution of a parabolic equation, being continuous and piecewise linear in time, is locally reconstructed by a continuous and piecewise quadratic polynomial in time. For this reconstruction they derive optimal order a posteriori error estimates. We define a spatial local reconstruction operator as follows.

Definition 2.7 (Local reconstruction operator)**.** *We define* $S_H^k := \{s_H \in C^0(\Omega_{1D}) : s_{H|\mathcal{T}_i} \in \mathbb{P}_k^1(\mathcal{T}_i), \mathcal{T}_i \in \mathcal{T}_H\}$ *and* $W_h^l := \{w_h \in C^0(\widehat{\omega}) : w_{h|\tau_j} \in \mathbb{P}_l^1(\tau_j), \tau_j \in \tau_h\}$*, where* $\mathbb{P}_k^1$ *is the space of polynomials of order* $\leq k$ *in one variable. Then we introduce the local reconstruction operators*

(i) $\mathfrak{R}_x : S_H^k \to S_H^{k+1}$ *with* $\mathfrak{R}_x(u) \in X$ *for* $u \in X^H$*,*

(ii) $\mathfrak{R}_y : W_h^l \to W_h^{l+1}$ *with* $\mathfrak{R}_y(q) \in Y$ *for* $q \in Y^h$*,*

where X^H *and* Y^h *have been defined in §2.1.3 and §2.3.3, respectively.*

We define a reconstructed discrete reduced solution $p_{m,rec}^H$ as

$$\begin{aligned} p_{m,rec}^H(x,\psi^{-1}(\hat{y};x)) &= \sum_{l=1}^{m} \bar{p}_{l,rec}^H(x)\cdot\phi_{l,rec}(\hat{y}) + g_D(x,\psi^{-1}(\hat{y};x)), \\ \text{where } \phi_{l,rec} &:= \begin{cases} \mathfrak{R}_y(\phi_l) & \text{if } \phi_l \in Y^h, \\ \phi_l & \text{if } \phi_l \text{ is a smooth function} \end{cases} \quad \text{and } \bar{p}_{l,rec}^H := \mathfrak{R}_x(\bar{p}_l^H). \end{aligned} \tag{2.50}$$

Let S be an edge of an element $T_{i,j}$ and $w \in L^2(\widehat{\Omega})$ with $w|_{T_{i,j}} \in C^0(T_{i,j})$ for all $T_{i,j} \in \widehat{T}$. Then we define the jump of w across S in the direction of the outer normal ν as $[w] := \lim_{t\to 0+} w((x,\hat{y}) + t\nu) - \lim_{t\to 0+} w((x,\hat{y}) - t\nu)\ \forall (x,\hat{y}) \in T_{i,j}$. The localized error estimator then reads as follows.

Theorem 2.8 (A localized residual-type a posteriori error estimator)**.** *Let* $\Psi : \Omega \to \widehat{\Omega}$ *be the mapping of* Ω *onto* $\widehat{\Omega}$*,* $\widehat{T} = \mathcal{T}_H \times \tau_h$ *the induced partition on* $\widehat{\Omega}$ *and let* Ψ *and* Ω *fulfill the assumptions in §2.1. Let* $\{\bar{p}_{j,rec}^H\}_{j=1}^m$ *denote the set of reconstructed discrete coefficient functions,* $\{\phi_{j,rec}\}_{j=1}^m$ *the set of reconstructed basis functions and* $p_{m,rec}^H$ *the reconstructed discrete reduced solution. Furthermore, the basis functions* $\{\phi_l\}_{l=1}^m$ *shall fulfill Assumption 2.5. We then have*

$$\|p - p_m^H\|_V \leq C(\Omega)\,\Delta_m^{rec} + \sqrt{c_4}\|p_{m,rec}^H - p_m^H\|_V, \quad \textit{with} \quad \Delta_m^{rec} := \left(\sum_{T_{i,j}\in\widehat{T}} \Delta_{m,T_{i,j}}^{rec}\right)^{1/2} \tag{2.51}$$

and

$$\begin{aligned} \Delta_{m,T_{i,j}}^{rec} := \Big\| \big|\mathcal{D}_2^{-1}(x,\psi^{-1}(\hat{y};x))\big|^{-\frac{1}{2}} \Big(&\operatorname{div}\left[k(x,\psi^{-1}(\hat{y};x)) d_m^H(x,\hat{y})\,\big|\mathcal{D}_2^{-1}(x,\psi^{-1}(\hat{y};x))\big|\right]\Big) \\ &+ s(x,\psi^{-1}(\hat{y};x))\,\big|\mathcal{D}_2^{-1}(x,\psi^{-1}(\hat{y};x))\big|^{\frac{1}{2}} \Big\|_{L^2(T_{i,j})}^2 \\ + \frac{1}{2}\sum_{S\subset\partial T_{i,j}\setminus\partial\widehat{\Omega}} &\Big\| \big[\, k(x,\psi^{-1}(\hat{y};x))\, d_m^H(x,\hat{y})\cdot\nu\big]\cdot\big|\mathcal{D}_2^{-1}(x,\psi^{-1}(\hat{y};x))\big|^{\frac{1}{2}}\Big\|_{L^2(S)}^2 \\ + \sum_{S\subset\partial T_{i,j}\cap\Psi(\Sigma_N)} &\Big\| \big(\, g_N(x,\psi^{-1}(\hat{y};x)) - k(x,\psi^{-1}(\hat{y};x))\, d_m^H(x,\hat{y})\cdot\nu\big)\cdot\big|\mathcal{D}_2^{-1}(x,\psi^{-1}(\hat{y};x))\big|^{\frac{1}{2}}\Big\|_{L^2(S)}^2, \end{aligned}$$

where

$$d_m^H(x,\hat{y}) := \left[\left(\sum_{j=1}^{m}\bar{p}^H_{j,rec}(x)\phi'_{j,rec}(\hat{y})\right) + \frac{dg_D(x,\psi^{-1}(\hat{y};x))}{d\hat{y}}\right]\begin{pmatrix}\mathcal{D}_1(x,\psi^{-1}(\hat{y};x))\\ \mathcal{D}_1^2(x,\psi^{-1}(\hat{y};x)) + \mathcal{D}_2^2(x,\psi^{-1}(\hat{y};x))\end{pmatrix}$$
$$+\left[\left(\sum_{j=1}^{m}\phi_{j,rec}(\hat{y})\frac{d\bar{p}^H_{j,rec}(x)}{dx}\right) + \frac{dg_D(x,\psi^{-1}(\hat{y};x))}{dx}\right]\begin{pmatrix}1\\ \mathcal{D}_1(x,\psi^{-1}(\hat{y};x))\end{pmatrix}$$

and $C(\Omega) := \max\{(3c_p/\sqrt{c_3}), (3c_t(c_p+1)/\sqrt{c_3})\}$ *and* c_t *and* c_p *denote the constants in the trace theorem and the Poincaré inequality, respectively.*

For the sake of clarity we do not prove Theorem 2.8 but the following Corollary 2.9, which is the analogue of Theorem 2.8 for a rectangular domain Ω. The ideas for the proofs of Theorem 2.8 and Corollary 2.9 are the same and the proofs only differ in the more complicated computations due to the transformation Ψ in the case of a non-rectangular domain.

Corollary 2.9 (A localized residual-type a posteriori error estimator for rectangular domains)**.** *Let* Ω *be a rectangle,* $\widehat{T} = \mathcal{T}_H \times \tau_h$ *and* $p^H_{m,rec}$ *the reconstructed discrete reduced solution. Furthermore, the basis functions* $\{\phi_l\}_{l=1}^m$ *shall satisfy Assumption 2.5. Then there holds*

$$\|p - p_m^H\|_V \leq C(\Omega)\,\Delta_m^{rec} + \sqrt{c_4}\|p^H_{m,rec} - p^H_m\|_V \quad \textit{with} \quad \Delta_m^{rec} = \left(\sum_{T_{i,j}\in\widehat{T}} \Delta^{rec}_{m,T_{i,j}}\right)^{1/2} \tag{2.52}$$

and

$$\begin{aligned}\Delta^{rec}_{m,T_{i,j}} &= \|s + \operatorname{div}\left(k\nabla\, p^H_{m,rec}\right)\|^2_{L^2(T_{i,j})} + \tfrac{1}{2}\sum_{S\subset\partial T_{i,j}\setminus\partial\Omega}\|[k\nabla\, p^H_{m,rec}\cdot\nu]\|^2_{L^2(S)}\\ &\quad + \sum_{S\subset\partial T_{i,j}\cap\Sigma_N}\|g_N - k\nabla\, p^H_{m,rec}\cdot\nu\|^2_{L^2(S)}.\end{aligned}$$

Proof. Proposition 2.6 and continuity of $a(\cdot,\cdot)$ yields

$$\|p - p_m^H\|_V \leq \frac{1}{\sqrt{c_3}}\sup_{\substack{w\in V\\ w\neq 0}}\frac{\left|\int_\Omega sw - k\nabla p^H_{m,rec}\nabla w\,dx\,dy + \int_{\Sigma_N} g_N w\,d\sigma\right|}{\|\nabla w\|_{L^2(\Omega)}} + \sqrt{c_4}\|p^H_{m,rec} - p^H_m\|_V. \tag{2.53}$$

We exploit $p^H_{m,rec} \in H^1(T_{i,j}; div)$ for $T_{i,j} \in \widehat{T}$, the trace theorem, the Cauchy-Schwarz inequality and the Poincaré inequality to further estimate the first term on the right side of (2.53).

$$\begin{aligned}\left|\int_\Omega sw - k\nabla p^H_{m,rec}\nabla w + \int_{\Sigma_N} g_N w\right| &= \left|\sum_{T_{i,j}\in\widehat{T}}\int_{T_{i,j}} sw - k\nabla p^H_{m,rec}\nabla w + \int_{\Sigma_N\cap T_{i,j}} g_N w\right|\\ &= \left|\sum_{T_{i,j}\in\widehat{T}}\int_{T_{i,j}} sw + \operatorname{div}(k\nabla p^H_{m,rec})w - \sum_{S\subset\partial T_{i,j}\setminus\partial\Omega}\int_S k\nabla p^H_{m,rec}\cdot\nu w\right.\\ &\quad \left. + \sum_{S\subset\partial T_{i,j}\cap\Sigma_N}\int_S \left(g_N w - k\nabla p^H_{m,rec}\cdot\nu w\right)\right|\end{aligned}$$

$$
\begin{aligned}
&\leq \sum_{T_{i,j}\in\widehat{T}} \Bigg(\| s + \operatorname{div}\left(k\nabla p^H_{m,rec}\right) \|_{L^2(T_{i,j})} \|w\|_{L^2(T_{i,j})} + \frac{1}{2} \sum_{S\subset\partial T_{i,j}\setminus\partial\Omega} \int_S \|[k\nabla p^H_{m,rec}\cdot\nu]\|_{L^2(S)} \|w\|_{L^2(S)} \\
&\qquad + \sum_{S\subset\partial T_{i,j}\cap\Sigma_N} \int_S \|g_N - k\nabla p^H_{m,rec}\cdot\nu\|_{L^2(S)} \|w\|_{L^2(S)} \Bigg) \\
&\leq \sum_{T_{i,j}\in\widehat{T}} \Bigg(\| s + \operatorname{div}\left(k\nabla p^H_{m,rec}\right) \|_{L^2(T_{i,j})} \|w\|_{L^2(T_{i,j})} \\
&\qquad + \frac{c_t}{2} \sum_{S\subset\partial T_{i,j}\setminus\partial\Omega} \int_S \|[k\nabla p^H_{m,rec}\cdot\nu]\|_{L^2(S)} \|w\|_{H^1(T_{i,j})} \\
&\qquad + c_t \sum_{S\subset\partial T_{i,j}\cap\Sigma_N} \int_S \|g_N - k\nabla p^H_{m,rec}\cdot\nu\|_{L^2(S)} \|w\|_{H^1(T_{i,j})} \Bigg) \\
&\leq \left(\sum_{T_{i,j}\in\widehat{T}} \| s + \operatorname{div}\left(k\nabla p^H_{m,rec}\right) \|^2_{L^2(T_{i,j})} \right)^{\frac{1}{2}} \|w\|_{L^2(\Omega)} \\
&\qquad + \frac{c_t}{2} \left(\sum_{T_{i,j}\in\widehat{T}} \sum_{S\subset\partial T_{i,j}\setminus\partial\Omega} \int_S \|[k\nabla p^H_{m,rec}\cdot\nu]\|^2_{L^2(S)} \right)^{\frac{1}{2}} \|w\|_{H^1(\Omega)} \\
&\qquad + c_t \left(\sum_{T_{i,j}\in\widehat{T}} \sum_{S\subset\partial T_{i,j}\cap\Sigma_N} \int_S \|g_N - k\nabla p^H_{m,rec}\cdot\nu\|^2_{L^2(S)} \right)^{\frac{1}{2}} \|w\|_{H^1(\Omega)} \\
&\leq c_p \left(\sum_{T_{i,j}\in\widehat{T}} \| s + \operatorname{div}\left(k\nabla p^H_{m,rec}\right) \|^2_{L^2(T_{i,j})} \right)^{\frac{1}{2}} \|\nabla w\|_{L^2(\Omega)} \\
&\qquad + \frac{c_t(c_p+1)}{2} \left(\sum_{T_{i,j}\in\widehat{T}} \sum_{S\subset\partial T_{i,j}\setminus\partial\Omega} \int_S \|[k\nabla p^H_{m,rec}\cdot\nu]\|^2_{L^2(S)} \right)^{\frac{1}{2}} \|\nabla w\|_{L^2(\Omega)} \\
&\qquad + c_t(c_p+1) \cdot \left(\sum_{T_{i,j}\in\widehat{T}} \sum_{S\subset\partial T_{i,j}\cap\Sigma_N} \int_S \|g_N - k\nabla p^H_{m,rec}\cdot\nu\|^2_{L^2(S)} \right)^{\frac{1}{2}} \|\nabla w\|_{L^2(\Omega)}.
\end{aligned}
$$

□

Finally, we present an example for the reconstruction operator $\mathfrak{R}_y : W^1_h \to W^2_h$ introduced in Definition 2.7. The same technique can be used for $\mathfrak{R}_x : S^1_H \to S^2_H$. Let $\phi_l(\hat{y})$ be computed using linear FE. To reconstruct $\phi_l(\hat{y})$ on the interval $\tau_j = (\hat{y}_{j-1}, \hat{y}_j)$, we also take into account the values $\phi_l(\hat{y}_{j-2})$ and $\phi_l(\hat{y}_{j+1})$ of the two adjacent nodes on the left and right side of the interval. Then one possible and cheap reconstruction is to keep the linear function on the interval τ_j and add a quadratic correction of the form $a_2\cdot(\hat{y}-\hat{y}_s)^2 - a_2\cdot(h_j^2/4)$, where $\hat{y}_s$ denotes the barycenter of τ_j. The coefficient a_2 is computed by a least square approach, demanding that the quadratic polynomial also interpolates the values $\phi_l(\hat{y}_{j-2})$ and $\phi_l(\hat{y}_{j+1})$. If we use this reconstruction technique, there holds $\phi_{l,rec} \in Y$ and respectively $\overline{p}^H_{l,rec} \in X$.

2.5 Analysis of the computational costs of the HMR-RB approach

In this section we compare the total computational costs for the computation of the discrete reduced solution p_m^H using the HMR-RB approach with the costs for the computation of the associated reference solution $p^{H\times h}$ of (2.40). As all numerical experiments have been conducted using linear FE in both directions, we restrict ourself in this section also for the sake of clarity to the case $X^H = \left\{v^H \in C^0(\Omega_{1D}) : v^H|_{\mathcal{T}_i} \in \mathbb{P}_1^1(\mathcal{T}_i), \mathcal{T}_i \in \mathcal{T}_H\right\}, Y^h = \left\{v^h \in C^0(\widehat{\omega}) : v^h|_{\tau_j} \in \mathbb{P}_1^1(\tau_j), \tau_j \in \tau_h\right\}$, and $V^{H\times h} = \{v^{H\times h} \in C^0(\widehat{\Omega}) : v^{H\times h}|_{T_{i,j}} \in \mathbb{Q}_{1,1}, T_{i,j} \in \hat{T}\}$. Analogous to the RB framework [97,110] the computation of the reduced solution p_m^H can be decomposed in an n_h-dependent offline stage where we construct the reduction space Y_m^h and a subsequent n_h-independent online stage where the coupled system (2.12) is solved. The total computational costs for computing p_m^H consist of both offline- and online costs and can be derived as follows.

(i) *Offline stage: Construction of Y_m^h by Algorithm 2.3.2 (*Adaptive-HMR-POD*):* First, we assemble the matrices and right hand sides of the linear systems of equations for the computation of the snapshots $\mathcal{P}^h(\mu)$ (2.32) and the reduced solutions $p_m^{H'}$ in $\mathcal{O}(n_h)$ and $\mathcal{O}(N_{H'})$ operations, respectively. Re-utilizing these matrices we can assemble the V-inner product for the computation of the Riesz representative based error estimator Δ_m (2.44) in $\mathcal{O}(n_h N_{H'})$ operations. When using the localized error estimator Δ_m^{rec} (2.51) we precompute the integrals on the elements $T_{i,j} \in \widehat{T}$ in $\mathcal{O}(n_h N_{H'})$ operations. In Algorithm 2.3.2 Adaptive-HMR-POD we compute the set of snapshots $\mathcal{P}^h(\mu)$, $\mu \in \Xi_{train}$, in $\mathcal{O}(n_{train} n_h)$ operations by a Thomas algorithm [107]. The associated reduced solutions $p_m^{H'}$ are computed in $\mathcal{O}(n_{train} N_{H'})$ operations by a preconditioned conjugate gradient (pcg) or preconditioned stabilized bi-conjugate gradient (bi-cgstab) method, which scaled linearly in the offline stage for the considered test cases in §2.6. We then either compute the error estimators Δ_m or Δ_m^{rec} in $\mathcal{O}(n_{train} n_h N_{N'})$ operations using a pcg method for the computation of the former. The costs for the PODs in Algorithm 2.3.1 are dominated by the costs for the POD after the refinement of the parameter space which requires $\mathcal{O}(n_{train}^2 n_h)$ operations for the formation of the correlation matrix and $\mathcal{O}(n_{train}^3)$ operations for the solution of the eigenvalue problem. Finally, we compute the integrals in y-direction in (2.12) depending on the basis functions $\{\phi_l\}_{l=1}^m$ in $\mathcal{O}(m^2 n_h)$ operations.

(ii) *Online stage: Solution of the coupled system* (2.12)*:* We assemble the coupled system (2.12) in $\mathcal{O}(m^2 N_H)$ operations. The solution of the resulting linear system of equations (2.12) with a pcg (§2.6, test case 2) or bi-cgstab method (§2.6, test case 3) required $\mathcal{O}(N_H m^2)$ and $\mathcal{O}(N_H^{1.4} m^2)$ operations, respectively.

Analyzing these results, we detect a threshold in the offline costs due to the mesh size independent factor n_{train}. If $N_{H'}$ is chosen independently of N_H, the offline costs, dominated by the computational costs for the error estimator, amount to $\mathcal{O}(n_{train} n_h)$ operations. As the offline costs in turn dominate the online costs, we thus expect a linear scaling of the HMR-RB approach in $\max\{n_h, N_H\}$, if $N_{H'}$ is chosen constant. The numerical experiments in the next section §2.6 show that the latter is sensible.
For the computation of the reference solution $p^{H\times h}$ we assemble the linear system of equations in $\mathcal{O}(N_H n_h)$ operations. Its solution with a pcg (§2.6, test case 2) or bi-cgstab method (§2.6, test case 3) required $\mathcal{O}(N_H^{2.5})$ and $\mathcal{O}(N_H^3)$ operations, respectively. We conclude that if n_{train} is sufficiently small compared to the mesh sizes N_H and n_h, we expect that starting from a certain mesh size the HMR-RB approach - including offline and online parts - outperforms the bilinear FEM. Although

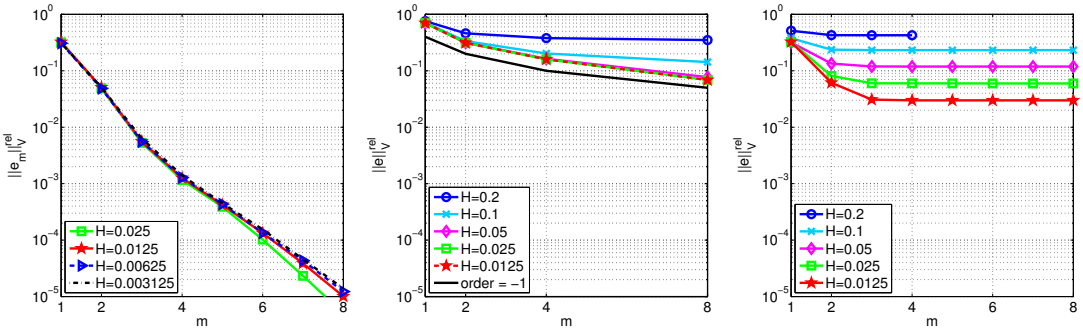

(a) $\|e_m\|_V^{rel}$ of HMR-RB (b) $\|e\|_V^{rel}$ of HMR [101] (c) $\|e\|_V^{rel}$ of HMR-RB

Figure 2.2: Test case 1: The relative model error $\|e_m\|_V^{rel}$ of the HMR-RB ansatz for increasing m and different H (a). Comparison of the relative total error $\|e\|_V^{rel}$ of the HMR approach [101] (b) and the HMR-RB approach (c) for increasing model order m and different mesh sizes H.

the sample size has to increase for more complex problems, we anticipate that in these situations also the grid resolution and hence N_H has to increase due to the higher complexities, and the HMR-RB approach still outperforms the bilinear FEM. The comparison of the total computational costs of the HMR-RB approach and bilinear FEM in test case 2 and 3 of §2.6 supports these two claims. Finally, we discuss the memory aspect. For the bilinear FEM in particular a sparse matrix with $9n_hN_H$ non-zero elements has to be stored. For the HMR-RB approach, most storage is needed for the full $n_{train} \times n_h$-matrix containing the snapshots, and for the sparse matrix of the coupled system with $3m^2N_H$ non-zero elements. Therefore, in general, less memory is needed for the HMR-RB approach than for the bilinear FEM.

2.6 Numerical experiments

In this section we present several numerical test cases to demonstrate the approximation properties and computational efficiency of the proposed method. First, we study the convergence rate of the HMR-RB approach on a numerical example with an analytical solution, where we observe an exponential order of convergence in the model order m. We compare these rates with the results of the HMR approach with sine functions presented in [102]. The solution of the second test case exhibits little spatial regularity both in the dominant and transverse direction as the source term is only in $H^1(\Omega) \cap C^0(\Omega)$ and not more. Nevertheless, we observe an exponential convergence rate in the model order m. In the third test case we consider an advection-diffusion equation in a long symmetric channel with sinusoidal wavy walls. Due to a strong advective field the solution exhibits a main stream and dominant spatial features along the x-direction. Finally, we test the proposed method on a Poisson problem whose source term cannot be expressed as a sum of tensor products. Again, we compare the outcome with the results obtained by the HMR approach with sine functions [48, 102]. All test cases are computed using linear FE in x- and y-direction, i.e. $X^H = \left\{v^H \in C^0(\Omega_{1D}) : v^H|_{\mathcal{T}_i} \in \mathbb{P}_1^1(\mathcal{T}_i), \mathcal{T}_i \in \mathcal{T}_H\right\}, Y^h = \left\{v^h \in C^0(\widehat{\omega}) : v^h|_{\tau_j} \in \mathbb{P}_1^1(\tau_j), \tau_j \in \tau_h\right\}$, and $V^{H\times h} = \{v^{H\times h} \in C^0(\widehat{\Omega}) : v^{H\times h}|_{T_{i,j}} \in \mathbb{Q}_{1,1}, T_{i,j} \in \hat{T}\}$. The relative model error in the V- or L^2-norm is defined as $\|e_m\|_V^{rel} := \|e_m\|_V / \|p^{H\times h}\|_V$, or $\|e_m\|_{L^2(\Omega)}^{rel} := \|e_m\|_{L^2(\Omega)} / \|p^{H\times h}\|_{L^2(\Omega)}$, respectively, for $e_m = p^{H\times h} - p_m^H$. To take into account the discretization error, we compare the discrete reduced solution p_m^H either with the exact solution p of (2.1) (test case 1) or with a

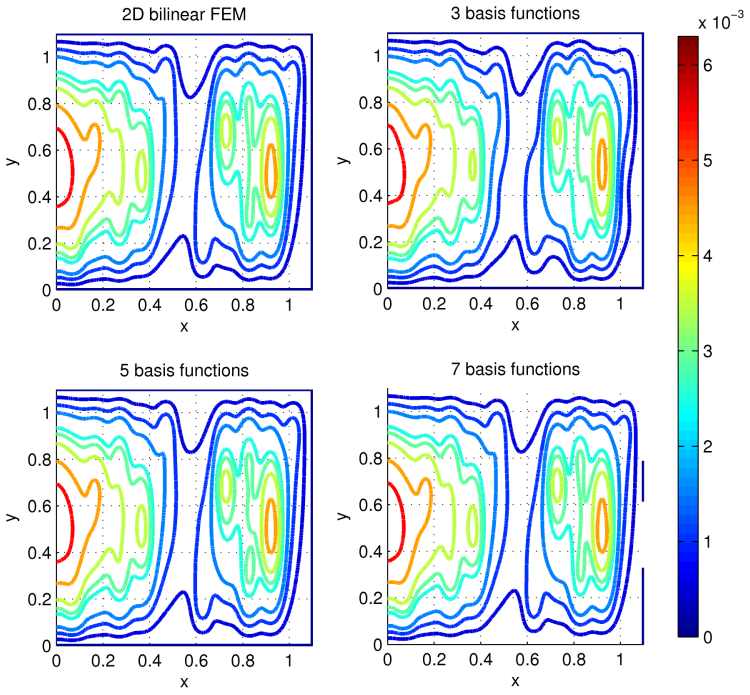

Figure 2.3: Test case 2: In comparison from left to right and top to bottom: the reference 2D bilinear FE solution $p^{H\times h}$ and the discrete reduced solution p_m^H using 3, 5 and 7 basis functions; $N_H = n_h = 800$, $N_{H'} = 80$.

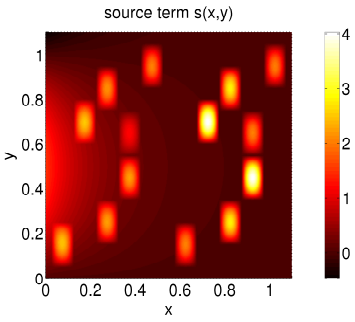

Figure 2.4: Test case 2: Source term $s(x, y)$ defined in (A.25) in §A.3

very finely resolved bilinear finite element solution p_{fine} (test cases 2, 3 and 4). We denote the relative total error in the V-norm $\|e\|_V^{rel} := \|p - p_m^H\|_V / \|p\|_V$ and $\|e\|_V^{rel} := \|p_{fine} - p_m^H\|_V / \|p_{fine}\|_V$, respectively. e can be decomposed into the model error e_m and the discretization error e^H. We also define relative error estimators $\Delta_m^{rel} := \Delta_m / \|p^{H\times h}\|_V$ and $\Delta_{m,rec}^{rel} := ((3/\sqrt{c_3})\Delta_m^{rec} + \sqrt{c_4}\|p_{m,rec}^H - p_m^H\|_V)/\|p_{fine}\|_V$. To discuss the decay behavior of the coefficient functions we introduce $\bar{e}_m^{L^2} := (\sum_{j=m+1}^M \|\bar{p}_j^H\|^2_{L^2(\Omega_{1D})})^{1/2}$ and $\bar{e}_m^{H^1} := (\sum_{j=m+1}^M \|\partial_x \bar{p}_j^H\|^2_{L^2(\Omega_{1D})})^{1/2}$, where M is the dimension of Y_M^h. We will see below that we usually have $M \ll n_{train}$. The implementation of our algorithm has been done in MATLAB. For the computation of the integrals we have used a composite trapezoidal rule. As the result of Algorithm 2.3.2 Adaptive-HMR-POD depends on a random choice of parameters, we performed several runs and determined averages for our error plots. For the first, second and third test case we performed 200 runs, and for the last test case we did 50 runs. For the generation and refinement of Ξ_{train} we have used the same sequence of randomly generated numbers drawn from the standard uniform distribution for each block of 200/200/200/50 runs. Furthermore, we have used equidistant grids in x- and y-direction for the computations of all four test cases and for the reconstruction we have applied the technique introduced at the end of §2.4.2. Unless otherwise stated the Riesz representative based error estimator has been used in Algorithm 2.3.2. All computations were done on a computer with an Intel Core i7 (4 cores) with 2.8 GHz.

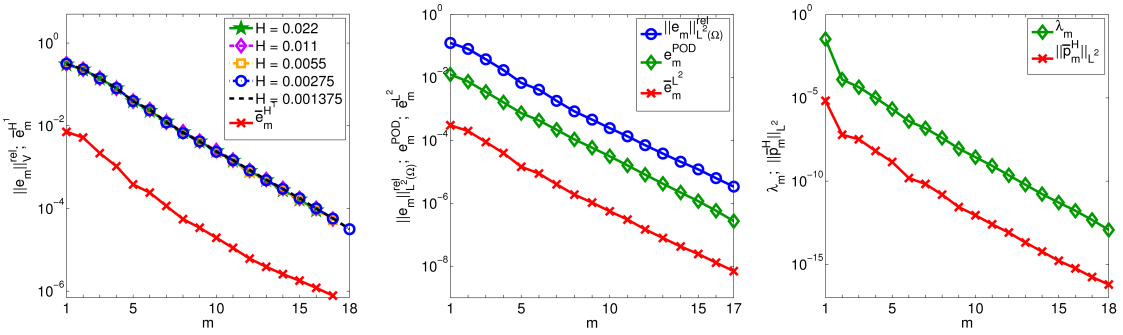

(a) $\|e_m\|_V^{rel}$ and $\bar{e}_m^{H^1}$ (b) $\|e_m\|_{L^2(\Omega)}^{rel}, e_m^{\mathrm{POD}}$ and $\bar{e}_m^{L^2}$ (c) λ_m and $\|\bar{p}_m^H\|_{L^2(\Omega_{1D})}$

Figure 2.5: Test case 2: Illustration of the model error convergence (a) $\|e_m\|_V^{rel}$ for different H and $\bar{e}_m^{H^1}$ for $H = 0.001375$, (b) $\|e_m\|_{L^2(\Omega)}^{rel}, e_m^{\mathrm{POD}}$ and $\bar{e}_m^{L^2}$ for $H = 0.001375$, and (c) λ_m and $\|\bar{p}_m^H\|_{L^2(\Omega_{1D})}$ for $H = 0.001375$.

Test case 1

First, we consider a numerical example with an analytical solution. We choose test case 2 of [102] in order to compare the convergence behavior of our new HMR-RB approach with the one of the HMR framework introduced in [48,102]. We solve a Poisson problem on $\Omega = (0,2) \times (0,1)$. The analytical solution is chosen to be $p(x,y) = y^2(1-y)^2(0.75-y)x(2-x)\exp(\sin(2\pi x))$. The error values of the HMR ansatz are taken from [101] and have been divided by $\|p\|_V$ to obtain relative errors. We use the same mesh sizes H in x-direction as in [101] and choose $h = H$. If we analyze the behavior of the model error $\|e_m\|_V^{rel}$ of the HMR-RB approach (Fig. 2.2a), we see that $\|e_m\|_V^{rel}$ converges exponentially fast in m. In contrast, the usage of sine functions in the orthonormal expansion of the HMR approach excludes a priori exponential convergence rates also for smooth functions like C^∞-functions [25]. The expected convergence rate of the model error for the present example is m^{-1} [26]. This rate can be detected for a sufficiently small H (here $H \leq 0.025$) in Fig. 2.2b, where the total error $\|e\|_V^{rel}$ of the HMR ansatz is depicted, as for $H \leq 0.025$ the model error dominates the discretization error. Hence, the slope of $\|e\|_V^{rel}$ most closely approximates the one of $\|e_m\|_V^{rel}$ for $H = 0.0125$. Regarding the convergence behavior of the total error $\|e\|_V^{rel}$ of the HMR-RB approach (Fig. 2.2c), we see that for $m \geq 3$ or even $m \geq 2$ the discretization error dominates the model error. For the HMR ansatz and $H \leq 0.05$ this is not even the case for a model order $m = 16$.

Test case 2

This test case has been chosen in order to demonstrate that it is possible that the HMR-RB approach approximates a full solution exponentially fast, which exhibits both little spatial and parametric regularity. In detail, we choose $\Omega = (0, 1.1) \times (0, 1.1)$ and a diffusion tensor

$$K = \begin{pmatrix} 0.25 & 0 \\ 0 & 25 \end{pmatrix}. \tag{2.54}$$

The source term s is depicted in Fig. 2.4 and defined in (A.25) in the appendix. We emphasize that $s \in H^1(\Omega) \cap C^0(\Omega)$ but $s \notin H^2(\Omega)$. On Γ_0 — defined in (2.4) — we prescribe homogeneous Neumann boundary conditions and on the remaining part of $\partial\Omega$ homogeneous Dirichlet boundary conditions. The reference solution $p^{H\times h}$ for $N_H = n_h = 800$ is displayed in the first picture of Fig. 2.3 and shows a stronger variation in x-direction. We have done a convergence study to ensure that $p^{H\times h}$ contains all essential features of the exact solution. We compare $p^{H\times h}$ with the discrete

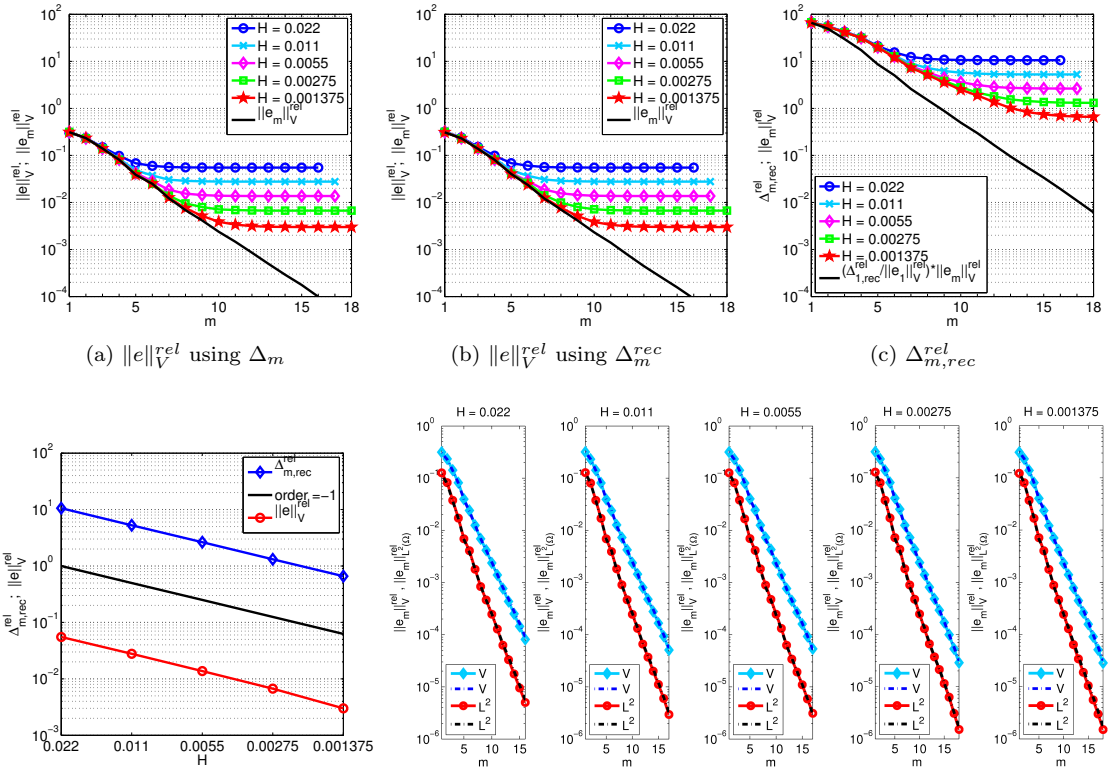

(a) $\|e\|_V^{rel}$ using Δ_m (b) $\|e\|_V^{rel}$ using Δ_m^{rec} (c) $\Delta_{m,rec}^{rel}$

(d) $\|e\|_V^{rel}$, $\Delta_{m,rec}^{rel}$ (e) $\|e_m\|_V^{rel}(V)$, $\|e_m\|_{L^2(\Omega)}^{rel}(L^2)$ for Δ_m (solid) and Δ_m^{rec} (dash-dotted)

Figure 2.6: Test case 2: $\|e\|_V^{rel}$ for increasing m and different mesh sizes H and $\|e_m\|_V^{rel}$ for $H = 0.001375$ using Δ_m (a) and Δ_m^{rec} (b); $\Delta_{m,rec}^{rel}$ for increasing m and $\|e_m\|_V^{rel}$ for $H = 0.001375$ (c); $\|e\|_V^{rel}$ and $\Delta_{m,rec}^{rel}$ for decreasing H (d); Comparison of $\|e_m\|_V^{rel}$ and $\|e_m\|_{L^2(\Omega)}^{rel}$ for using Δ_m (solid) and Δ_m^{rec} (dash-dotted) (e).

reduced solution p_m^H for $m = 3, 5, 7$, $N_H = n_h = 800$ and $N_{H'} = 80$ (Fig. 2.3), where $N_{H'}$ has been defined in §2.1.3. We see a very good visual agreement of $p^{H\times h}$ and p_7^H. Furthermore, already p_5^H contains all essential features of the reference solution.

In order to quantify the approximation properties of the HMR-RB approach, we study the convergence behavior of the model error, the coefficient functions and the POD error for increasing model order m. In Fig. 2.5a, $\|e_m\|_V^{rel}$ is depicted for various values of H in a semi-logarithmic scale and compared with $\bar{e}_m^{H^1}$ for $H = 0.001375$. It can be seen that $\|e_m\|_V^{rel}$ converges exponentially fast in m. We remark that by exploiting the fact that $V^{H\times h}$ is a finite dimensional space it is always possible to derive an exponential rate, which, however, depends on the mesh size of the discretization (cf. [24] for the proof of this statement for the Proper General Decomposition approach). As the convergence rate of $\|e_m\|_V^{rel}$ in Fig. 2.5a does not change for decreasing mesh size, and stays the same even for very fine meshes, we argue that this exponential convergence rate does not result from the fact that $V^{H\times h}$ is of finite dimension. Moreover, we see that the convergence rates of $\|e_m\|_V^{rel}$ and $\bar{e}_m^{H^1}$ agree very well. In Fig. 2.5b we compare $\|e_m\|_{L^2(\Omega)}^{rel}, e_m^{\mathrm{POD}}$ (2.37) and $\bar{e}_m^{L^2}$ for $H = 0.001375$, again in a semi-logarithmic scale. All three quantities exhibit the same exponential convergence rate. Finally, also the convergence behavior of the eigenvalues of the POD λ_m and of

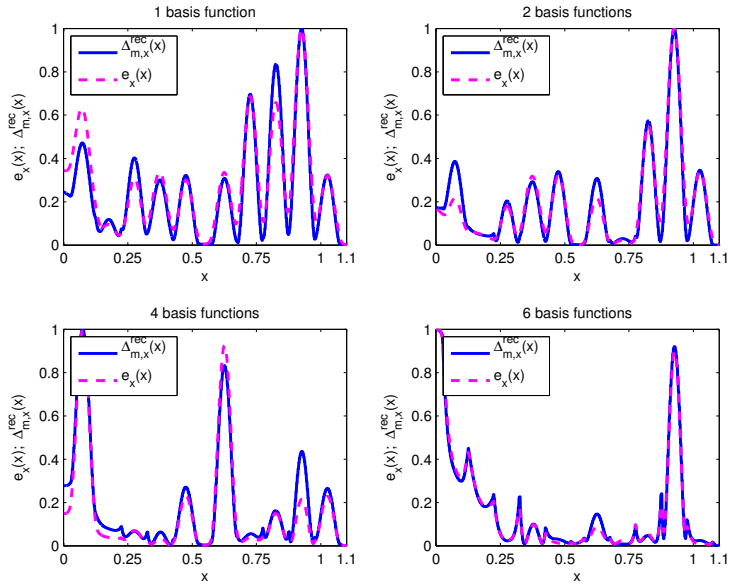

Figure 2.7: Test case 2: Comparison of $\Delta^{rec}_{m,x}(x)$ (solid) and $e_x(x)$ (dashed) — both defined in (2.55) — for discrete reduced solutions p^H_m using $1, 2, 4$ and 6 basis functions and $N_H = n_h = 400$ and $N_{H'} = 40$.

$\|\bar{p}^H_m\|_{L^2(\Omega_{1D})}$ coincide, as depicted in Fig. 2.5c. We have chosen $N_{H'} = N_H/10$ for the computations of all quantities in Fig. 2.5. Altogether, we infer that the convergence behavior of the POD transfers to the coefficients $\|\bar{p}^H_m\|_{L^2(\Omega_{1D})}$, $\bar{e}^{L^2}_m$, $\bar{e}^{H^1}_m$ and to the model error $\|e_m\|^{rel}_{L^2(\Omega)}$,$\|e_m\|^{rel}_V$. We therefore conclude that the discrete solution manifold Y^h_M (2.33) and the reference solution $p^{H\times h}$ are approximated with the same approximation quality by the reduction space Y^h_m. If we compare the total error $\|e\|^{rel}_V$ for increasing m and various mesh sizes H with the model error $\|e_m\|^{rel}_V$ for $H = 0.001375$ (Fig. 2.6a), we detect an interaction of the model error and the discretization error. Up to a certain model order m, for example $m = 8$ for $H = 0.001375$, the model error clearly dominates the discretization error. Then the proportion of the discretization error increases and finally dominates the model error for higher orders of m (for instance $m \geq 11$ for $H = 0.001375$). We also observe in Fig. 2.6a that the total error $\|e\|^{rel}_V$ converges linearly in H, which is the expected rate. Using the localized error estimator Δ^{rec}_m (2.51) in Algorithm 2.3.2 produces the same behavior of the total error $\|e\|^{rel}_V$ (Fig. 2.6b). Moreover, if we compare $\|e_m\|^{rel}_V$ and $\|e_m\|^{rel}_{L^2(\Omega)}$ for the two error estimators Δ_m (2.44) and Δ^{rec}_m (2.51) for increasing m and various mesh sizes H in Fig. 2.6e, we observe only very small differences. Thus we conclude that at least for the present test case the choice of the error estimator has barely any influence on the outcome of the proposed HMR-RB method. As the bilinear form $a(\cdot,\cdot)$ is symmetric we have $\Delta_m = \|e_m\|_V$ (see §2.4.1) and the behavior of Δ^{rel}_m can therefore be seen in Fig. 2.5a. Concerning $\Delta^{rel}_{m,rec}$, we observe in Fig. 2.6c that the relative error estimator clearly overestimates the relative error, but captures the qualitative behavior. Furthermore, the convergence rate of $\Delta^{rel}_{m,rec}$ in m is worse than the actual rate of $\|e_m\|^{rel}_V$ in m. This can be explained by the fact that $\Delta^{rel}_{m,rec}$ does not contain information stemming from an interpolation estimate for $\|\nabla v - \nabla v_m\|_{L^2(\Omega)}$, $v \in V$, $v_m \in V_m$ (cf. §2.4.2). However, we see in Fig. 2.6d, that the reconstruction technique introduced in §2.4.2 produces the expected linear order in H. As we do not use $\Delta^{rel}_{m,rec}$ as a stopping criterion in Algorithm 2.3.2 Adaptive-HMR-POD, the reduced rate with respect to m does not influence our adaptive algorithm. It is much more important that the error estimator detects relevant structures of the solution in x-direction and

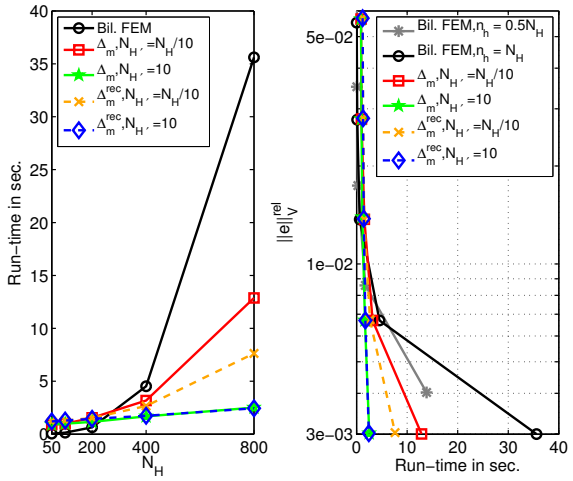

Figure 2.8: Test case 2: Comparison of the total run-time [s] of the bilinear FEM and the HMR-RB approach ($N_{H'} = N_H/10, 10$) for $N_H = n_h = 50, 100, ..., 800$ elements (left) and versus $\|e\|_V^{rel}$ (right) using Δ_m (2.44) and Δ_m^{rec} (2.51).

that the right regions of the parameter space $\mathcal{D}$ are refined. To analyze this, we define

$$\Delta_{m,x}^{rec}(x) := \frac{\sum_{j=1}^{\tilde{n}_h} \Delta_{m,T_{i,j}}^{rec}}{\max_{i\in\{1,...,\tilde{N}_H\}} \left(\sum_{j=1}^{\tilde{n}_h} \Delta_{m,T_{i,j}}^{rec} \right)}, \quad e_x(x) := \frac{\sum_{j=1}^{\tilde{n}_h} e_{T_{i,j}}}{\max_{i\in\{1,...,\tilde{N}_H\}} \left(\sum_{j=1}^{\tilde{n}_h} e_{T_{i,j}} \right)}, \tag{2.55}$$

for $(i-1)H \le x < iH, i = 1, ..., \tilde{N}_H$, where $\tilde{N}_H$ denotes the number of elements $\mathcal{T}_i \in \mathcal{T}$, $e_{T_{i,j}} := \|K\nabla(p_{fine} - p_m)\|^2_{L^2(T_{i,j})}$, $T_{i,j} \in \widehat{T}$, and $\Delta_{m,T_{i,j}}^{rec}$, $T_{i,j} \in \widehat{T}$, has been defined in (2.52). To make the values comparable, we have normalized $\Delta_{m,x}^{rec}$ and e_x. In Fig. 2.7 we compare $\Delta_{m,x}^{rec}(x)$ with $e_x(x)$ for discrete reduced solutions p_m^H computed with $m = 1, 2, 4$ and 6 basis functions and $N_H = n_h = 400$. The locations of all peaks of $e_x(x)$ are reproduced exactly by $\Delta_{m,x}^{rec}(x)$. In addition, also the graphs of $\Delta_{m,x}^{rec}(x)$ and $e_x(x)$ coincide for $m = 1, 2, 6$ except for some small discrepancies. Hence, the local indicators $\Delta_{m,x}^{rec}$ capture the behavior of the total local error in x-direction e_x very well.

Next, we compare the run-times of the HMR-RB approach with the ones of the standard bilinear FEM for various mesh sizes N_H. For the computation of the reference solution $p^{H\times h}$ we have run the algorithm 200 times to determine averaged run-times. To compute p_m^H we have run Algorithm 2.3.2 Adaptive-HMR-POD with a subsequent solve of the coupled system (2.12) 200 times for each value of N_H and $N_{H'}$, where $N_{H'}$ has been defined in §2.1.3. We emphasize that the run-times of the HMR-RB approach depicted in Fig. 2.8 are total run-times, including both offline and online costs. To make the run-times of the HMR-RB approach and the bilinear FEM fully comparable we have used the same routines for the assembling of matrixes and right hand sides and the same pcg method with the same settings for the solution of the linear systems of equations. The tolerance for the POD (see §2.3.4) has been chosen as $\varepsilon_{\text{tol}} = 10^{-5}$. In the left picture of Fig. 2.8 the average run-times of the bilinear FEM and the HMR-RB approach for $N_{H'} = N_H/10$ and $N_{H'} = 10$ are compared for $N_H = n_h = 50, 100, 200, 400$ and 800 using one time the estimator Δ_m (2.44) in Al-

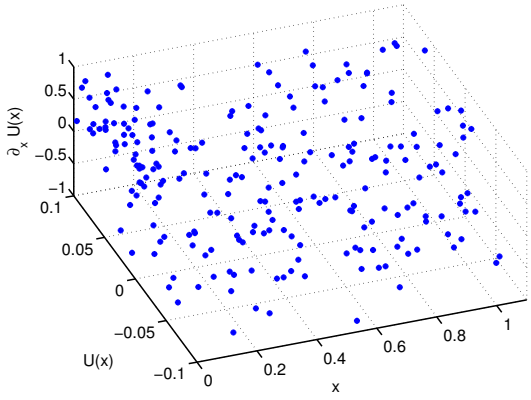

Figure 2.9: Test case 2: Plot of the adaptively refined training set generated by Algorithm 2.3.2 ADAPTIVE-HMR-POD.

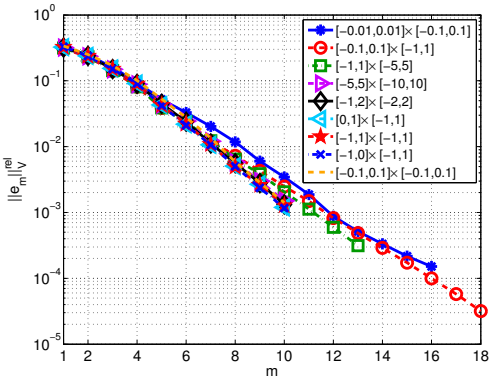

Figure 2.10: Test case 2: $\|e_m\|_V^{rel}$ for different parameter spaces $\mathcal{D} = \Omega_{1D} \times \cdots$

gorithm 2.3.2 and the other time Δ_m^{rec} (2.51). An actual run-time complexity of the bilinear FEM between $O(N_H^2)$ and $O(N_H^3)$ can be detected. In contrast, the HMR-RB approach scales linearly in N_H for $N_{H'} = 10$ and a bit worse than linearly for $N_{H'} = N_H/10$. This confirms the theoretical run-time complexities derived in §2.5. Also the supposed threshold due to the factor n_{train} can be detected. The average run-times for $N_{H'} = N_H/10$ lie well above the ones for $N_{H'} = 10$ for $N_H = 400, 800$, which can be explained by the higher costs of Algorithm 2.3.1 ADAPTIVEPARAMETERREFINEMENT for higher values of $N_{H'}$. While the total run-times for the usage of Δ_m and Δ_m^{rec} coincide for $N_{H'} = 10$, the computational costs when using Δ_m are much higher than the ones for the usage of Δ_m^{rec} for $N_{H'} = N_H/10$. This can be explained by the fact that when calculating Δ_m^{rec} the vast majority of the computations can be conducted either in $\mathcal{O}(n_h)$ or $\mathcal{O}(N_{H'})$ operations, whereas the computational costs of Δ_m are clearly dominated by the ones of the pcg method, which solves the linear system of equations (2.43) in $\mathcal{O}(n_h N_{H'})$ operations. In the right picture of Fig. 2.8 the total computational costs of the bilinear FEM and the HMR-RB approach are plotted versus the respective relative total error $\|e\|_V^{rel}$. As $N_{H'} = 10$ yields the same relative total error in a much shorter run-time than $N_{H'} = N_H/10$ for both estimators, we conclude that it is sufficient and most efficient to use only $N_{H'} = 10$ finite elements in the dominant direction in Algorithm 2.3.1 for the present example. Finally, we emphasize that for $\|e\|_V^{rel} \leq 10^{-2}$ the HMR-RB approach with $N_{H'} = 10$ clearly outperforms the bilinear FEM for $N_H = n_h$ and also when using a coarser discretization in y-direction with $n_h = 0.5N_H$ in the bilinear FEM. For smaller values of $\|e\|_V^{rel}$ the gain of using the HMR-RB approach instead of the standard bilinear FEM increases.

In Fig. 2.9 a plot of an adaptively refined training set Ξ_{train} constructed with Algorithm 2.3.2 ADAPTIVE-HMR-POD for $\mathcal{D} = [0, 1.1] \times [-0.1, 0.1] \times [-1, 1], m_{max} = 2, i_{max} = 1, n_\Xi = 6$ and $\theta = 0.05$ is depicted. All results that have been reported for this test case so far have been computed with these settings. Based on the obtained numerical results, we choose $\sigma_{thres} = (i_{max}-1)\cdot\lceil \text{diam}(g)\rceil+1$, to achieve $(i_{max} - 1) \cdot \text{diam}(g) \leq \sigma_{thres} \leq i_{max} \cdot \lceil \text{diam}(g)\rceil$, where $\text{diam}(g)$ is the length of the diagonal of an element of the initial grid $G_0 = [0, 0.275, 0.55, 0.825, 1.1] \times [-0.1, 0.1] \times [-1, 1]$ in the parameter space $\mathcal{D}$ and $\lceil\cdot\rceil$ denotes the ceiling function. This choice of σ_{thres} causes a nonrecurring refinement of all elements which have not been marked for refinement by the first element indicator $\eta(g)$. Altogether, this results in a sample size of $n_{\text{train}} \approx 220$. It can be seen in Fig. 2.9 that the first error indicator $\eta(g)$ causes a refinement of $\mathcal{D}$ in the region $0 \leq x \leq 0.2$ due to the source term

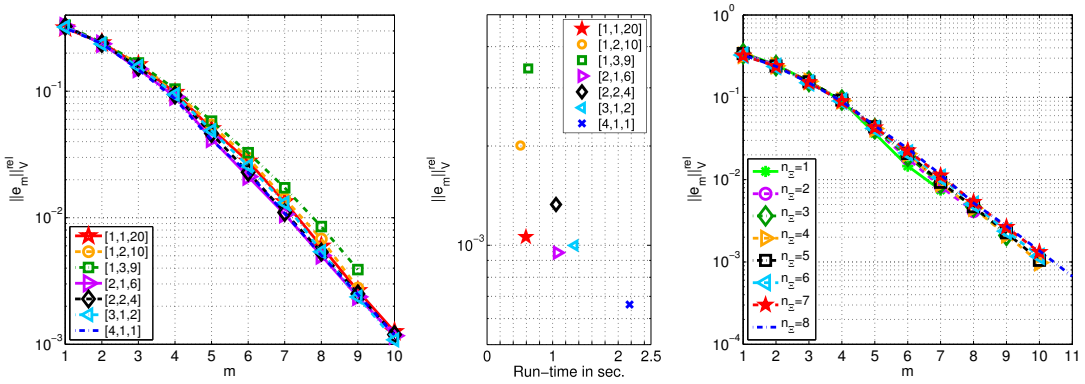

(a) $\|e_m\|_V^{rel}$ for $[m_{\max}, i_{\max}, n_\Xi]$ (b) Run-time vs. $\|e_m\|_V^{rel}$ (c) $\|e_m\|_V^{rel}$; varying n_Ξ

Figure 2.11: Test case 2: $\|e_m\|_V^{rel}$ for $\mathcal{D} = [0, 1.1] \times [-1, 0] \times [-1, 1]$ for different combinations of inputs of Algorithm 2.3.2 ADAPTIVE-HMR-POD: Varying $[m_{max}, i_{max}, n_\Xi]$ for $n_{train} \approx 220$ (a) with associated total run-times (b); $m_{max} = 2, i_{max} = 1$ and varying n_Ξ (c).

(see Fig. 2.4) and the Neumann boundary at Γ_0. Due to the second indicator $\sigma(g)$ also the rest of the parameter space is refined once, such that the local maxima in the solution between $x = 0.4$ and $x = 0.7$ are detected, too, and included in the discrete reduced solution p_m^H (see Fig. 2.3). We conclude that $\eta(g)$ causes a refinement of the relevant parts of $\mathcal{D}$ and that also small structures in the solution are detected due to the second indicator. To address the choice of the intervals I_k, $k = 0, 1$, which enclose the ranges of $\partial_x^k U(x)$, $k = 0, 1$, and have been defined in §2.3.1, we compare in Fig. 2.10 the relative model error $\|e_m\|_V^{rel}$ for different values of I_0 and I_1. First, we state that neither the size of I_0 and I_1, the sign of their limits, or the ratio of I_0/I_1 seem to have much influence on the convergence rate of $\|e_m\|_V^{rel}$. Although the reference solution $p^{H\times h}$ ranges from 0 to 0.007 (see Fig. 2.3), also the choice $I_0 = [-5, 5]$ yields a very good model convergence rate. The fact that $\mathcal{D} = [0, 1.1] \times [-0.01, 0.01] \times [-0.1, 0.1]$ performs worst might be explained by the fact that I_0 is chosen too small and hence does not allow enough variation in the parameter to include all essential features of the full solution in the manifold $\mathcal{M}^h$.

Finally, we discuss the choice of the inputs m_{max}, i_{max} and n_Ξ of Algorithm 2.3.2 ADAPTIVE-HMR-POD (see §2.3.4), where $\mathcal{D} = [0, 1.1] \times [-1, 0] \times [-1, 1]$. First, we observe a low sensitivity of $\|e_m\|_V^{rel}$ with respect to a change in the input parameters for a fixed sample size of approximately 220, where $n_{train} \approx 280$ for $m_{max} = 4$, $i_{max} = 1$ and $n_\Xi = 1$ (Fig. 2.11a). Nevertheless, we detect that the convergence rate becomes better from $m_{max} = 1$ to $m_{max} = 2$, but a further increase produces no additional improvement. Regarding i_{max} it can be stated that an increase of i_{max} deteriorates the convergence rate. The associated total run-times for $N_H = n_h = 200$ in Fig. 2.11b support these findings as the choice of $i_{max} = 1$ always performs best by yielding a better relative error for comparable run-times. As the choice $m_{max} = 3$ performs worse than $m_{max} = 2$ and the choice $m_{max} = 4$ reduces the relative error only at considerably additional cost, we conclude that m_{max} should be chosen either equal to one or two and that $i_{max} = 1$ is the best choice. Fixing $m_{max} = 2$ and $i_{max} = 1$, we see in Fig. 2.11c that the convergence rate of $\|e_m\|_V^{rel}$ gets worse for growing n_Ξ whereas $M = \dim(Y_M^h)$ increases. The same behavior can be observed for the other combinations of m_{max} and i_{max} listed in Fig. 2.11a, except for $m_{max} = 1$ and $i_{max} = 1$, where the model error improves for increasing n_Ξ until $n_\Xi = 6$. We further see in Fig. 2.11c that for $n_\Xi \leq 3$ a

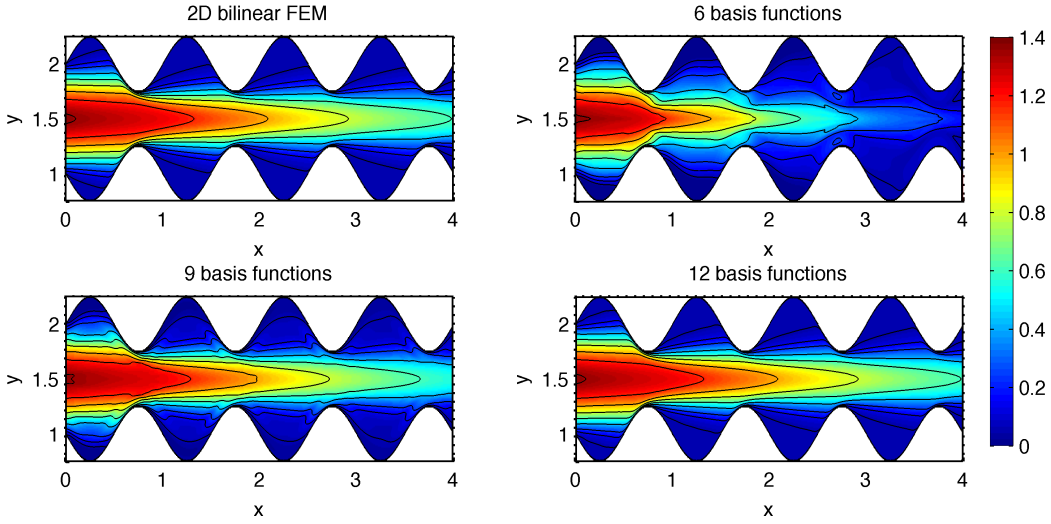

Figure 2.12: Test case 3: In comparison from left to right and top to bottom: the reference 2D bilinear FE solution $p^{H\times h}$ and the discrete reduced solution p_m^H using 6, 9 and 12 basis functions; $N_H = 1200, n_h = 400, N_{H'} = 20$.

tolerance of 10^{-3} can in general not be achieved, as the number M of linear independent snapshots in Ξ_{train} is too small. Trading off the worsening of the convergence rate and the increase of the computational costs for growing n_Ξ against the augmentation of M, we have chosen $n_\Xi = 6$, but $n_\Xi = 5, ..., 8$ yields comparable results.

Test case 3

This test case, which is very similar to test case 4 in [102], comes from the field of hemodynamics, modeling a Bellhouse membrane oxygenator for extracorporeal circulation (cf. [15]). We model oxygen transport within a symmetric channel with sinusoidal wavy walls, which is a typical geometry in this context. To this end we define Ω as the domain which is bounded by the functions $x = 0$, $y = 1 - 0.25\sin(2\pi x)$, $x = 4$ and $y = 2 + 0.25\sin(2\pi x)$ and consider (2.9) for $k = 1$, $b = (100, 0)^t$ and $s = 0$, where p models the oxygen concentration in the blood. We prescribe non-homogeneous Dirichlet boundary conditions on the inflow boundary Γ_0 by setting $p(0, y) = \sqrt{2}\sin(\pi(y + 1))$, homogeneous Neumann boundary conditions on the outflow boundary Γ_1 and homogeneous Dirichlet boundary conditions on Γ_*. The reference solution $p^{H\times h}$ for $N_H = 1200$ and $n_h = 400$ is depicted in the first picture of Fig. 2.12 and shows a main stream along the dominant x-direction, where we have conducted a convergence study to ensure grid convergence. Boundary layers, caused by the curved boundary of Ω induce also a transverse behavior of the solution that is not negligible. Note that the mesh size of $H = 1/3 \cdot 10^{-3}$ yields a local Péclet number which is for the prescribed advection field strictly less than 1. Also for values of H resulting in local Péclet numbers that are greater than 1, no oscillations have been observed either, indicating that also for these discretizations the scheme is stable. Because of that we have not applied a stabilization scheme. We compare $p^{H\times h}$ with the discrete reduced solution p_m^H for $m = 6, 9, 12$, $N_H = 1200$, $n_h = 400$ and $N_{H'} = 20$ (Fig. 2.12). p_6^H reproduces the behavior of $p^{H\times h}$ for $0 \leq x \leq 0.75$ quite well, but shows a bad approximation quality for $x \geq 2$, due to a major refinement of $\mathcal{D}$ in the interval $[0.5, 1]$ during Algorithm 2.3.2 Adaptive-HMR-POD (Fig. 2.13). p_9^H already captures the behavior of the main stream very well but exhibits some oscillations caused by the irregular shape of Ω. We finally see a very good visual agreement of $p^{H\times h}$ and p_{12}^H. Fig. 2.13 shows that during Algorithm 2.3.2 the

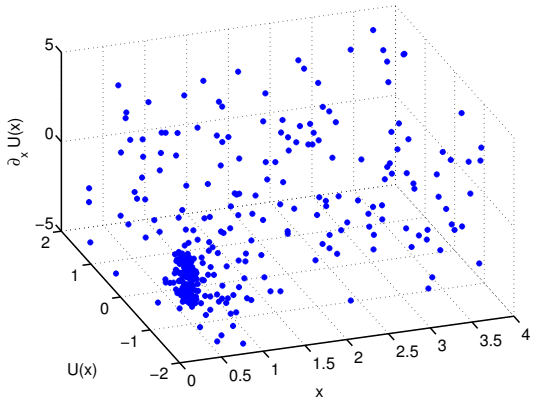

Figure 2.13: Test case 3: Adaptively refined training set generated by Algorithm 2.3.2 Adaptive-HMR-POD.

parameter space $\mathcal{D} = [0, 4] \times [-2, 2] \times [-5, 5]$ is mostly refined at the constriction of the domain Ω at $x = 0.75$. The other parts of $\mathcal{D}$ are refined only once due to the second indicator $\sigma(g)$. We therefore conclude that Algorithm 2.3.2 Adaptive-HMR-POD is able to detect recurring structures in the full solution p.

Studying the convergence behavior of $\|e_m\|_V^{rel}$ (Fig. 2.14a) and $\|e_m\|_{L^2(\Omega)}^{rel}$ (Fig. 2.14b, solid line with circle), we detect an error plateau as the relative error does not drop until $m = 6$. However, for $m \geq 6$ we see that $\|e_m\|_V^{rel}$ and $\|e_m\|_{L^2(\Omega)}^{rel}$ converge exponentially fast and that the convergence rates of $\|e_m\|_{L^2(\Omega)}^{rel}$ and e_m^{POD} coincide (Fig. 2.14b, solid lines). If we compare λ_m and $\|\bar{p}_m^H\|_{L^2(\Omega_{1D})}$ (Fig. 2.14c, solid lines), we observe that $\|\bar{p}_m^H\|_{L^2(\Omega_{1D})}$ increases until $m = 5$, subsequently drops and for $m \geq 8$ exhibits the same convergence rate as λ_m. We therefore conclude that the coefficients in the dominant direction add relevant information to the reduced solution p_m^H, which has not been included in the solution manifold $\mathcal{M}^h$. This could also explain the flattening of $\|\bar{p}_m^H\|_{L^2(\Omega_{1D})}$ for $m = 14$ in Fig. 2.14c and $\bar{e}_m^{H^1}$ in Fig. 2.14a, which vanishes for higher sample sizes n_{train}. These computations have been done using one quadrature point in the derivation of the parameter dependent 1D problem (see §2.3.1) with weights as defined in (2.29). To increase the amount of information from the dominant direction in the basis functions, we have recomputed the HMR-RB approximation for approximately the same sample size using a modified two point-rectangle formula (2.29) or a three point-trapezoidal rule. The convergence rate of $\|\bar{p}_m^H\|_{L^2(\Omega_{1D})}$ improves considerably, as there is only a small increase of $\|\bar{p}_m^H\|_{L^2(\Omega_{1D})}$ until $m \leq 3$ before the subsequent drop (Fig. 2.14c). This transfers to the convergence behavior of $\|e_m\|_V^{rel}$ (Fig. 2.14d) and $\|e_m\|_{L^2(\Omega)}^{rel}$ (Fig. 2.14b, dashed line with circle), which exhibit only a small error plateau for $m \leq 3$ and a significantly improved rate. We remark that the trapezoidal rule performs slightly better than the two point-rectangle formula. Altogether we conclude that due to the strong advection field b, which is reinforced by the transformation Ψ (Fig. 2.1), the usage of one quadrature point yields a bad convergence behavior for smaller m, as the discrete solution manifold Y_M^h (2.33) does not contain all essential features of the solution (in contrast to test case 2). Using a quadrature rule with higher accuracy improves the convergence rates significantly. Comparing the behavior of the total error $\|e\|_V^{rel}$ for one quadrature point in Fig. 2.14e with $\|e\|_V^{rel}$ of test case 2 (Fig. 2.6a), we observe that in test case 3 substantially more basis functions — for example 15 for $\|e\|_V^{rel} = 0.0131955$ ($H = 1/300$) — are needed to balance the influences of the model and the discretization error than in test case 2, where we need 9 basis functions to obtain $\|e\|_V^{rel} = 0.00799781$ ($H = 0.00275$). Again, we detect

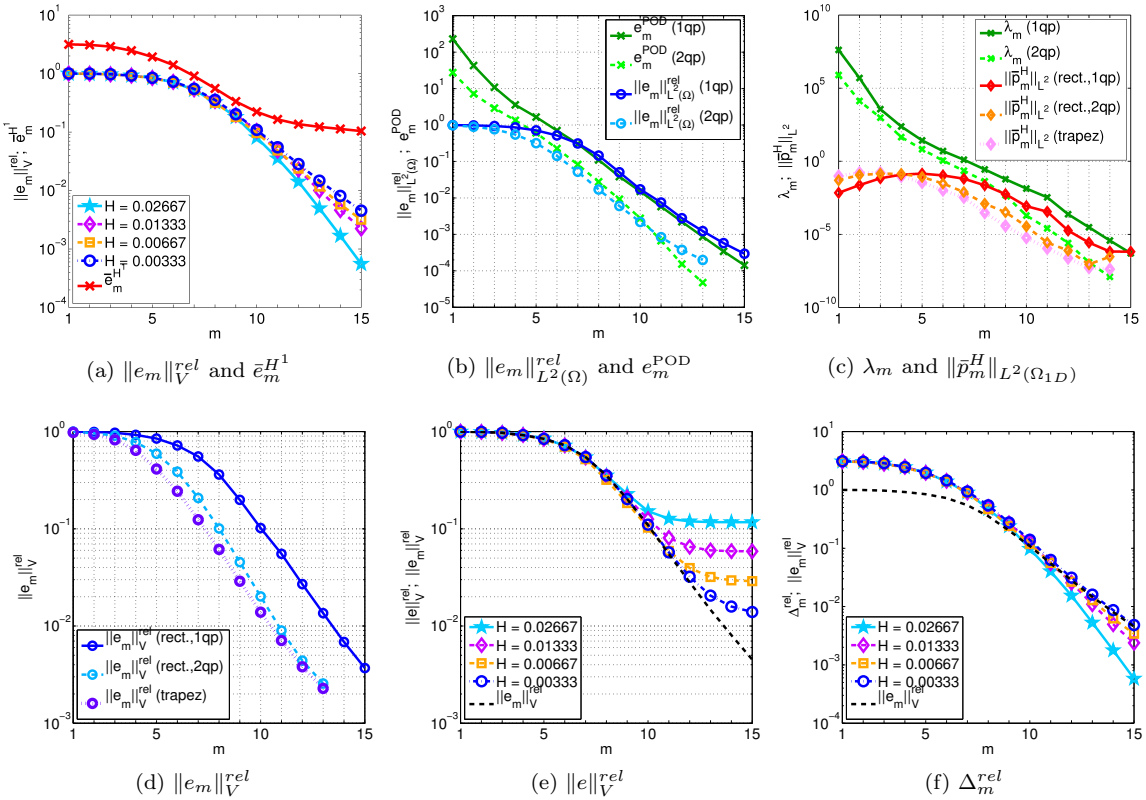

(a) $\|e_m\|_V^{rel}$ and $\bar{e}_m^{H^1}$ (b) $\|e_m\|_{L^2(\Omega)}^{rel}$ and e_m^{POD} (c) λ_m and $\|\bar{p}_m^H\|_{L^2(\Omega_{1D})}$

(d) $\|e_m\|_V^{rel}$ (e) $\|e\|_V^{rel}$ (f) Δ_m^{rel}

Figure 2.14: Test case 3: Comparison of the model error convergence for different quadrature rules for $N_{H'} = N_H/10$ in the V-norm/H^1-half-norm : (a) $\|e_m\|_V^{rel}$ for different H and $\bar{e}_m^{H^1}$ for $H = 0.00333$ for the one point rectangle formula (1qp), and for $H = 0.00333$ in the L^2-norm: (b) $\|e_m\|_{L^2(\Omega)}^{rel}$ and e_m^{POD} for the one point- and two point-rectangle formula (2qp), (c) λ_m and $\|\bar{p}_m^H\|_{L^2(\Omega_{1D})}$ for one point-, two point-rectangle formula and the trapezoidal rule (trapez), (d) $\|e_m\|_V^{rel}$ for the one point-, two point-rectangle formula and the trapezoidal rule, (e) relative total error $\|e\|_V^{rel}$ for different H and $\|e_m\|_V^{rel}$ for $H = 0.00333$ and (f) Δ_m^{rel} for different H and $\|e_m\|_V^{rel}$ for $H = 0.00333$ both for the one point-rectangle formula.

the expected linear convergence rate in H. Validating Δ_m, a slight overestimation of $\|e_m\|_V^{rel}$ for smaller m can be detected, which can be explained by the fact that the bilinear form $a(\cdot,\cdot)$ of this test case is non-symmetric. For higher values of m ($m \geq 8$) the effectivity indices are very close to 1.

For the comparison of the run-times of the HMR-RB approach with standard bilinear FEM we have run the respective algorithms 200 times, using the same routines for the assembling and the solution of the respective linear systems of equations. Again, the reported run-times include the total computational costs for the computation of the reference solution $p^{H\times h}$ and the discrete reduced solution p_m^H, respectively. The tolerance for the POD (see §2.3.4) has been set to $\varepsilon_{\mathrm{tol}} = 10^{-4}$. In order to account for the geometry of Ω, we have chosen $n_h = 1/3N_H$. Comparing the averaged run-times of the bilinear FEM and the HMR-RB approach for the one point- and two point-rectangle formula and the three point-trapezoidal rule for $N_{H'} = 10$ and $N_{H'} = 20$, we detect an actual run-time complexity of the bilinear FEM between $O(N_H^2)$ and $O(N_H^3)$, whereas the HMR-RB approach scales

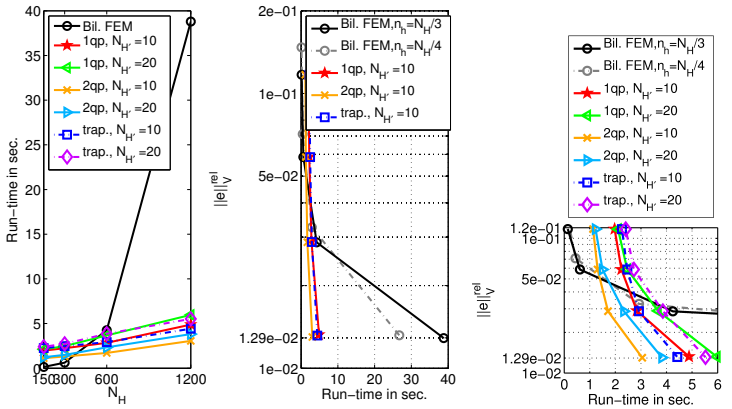

Figure 2.15: Test case 3: Comparison of the run-time [s] of bilinear FEM and the HMR-RB approach ($N_{H'} = 10, 20$) for the one point- (1qp) and two point-rectangle formula (2qp) and the trapezoidal rule (trap.) for $n_h = 1/3N_H$ (left) and per $\|e\|_V^{rel}$ (middle and right).

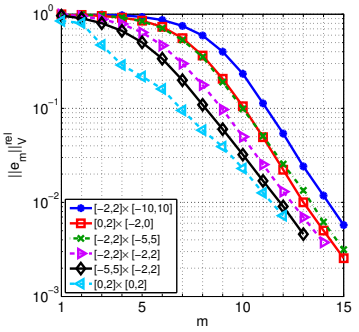

Figure 2.16: Test case 3: $\|e_m\|_V^{rel}$ for different parameter spaces $\mathcal{D} = \Omega_{1D} \times \cdots$

linearly in N_H (Fig. 2.15, left picture). Also for this test case the theoretical run-time complexities derived in §2.5 are confirmed and the supposed threshold due to the factor n_{train} can be detected. If we compare the run-times of the HMR-RB approach for the considered quadrature rules, we observe that the run-time for the one point-rectangle formula is highest, closely followed by the one for the three point-trapezoidal rule, and that both are significantly higher than the run-time for the two point-rectangle formula (Fig. 2.15). As all three quadrature rules yield the same relative total error $\|e\|_V^{rel}$, we conclude that the two point-rectangle formula performs best for the present test case. Since $N_{H'} = 10$ yields the same relative total error in a much shorter run-time than $N_{H'} = 20$ for all three quadrature rules, we further conclude that it is sufficient and most efficient to choose also for this numerical example $N_{H'} = 10$. Finally, for $\|e\|_V^{rel} \leq 0.03$ the HMR-RB approach with $N_{H'} = 10$ clearly outperforms the bilinear FEM for $n_h = 1/3N_H$ and also for the coarser discretization in y-direction with $n_h = 1/4N_H$ for the bilinear FEM. Moreover, the advantage of using the HMR-RB approach instead of the standard bilinear FEM increases significantly for decreasing $\|e\|_V^{rel}$. We emphasize that although Ξ_{train} is twice as large as in test case 2, the HMR-RB approach outperforms the bilinear FEM even for higher values of the relative total error $\|e\|_V^{rel}$ — 0.03 in the present example and 0.01 in test case 2 — as the boundary layers (Fig. 2.12) require in relation to test case 2 a much higher grid resolution. As Algorithm 2.3.1 AdaptiveParameterRefinement is able to detect recurring structures in the full solution (Fig. 2.13) and thus possibly limits the growth of the sample size also for more complex problems to some extent, we expect that the increase of n_{train} and the grid resolution balance for more complex problems as in the present test case, and hence the HMR-RB approach still outperforms the bilinear FEM.

Finally, we address the choice of the input parameters of Algorithm 2.3.2 Adaptive-HMR-POD. First, we detect a much stronger sensitivity of $\|e_m\|_V^{rel}$ with respect to the values of I_0 and I_1 (Fig. 2.16) than in test case 2 (Fig. 2.10). However, except for $\mathcal{D} = [0, 4] \times [0, 2] \times [0, 2]$, all choices exhibit the same convergence rate after the error plateau. If we choose the same intervals I_0 and I_1 also for the respective intervals in the quadrature formulas of higher accuracy, except for $\mathcal{D} = [0, 4] \times [0, 2] \times [0, 2]$ all choices yield a comparable gain, whereas the gain for the latter is very small. Concerning the required run-time per $\|e\|_V^{rel}$ we have observed that all considered

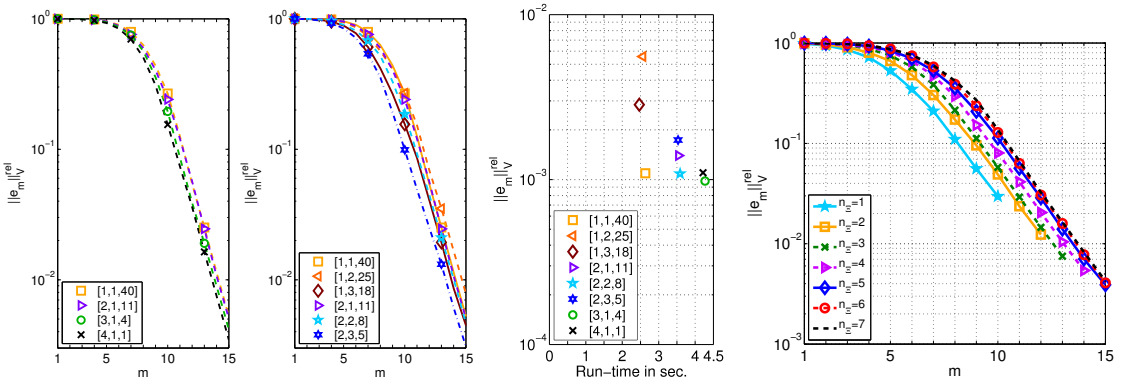

(a) $\|e_m\|_V^{rel}$ for $[m_{max}, i_{max}, n_\Xi]$ (b) Run-time vs $\|e_m\|_V^{rel}$ (c) $\|e_m\|_V^{rel}$; varying n_Ξ

Figure 2.17: Test case 3: $\|e_m\|_V^{rel}$ for $\mathcal{D} = [0,4] \times [-2,2] \times [-5,5]$ for different combinations of inputs of Algorithm 2.3.2 ADAPTIVE-HMR-POD: Varying $[m_{max}, i_{max}, n_\Xi]$ for $n_{train} \approx 440$ (a) with associated total run-times (b); $m_{max} = 2, i_{max} = 3$ and varying n_Ξ (c).

domains require less or the same run-time than the choice $\mathcal{D} = [0,4] \times [-2,2] \times [-5,5]$ for the same $\|e\|_V^{rel}$ and that the differences between the parameter domains are relatively small— for instance one second between the smallest and the highest run-time for $N_H = 1200$, $n_h = 400$ and $N_{H'} = 20$. We therefore conclude that in spite of the relatively high sensitivity of the convergence rate $\|e_m\|_V^{rel}$ with respect to the values of I_0 and I_1, the choice of I_0 and I_1 has little influence on the performance of the HMR-RB approach, when considering the required run-time per $\|e\|_V^{rel}$. Regarding the choice of m_{max}, i_{max} and n_Ξ we detect for $\mathcal{D} = [0,4] \times [-2,2] \times [-5,5]$ a low sensitivity of $\|e_m\|_V^{rel}$ with respect to a change in the input parameters for a fixed sample size of approximately 440, where $n_{train} \approx 403$ for $m_{max} = 3$, $i_{max} = 1$ and $n_\Xi = 4$ and $n_{train} \approx 337$ for $m_{max} = 4$, $i_{max} = 1$ and $n_\Xi = 1$ (Fig. 2.17a). However, we observe an improvement of the convergence rate for increasing m_{max} (Fig. 2.17a, left picture) and except for $m_{max} = 1$, $i_{max} = 1$ also an improvement for growing i_{max} (Fig. 2.17a, right picture). The associated run-times for growing m_{max} increase, whereas for i_{max} no trend is detectable (Fig. 2.17b). Because of the strong variation for $m_{max} = 1$ (Fig. 2.17a, Fig. 2.17b), which makes it difficult to determine a suitable choice of n_Ξ, and the fact that $m_{max} = 2$ performs better than $m_{max} = 3$ or $m_{max} = 4$, we prefer $m_{max} = 2$. Fixing $m_{max} = 2$ and $i_{max} = 3$, we see in Fig. 2.17c that the convergence rate of $\|e_m\|_V^{rel}$ gets worse for growing n_Ξ whereas M increases. An equal behavior can be detected for all other combinations of m_{max} and i_{max} listed in Fig. 2.17a. To trade off the worse convergence behavior for growing n_Ξ against the increase of M, $n_\Xi = 4, ..., 7$ are reasonable choices, where all computations for this test case have been conducted for $m_{max} = 2$, $i_{max} = 3$ and $i_{max} = 5$ for the one point-rectangle formula. For the two point-rectangle formula we have chosen $m_{max} = i_{max} = 1$ and $n_\Xi = 5$ and for the trapezoidal rule $m_{max} = 2$, $i_{max} = 1$ and $i_{max} = 6$ and for both $\theta = 0.025$ and $\sigma_{thres} = i_{max}\lceil diam(g) \rceil + 1$.

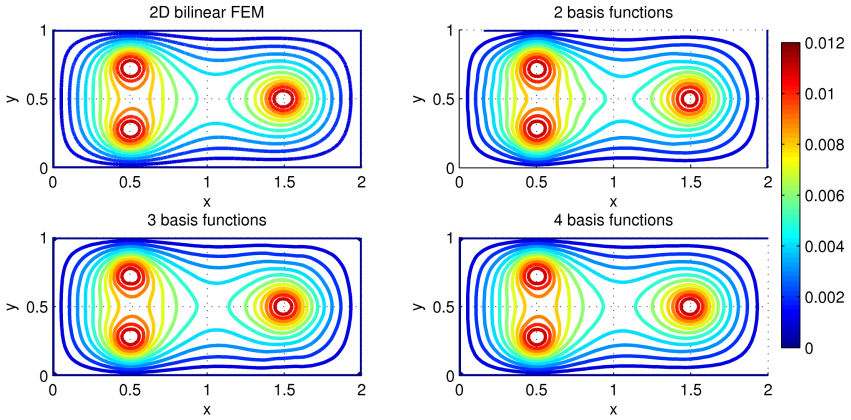

Figure 2.18: Test case 4: In comparison from left to right and top to bottom: the 2D bilinear FE solution $p^{H\times h}$ for $N_H = 640$ and $n_h = 320$ and the discrete reduced solution p_m^H using 2, 3 and 4 basis functions for $N_H = 80, n_h = 40$ and $N_{H'} = 10$.

Test case 4

As a last experiment, we consider a test case with a source term that cannot be expressed as a linear combination of tensor products. We choose the numerical example from [48], which is revisited as test case 5 in [102]. Hence, we consider a Poisson problem in $\Omega = (0,2)\times(0,1)$ with homogeneous Dirichlet boundary conditions. The source term is the characteristic function $s(x,y) = \chi_{D_1\cup D_2\cup D_3}$, where $D_1 = \{(x,y)\in\Omega : (x-0.5)^2+(y-0.25)^2 \leq 0.01\}$, $D_2 = \{(x,y)\in\Omega : (x-0.5)^2+(y-0.75)^2 \leq 0.01\}$, and $D_3 = \{(x,y)\in\Omega : (x-1.5)^2+(y-0.5)^2 \leq 0.01\}$. The circular plateaus in the source term yield a quite challenging test case for an approach based on a truncated tensor product decomposition. The bilinear FE solution $p^{H\times h}$ for $N_H = 640$ and $n_h = 320$ is displayed in the first picture of Fig. 2.18 and exhibits peaks at the centers of the circles D_i, $i = 1,2,3$. Again a convergence study has been done to ensure that $p^{H\times h}$ contains all essential features of the exact solution. The HMR approach requires eight sine functions for a good approximation for $N_H = 100$ [48]. If the domain Ω is split into two subdomains $\Omega_1 = (0,1)\times(0,1)$ and $\Omega_2 = (1,2)\times(0,1)$ and a domain decomposition scheme is applied, $m = 7$ in Ω_1 and $m = 5$ in Ω_2 sine functions should be used to get a good approximation for $H = 0.02$ [102]. For the HMR-RB approach, we compare $p^{H\times h}$ with the discrete reduced solution p_m^H using $m = 2,3$ and 4 basis functions for $N_H = 80$, $n_h = 40$ and $N_{H'} = 10$ in Fig. 2.18. Already p_2^H contains all essential features of the full solution, namely the three peaks, and p_3^H exhibits only small deviations from $p^{H\times h}$ around $x = 1.5$. Finally, the contour lines of $p^{H\times h}$ and p_4^H coincide. Thus, also for this test case, we observe a much better modal convergence behavior of the HMR-RB approach than the HMR ansatz. This statement is supported by the convergence behavior of the model error $\|e_m\|_V^{rel}$ for increasing m. As $s\in L^2(\Omega)$, we expect the HMR ansatz to converge linearly in m^{-1} [26]. If we analyze the convergence behavior of $\|e_m\|_V^{rel}$ of the HMR-RB approach (Fig. 2.19d), we detect a limit convergence rate of $m^{-1.8}$. For $H = 0.025$, $m \geq 10$, and $H = 0.0125$, $m \geq 20$, we even observe an exponential convergence rate, which however depends heavily on the mesh size. As expected, the error in the L^2-norm is one order better and we detect a rate of $m^{-2.8}$ for $\|e_m\|_{L^2(\Omega)}^{rel}$ in Fig. 2.19b. As can be seen in Fig. 2.19a,2.19b, the rates for $\|e_m\|_V^{rel}$ and $\bar{e}_m^{H^1}$, as well as $\|e_m\|_{L^2(\Omega)}^{rel}$ and $\bar{e}_m^{L^2}$ coincide perfectly for $H = 0.003125$. Also the rates for e_m^{POD} and $\|e_m\|_{L^2(\Omega)}^{rel}$ are quite comparable, although e_m^{POD} converges slightly better for $m \geq 30$. Likewise, λ_m converges approximately with the same order as $\|\bar{p}_m^H\|_{L^2(\Omega_{1D})}$ (Fig. 2.19c). We thus conclude that the convergence rate of the POD seems to

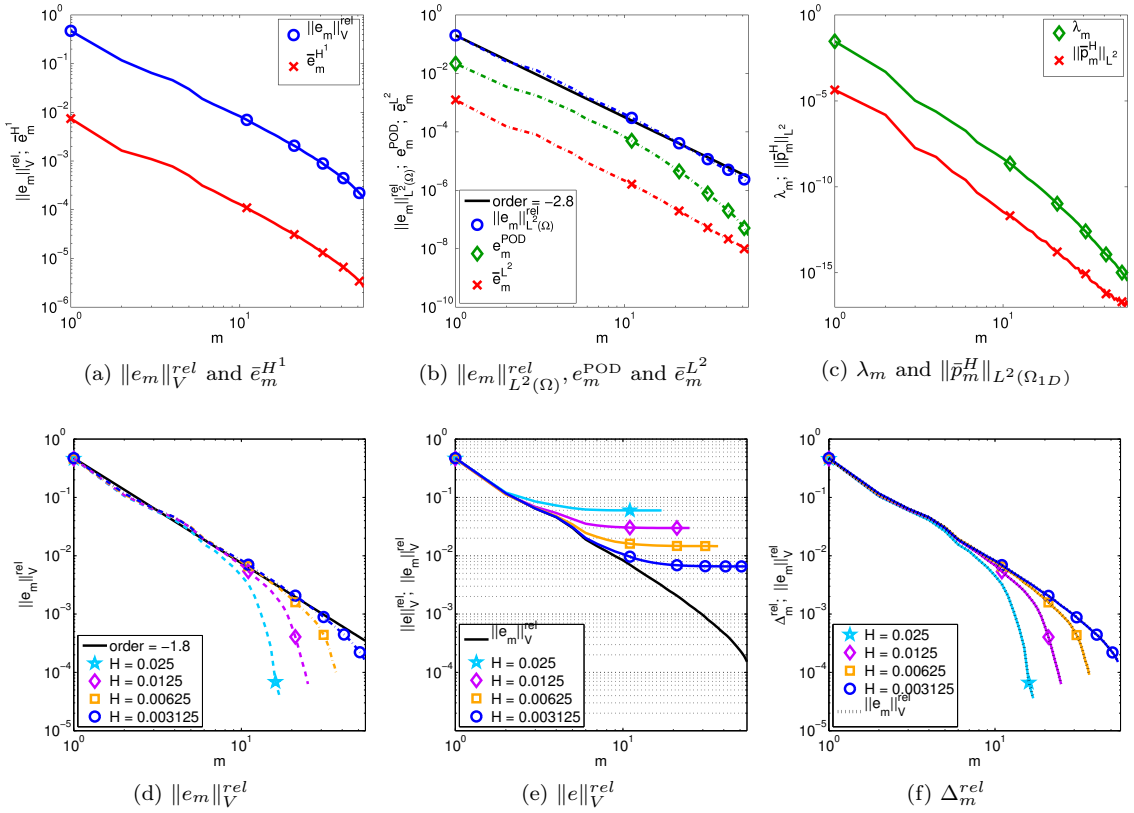

(a) $\|e_m\|_V^{rel}$ and $\bar{e}_m^{H^1}$ (b) $\|e_m\|_{L^2(\Omega)}^{rel}, e_m^{\mathrm{POD}}$ and $\bar{e}_m^{L^2}$ (c) λ_m and $\|\bar{p}_m^H\|_{L^2(\Omega_{1D})}$

(d) $\|e_m\|_V^{rel}$ (e) $\|e\|_V^{rel}$ (f) Δ_m^{rel}

Figure 2.19: Test case 4: Illustration of the error convergence for $N_{H'} = N_H/10$ for $H = 0.003125$ in the V-norm/H^1-half-norm: (a) $\|e_m\|_V^{rel}$ and $\bar{e}_m^{H^1}$, and the L^2-norm: (b) $\|e_m\|_{L^2(\Omega)}^{rel}, e_m^{\mathrm{POD}}$ and $\bar{e}_m^{L^2}$, (c) λ_m and $\|\bar{p}_m^H\|_{L^2(\Omega_{1D})}$ and in the V-norm for different H (d) $\|e_m\|_V^{rel}$, (e) $\|e\|_V^{rel}$, and (f) Δ_m^{rel} .

transfer to the coefficients $\|\bar{p}_m^H\|_{L^2(\Omega_{1D})}$, $\bar{e}_m^{L^2}$, $\bar{e}_m^{H^1}$ and to the model error $\|e_m\|_{L^2(\Omega)}^{rel}$,$\|e_m\|_V^{rel}$. Hence, the discrete solution manifold Y_M^h and the reference solution $p^{H\times h}$ are approximated with the same accuracy by the reduction space Y_m^h. Although the modal convergence rate is only polynomial for this test case, we see in Fig. 2.19e that comparatively few basis functions are needed to balance the contributions of the model and the discretization error. For instance, for $H \leq 0.00625$ eleven basis functions and for $H = 0.003125$ $m = 17$ basis functions are sufficient to diminish the contribution of the model error to less than ten percent. Therefore, we conclude that also for this test case the HMR-RB approach performs very well. As in the present example the coercivity constant c_0 equals to 1 and the bilinear form $a(\cdot,\cdot)$ is symmetric and hence $\|e_m\|_V^{rel} = \Delta_m^{rel}$ (see §2.4.1), we expect for Δ_m^{rel} an effectivity index of 1, which is demonstrated in Fig. 2.19f. As in test case 2 we observe the same behavior of $\|e\|_V^{rel}$ (Fig. 2.20a) when replacing Δ_m (2.44) by Δ_m^{rec} (2.51) in Algorithm 2.3.2. Also the comparison of $\|e_m\|_V^{rel}$ and $\|e_m\|_{L^2(\Omega)}^{rel}$ for the two error estimators Δ_m and Δ_m^{rec} in Fig. 2.20d and Fig. 2.20e shows only very small variations in the error behavior when changing the estimator. Hence we conclude that also for the present example the choice of the error estimator does hardly affect the outcome of the HMR-RB method. In Fig. 2.20b it can be seen that $\Delta_{m,rec}^{rel}$ overestimates the relative error, but captures the qualitative behavior. In contrast to test case 2 the expected linear convergence rate in H is not recovered for $\Delta_{m,rec}^{rel}$ (Fig. 2.20c), which can

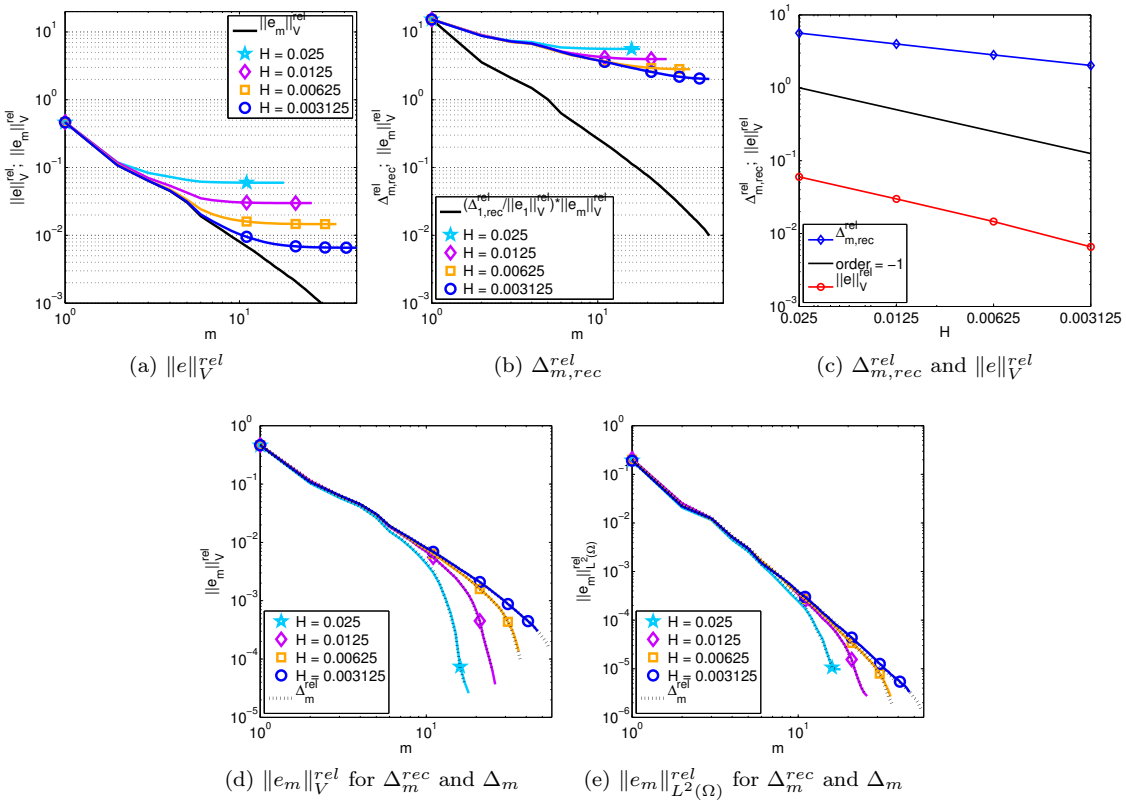

(a) $\|e\|_V^{rel}$ (b) $\Delta_{m,rec}^{rel}$ (c) $\Delta_{m,rec}^{rel}$ and $\|e\|_V^{rel}$

(d) $\|e_m\|_V^{rel}$ for Δ_m^{rec} and Δ_m (e) $\|e_m\|_{L^2(\Omega)}^{rel}$ for Δ_m^{rec} and Δ_m

Figure 2.20: Test case 4: Comparison of $\|e\|_V$ (a) and $\Delta_{m,rec}^{rel}$ (b) for increasing model order m and different mesh sizes H. Both are also compared with $\|e_m\|_V^{rel}$ for $H = 0.003125$. $\Delta_{m,rec}^{rel}$ and $\|e\|_V^{rel}$ for decreasing mesh size H and model order $m = M$ (c). $\|e_m\|_V^{rel}$ (d) and $\|e_m\|_{L^2(\Omega)}^{rel}$ (e) for Δ_m^{rec} (solid) and Δ_m (dashed).

be ascribed to the discontinuities in s in combination with our proposed reconstruction technique (see §2.4.2). To analyze whether $\Delta_{m,rec}^{rel}$ detects the relevant structures in x-direction, we compare $\Delta_{m,x}^{rec}(x)$ and $e_x(x)$ (2.55) in Fig. 2.21 for discrete reduced solutions p_m^H computed with $m = 1, 2$ and 4 basis functions and $N_H = 640$, $n_h = 320$, $N_{H'} = 64$. We see that also for the present test case the peaks of e_x are exactly recovered by $\Delta_{m,x}^{rec}$. Also the graphs for $e_x(x)$ and $\Delta_{m,x}^{rec}(x)$ match pretty well.

The input arguments of Algorithm 2.3.2 ADAPTIVE-HMR-POD, have been chosen as $G_0 = [0, 0.4, 0.8, 1.2, 1.6, 2] \times [-0.2, 0.2] \times [-1, 1]$, $m_{\max} = 2$, $i_{max} = 2$, $n_\Xi = 6$, $\theta = 0.05$, $\sigma_{thres} = (i_{max} - 1) \cdot \lceil \mathrm{diam}(g) \rceil + 1$ for an element $g \in G_0$ and $\varepsilon_{tol} = 5 \cdot 10^{-5}$ for all computations for this test case. The average sample size is $n_{\text{train}} \approx 335$. In Fig. 2.22 the adaptive training set constructed with Algorithm 2.3.1 ADAPTIVEPARAMETERREFINEMENT is displayed. The scatter plot shows that the element indicator $\eta(g)$ detects the essential features of the solution, here induced by the heterogeneities in the source term around $x = 0.5$ and $x = 1.5$. Regarding the choice of I_0 and I_1, we observed a very low sensitivity of $\|e\|_V^{rel}$ with respect to the values of I_0 and I_1, being even lower than in test case 2. In contrast to test case 2 and 3, the relative model error $\|e_m\|_V$ decreases for increasing m_{max}, i_{max} and n_Ξ until it reaches the limit convergence rate $m^{-1.8}$, which can be observed in Fig. 2.23a for $m_{max} = 2$, $i_{max} = 2$ and growing n_Ξ. This can be

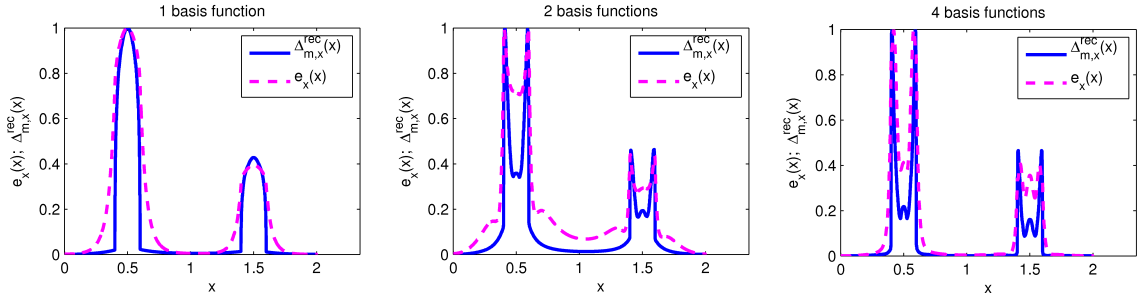

Figure 2.21: Test case 4: Comparison of $\Delta^{rec}_{m,x}(x)$ (solid) and $e_x(x)$ (dashed) for discrete reduced solutions p^H_m using $1, 2$ and 4 basis functions and $N_H = 640$, $n_h = 320$, $N_{H'} = 64$.

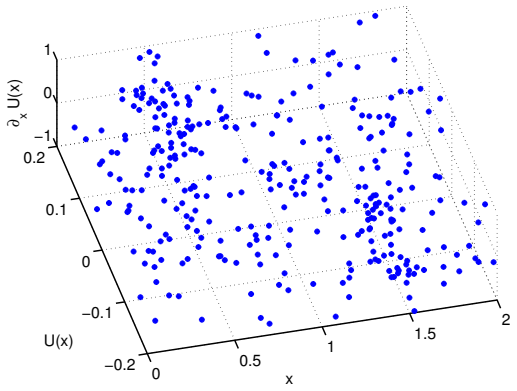

Figure 2.22: Test case 4: Adaptively refined training set generated by Algorithm 2.3.2 ADAPTIVE-HMR-POD.

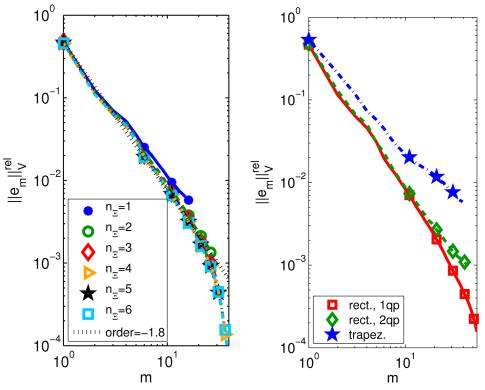

(a) $m_{max} = 2$, $i_{max} = 2$ (b) *Quadratures*

Figure 2.23: Test case 4: $\|e_m\|^{rel}_V$ for increasing n_Ξ (a) and different quadratures (b).

explained by the fact that each refinement of $\mathcal{D}$ around $x = 0.5$ and $x = 1.5$ seems to add relevant information to the discrete solution manifold Y^h_M (2.33) and thus improve the convergence rate of $\|e_m\|^{rel}_V$ until a certain saturation is reached. Comparing different quadrature rules in Fig. 2.23b we observe that the one point-rectangle rule yields the best convergence rate of $\|e_m\|^{rel}_V$ followed by the two point-rectangle formula, whereas for the three point-trapezoidal rule $\|e_m\|^{rel}_V$ exhibits a worse convergence rate of order -1.3. As moreover for the two point-rectangle formula Algorithm 2.3.1 refined for the second quadrature point the parts of $\mathcal{D}$, where s equals 0, we conclude that for the present test case it is best to construct Y^h_M using snapshots which contain only the information at one quadrature point in Ω_{1D}. Here, we have chosen $m_{max} = 1$, $i_{max} = 1$, $n_\Xi = 4$ for the two point-rectangle formula, $m_{max} = 2$, $i_{max} = 1$, $n_\Xi = 6$ for the trapezoidal rule, and $\theta = 0.025$ and $\sigma_{thres} = i_{max}\lceil diam(g)\rceil + 1$ for both of them.

We conclude the numerical experiments with some remarks on the choice of the input parameters of Algorithm 2.3.2. Test cases 1,2 and 4 demonstrate that it is sufficient to use the one point-rectangle formula (2.29) for purely diffusive problems, whereas for advection-dominated problems as the one in test case 3 quadrature rules of higher accuracy should be used. Due to its better performance in the test cases 3 and 4 the two point-rectangle formula seems to be preferable to the three point-

trapezoidal rule. We have observed a low sensitivity of the performance of the HMR-RB approach with respect to the choice of the intervals I_k, defined in §2.3.1 for intervals of length $0.1 - 20$, where the sign of the interval boundary seems to have no influence on the outcome. Using the one point-rectangle formula $m_{max} = 2$, $i_{max} = 2$ and $n_{\Xi} = 5, ..., 8$ yielded good result for all considered test cases. For the two point-rectangle formula $m_{max} = 1$, $i_{max} = 1$ and $n_{\Xi} = 4, ..., 8$ performed well.

Chapter 3

Application of the HMR-RB approach to nonlinear partial differential equations

This chapter is devoted to the adaption of the HMR-RB approach to nonlinear PDEs with a nonlinear operator $A : H_0^1(\Omega) \to H^{-1}(\Omega)$. The results are exemplified for the nonlinear diffusion equation with an elliptic and bounded nonlinearity. Due to the assumptions on A the obtained results also apply to the stationary Kirchhoff transformed Richards equation (cf. [16])

$$-\operatorname{div}(\nabla u + k(b^{-1}(u))\mathbf{g}) = 0.$$

Here, u is the so-called generalized pressure, k is the relative permeability, b^{-1} is the inverse of the Kirchhoff transformation and $\mathbf{g}$ denotes the gravity vector.
This chapter is organized as follows. First, we derive the reduced problem in the HMR setting and formulate a Newton method for the solution of the discrete reduced problem in Section 3.1. As the nonlinear operator A prevents the conduction of a dimensional reduction, we introduce the Empirical Projection Method (EPM) in Section 3.2. The key idea in the design of the EPM is to use an orthonormal expansion in a L^2-orthonormal basis on the transverse direction and approximate the integrals in the coefficients by an automatic numerical integration program based on the Empirical Interpolation Method [12]. This allows us to control the integration error in the coefficients and to derive rigorous a priori and a posteriori bounds. In this section we also give an overview on the literature on the Empirical Interpolation Method and its variants. In Section 3.3 we first formulate the HMR-RB approximation using the EPM for nonlinear PDEs. Afterwards, the derivation of a parametrized nonlinear 1D PDE and of parametrized 1D operator evaluations in the transverse direction is described. The reduction and collateral basis space are generated by Algorithm 3.3.3, which is subsequently introduced. In Section 3.4 we derive a reliable and efficient a posteriori error bound based on the Brezzi-Rappaz-Raviart theory [20, 23] extending the results in [27] from quadratically nonlinear to general nonlinear PDEs. By employing the a priori and a posteriori bounds for the EPM to estimate the error caused by the approximation of the nonlinear operator, we obtain a fully rigorous a posteriori error bound. As the requirements for the application of the error estimator based on the BRR-theory can be too restrictive for small ellipticity constants and thus small inf-sup stability factors, we derive a second error estimator similar to the one in [121], which is less sharp but whose requirements for the application are less strict. Again, we prove the reliability and effectivity of the error bound under certain assumptions. Finally, based on the results

in [41] we define a third error estimator which is particularly suited for degenerate equations as it does not depend on the inf-sup stability factor. However, to our best knowledge it cannot be proved that the latter is a reliable error bound. We close this section by proposing a method for the efficient computation of the inf-sup stability factor which is based on the ideas in [127]. In Section 3.5 we discuss the computational complexity of the HMR-RB approach in the nonlinear setting. In the numerical experiments in Section 3.6 we analyze the convergence behavior and the computational efficiency of the HMR-RB approach for the elliptic nonlinear diffusion equation. Furthermore, we investigate the reliability and effectivity of the proposed error estimators and test the applicability of the a priori and a posteriori bounds for the EPM. Finally, we study the applicability of the HMR-RB approach for decreasing ellipticity constants to get an idea of its performance for degenerate equations.

3.1 The Hierarchical Model Reduction framework for nonlinear partial differential equations

Let $\Omega \subset \mathbb{R}^2$ be a computational domain with Lipschitz boundary $\partial\Omega$. We follow the hierarchical model reduction framework introduced in [48, 102] and described in detail in §2.1 in Chapter 2 and therefore assume that Ω can be considered as a two-dimensional fiber bundle

$$\Omega = \bigcup_{x \in \Omega_{1D}} \{x\} \times \omega_x,$$

where $\Omega_{1D} =]x_0, x_1[$ denotes the computational domain in the dominant direction and ω_x is the fiber associated with $x \in \Omega_{1D}$. $\widehat{\omega} =]y_0, y_1[$ denotes the reference fiber in the transverse direction and the mapping $\psi(\cdot; x)$ is defined as $\psi(\cdot; x) : \omega_x \to \widehat{\omega}$ for $x \in \Omega_{1D}$. For the sake of simplicity we restrict ourselves in this chapter to homogeneous Dirichlet boundary conditions and choose the solution space $H_0^1(\Omega)$. We denote with $\langle \cdot, \cdot \rangle$ the dual pairing between $H^{-1}(\Omega)$ and $H_0^1(\Omega)$. Let $A : H_0^1(\Omega) \to H^{-1}(\Omega)$ be a nonlinear operator and $f \in H^{-1}(\Omega)$ a continuous linear form. We consider the nonlinear problem

$$\text{Find } p \in H_0^1(\Omega): \quad \langle A(p), v \rangle = \langle f, v \rangle \quad \forall v \in H_0^1(\Omega), \tag{3.1}$$

or, to shorten notations,

$$\text{Find } p \in H_0^1(\Omega): \quad \langle F(p), v \rangle = 0 \quad \forall v \in H_0^1(\Omega), \tag{3.2}$$

where $\langle F(p), v \rangle := \langle A(p), v \rangle - \langle f, v \rangle$. The problem (3.1) is denoted as the full problem and the existence and uniqueness of a solution $p \in H_0^1(\Omega)$ of (3.1) is assumed.

The following nonlinear diffusion equation will serve as a model problem for (3.1) in this whole chapter:

$$\langle A(p), v \rangle := \int_\Omega d(p) \nabla p \nabla v \, dxdy \quad \text{and} \quad \langle f, v \rangle := \int_\Omega sv \, dxdy \quad \forall p, v \in H_0^1(\Omega), \tag{3.3}$$

where $s \in L^2(\Omega)$ and $d : \mathbb{R} \to \mathbb{R}^+$ is in $C^2(\mathbb{R})$ and uniformly elliptic and bounded, i.e. there exist constants $c_k > 0$, $k = 0, 1, 2, 3$, such that

$$\begin{aligned} c_0 \|w\|^2 &\leq d(p) w \cdot w, \quad \|d(p)w\| \leq c_1 \|w\|, \\ \|d'(p)w\| &\leq c_2 \|w\|, \quad \|d''(p)w\| \leq c_3 \|w\|, \quad \forall w \in \mathbb{R}^2, \quad \forall p \in \mathbb{R}. \end{aligned} \tag{3.4}$$

Theorem 3.1. *The problem*

$$\text{Find } p \in H_0^1(\Omega): \quad \langle A(p), v\rangle = \langle f, v\rangle \quad \forall v \in H_0^1(\Omega), \tag{3.5}$$

for $A : H_0^1(\Omega) \to H^{-1}(\Omega)$ and $f \in H^{-1}(\Omega)$ as defined in (3.3) has a unique solution $p \in H_0^1(\Omega)$. Moreover, for $s \in L^\infty(\Omega)$, we have $p \in W_0^{2,q}(\Omega)$, $1 \le q < \infty$.

Proof. The existence and uniqueness of a solution $p \in H_0^1(\Omega)$ is proven in [35] with the aid of the Kirchhoff transformation $u(x,y) := \int_0^{p(x,y)} d(z)\,dz$ and the Lax-Milgram theorem. The improved regularity can be proven using standard elliptic regularity results as the function $\kappa(t) := \int_0^t d(z)\,dz$ is in $C^1(\mathbb{R}^+)$ and a monotone increasing function (cf. [23]), and we require that Ω has a Lipschitz boundary (cf. [4], p. 430). □

3.1.1 Formulation of the reduced problem

We introduce a set of L^2-orthonormal basis functions $\{\phi_k\}_{k\in\mathbb{N}} \in H_0^1(\widehat{\omega})$. At this point we assume that the basis functions $\{\phi_k\}_{k\in\mathbb{N}}$ are given to us. Possible choices are sine functions or Legendre polynomials [102] or a posteriori determined basis functions, whose construction will be described in §3.3. We combine the reduction space $Y_m := \text{span}(\phi_1, ..., \phi_m)$ with $H_0^1(\Omega_{1D})$ and define the reduced space

$$V_m = \left\{ v_m(x,y) = \sum_{k=1}^m \overline{v}_k(x)\,\phi_k(\psi(y;x)), \text{ with } \overline{v}_k(x) \in H_0^1(\Omega_{1D}),\, x \in \Omega_{1D},\, y \in \omega_x \right\}, \tag{3.6}$$

where

$$\overline{v}_k(x) = \int_{\widehat{\omega}} v_m(x, \psi^{-1}(\hat{y};x))\,\phi_k(\hat{y})\,d\hat{y}, \qquad k = 1, ..., m.$$

We use a Galerkin projection onto V_m and obtain the reduced problem:

$$\text{Find } p_m \in V_m: \quad \langle A(p_m), v_m\rangle = \langle f, v_m\rangle \quad \forall v_m \in V_m. \tag{3.7}$$

Exploiting the orthonormal expansion of p_m, namely, $p_m(x,y) = \sum_{k=1}^m \overline{p}_k(x)\,\phi_k(\psi(y;x))$, (3.7) can be rewritten as: Find $\overline{p}_k \in H_0^1(\Omega_{1D}), k = 1, ..., m$, such that

$$\left\langle A\left(\sum_{k=1}^m \overline{p}_k\phi_k\right), \xi\phi_l \right\rangle = \langle f, \xi\phi_l\rangle \;\; \forall\, \xi \in H_0^1(\Omega_{1D}) \text{ and } l = 1, ..., m. \tag{3.8}$$

To compute the coefficient functions $\overline{p}_l(x)$, $l = 1, ..., m$, we use the subdivision $\mathcal{T}_H$ of Ω_{1D} with elements $\mathcal{T}_i = (x_{i-1}, x_i)$ of width $H_i = x_i - x_{i-1}$ and maximal step size $H = \max_{\mathcal{T}_i} H_i$ defined in §2.1.3. We introduce an associated conforming Finite Element space $X^H \subset H_0^1(\Omega_{1D})$ with $\dim(X^H) = N_H < \infty$ and basis ξ_i^H, $i = 1, ..., N_H$. Moreover, we assume that for all $w \in H_0^1(\Omega_{1D})$ there exists a $w^H \in X^H$ such that $\lim_{H\to 0} \|w^H - w\|_{H^1(\Omega_{1D})} \to 0$ (density hypothesis). By combining X^H with Y_m we define the discrete reduced space

$$V_m^H = \left\{ v_m^H(x,y) = \sum_{k=1}^m \overline{v}_k^H(x)\,\phi_k(\psi(y;x)), \text{ with } \overline{v}_k^H(x) \in X^H,\, x \in \Omega_{1D},\, y \in \omega_x \right\}. \tag{3.9}$$

Using a Galerkin projection onto V_m^H and rewriting the discrete reduced solution p_m^H as $p_m^H(x,y) = \sum_{k=1}^m \overline{p}_k^H(x)\,\phi_k(\psi(y;x))$, we obtain the discrete reduced problem: Find $\overline{p}_k^H \in X^H$, $k = 1, ..., m$, such that

$$\left\langle A\left(\sum_{k=1}^m \overline{p}_k^H\phi_k\right), \xi_i^H\phi_l \right\rangle = \langle f, \xi_i^H\phi_l\rangle \qquad \text{for } i = 1, ..., N_H \text{ and } l = 1, ..., m. \tag{3.10}$$

The existence of solutions of (3.10) is assumed. We emphasize that in contrast to the case of linear PDEs described in Chapter 2 the integrals in the transverse direction in (3.10) cannot be precomputed due to the nonlinear operator A. This implies that (3.10) is still of full dimension. We finally use the coarse subdivision $\mathcal{T}_{H'}$ of Ω_{1D} defined in §2.1.3 and define an associated low-dimensional conforming FE space $X^{H'} \subset H_0^1(\Omega_{1D})$ with $\dim(X^{H'}) = N_{H'} < N_H < \infty$. $V_m^{H'}$ and $p_m^{H'}$ denote the coarse counterparts of V_m^H and p_m^H.

The reduced problem for the model problem (3.3) reads as follows

$$\text{Find } p_m \in V_m : \int_\Omega d(p_m)\nabla p_m \nabla v_m \, dx\, dy = \int_\Omega s\, v_m \, dx\, dy \quad \forall v_m \in V_m. \tag{3.11}$$

Furthermore we obtain the discrete reduced problem: Find $\overline{p}_k^H \in X^H, k = 1, ..., m$, such that

$$\sum_{n=1}^{m} \int_\Omega d\left(\sum_{k=1}^{m} \overline{p}_k^H \phi_k\right) \nabla(\overline{p}_n^H \phi_n)\nabla(\xi_i^H \phi_l)\, dx\, dy = \int_\Omega s\, \xi_i^H \phi_l \, dx\, dy \tag{3.12}$$
$$\text{for } i = 1, ..., N_H, \;\; l = 1, ..., m.$$

Theorem 3.2. *Under the assumptions of Theorem 3.1 there exists a reduced solution $p_m \in V_m$ of problem (3.11) and a discrete reduced solution $p_m^H \in V_m^H$ of (3.12).*

Proof. Let m be fixed. As d is uniform elliptic (3.4), we have that $\frac{\langle A(u),u\rangle}{\|u\|_{H^1(\Omega)}} \to \infty$ for $\|u\|_{H^1(\Omega)} \to \infty$. Therefore, we can infer as in the proof of the Theorem of Browder and Minty in [111], that there exists $R > 0$, such that for all $\|u\|_{H^1(\Omega)} \geq R$

$$\langle A(u), u\rangle \geq (1 + 2\|f\|_{H^{-1}(\Omega)})\|u\|_{H^1(\Omega)} > 0.$$

Thus for $\|p_m^H\|_{H^1(\Omega)} = R$ we have

$$\langle A(p_m^H), p_m^H\rangle - \langle f, p_m^H\rangle \geq (1 + \|f\|_{H^{-1}(\Omega)})\|p_m^H\|_{H^1(\Omega)} > 0.$$

As $d \in C^1(\mathbb{R})$ we can apply a technical corollary (cf. [49], p.493) of Brouwer's fixed point theorem to deduce that there exists a solution $p_m^H \in V_m^H$ of (3.12) with $\|p_m^H\|_{H^1(\Omega)} \leq R$ with R independent of H. The boundedness of d (3.4) then yields $\|A(p_m^H)\|_{H^{-1}(\Omega)} \leq c_1 R$. Due to these a priori bounds we may extract weakly converging subsequences $p_m^{H_j} \rightharpoonup p_m$ $(H_j \to 0)$ in $H^1(\Omega)$ and $A(p_m^{H_i}) \rightharpoonup c$ $(H_i \to 0)$ in $H^{-1}(\Omega)$. Finally, the density hypothesis on X^H and the compactness of the embedding of $H_0^1(\Omega)$ into $L^2(\Omega)$ yield the convergence of the Galerkin method for $H \to 0$ and the existence of a solution of (3.11). □

3.1.2 Solution of the discrete reduced problem with Newton's method

Problem (3.10) can be solved by Newton's method. However, for some problems as for instance the model problem (3.3) the mapping $F : H_0^1(\Omega) \to H^{-1}(\Omega)$ is not C^1. In order to take also such type of problems into account, we require that the mapping F, considered from $W_0^{1,p}(\Omega)$ into $W^{-1,p}(\Omega)$, $p \geq 2$, has a Fréchet derivative $F'(z) : W_0^{1,p}(\Omega) \to W^{-1,p}(\Omega)$ for $z \in W_0^{1,p}$, $p \geq 2$. We therefore demand that

$$\phi_k \in W^{1,p}(\widehat{\omega}) \cap H_0^1(\widehat{\omega}), \quad k = 1, ..., m, \quad \text{for } p \geq 2. \tag{3.13}$$

As $\bar{p}_k^H \in X^H \subset W_0^{1,t}(\Omega_{1D})$, $t \geq 1$, we obtain $p_m^H \in W_0^{1,p}(\Omega)$, $p \geq 2$. We remark that these assumptions include both the cases where $F : H_0^1(\Omega) \to H^{-1}(\Omega)$ is in C^1, and where F has to be

considered as a mapping from $W_0^{1,p}(\Omega)$ into $W^{-1,p}(\Omega)$, $p > 2$. Next, we define the inf-sup stability factor and the continuity constant

$$\beta_{\text{HMR}}(z_m^H) := \inf_{\substack{w_m^H \in V_m^H \\ |w_m^H|_{W^{1,p}(\Omega)} \neq 0}} \sup_{\substack{v_m^H \in V_m^H \\ |v_m^H|_{W^{1,q}(\Omega)} \neq 0}} \frac{\langle F'(z_m^H) w_m^H, v_m^H \rangle_{W^{-1,p}(\Omega) W^{1,q}(\Omega)}}{|w_m^H|_{W^{1,p}(\Omega)} |v_m^H|_{W^{1,q}(\Omega)}} \quad \text{for } z_m^H \in V_m^H, \tag{3.14}$$

$$\gamma_{\text{HMR}}(z_m^H) := \sup_{\substack{w_m^H \in V_m^H \\ |w_m^H|_{W^{1,p}(\Omega)} \neq 0}} \sup_{\substack{v_m^H \in V_m^H \\ |v_m^H|_{W^{1,q}(\Omega)} \neq 0}} \frac{\langle F'(z_m^H) w_m^H, v_m^H \rangle_{W^{-1,p}(\Omega) W^{1,q}(\Omega)}}{|w_m^H|_{W^{1,p}(\Omega)} |v_m^H|_{W^{1,q}(\Omega)}} \quad \text{for } z_m^H \in V_m^H, \tag{3.15}$$

where $\frac{1}{p} + \frac{1}{q} = 1$, and $\langle \cdot, \cdot \rangle_{W^{-1,p}(\Omega) W^{1,q}(\Omega)}$ denotes the duality pairing between $W^{-1,p}(\Omega)$ and $W^{1,q}(\Omega)$. Finally, $|v|_{W^{1,p}(\Omega)} := \|\nabla v\|_{L^p(\Omega)}$ designates the $W^{1,p}$-half norm, which is equivalent to the $W^{1,p}$-norm in $W_0^{1,p}(\Omega)$ due to Poincaré's inequality.

Assumption 3.3. *We assume that $F'(z_m^H) : W_0^{1,p}(\Omega) \to W^{-1,p}(\Omega)$ is uniformly bounded, i.e. there exists a constant $\gamma < \infty$, independent of m and H, such that $\gamma_{HMR}(z_m^H) < \gamma < \infty$ for all $z_m^H \in V_m^H$. Furthermore we assume local inf-sup stability, i.e. there exists a constant $\beta(m, H) > 0$, such that $\beta_{HMR}(z_m^H) > \beta(m, H) > 0$ for all $z_m^H \in B(p_m^H, R) \subset V_m^H$, where $B(p_m^H, R) := \{v \in V : |v - p_m^H|_{W^{1,p}} \leq R\}$ denotes the ball around the solution p_m^H of (3.10) of radius R.*

Then for a suitable initial datum $p_{m,H}^0$ we solve in each Newton step for the correction $\delta p_{m,H}^j$:

$$\begin{aligned} \langle F'(p_{m,H}^j)\, \delta p_{m,H}^j, v_m^H \rangle &= -\langle F(p_{m,H}^j), v_m^H \rangle \quad \forall v_m^H \in V_m^H, \quad j = 0, 1, 2, ... \\ \text{and update} \qquad p_{m,H}^{j+1} &= p_{m,H}^j + \sigma \delta p_{m,H}^j, \end{aligned} \tag{3.16}$$

where σ is a damping parameter. As the local inf-sup stability implies that F' is invertible in an environment of p_m^H, Assumption 3.3 implies the convergence of the Newton iteration to the solution p_m^H of (3.2) if the initial datum $p_{m,H}^0$ is close enough to p_m^H [113]. If we further assume that F' is Lipschitz continuous, i.e.

$$\|F'(v_m^H) - F'(w_m^H)\|_{W^{1,p}(\Omega), W^{-1,p}(\Omega)} \leq L_{\text{HMR}} |\, v_m^H - w_m^H \,|_{W^{1,p}(\Omega)}, \tag{3.17}$$

where $\|\cdot\|_{W^{1,p}(\Omega), W^{-1,p}(\Omega)}$ denotes the operator norm, we obtain that the Newton scheme (3.16) converges quadratically for an initial datum $p_{m,H}^0$ close to p_m^H and $\sigma = 1$ [113]. For the damped Newton scheme with line search we have a global linear convergence [113] if we further suppose global inf-sup stability, i.e. $\beta_{\text{HMR}}(z_m^H) > \beta(m, H) > 0$ for all $z_m^H \in V_m^H$.
To compute an approximation of p_m^H with the Newton scheme (3.16) we have to assemble in each Newton step the jacobian and the residual. However, due to the nonlinearity of the operator A the integrals in the transverse direction cannot be precomputed. Hence, the assembling of the jacobian and the residual requires the computation of two-dimensional integrals, which is why solving for p_m^H is still a full dimensional problem. In order to obtain a one-dimensional problem in the dominant direction we introduce in the next section §3.2 the Empirical Projection Method and apply it in the HMR-RB framework in §3.3.1.

As indicated at the beginning of this subsection the mapping $F : H_0^1(\Omega) \to H^{-1}(\Omega)$ of our model problem (3.3) is in general not C^1. Thus we consider instead $F : W_0^{1,p}(\Omega) \to W^{-1,p}(\Omega)$ with $2 < p < \infty$:

$$\langle F(w), v \rangle_{W^{-1,p}(\Omega) W_0^{1,q}(\Omega)} = \int_\Omega d(w) \nabla w \nabla v \, dxdy - \int_\Omega sv \, dxdy, \quad \forall w \in W_0^{1,p}(\Omega), \ \forall v \in W_0^{1,q}(\Omega). \tag{3.18}$$

Denoting with $L(W,Z)$ the space of continuous linear mappings from the Banach space W into the Banach space Z and with $C^1(W,Z)$ the space of functions that are continuous differentiable for all $w \in W$, we obtain the following result.

Theorem 3.4. *Under the hypotheses of Theorem 3.1, the mapping $F : W_0^{1,p}(\Omega) \to W^{-1,p}(\Omega)$ is in $C^1(W_0^{1,p}(\Omega), W^{-1,p}(\Omega))$ for $2 < p < \infty$ and for the solution p of (3.3) the Fréchet derivative $F'(p) \in L(W_0^{1,p}(\Omega), W^{-1,p}(\Omega))$ is an isomorphism. Furthermore, there exist constants γ_{mod}, β_{mod} and L_{mod} such that*

$$0 < \beta_{mod} \leq \inf_{\substack{w \in W_0^{1,p}(\Omega) \\ |w|_{W^{1,p}(\Omega)} \neq 0}} \sup_{\substack{v \in W_0^{1,q}(\Omega) \\ |v|_{W^{1,q}(\Omega)} \neq 0}} \frac{\langle F'(p)w, v\rangle_{W^{-1,p}(\Omega)W_0^{1,q}(\Omega)}}{|w|_{W^{1,p}(\Omega)}|v|_{W^{1,q}(\Omega)}}, \tag{3.19}$$

$$\text{and} \quad \infty > \gamma_{mod} \geq \sup_{\substack{w \in W_0^{1,p}(\Omega) \\ |w|_{W^{1,p}(\Omega)} \neq 0}} \sup_{\substack{v \in W_0^{1,q}(\Omega) \\ |v|_{W^{1,q}(\Omega)} \neq 0}} \frac{\langle F'(z)w, v\rangle_{W^{-1,p}(\Omega)W_0^{1,q}(\Omega)}}{|w|_{W^{1,p}(\Omega)}|v|_{W^{1,q}(\Omega)}} \quad \forall z \in W_0^{1,p}(\Omega), \tag{3.20}$$

$$\|F'(v) - F'(w)\|_{W^{1,p}(\Omega),W^{-1,p}(\Omega)} \leq L_{mod} |\, v - w \,|_{W^{1,p}(\Omega)}. \tag{3.21}$$

Proof. As $W^{1,p}(\Omega) \hookrightarrow C^0(\Omega)$ for $p > 2$ and $\Omega \subset \mathbb{R}^2$ (cf. [49], p. 270), it is easy to prove that under the assumptions on d (3.4), $F \in C^1(W_0^{1,p}(\Omega), W^{-1,p}(\Omega))$. The Fréchet derivative can be determined as

$$\begin{aligned} \langle F'(z)w, v\rangle_{W^{-1,p}(\Omega)W_0^{1,q}(\Omega)} &= \int_\Omega d'(z)w\nabla z\nabla v + d(z)\nabla w\nabla v \, dxdy \\ &= \int_\Omega \nabla(d(z)w)\nabla v \, dxdy \quad \forall z, w \in W_0^{1,p}(\Omega), \ \ \forall v \in W_0^{1,q}(\Omega). \end{aligned} \tag{3.22}$$

Again employing the assumptions on d (3.4) we obtain that (3.20) and (3.21) apply, where

$$\begin{aligned} \gamma_{\text{mod}} &= c_2 c_s (1 + c_p^p)^{1/p} |\, z \,|_{W^{1,p}(\Omega)} + c_1, \\ L_{\text{mod}} &= c_s (1 + c_p^p)^{1/p} (2c_2 + c_3 c_s (1 + c_p^p)^{1/p}) \min\{|\, v \,|_{W^{1,p}(\Omega)}, |\, w \,|_{W^{1,p}(\Omega)}\}. \end{aligned}$$

Here, c_k, $k = 0, ..., 3$, are the ellipticity and continuity constants of d, defined in (3.4), c_p is the constant in Poincaré's inequality and c_s denotes the Sobolev embedding constant in the estimate $\|v\|_{C^{0,1-(2/p)}(\Omega)} \leq c_s \|v\|_{W^{1,p}(\Omega)}$. As the Laplacian operator with homogeneous boundary conditions is an isomorphism from $W_0^{1,p}(\Omega)$ onto $W^{-1,p}(\Omega)$ [105] we infer that $F'(p) \in L(W_0^{1,p}(\Omega), W^{-1,p}(\Omega))$ is an isomorphism and hence (3.19). For details see [105]. □

Remark 3.5. *Following the argumentation in [105], one can prove by using the Hahn-Banach theorem that $F'(p) \in L(W_0^{1,p}(\Omega), W^{-1,p}(\Omega))$ admits a continuous extension from $H_0^1(\Omega)$ into $H^{-1}(\Omega)$. The Lax-Milgram theorem then yields that the Laplacian operator is an isomorphism from $H_0^1(\Omega)$ onto $H^{-1}(\Omega)$ and thus, that $F'(p)$ is an isomorphism from $H_0^1(\Omega)$ onto $H^{-1}(\Omega)$. Hence, we obtain*

$$\inf_{\substack{w \in H_0^1(\Omega) \\ |w|_{H^1(\Omega)} \neq 0}} \sup_{\substack{v \in H_0^1(\Omega) \\ |v|_{H^1(\Omega)} \neq 0}} \frac{\langle F'(p)w, v\rangle}{|w|_{H^1(\Omega)}|v|_{H^1(\Omega)}} \geq \beta_{mod}^{H^1} > 0. \tag{3.23}$$

3.2 The Empirical Projection Method (EPM)

As noted in the previous section the nonlinearity of the operator $A : H_0^1(\Omega) \to H^{-1}(\Omega)$ in (3.10) prevents a dimensional reduction of the full problem. The goal of this section is thus to derive an efficient approximation of possibly non-smooth nonlinear operators $A : H_0^1(\Omega) \to H^{-1}(\Omega)$ allowing for the derivation of a lower dimensional coupled system for the coefficients $\bar{p}_l^H \in X^H$. Due to the Theorem on the characterization of H^{-1} (cf. [49], p. 283) there exist functions $u_1, u_2 \in L^2(\Omega)$ such that

$$\langle A(z), v\rangle = \int_\Omega u_1\, \partial_x v + u_2\, \partial_y v \, dx\, dy \quad \text{for } v, z \in H_0^1(\Omega). \tag{3.24}$$

For the sake of clarity we restrict our exposition in this section to functions $u \in L^2(\Omega)$, which are either given or can be identified with $A(z) \in H^{-1}(\Omega)$, $z \in H_0^1(\Omega)$, $A : H_0^1(\Omega) \to H^{-1}(\Omega)$, via (3.24). In the latter case, the Empirical Projection Method has to be applied to u_1 and u_2 separately. The key idea in the design of the Empirical Projection Method (EPM) is to use an orthonormal expansion in L^2-orthonormal basis functions $\{\kappa_n\}_{n\in\mathbb{N}} \in L^2(\widehat{\omega})$ and approximate the integrals $\int_{\widehat{\omega}} u\, \kappa_n \, d\hat{y}$ by an automatic numerical integration program based on the Empirical Interpolation Method [12]. The main novelty is that we are able to prove rigorous a priori and a posteriori bounds in the continuous setting for the Empirical Projection Method, which do not require additional regularity of u. Next, we describe the construction of the EPM in detail and subsequently derive the error bounds. Let $W_K := \{u(\mu, \hat{y}),\, \mu \in \Xi_{1D}\}$ be a given set of snapshots of the function u, where $\Xi_{1D} \subset \Omega_{1D}$ is a finite dimensional train sample of size $|\Xi_{1D}| = n$. The orthonormal basis functions $\{\kappa_n\}_{n=1}^k \in L^2(\widehat{\omega})$, the so-called collateral basis, is then computed by a POD and the collateral basis space $W_k = \text{span}\{\kappa_1, ..., \kappa_k\}$ is thus defined as

$$W_k = \arg \inf_{\substack{\tilde{W}_k \subset \text{span}\{W_K\} \\ \dim(\tilde{W}_k)=k}} \left(\frac{1}{n} \sum_{\mu\in\Xi_{1D}} \inf_{\tilde{w}_k \in \tilde{W}_k} \|u(\mu, \cdot) - \tilde{w}_k\|^2_{L^2(\widehat{\omega})} \right). \tag{3.25}$$

In case u can be identified with $A(z) \in H^{-1}(\Omega)$, $z \in H_0^1(\Omega)$, $A : H_0^1(\Omega) \to H^{-1}(\Omega)$, we will introduce a new ansatz for the derivation of the snapshot set W_K and thus the collateral basis functions $\{\kappa_n\}_{n=1}^k$ in the next section §3.3.

For the orthogonal projection

$$P_k[u](x, y) := \sum_{n=1}^k \int_{\widehat{\omega}} u(x, \psi^{-1}(\hat{y}; x))\, \kappa_n(\hat{y})\, d\hat{y}\ \kappa_n(\psi(y; x)) \tag{3.26}$$

of u onto $\mathcal{W}_k := \left\{ w_k(x, y) = \sum_{n=1}^k \tilde{w}_n(x)\kappa_n(\psi(y; x)),\ \ \tilde{w}_n(x) \in L^2(\Omega_{1D}),\, x \in \Omega_{1D},\, y \in \widehat{\omega} \right\}$ we have

$$\|u - P_k[u]\|_{L^2(\Omega)} = \inf_{w_k\in\mathcal{W}_k} \|u - w_k\|_{L^2(\Omega)}. \tag{3.27}$$

Thus the coefficients $\int_{\widehat{\omega}} u(x, \psi^{-1}(\hat{y}; x))\, \kappa_n(\hat{y})\, d\hat{y}$, $n = 1, ..., k$, are optimal in a L^2-sense and in order to compute $P_k[u]$ we have to find an efficient quadrature formula for the integrals $\int_{\widehat{\omega}} u(x, \psi^{-1}(\hat{y}; x))$ $\kappa_n(\hat{y})\, d\hat{y}$, $n = 1, ..., k$. Here, we use the term efficient in the sense that a quadrature formula is more efficient than another if it requires less evaluations of u to achieve the same accuracy. As standard Newton-Cotes formulae lack efficiency and the computation of generalized Gaussian quadratures requires, at least to our knowledge, that the basis functions $\{\kappa_n\}_{n=1}^k$ form a Chebychev

Algorithm 3.2.1: Empirical interpolation - Construction of the interpolation points

EIM(W_k,$\widehat{\omega}$)

Set

$$t_1 := \arg \operatorname*{ess\,sup}_{y \in \widehat{\omega}} |\kappa_1(\hat{y})|, \quad \zeta_1 = \frac{\kappa_1}{\kappa_1(t_1)}, \quad \text{and} \quad B^1_{11} = 1.$$

for $l = 1, \ldots, k$ **do**

Solve for the coefficients σ_j^{l-1}:

$$\sum_{j=1}^{l-1} \sigma_j^{l-1} \zeta_j(t_i) = \kappa_l(t_i), \;\; i = 1, ..., l-1.$$

Compute the residual

$$r_l(\hat{y}) := \kappa_l(\hat{y}) - \sum_{j=1}^{l-1} \sigma_j^{l-1} \zeta_j(\hat{y}).$$

Set

$$t_l = \arg \operatorname*{ess\,sup}_{y \in \widehat{\omega}} |r_l(\hat{y})|, \quad \zeta_l = \frac{r_l}{r_l(t_l)}, \quad \text{and} \quad B^l_{ij} = \zeta_j(t_i), \quad 1 \leq i, j \leq l.$$

end

return T_k, $Z_k := \{\zeta_1, ..., \zeta_k\}$, B^k

system[1] [79, 128], which is in general not the case, we have to pursue a more subtle approach. We propose to approximate the function u in the integrals by an empirical Lagrangian interpolant $\mathcal{I}_L[u]$, where the interpolation points are determined using the Empirical Interpolation Method (EIM), introduced in [12] and analyzed more detailed in [59, 80, 118]. The EIM was originally introduced in [12] as a strategy to determine an efficient offline-online decomposition of a bilinear or linear form in a parametrized PDE in the case of a non-affine parameter dependence. The idea is to approximate a non-affine parametrized data function $g : \Omega \times \mathcal{D} \to \mathbb{R}$, $g(\cdot; \mu) \in L^\infty(\Omega)$, with a Lagrangian interpolant $\mathcal{I}_L[g] = \sum_{n=1}^{L} \gamma_n(\mu)\zeta_n(x)$, such that already for a very small number L a high accuracy can be achieved. To this end the collateral basis space W_k is computed by a greedy algorithm of the same type as Algorithm 2.2.1. The construction of the interpolation points $T_k := \{t_1, ..., t_k\}$, sometimes also called 'magic points' [80], for the collateral space W_k over $\widehat{\omega}$ is decribed in Algorithm 3.2.1. Here, we have simplified the notation by setting $\kappa_l(t_i) := \lim_{\varepsilon \to 0} \frac{1}{|B_\varepsilon(t_i)|} \int_{B_\varepsilon(t_i)} \kappa_l(\hat{y})\, d\hat{y}$. We remark that we compute the space W_k by a POD, as the POD is optimal in a L^2-sense (cf. 2.2.1), which better fits our goal to approximate u with respect to the L^2-norm. The following lemma collects some well-known statements on the EIM.

Lemma 3.6. *Let the collateral basis space W_k be given and the set of interpolation points T_k be constructed by Algorithm 3.2.1. Then we have*

1. *The matrix B is invertible. As a consequence the construction of the interpolation points T_k is well-defined.*

[1] Following Karlin and Studden [71] a collection of k real-valued continuous functions $q_1, ..., q_k$ defined on an interval $I \subset \mathbb{R}$ is a Chebyshev system if any nontrivial linear combination, i.e. a combination where not all coefficients are zero, has at most $k-1$ distinct zeros in I.

2. The interpolation is exact for all $w \in W_k$.

Proof. The proof of 1. can be found in [12] and for the proof of 2. see [80]. □

We remark that constructing the interpolation points T_k with the 'best points' interpolation method [87] is also an option. But as the computation of the 'best points' requires the solution of a least-squares minimization problem, which has to be solved in the context of HMR-RB for every parameter value in the train sample Ξ_{train} (see §3.3.5), we have opted for the EIM.

Algorithm 3.2.2: Empirical Projection Method

1 EPM(W_k, W_K, $\varepsilon_{\text{tol}}^{\text{int}}$, $N_{\max}^{\text{int}}$, Ξ_{1D})
2 **Initialize** $I = \widehat{\omega}$, and $a^I = y_0$, $b^I = y_1$.
3 Compute $[T_k^I, Z_k^I, B_k^I]$= EIM(W_k,I).
4 **for** $j = 1, ..., N_{max}^{int}$ **do**
5 **foreach** $I \in \mathfrak{I}$ **do**
6 Compute

$$e_j^I := \frac{1}{n} \sum_{\mu \in \Xi_{1D}} \| \sum_{l=1}^{k} \int_{\widehat{\omega}} (u(\mu, \hat{y}) - \mathcal{I}_L[u](\mu, \hat{y})) \kappa_l(\hat{y}) \, d\hat{y} \, \kappa_l \|_{L^2(I)}^2 \tag{3.28}$$

7 **if** $e_j^I \leq \frac{|I|}{|\widehat{\omega}|} \cdot \varepsilon_{tol}^{int}$ **then**
8 **Continue**
9 **else**
10 Set
11 $I_{left} := [a^I, (a^I + b^I)/2]$,
12 $I_{right} := [(a^I + b^I)/2, b^I]$.
13 Compute
14 $[T_k^{I_{left}}, Z_k^{I_{left}}, B_k^{I_{left}}] = \text{EIM}(W_k|_{I_{left}}, I_{left})$,
15 $[T_k^{I_{right}}, Z_k^{I_{right}}, B_k^{I_{right}}] = \text{EIM}(W_k|_{I_{right}}, I_{right})$,
16 Update $\mathfrak{I}$
17 **end**
18 **end**
19 Set $e_{\text{int}} = \sum_{I \in \mathfrak{I}} e_j^I$.
20 **if** $e_{int} \leq \varepsilon_{tol}^{int}$ **then**
21 **Break**
22 **end**
23 **end**
24 **return** $T_k^{\mathfrak{I}}$, $Z_k^{\mathfrak{I}}$, $B_k^{\mathfrak{I}}$, e_{int}.

To formulate an adaptive integration algorithm and thus the Empirical Projection Method 3.2.2, we introduce a non-uniform partition $\mathfrak{I}$ of $\widehat{\omega}$ with cells I. a^I and b^I denote the left and right interval boundary of I, respectively. We first compute the standard EIM for the whole reference fiber $\widehat{\omega}$ in line 3. If the integration error

$$e_j^{\widehat{\omega}} := \frac{1}{n} \sum_{\mu \in \Xi_{1D}} \| \sum_{l=1}^{k} \int_{\widehat{\omega}} (u(\mu, \hat{y}) - \mathcal{I}_L[u](\mu, \hat{y})) \kappa_l(\hat{y}) \, d\hat{y} \, \kappa_l \|_{L^2(\widehat{\omega})}^2,$$

is smaller then the prescribed tolerance $\varepsilon_{\text{tol}}^{\text{int}}$ we stop without refining at all. Otherwise we bisect in each iteration those intervals for which $e_j^I > (|I|/|\widehat{\omega}|)\cdot\varepsilon_{\text{tol}}^{\text{int}}$ holds. On the new intervals we perform the EIM to contruct the local interpolants $\mathcal{I}_L^{I_{left}}[u]$ and $\mathcal{I}_L^{I_{right}}[u]$. We stop either if $e_{\text{int}} = \sum_{I\in\mathfrak{I}} e_j^I \leq \varepsilon_{\text{tol}}^{\text{int}}$ or if the maximal number of iterations $N_{\max}^{\text{int}}$ is reached. The approximation of u can then be computed as

$$P_k^L[u](x,y) := \sum_{n=1}^{k} \int_{\widehat{\omega}} \mathcal{I}_L[u](x,\psi^{-1}(\hat{y};x))\,\kappa_n(\hat{y})\,d\hat{y}\;\kappa_n(\psi(y;x)), \tag{3.29}$$

where

$$\mathcal{I}_L[u](x,\psi^{-1}(\hat{y};x)) := \sum_{l=1}^{L} u(x,t_l)\vartheta_l(\hat{y}), \tag{3.30}$$

and the ϑ_l fulfill $\vartheta_l(t_i) = \delta_{i,l}$ for all $t_i \in T_k^{\mathfrak{I}}$. The ϑ_l are computed on the respective interval $I \in \mathfrak{I}$ as $\sum_{l=1}^{k} B_{il}^I \vartheta_l^I = \zeta_i^I$, $i = 1,...,k$, and extended by zero to the other intervals $I \in \mathfrak{I}$. We have proven in §B.1 in the discrete setting under certain additional assumptions the convergence of Algorithm 3.2.2. Unfortunately the used technique cannot be applied in the continuous setting. For the EIM, at least to our knowledge, only one a priori result has been proven until now (cf. [80]), which cannot be invoked either as the proof heavily relies on the fact that the collateral basis functions are chosen as $\zeta_l := \arg\max_{w_K\in W_K} \|w_K - \mathcal{I}_{l-1}[w_K]\|_{L^\infty(\widehat{\omega})}$. As numerical experiments for the EIM and also the quadrature formula based on the EIM yield very good convergence results (see amongst others [43, 59, 80] for the former and §3.6 for the latter), we expect that the employed quadrature formula indeed converges. If Algorithm 3.2.2 EPM does not converge, the integration error e_{int} is returned and can be used to derive fully rigorous a priori and a posteriori bounds (§3.2.1). Before moving to this subject we compare the EPM to some related methods.

It has been demonstrated in [119] for the so-called Least-Squares Empirical Interpolation Method, that for functions lacking spatial regularity, choosing $L > k$ can improve the convergence rate of the EIM significantly. Here, a least-squares problem is solved to fit the coefficients to additional interpolation points. We emphasize that in contrast to the Least-Squares Empirical Interpolation Method, the interpolant $\mathcal{I}_L[u]$ (3.30) still fulfills $\mathcal{I}_L[u](x,\psi^{-1}(t_i;x)) = u(x,\psi^{-1}(t_i;x))$, $i = 1,\dots,L$, as it is computed locally by a EIM. Thus, the properties collected in Lemma 3.6 still apply locally. Compared to the EIM, the EPM might seem inefficient as it requires the computation of the additional integrals over $\widehat{\omega}$ in (3.29). However, for the special case $k = L$, we have the following lemma.

Lemma 3.7. *Let the collateral basis space W_k be given and let the set of interpolation points T_k be computed by Algorithm 3.2.1. Then the computation of $P_k^L[u]$ with Algorithm 3.2.2 and $N_{max}^{int} = 0$ is equivalent to the Proper Orthogonal Interpolation Method (POIM) introduced in [119] and yields the same approximation as the Discrete Empirical Interpolation Method (DEIM), which has been introduced in [31] and is described in Algorithm B.1.1 in §B.1.*

Proof. First, we note that in [119] the application of the EIM for a POD basis is denoted as Proper Orthogonal Interpolation Method (POIM), which yields for $k = L$ $\mathcal{I}_L[u]$ in (3.29). Furthermore, it is shown in [119] that the DEIM and the POIM yield the same interpolant and the same interpolation points. For the sake of completeness we invoke the main steps of the proof. Obviously t_1 is the same for both methods. We then proceed by induction and assume that the two methods result in the same set of interpolation points T_{k-1}. As both the POIM basis $\{\zeta_1,...,\zeta_k\}$ and the DEIM basis $\{\kappa_1,...,\kappa_k\}$ span the same space, there exists a matrix M such that $Z_{k-1} = W_{k-1}\cdot M$, which implies $(\zeta_j(t_i))_{i,j=1}^{k-1} = (\kappa_j(t_i))_{i,j=1}^{k-1}\cdot M$ and thus that the interpolants coincide for $k-1$. Finally,

both methods maximize the same residual to compute t_k and thus yield the same set of interpolation points T_k. Due to the orthonormality of the collateral basis $\{\kappa_l\}_{l=1}^k$ the integrals in (3.29) disappear and using the transformation matrix M we end up with a POIM approximation. □

We finally remark that the DEIM has been introduced in [31] for the interpolation of discrete operators in nonlinear systems of ordinary differential equations coming for instance from the discretization of a nonlinear PDE with a finite difference scheme. The DEIM is very similar to the Gauss-Newton with Approximated Tensors (GNAT) method [28–30], which uses a gappy POD method [50] and the more general Empirical Operator Interpolation Method [42, 43], designed for the interpolation of discrete nonlinear operators stemming from the discretization of a nonlinear PDE by for example a finite volume scheme or a discontinuous Galerkin method.

3.2.1 Rigorous a priori and a posteriori error analysis for the EPM

First, we derive a rigorous a priori bound for the EPM. In [72, 73] Kunisch and Volkwein derived error estimates for a POD-Galerkin approximation of parabolic nonlinear PDEs, where the POD is applied to snapshots of the solution for different instants of time. The respective estimates contain both the standard discretization and the POD error. This approach has been applied in [32] for the DEIM in the discrete setting for systems of nonlinear ODEs. To control the projection error $\|u - P_k[u]\|_{L^2(\Omega)}$ by the POD error (2.22) we interpret the discrete L^2-norm occurring in the definition of the POD-space (3.25) as a numerical approximation of the corresponding integral with the Monte Carlo method, which is one new contribution of the proof, and subsequently use ideas of Kunisch and Volkwein [73]. The main new contribution of Theorem 3.8 is the control of the term $\|P_k[u] - P_k^L[u]\|_{L^2(\Omega)}$, which is possible because of the design of the EPM and again the usage of the Monte Carlo method. We obtain the following result.

Theorem 3.8 (An a priori error bound for the EPM)**.** *We assume that the parameter values $\mu \in \Xi_{1D}$ are sampled from the uniform distribution over Ω_{1D} and denote with $\{\lambda_l^n\}_{l=1}^{d(n)}$ the set of eigenvalues of the correlation matrix eigenvalue problem that is equivalent to the optimization problem* (3.25)*. If Algorithm 3.2.2 converges till the given tolerance ε_{tol}^{int}, there exists an N such that for all $n > N$*

$$\|u - P_k^L[u]\|_{L^2(\Omega)} \leq \left(\sum_{l=k+1}^{d(n)} \lambda_l^n \right)^{1/2} + (\varepsilon_{tol}^{int})^{1/2} + \mathcal{O}(n^{-1/4}). \tag{3.31}$$

If furthermore $\lambda_k^{I,\infty} \neq \lambda_{k+1}^{I,\infty}$ there exists an N such that for all $n > N$

$$\|u - P_k^L[u]\|_{L^2(\Omega)} \leq \sqrt{2} \left(\sum_{l=k+1}^{\infty} \lambda_l^{\infty} \right)^{1/2} + (\varepsilon_{tol}^{int})^{1/2} + \mathcal{O}(n^{-1/4}), \tag{3.32}$$

and $\lambda_l^n \to \lambda_l^{\infty}$ for $1 \leq l \leq k$ as $n \to \infty$ and $\lim_{n\to\infty} \kappa_l^n = \kappa_l^{\infty}$ for $1 \leq l \leq k$, where $\{\lambda_l^{\infty}\}_{l=1}^{\infty}$ are the eigenvalues and κ_l^{∞} are the eigenfunctions of the operator $B : L^2(\widehat{\omega}) \to L^2(\widehat{\omega})$, defined as

$$B(v) = \int_{\Omega_{1D}} \int_{\widehat{\omega}} v(\hat{y}) u(x, \hat{y}) \, d\hat{y} \, u(x, \hat{y}) \, dx \quad \text{for } v \in L^2(\widehat{\omega}). \tag{3.33}$$

If Algorithm 3.2.2 stops at iteration N_{max}^{int} without reaching the prescribed tolerance ε_{tol}^{int}, there exists

an N such that for all $n > N$

$$\|u - P_k^L[u]\|_{L^2(\Omega)} \leq \left(\sum_{l=k+1}^{d(n)} \lambda_l^n \right)^{1/2} + e_{int}^{1/2} + \mathcal{O}(n^{-1/4}). \tag{3.34}$$

If furthermore $\lambda_k^{I,\infty} \neq \lambda_{k+1}^{I,\infty}$ there exists an N such that for all $n > N$

$$\|u - P_k^L[u]\|_{L^2(\Omega)} \leq \sqrt{2} \left(\sum_{l=k+1}^{\infty} \lambda_l^{\infty} \right)^{1/2} + e_{int}^{1/2} + \mathcal{O}(n^{-1/4}). \tag{3.35}$$

Proof. We start by splitting the error in a projection error and an integration error:

$$\|u - P_k^L[u]\|_{L^2(\Omega)} \leq \|u - P_k[u]\|_{L^2(\Omega)} + \|P_k[u] - P_k^L[u]\|_{L^2(\Omega)}. \tag{3.36}$$

Due to the assumptions on Ξ_{1D}, we can interpret for an arbitrary function $f \in L^2(\Omega)$, the term $I_n(f) := (1/n) \sum_{\mu \in \Xi_{1D}} \|f(\mu, \cdot)\|^2_{L^2(\widehat{\omega})}$ as a numerical approximation of the integral $I(f) = \int_{\Omega_{1D}} \int_{\widehat{\omega}} f^2 \, d\hat{y} \, dx$ with the Monte Carlo method [22, 107]. Thus the strong law of large numbers ensures with probality 1 the convergence of $I_n(f)$ to $I(f)$ as $n \to \infty$ with a convergence rate of $\mathcal{O}(n^{-1/2})$ [22,107]. This yields together with the definition of the POD-error (2.22) that there exists an N such that for all $n > N$

$$\begin{aligned}
\|u - P_k[u]\|^2_{L^2(\Omega)} &= \left(\frac{1}{n} \sum_{\mu \in \Xi_{1D}} \|u(\mu, \cdot) - \sum_{l=1}^{k} \int_{\widehat{\omega}} u(\mu, \hat{y}) \kappa_l(\hat{y}) \, d\hat{y} \, \kappa_l \|^2_{L^2(\widehat{\omega})} \right) + \mathcal{O}(n^{-1/2}) \\
&\leq \left(\sum_{l=k+1}^{d(n)} \lambda_l^n \right) + \mathcal{O}(n^{-1/2}).
\end{aligned}$$

Approximating also the integral of the second term in (3.36) with a Monte Carlo method and using the outcome of Algorithm 3.2.2, we obtain

$$\begin{aligned}
&\|P_k[u] - P_k^L[u]\|^2_{L^2(\Omega)} \\
&\quad = \left(\frac{1}{n} \sum_{\mu \in \Xi_{1D}} \| \sum_{l=1}^{k} \int_{\widehat{\omega}} u(\mu, \hat{y}) \kappa_l(\hat{y}) \, d\hat{y} \, \kappa_l - \sum_{l=1}^{k} \int_{\widehat{\omega}} \mathcal{I}_L[u(\mu, \hat{y})] \kappa_l(\hat{y}) \, d\hat{y} \, \kappa_l \|^2_{L^2(\widehat{\omega})} \right) + \mathcal{O}(n^{-1/2}) \\
&\quad = \left(\frac{1}{n} \sum_{\mu \in \Xi_{1D}} \| \sum_{l=1}^{k} \int_{\widehat{\omega}} (u(\mu, \hat{y}) - \mathcal{I}_L[u(\mu, \hat{y})]) \kappa_l(\hat{y}) \, d\hat{y} \, \kappa_l \|^2_{L^2(\widehat{\omega})} \right) + \mathcal{O}(n^{-1/2}) \\
&\quad \leq e_{\text{int}} + \mathcal{O}(n^{-1/2}).
\end{aligned}$$

The operator $T : L^2(\widehat{\omega}) \to L^2(\Omega_{1D})$, defined as

$$(Tv)(x) := \int_{\widehat{\omega}} u(x, \hat{y}) v(\hat{y}) \, d\hat{y}, \quad \text{for } v \in L^2(\widehat{\omega}),$$

is a Hilbert-Schmidt integral operator and thus compact [4]. Boundedness of the operator $\mathcal{Y} : L^2(\Omega_{1D}) \to L^2(\widehat{\omega})$, defined as

$$\mathcal{Y}(w) := \int_{\Omega_{1D}} u(x, \hat{y}) w(x) \, dx, \quad \text{for } w \in L^2(\Omega_{1D}),$$

yields that B is a compact operator as well. The remaining assertions can then be proven completely analogous to the argumentation in subsection 3.2 of [73]. □

We remark that the assumptions on Ξ_{1D} can be weakened in the sense that also an adaptive sampling strategy can be considered. This can change the convergence rate of the Monte Carlo method, but does not affect the proof of Theorem 3.8. Alternatively, a quasi-Monte Carlo method, based on quasi-random points, can be used, which has an improved convergence rate of approximately $\mathcal{O}((\log n)^c n^{-1})$ for some constant c [22]. Next, we employ the a priori bounds (3.31) and (3.34) in Theorem 3.8 to derive a rigorous a posteriori bound by using a better approximation $P_{k'}^{L'}[u]$ and considering the error $\|P_{k'}^{L'}[u] - P_k^L[u]\|_{L^2(\Omega)}$. This idea, sometimes called the M'-trick, has been introduced in [43] and applied within the context of DEIM in [127] and POIM in [119]. We emphasize that in contrast to the cited works the a posteriori error bound we will derive is completely rigorous due to the application of the a priori bound of Theorem 3.8 for the determination of a suitable better approximation $P_{k'}^{L'}[u]$.

Proposition 3.9 (An a posteriori error bound for the EPM)**.** *Let the assumptions of Theorem 3.8 be fulfilled and let ε_{tol} be a given tolerance. Then the error estimator*

$$\Delta^{EPM} := \|P_{k'}^{L'}[u] - P_k^L[u]\|_{L^2(\Omega)} \tag{3.37}$$

satisfies

$$\|u - P_k^L[u]\|_{L^2(\Omega)} \leq \varepsilon_{tol} + \Delta^{EPM} + e_{int}^{1/2} + \mathcal{O}(n^{-1/4}), \tag{3.38}$$

where k' can be automatically chosen by employing the a priori bounds of Theorem 3.8 and L' is determined by Algorithm 3.2.2 EPM.

Proof. Depending on whether Algorithm 3.2.2 converges or not, applying (3.31) or (3.34) results in

$$\|u - P_k^L[u]\|_{L^2(\Omega)} \leq \left(\sum_{l=k+1}^{d(n)} \lambda_l^n\right)^{1/2} + e_{\text{int}}^{1/2} + \mathcal{O}(n^{-1/4}).$$

Choosing

$$k' := \underset{l=k+1,\ldots,d(n)}{\arg\min} \left(\sum_{j=l}^{d(n)} \lambda_j^n\right)^{1/2} \leq \varepsilon_{\text{tol}},$$

and computing $P_{k'}^{L'}[u]$ with Algorithm 3.2.2 EPM yields

$$\|u - P_k^L[u]\|_{L^2(\Omega)} \leq \varepsilon_{\text{tol}} + \|P_{k'}^{L'}[u] - P_k^L[u]\|_{L^2(\Omega)} + e_{\text{int}}^{1/2} + \mathcal{O}(n^{-1/4})$$

and thus the claim. □

Note that theoretically also the a posteriori bound for the EIM derived in [45] can be employed to obtain an a posteriori estimate for the EPM. As the theory developed in [45] however requires that the considered functions are smooth, it is unfortunately not applicable in our context. We emphasize that by running Algorithm 3.2.2 with $N_{\max}^{\text{int}} = 0$ and additionally computing $e_1^{\widehat{\omega}}$ in (3.28), Theorem 3.8 and Proposition 3.9 yield rigorous a priori and a posteriori bounds for the POIM [119] and the continuous version of the DEIM [31] (Algorithm B.1.1), when the $L^2(\Xi_{1D}; L^2(\widehat{\omega}))$-norm (2.16) is considered.

3.3 The Hierarchical Model Reduction-Reduced Basis approach for nonlinear partial differential equations (using the EPM)

The goal of this section is the efficient construction of a low-dimensional reduction space Y_m and a collateral basis space W_k which yield a fast convergence of the HMR-RB approximation to the full solution. Following the approach in §2.3.1 we derive in §3.3.2 a parametrized nonlinear 1D PDE, whose solution is employed for the definition of parametrized 1D operator evaluations in the transverse direction in §3.3.3. The sets of solution and operator snapshots are generated simultaneously by an adaptive training set extension algorithm in §3.3.5, resembling the one in §2.3.4. The principal components of the snapshot sets then form the reduction space Y_m and the collateral basis space W_k. We begin with formulating the HMR-RB approach with the Empirical Projection Method in §3.3.1.

3.3.1 Formulation of the reduced problem in the HMR-RB framework employing the EPM

We assume that a set of reduced basis functions $\{\phi_l\}_{l=1}^m$ and a set of collateral basis functions $\{\kappa_n\}_{n=1}^k$ are given to us. The reduced problem with EPM then reads

$$\text{Find } p_{m,k} \in V_m: \quad \langle P_k^L[A(p_{m,k})], v_m\rangle = \langle f, v_m\rangle \quad \forall v_m \in V_m, \tag{3.39}$$

$$\begin{aligned}\text{where} \quad P_k^L[A(p_{m,k})](x,y) &= \sum_{n=1}^{k} \int_{\widehat{\omega}} \mathcal{I}_L[A(p_{m,k})](x,\psi^{-1}(\hat{y};x))\,\kappa_n(\hat{y})\,d\hat{y}\;\kappa_n(\psi(y;x)) \\ &= \sum_{n=1}^{k}\sum_{l=1}^{L} \int_{\widehat{\omega}} A(p_{m,k}(x,\psi^{-1}(t_l;x)))\,\vartheta_l(\hat{y})\,\kappa_n(\hat{y})\,d\hat{y}\;\kappa_n(\psi(y;x)).\end{aligned}$$

Note that depending on the structure of the nonlinear operator it might be necessary to apply the EPM componentwise. Rewriting $p_{m,k}$ as $p_{m,k}(x,y) = \sum_{s=1}^m \overline{p}_{s,k}(x)\,\phi_s(\psi(y;x))$ we obtain: Find $\overline{p}_{s,k} \in H_0^1(\Omega_{1D}), s = 1,...,m$, such that

$$\sum_{n=1}^{k}\sum_{l=1}^{L} \left\langle A\left(\sum_{s=1}^{m} \overline{p}_{s,k}\phi_s(t_l)\right) \int_{\widehat{\omega}} \vartheta_l(\hat{y})\,\kappa_n(\hat{y})\,d\hat{y}\,\kappa_n, \xi\phi_j \right\rangle = \langle f, \xi\phi_j\rangle \tag{3.40}$$
$$\forall\, \xi \in H_0^1(\Omega_{1D}) \text{ and } j = 1,...,m.$$

The corresponding discrete reduced problem reads: Find $\overline{p}_{s,k}^H \in X^H$, $s = 1,...,m$, such that

$$\sum_{n=1}^{k}\sum_{l=1}^{L} \left\langle A\left(\sum_{s=1}^{m} \overline{p}_{s,k}^H\phi_s(t_l)\right) \int_{\widehat{\omega}} \vartheta_l(\hat{y})\,\kappa_n(\hat{y})\,d\hat{y}\,\kappa_n, \xi_i^H\phi_j \right\rangle = \langle f, \xi_i^H\phi_j\rangle \tag{3.41}$$
$$\text{for } i = 1,...,N_H \text{ and } j = 1,...,m,$$

or shortened

$$\text{Find } p_{m,k}^H \in V_m^H: \quad \langle P_k^L[F(p_{m,k}^H)], \xi_i^H\phi_j\rangle = 0 \quad \text{for } i = 1,...,N_H \text{ and } j = 1,...,m, \tag{3.42}$$

where $\langle P_k^L[F(p_{m,k}^H)], \xi_i^H\phi_j\rangle = \langle P_k^L[A(p_{m,k}^H)], \xi_i^H\phi_j\rangle - \langle f, \xi_i^H\phi_j\rangle$, $i = 1,...,N_H$, $j = 1,...,m$. We emphasize that due to the application of the EPM we can now precompute the integrals in the

transverse direction in (3.40) and (3.41) and as a result the computation of $\bar{p}_{s,k}$ and $\bar{p}^H_{s,k}$ reduces to the solution of a coupled system of nonlinear one-dimensional PDEs of size m (3.40) or $m \cdot N_H$ (3.41).

Problem (3.41) can be efficiently solved by Newton's method. It is possible to reuse the collateral basis for a nonlinear operator also for the approximation of its Fréchet derivative [30,43]. To obtain a better approximation of $A'(p^H_{m,k}(x,\hat{y}))$ and thus hopefully a faster convergence of the Newton scheme solving for $p^H_{m,k}$, we propose to use a second collateral basis space $W_{f,k_f} := \{\kappa^f_1, ..., \kappa^f_{k_f}\}$ for this approximation. Assuming that W_{f,k_f} is given to us and that the analogue of Assumption 3.3 is satisfied, we solve in each Newton step for the correction $\delta(p^H_{m,k})^j$:

$$\begin{aligned} \langle P^{L_f}_{k_f}[F'((p^H_{m,k})^j)]\,\delta(p^H_{m,k})^j, v^H_m\rangle &= -\langle P^L_k[F((p^H_{m,k})^j)], v^H_m\rangle \quad \forall v^H_m \in V^H_m, \quad j = 0,1,2,... \\ \text{and update} \qquad (p^H_{m,k})^{j+1} &= (p^H_{m,k})^j + \sigma\delta(p^H_{m,k})^j, \end{aligned} \tag{3.43}$$

where σ is a damping parameter, $(p^H_{m,k})^0$ is a suitable initial datum and $P^{L_f}_{k_f}[F'(p^H_{m,k})]$ is computed analogous to $P^L_k[F(p^H_{m,k})]$ with the EPM substituting W_k by W_{f,k_f}. We remark that we do not apply the Tensorized Empirical Interpolation Method (TEIM) [68] and compress the spaces W_k and W_{f,k_f} in one collateral basis space as the latter in general would have a higher dimension as k and k_f and thus would increase the costs for assembling the jacobian and the residual of (3.43).

3.3.2 Derivation of a parametrized 1D problem in transverse direction

To derive a lower dimensional parametrized PDE in the transverse direction we proceed as in §2.3.1 in Chapter 2 and assume that

$$p(x,\hat{y}) \approx U(x) \cdot \mathcal{P}(\hat{y}), \tag{3.44}$$

where the function $U(x)$ represents the unknown behavior of the full solution in the dominant direction. Using the test functions $v(x,y) = U(x) \cdot v(\hat{y})$ for all $v \in H^1_0(\widehat{\omega})$ yields the reduced problem: Given any $U \in H^1_0(\Omega_{1D})$, find $\mathcal{P} \in H^1_0(\widehat{\omega})$ such that

$$\langle A(U\mathcal{P}), Uv\rangle = \langle f, Uv\rangle \ \ \forall v \in H^1_0(\widehat{\omega}). \tag{3.45}$$

Next, we introduce for an integral $I(t) := \int_{\widehat{\omega}} \int_{\Omega_{1D}} t(x,\hat{y})\, dx d\hat{y}$ with an integrand $t \in L^1(\widehat{\Omega})$ the quadrature formula

$$Q(t) := \sum_{l=1}^{Q} \alpha_l \int_{\widehat{\omega}} \tilde{t}(x^q_l, \hat{y})\ d\hat{y}, \quad \tilde{t}(x^q_l,\hat{y}) := \lim_{\varepsilon\to 0} \frac{1}{|B_\varepsilon(x^q_l)|} \int_{B_\varepsilon(x^q_l)} t(x,\hat{y})\, dx, \tag{3.46}$$

with weights α_l, $l = 1,...,Q$, and quadrature points x^q_l, $l = 1,...,Q$. We denote with $\langle\cdot,\cdot\rangle^q$ the approximation obtained by substituting the integral $I(t)$ in $\langle\cdot,\cdot\rangle$ by the quadrature rule $Q(t)$ (3.46). In this way we get the reduced problem with quadrature:

$$\text{Given any } U \in H^1_0(\Omega_{1D}), \text{ find } \mathcal{P} \in H^1_0(\widehat{\omega}): \quad \langle A(U\mathcal{P}), Uv\rangle^q = \langle f, Uv\rangle^q \ \ \forall v \in H^1_0(\widehat{\omega}). \tag{3.47}$$

To include the unknown influence of the dynamics in the dominant direction U on the lower-dimensional problems in the transverse direction and to find the optimal locations of the quadrature points with RB methods (see §2.2 and §3.3.5) we parametrize (3.47). Therefore we introduce a parameter vector $\mu = (x^q_l, U(x^q_l), \partial^k_x U(x^q_l))$, $l = 1,...,Q$, $k = 1,...,n$, where for x_0 or $x_1 \in \{x^q_l\}^Q_{l=1}$, the associated quadrature point(s) and the evaluations $U(x_i)$, $i = 0,1$ in the interval boundaries x_0 and x_1 of Ω_{1D} can be omitted. The P-dimensional parameter space $\mathcal{D}$ containing all admissible

parameter values of μ, is defined as $\mathcal{D} := [\Omega_{1D} \times I_0 \times \cdots \times I_n]^Q$, where the intervals $I_k \subset \mathbb{R}$, $k = 0, ..., n$, enclose the ranges of $\partial_x^k U(x)$, $k = 0, ..., n$. We expect a greater sensitivity of the HMR-RB approach with respect to the choice of the intervals $I_k \subset \mathbb{R}$, $k = 0, ..., n$, compared to the linear setting as the nonlinearity of A also applies to the parameter via the term $A(U\mathcal{P})$. This can indeed be observed in the numerical experiments §3.6. To get a rough estimate on the possible ranges of $\partial_x^k U(x)$, $k = 0, ..., n$, and therefore obtain an optimal convergence rate of the HMR-RB approach for instance a coarse approximation of the solution p of (3.1) can be precomputed. Finally the parametrized 1D nonlinear partial differential equation in the transverse direction reads as follows:

$$\text{Given any } \mu \in \mathcal{D}, \text{ find } \mathcal{P}(\mu) \in H_0^1(\widehat{\omega}) : \langle A(\mathcal{P}(\mu); \mu), \upsilon; \mu\rangle^q = \langle f, \upsilon; \mu\rangle^q \ \forall \upsilon \in H_0^1(\widehat{\omega}), \tag{3.48}$$

or shortened:

$$\text{Given any } \mu \in \mathcal{D}, \text{ find } \mathcal{P}(\mu) \in H_0^1(\widehat{\omega}) : \langle F(\mathcal{P}(\mu); \mu), \upsilon; \mu\rangle^q = 0 \ \forall \upsilon \in H_0^1(\widehat{\omega}), \tag{3.49}$$

where $\langle F(\mathcal{P}(\mu); \mu), \upsilon; \mu\rangle^q := \langle A(\mathcal{P}(\mu); \mu), \upsilon; \mu\rangle^q - \langle f, \upsilon; \mu\rangle^q$ for all $\mu \in \mathcal{D}$. One possible choice for the α_l, $l = 1, ..., Q$, in (3.46) are the weights

$$\alpha_1 := \frac{x_1^q + x_2^q}{2} - x_0, \quad \alpha_l := \frac{x_{l+1}^q - x_{l-1}^q}{2}, \ l = 2, ..., Q-1, \quad \alpha_Q := x_1 - \frac{x_{Q-2}^q + x_{Q-1}^q}{2}, \tag{3.50}$$

where the quadrature points x_l^q, $l = 1, ..., Q$ are expected to be sorted in ascending order. The choice (3.50) yields a modified rectangle formula. Alternatively, for instance a standard composite trapezoidal rule (cf. [107]) can be considered. The number of quadrature points is chosen automatically by an adaptive algorithm, described in §3.3.5.

To compute snapshots we use the subdivision τ_h of $\widehat{\omega}$ with elements $\tau_j = (\hat{y}_{j-1}, \hat{y}_j)$ of width $h_j = \hat{y}_j - \hat{y}_{j-1}$ and maximal step size $h := \max_{\tau_j} h_j$ introduced in §2.3.3. We introduce an associated conforming Finite Element space $Y^h \subset H_0^1(\widehat{\omega})$ with $\dim(Y^h) = n_h < \infty$, and basis υ_j^h, $j = 1, ..., n_h$. We obtain the parameter dependent discrete 1D problem:

$$\text{Given any } \mu \in \mathcal{D}, \text{ find } \mathcal{P}^h(\mu) \in Y^h : \langle A(\mathcal{P}^h(\mu); \mu), \upsilon_j^h; \mu\rangle^q = \langle f, \upsilon_j^h; \mu\rangle^q \text{ for } j = 1, ..., n_h, \tag{3.51}$$

which can be solved by Newton's method. Therefore we define the parameter dependent inf-sup stability factor and the continuity constant

$$\beta_{1D}(z^h; \mu) := \inf_{\substack{w^h \in Y^h \\ |w^h|_{W^{1,p}(\widehat{\omega})} \neq 0}} \sup_{\substack{v^h \in Y^h \\ |v^h|_{W^{1,q}(\widehat{\omega})} \neq 0}} \frac{\langle F'(z^h; \mu) w^h, v^h; \mu\rangle^q_{W^{-1,p}(\widehat{\omega}) W^{1,q}(\widehat{\omega})}}{|w^h|_{W^{1,p}(\widehat{\omega})} |v^h|_{W^{1,q}(\widehat{\omega})}} \quad \text{for } z^h \in Y^h, \tag{3.52}$$

$$\gamma_{1D}(z^h; \mu) := \sup_{\substack{w^h \in Y^h \\ |w^h|_{W^{1,p}(\widehat{\omega})} \neq 0}} \sup_{\substack{v^h \in Y^h \\ |v^h|_{W^{1,q}(\widehat{\omega})} \neq 0}} \frac{\langle F'(z^h; \mu) w^h, v^h; \mu\rangle^q_{W^{-1,p}(\widehat{\omega}) W^{1,q}(\widehat{\omega})}}{|w^h|_{W^{1,p}(\widehat{\omega})} |v^h|_{W^{1,q}(\widehat{\omega})}} \quad \text{for } z^h \in Y^h, \tag{3.53}$$

where $\frac{1}{p} + \frac{1}{q} = 1$. As there might be parameters for which no solution of (3.51) exists, the conditions for the convergence of Newton's method, i.e. the boundedness of $F'(\mathcal{P}^h(\mu); \mu) : W_0^{1,p}(\widehat{\omega}) \to W^{-1,p}(\widehat{\omega})$ and the local inf-sup stability (see Assumption 3.3) have to be verified a posteriori [27]. If the analogue of Assumption 3.3 for the 1D case is fulfilled, we solve in each Newton iteration for the correction $\delta\mathcal{P}_j^h$:

$$\begin{aligned} \langle F'(\mathcal{P}_j^h(\mu); \mu)\, \delta\mathcal{P}_j^h(\mu), v^h; \mu\rangle^q &= -\langle F(\mathcal{P}_j^h(\mu); \mu), v^h; \mu\rangle^q \quad \forall v^h \in Y^h, \quad j = 0, 1, 2, ... \\ \text{and update} \qquad \mathcal{P}_{j+1}^h(\mu) &= \mathcal{P}_j^h(\mu) + \sigma\delta\mathcal{P}_j^h(\mu), \end{aligned} \tag{3.54}$$

where $\mathcal{P}_0^h(\mu)$ is an appropriate initial datum and σ is a damping parameter.

3.3.3 The generation of parametrized 1D operator evaluations

In this subsection we introduce an approach for the generation of parametrized 1D operator evaluations of the nonlinear operator A in the transverse direction. For this purpose we consider (3.48) and define a parametrized 1D operator evaluation $\mathcal{A}(\hat{y};\mu)$ of the operator $A(p(x,\hat{y}))$ as

$$\mathcal{A}(\hat{y};\mu) := \sum_{l=1}^{Q} \frac{\alpha_l}{|\Omega_{1D}|} A(\mathcal{P}(\hat{y};\mu);\mu_l), \tag{3.55}$$

where $\mu_l := (x_l^q, U(x_l^q), \partial_x^k U(x_l^q))$, $|\Omega_{1D}|$ denotes the length of the interval Ω_{1D} and $\mathcal{P}(\hat{y};\mu)$ is the solution of (3.48). Provided that $\mathcal{P}(\hat{y};\mu)$ is able to capture the behavior of the full solution p in the transverse direction, we expect that $\mathcal{A}(\hat{y};\mu)$ is a good approximation of the range of $A(p(x,\hat{y}))$ in that direction, which will be validated in §3.6. For $V^{H\times h}$ defined in (2.39) we denote with $p^{H\times h} \in V^{H\times h}$ the reference FEM solution of

$$\text{Find } p^{H\times h} \in V^{H\times h}: \quad \langle A(p^{H\times h}), v^{H\times h}\rangle = \langle f, v^{H\times h}\rangle \quad \forall\, v^{H\times h} \in V^{H\times h}, \tag{3.56}$$

which will be discussed in greater detail in §3.4. A parametrized 1D operator evaluation of $A(p^{H\times h}(x,\hat{y}))$ can the be defined as

$$\mathcal{A}^h(\hat{y};\mu) := \sum_{l=1}^{Q} \frac{\alpha_l}{|\Omega_{1D}|} A(\mathcal{P}^h(\hat{y};\mu);\mu_l), \tag{3.57}$$

where $\mathcal{P}^h(\hat{y};\mu)$ solves (3.51). Finally, we define a parametrized 1D operator evaluation of $A'(p^{H\times h}(x,\hat{y}))$ as

$$\mathcal{A}_f^h(\hat{y};\mu) := \sum_{l=1}^{Q} \frac{\alpha_l}{|\Omega_{1D}|} A'(\mathcal{P}^h(\hat{y};\mu);\mu_l). \tag{3.58}$$

3.3.4 Example: The nonlinear diffusion equation

We exemplify the derivation of the parametrized 1D partial differential equation and the generation of parametrized 1D operator evaluations of $A(p^{H\times h}(x,\hat{y}))$ for our model problem (3.3) on a rectangular domain Ω, which implies $\Omega = \widehat{\Omega}$ and $y = \hat{y}$. First, we use the quadrature formula (3.46) to get the reduced problem with quadrature: Given any $U \in X$, find $\mathcal{P} \in H_0^1(\widehat{\omega})$ such that:

$$\begin{aligned}\sum_{l=1}^{Q} \alpha_l \Big(\int_{\widehat{\omega}} d(\mathcal{P}\,U(x_l^q))\, \frac{d\mathcal{P}}{dy}\, \frac{d\upsilon}{dy}\, U^2(x_l^q) + \int_{\widehat{\omega}} d(\mathcal{P}\,U(x_l^q))\, \mathcal{P}\,\upsilon\, (\partial_x U(x_l^q))^2 \Big) \\ = \sum_{l=1}^{Q} \alpha_l \int_{\widehat{\omega}} s(x_l^q, y)\, \upsilon\, U(x_l^q) \quad \forall \upsilon \in H_0^1(\widehat{\omega}),\end{aligned} \tag{3.59}$$

where we have omitted the $\backsim$ on the integrands (cf. (3.46)) to simplify notation. Assuming that $x_0, x_1 \notin \{x_l^q\}_{l=1}^Q$ we obtain $\mu = (x_l^q, U(x_l^q), \partial_x U(x_l^q))$, $l = 1, ..., Q$, and $\mathcal{D} := [\Omega_{1D} \times I_0 \times I_1]^Q$. By replacing x_l^q by $\mu_{l,1}$, $U(x_l^q)$ by $\mu_{l,2}$ and $\partial_x U(x_l^q)$ by $\mu_{l,3}$, the parameter vector can be shortened to $\mu = [\mu_{l,1}, \mu_{l,2}, \mu_{l,3}]_{l=1}^Q$ and the parametrized 1D nonlinear PDE in transverse direction reads as

follows: Given any $\mu \in \mathcal{D}$, find $\mathcal{P}(\mu) \in H_0^1(\widehat{\omega})$ such that

$$\begin{aligned}\sum_{l=1}^{Q}\alpha_l\Big(\int_{\widehat{\omega}} d(\mathcal{P}(\mu)\,\mu_{l,2})\,\frac{d\mathcal{P}(\mu)}{dy}\,\frac{dv}{dy}\,\mu_{l,2}^2 + \int_{\widehat{\omega}} d(\mathcal{P}(\mu)\,\mu_{l,2})\,\mathcal{P}(\mu)\,v\,\mu_{l,3}^2\Big)\\ = \sum_{l=1}^{Q}\alpha_l\int_{\widehat{\omega}} s(\mu_{l,1},y)\,v\,\mu_{l,2}\quad \forall v\in H_0^1(\widehat{\omega}).\end{aligned} \tag{3.60}$$

To solve the coupled system (3.10) with Newton's method, we have additionally required in (3.13) that the basis functions $\phi_k(\hat{y})$, $k = 1, ..., m$, are in $W^{1,p}(\widehat{\omega})$. Regarding the existence of solutions $\mathcal{P}(\mu)$ of (3.60) and their boundary regularity we have the following proposition.

Proposition 3.10. *Let the assumptions* (3.4) *on d be fulfilled and let s be in $L^2(\Omega_{1D}, H^1(\widehat{\omega})) \cap C^0(\Omega)$. Then for any given parameter $\mu \in \mathcal{D}$ there exists a solution $\mathcal{P}(\mu) \in H_0^1(\widehat{\omega})$. Furthermore, we have $\mathcal{P}(\mu) \in H^2(\widehat{\omega}) \cap W^{1,\infty}(\widehat{\omega})$.*

Proof. For $\mu_{l,2} = 0$ we have the trivial solution $\mathcal{P} \equiv 0$. Let us thus assume that $\mu_{l,2} \neq 0$. As the terms $\mu_{l,2}^2$ and $\mu_{l,3}^2$ are positive and therefore do not affect the structure of the PDE it is sufficient to verify if the assumptions on the data functions d and s allow for a solution $\mathcal{P} \in H^2(\widehat{\omega}) \cap W^{1,\infty}(\widehat{\omega})$. Due to the uniform ellipticity of d, the boundedness of d and d' (3.4) and the required regularity of s the assumption (3.1), (3.2) and (5.7) in Chapter 4 of [74] are fulfilled. The assertion then follows with Theorem 4.1, Theorem 5.2 and Theorem 8.2 in [74] (Chapter 4, pp. 270, 277, 297). □

For the discretization of (3.60) we use the subdivision τ_h of $\widehat{\omega}$ introduced in §2.3.3 and the associated FE space $Y^h \subset H_0^1(\widehat{\omega})$ with basis v_j^h, $j = 1, ..., n_h$, from the previous subsection. We obtain the parameter dependent discrete 1D problem: Given any $\mu \in \mathcal{D}$, find $\mathcal{P}^h(\mu) \in Y^h$ such that

$$\begin{aligned}\sum_{l=1}^{Q}\alpha_l\Big(\int_{\widehat{\omega}} d(\mathcal{P}^h(\mu)\,\mu_{l,2})\,\frac{d\mathcal{P}^h(\mu)}{dy}\,\frac{dv_j^h}{dy}\,\mu_{l,2}^2 + \int_{\widehat{\omega}} d(\mathcal{P}^h(\mu)\,\mu_{l,2})\,\mathcal{P}^h(\mu)\,v_j^h\,\mu_{l,3}^2\Big)\\ = \sum_{l=1}^{Q}\alpha_l\int_{\widehat{\omega}} s(\mu_{l,1},y)\,v_j^h\,\mu_{l,2}\quad \text{for } j=1,...,n_h.\end{aligned} \tag{3.61}$$

Due to the embedding $H^1(\widehat{\omega}) \hookrightarrow C^0(\widehat{\omega})$ for $\widehat{\omega} \subset \mathbb{R}$ we have that $F : H_0^1(\widehat{\omega}) \to H^{-1}(\widehat{\omega})$ is in C^1 and its Fréchet derivative at the solution $\mathcal{P}^h(\mu)\mu_2$ can be computed as

$$\begin{aligned}&\langle F'(\mathcal{P}^h(\mu)\mu_2)\vartheta^h, v^h\rangle^q = \\ &\sum_{l=1}^{Q}\alpha_l\Big(\int_{\widehat{\omega}} d'(\mathcal{P}^h(\mu)\mu_{2,l})\,\vartheta^h\,\frac{d\mathcal{P}^h(\mu)}{dy}\,\frac{dv^h}{dy}\,\mu_{l,2}^3 + \int_{\widehat{\omega}} d(\mathcal{P}^h(\mu)\,\mu_{l,2})\,\frac{d\vartheta^h}{dy}\,\frac{dv^h}{dy}\,\mu_{l,2}^2\\ &\quad + \int_{\widehat{\omega}} d'(\mathcal{P}^h(\mu)\,\mu_{l,2})\,\vartheta^h\,\mathcal{P}^h(\mu)\,v^h\,\mu_{l,2}\,\mu_{l,3}^2 + \int_{\widehat{\omega}} d(\mathcal{P}^h(\mu)\,\mu_{l,2})\,\vartheta^h\,v_j^h\,\mu_{l,3}^2\Big).\end{aligned} \tag{3.62}$$

Note that due to the application of the chain rule we obtain the additional term $\mu_{l,2}$ in the first and third term of (3.62). The structure of the two-dimensional Fréchet derivative (3.22) is thus maintained. Finally, we define the parametrized 1D operator evaluations of $A(p^{H\times h}(x, y))$

$$\mathcal{A}_1^h(y;\mu) = \sum_{l=1}^{Q}\frac{\alpha_l}{|\Omega_{1D}|}\,d(\mathcal{P}^h(\mu)\mu_{l,2})\,\mathcal{P}^h(\mu)\mu_{l,3}\quad\text{and}\quad \mathcal{A}_2^h(y;\mu) = \sum_{l=1}^{Q}\frac{\alpha_l}{|\Omega_{1D}|}\,d(\mathcal{P}^h(\mu)\mu_{l,2})\,\frac{d\mathcal{P}^h(\mu)}{dy}\mu_{l,2}, \tag{3.63}$$

Algorithm 3.3.1: Computation of k'

EPM-INDICATOR($\mathcal{P}_G^h, \mathcal{A}_G^h, \varepsilon_{\text{tol}}^{err}, \text{tol}_{k'}, \varepsilon_{\text{tol}}^c, \varepsilon_{\text{tol}}^{\text{int}}, N_{\max}^{\text{int}}, m_{\max}, N_{H'}, \Xi_G$)
$\{\phi_l\}_{l=1}^{m_{\max}} := \text{POD}(\mathcal{P}_G^h, m_{\max})$
$[\{\kappa_l\}_{l=1}^{k_{POD}}, \{\lambda_l\}_{l=1}^{k_{POD}}] := \text{POD}(\mathcal{A}_G^h, \varepsilon_{\text{tol}}^{err})$
$[T_{k_{POD}}, Z_{k_{POD}}, B_{k_{POD}}, e_{\text{int}}]$:=EPM($\{\kappa_l\}_{l=1}^{k_{POD}}, \mathcal{A}_G^h, \varepsilon_{\text{tol}}^{\text{int}}, N_{\max}^{\text{int}}, \Xi_G, \{\phi_l\}_{l=1}^{m_{POD}}, N_{H'}$)
k' =EPM-APOSTERIORI-BOUND($e_{\text{int}}, \text{tol}_{k'} \cdot \varepsilon_{\text{tol}}^c, \{\lambda_l\}_{l=1}^{k_{POD}}$)
$W_{k'} := \{\kappa_l\}_{l=1}^{k'}$
$T_{k'}$:=EPM($\{\kappa_l\}_{l=1}^{k'}, \mathcal{A}_G^h, \varepsilon_{\text{tol}}^{\text{int}}, N_{\max}^{\text{int}}, \Xi_G, \{\phi_l\}_{l=1}^{m_{POD}}, N_{H'}$)
return $W_{k'}, T_{k'}$

and the parametrized 1D operator evaluations of $A'(p^{H\times h}(x,y))$

$$\mathcal{A}_{f,1}^h(y;\mu) = \sum_{l=1}^{Q} \frac{\alpha_l}{|\Omega_{1D}|}\, d'(\mathcal{P}^h(\mu)\mu_{l,2})\, \mathcal{P}^h(\mu)\mu_{l,3}, \quad \mathcal{A}_{f,2}^h(y;\mu) = \sum_{l=1}^{Q} \frac{\alpha_l}{|\Omega_{1D}|}\, d'(\mathcal{P}^h(\mu)\mu_{l,2})\, \frac{d\mathcal{P}^h(\mu)}{dy}\mu_{l,2},$$
$$\text{and} \quad \mathcal{A}_{f,3}^h(y;\mu) = \sum_{l=1}^{Q} \frac{\alpha_l}{|\Omega_{1D}|}\, d(\mathcal{P}^h(\mu)\mu_{l,2}). \tag{3.64}$$

3.3.5 Reduced and collateral basis generation with RB methods — the ADAPTIVE-HMR-RB algorithm

In this subsection we introduce the ADAPTIVE-HMR-RB algorithm which simultaneously constructs the reduction space $Y_m^h = \text{span}(\phi_1, \ldots, \phi_m) \subset Y^h$ and the collateral basis space $W_k^h = \text{span}(\kappa_1, \ldots, \kappa_k)$ using sampling strategies from the RB framework. Algorithm ADAPTIVE-HMR-RB is a modification of Algorithm 2.3.2 ADAPTIVE-HMR-POD, presented in §2.3.4. The solution manifold $\mathcal{M}^h$ and the discrete solution manifold Y_M^h, $M := \dim(Y_M^h)$, are defined as

$$\mathcal{M}^h := \{\mathcal{P}^h(\mu)\,|\,\mu \in \mathcal{D}\}, \qquad Y_M^h := \{\mathcal{P}^h(\mu)\,|\,\mu \in \Xi_{train}\}, \tag{3.65}$$

where $\Xi_{train} \subset \mathcal{D}$ is a finite dimensional (discrete) surrogate of $\mathcal{D}$ of size $n_{train} = |\Xi_{train}|$ and $\mathcal{P}^h(\mu)$ is the solution of (3.51). Analogously we can define an operator manifold $\mathcal{M}_A^h$ and its discrete counterpart W_K^h, $K := \dim(W_K^h)$ through

$$\mathcal{M}_A^h := \{\mathcal{A}^h(\mu)\,|\,\mu \in \mathcal{D}\}, \qquad W_K^h := \{\mathcal{A}^h(\mu)\,|\,\mu \in \Xi_{train}\}. \tag{3.66}$$

To simplify notations we assume in this subsection that $\mathcal{A}^h(\mu)$ denotes both the parameter dependent snapshot for the operator defined in (3.57) and its Fréchet derivative (3.58) and accordingly that W_k^h comprises $W_{f,k}^h$. The discrete manifolds Y_M^h and W_K^h are efficiently constructed in Algorithm 3.3.2, described below, by an adaptive training set extension very similar to the one applied in Algorithm 2.3.1 in Chapter 2 which in turn is based on [61, 62]. Finally, the reduction space Y_m^h and the collateral basis space W_k^h are formed by the principal components of Y_M^h and W_K^h, singled out by a POD (Algorithm 3.3.3).

Algorithm 3.3.2: Adaptive training set extension and snapshot generation

1 AdaptiveTrainExtension($G_0, \Xi_{G_0}, \Xi_c, m_{\max}, i_{max}, n_\Xi, \theta, \sigma_{thres}, N_{H'}, ...$
2 $...\varepsilon_{\text{tol}}^{err}, \varepsilon_{\text{tol}}^{c}, \text{tol}_{k'}, \varepsilon_{\text{tol}}^{\text{int}}, N_{\max}^{\text{int}}, Q_0, Q_{\max}$)
3 **Initialize** $G = G_0, \Xi_G = \Xi_{G_0}, \phi_0 = \emptyset, \kappa_0 = \emptyset, \rho_0(G) = 0, Q = Q_0$
4 Compute $\mathcal{P}_c^h(Q)$, $\mathcal{A}_c^h(Q)$
5 $[W_{k'}^h, T_{k'}]$ =EPM-Indicator($\mathcal{P}_c^h, \mathcal{A}_c^h, \varepsilon_{\text{tol}}^{err}, \text{tol}_{k'}, \varepsilon_{\text{tol}}^{c}, \varepsilon_{\text{tol}}^{\text{int}}, N_{\max}^{\text{int}}, m_{\max}, N_{H'}, \Xi_c$)
6 Q =QP-Indicator($\mathcal{P}_c^h, N_{H'}, W_{k'}^h, T_{k'}, Q_{\max}$)
7 Possibly adapt G and Ξ_G if Q has changed.
8 **for** $m = 1, \ldots, m_{max}$ **do**
9 Compute $\mathcal{P}_G^h(Q)$, $\mathcal{A}_G^h(Q)$
10 $[\eta(G), \sigma(G)]$ =ElementIndicators($\{\phi_k\}_{k=1}^{m-1}, \mathcal{P}_G^h, \{\kappa_k\}_{k=1}^{k_c}, \mathcal{A}_G^h, W_{k'}^h, T_{k'}, G, \rho(G), N_{H'}$)
11 **for** $i = 1, \ldots, i_{max}$ **do**
12 $\mathcal{G}$:= Mark($\eta(G), \sigma(G), \theta, \sigma_{thres}$)
13 (G, Ξ_G) := Refine($\mathcal{G}, \Xi_{\mathcal{G}}, n_\Xi$)
14 $\rho(G \setminus \mathcal{G}) = \rho(G \setminus \mathcal{G}) + 1$
15 Compute $\mathcal{P}_{\mathcal{G}}^h(Q)$, $\mathcal{A}_{\mathcal{G}}^h(Q)$
16 $[\eta(\mathcal{G}), \rho(\mathcal{G}), \sigma(\mathcal{G})]$ =ElementIndicators($\{\phi_k\}_{k=1}^{m-1}, \mathcal{P}_{\mathcal{G}}^h, \{\kappa_k\}_{k=1}^{k_c}, \mathcal{A}_{\mathcal{G}}^h, W_{k'}, T_{k'}, N_{H'}$)
17 **end**
18 $\{\phi_k\}_{k=1}^{m}$:= POD($\mathcal{P}_G^h, m$)
19 $\{\kappa_k\}_{k=1}^{k_c}$:= POD($\mathcal{A}_G^h, \varepsilon_{\text{tol}}^{c}$)
20 $[W_{k'}^h, T_{k'}]$ =EPM-Indicator($\mathcal{P}_G^h, \mathcal{A}_G^h, \varepsilon_{\text{tol}}^{err}, \text{tol}_{k'}, \varepsilon_{\text{tol}}^{c}, \varepsilon_{\text{tol}}^{\text{int}}, N_{\max}^{\text{int}}, m_{\max}, N_{H'}, \Xi_G$)
21 Q =QP-Indicator($\mathcal{P}_G^h, N_{H'}, W_{k'}^h, T_{k'}, Q_{\max}$)
22 Possibly adapt G and Ξ_G if Q has changed.
23 **end**
24 **return** Y_M^h, W_K^h, Ξ_G

Algorithm 3.3.2: AdaptiveTrainExtension We use the same notation as in Algorithm 2.3.1, which we shortly recall for the reader's convenience. G denotes a hyper-rectangular possibly non-conforming grid in the parameter space $\mathcal{D}$, g is a cell of G and N_G is the number of cells in G. The parameter values in the training set Ξ_g are sampled from the uniform distribution over the cell g, where Ξ_g has the same size n_Ξ for all cells g and $\Xi_G = \cup_{g \in G} \Xi_g$. As in Algorithm 2.3.1 and originally in [61, 62] we use a local mesh adaptation with a SOLVE → ESTIMATE → MARK → REFINE strategy for the generation of G and Ξ_G beginning with a given coarse partition G_0 and an associated initial training set Ξ_{G_0}. In §3.4 we derive an a posteriori error estimate Δ_m^k for the error between the solution $p_{m,k}^{H'}$ of (3.41) and the reference solution $p^{H' \times h}$ defined in (3.56) which takes into account both the model error and the error due to the approximation of the nonlinear operator. For the latter we use the a posteriori bound for the EPM derived in Proposition 3.9. A richer collateral basis space $W_{k'}^h$ with associated interpolation points $T_{k'}$ has thus to be provided before starting the SOLVE → ESTIMATE → MARK → REFINE-loop. Therefore we initially compute the snapshots $\mathcal{P}_c^h$ and $\mathcal{A}_c^h$ for a coarse train sample Ξ_c of G_0 in line 4. To compute $W_{k'}^h$ and the points $T_{k'}$ with Algorithm 3.3.1 EPM-Indicator, we first use a POD to find the principal components $\{\kappa_l\}_{l=1}^{k_{POD}}$ such that the POD-error $e_{k_{POD}}^{\text{POD}} = (\sum_{l=k_{POD}+1}^{n_{\text{train}}} \lambda_l)^{1/2} \leq \varepsilon_{\text{tol}}^{err}$, where $\varepsilon_{\text{tol}}^{err} < \varepsilon_{\text{tol}}^{\text{EPM}}$. Next, we apply Algorithm 3.2.2 EPM for the computation of the interpolation points $T_{k_{POD}}$, the basis $Z_{k_{POD}}$ and the matrix $B_{k_{POD}}$, where the computation of the interpolant in (3.29) necessitates the solution of (3.41) and thus the computation of $\{\phi_l\}_{l=1}^{m_{\max}}$ in line 2. As the error bound is only employed during the adaptive training set extension, it is sufficient to restrict to $m = m_{\max}$.

Algorithm 3.3.3: Construction of the reduction space Y_m^h and the collateral basis space W_k^h

1 ADAPTIVE-HMR-RB($G_0, m_{\max}, i_{\max}, n_\Xi, n_c, \theta, \sigma_{\text{thres}}, N_{H'}, \varepsilon_{\text{tol}}^{\text{HMR}}, \varepsilon_{\text{tol}}^{\text{EPM}}, ...$
2 $...\varepsilon_{\text{tol}}^{\text{err}}, \varepsilon_{\text{tol}}^{c}, \text{tol}_{k'}, \varepsilon_{\text{tol}}^{\text{int}}, N_{\max}^{\text{int}}, Q_0, Q_{\max})$
3 **Initialize** Ξ_{G_0}, Ξ_c
4 $[Y_M^h, W_K^h, \Xi_G]$ = ADAPTIVETRAINEXTENSION($G_0, \Xi_{G_0}, \Xi_c, m_{\max}, i_{\max}, n_\Xi, ...$
5 $...\theta, \sigma_{\text{thres}}, N_{H'}, \varepsilon_{\text{tol}}^{\text{err}}, \varepsilon_{\text{tol}}^{c}, \text{tol}_{k'}, \varepsilon_{\text{tol}}^{\text{int}}, N_{\max}^{\text{int}}, Q_0, Q_{\max})$
6 $Y_m^h := \text{POD}(\mathcal{P}_G^h, \varepsilon_{\text{tol}}^{\text{HMR}})$, such that $e_m^{\text{POD}} \leq \varepsilon_{\text{tol}}^{\text{HMR}}$.
7 $W_k^h := \text{POD}(\mathcal{A}_G^h, \varepsilon_{\text{tol}}^{\text{EPM}})$, such that $e_k^{\text{POD}} \leq \varepsilon_{\text{tol}}^{\text{EPM}}$.
8 T_k =EPM($W_k^h, \mathcal{A}_G^h, \varepsilon_{\text{tol}}^{\text{int}}, N_{\max}^{\text{int}}, \Xi_G, Y_m^h, N_{H'}$)
9 **return** Y_m^h, W_k^h, T_k

Then we use the a priori bound for the EPM from Theorem 3.8 to compute k', which yields $W_{k'}$ and apply again Algorithm 3.2.2 to determine $T_{k'}$. $W_{k'}$ and $T_{k'}$ are updated at the end of each loop over m in line 20 to include the information from the snapshots generated during lines 9 and 15.

Another main difference to Algorithm 2.3.1 is the usage of the QP-INDICATOR, which chooses the number of quadrature points Q used in (3.51). To decide whether Q has to be increased or not we apply a POD to $\mathcal{P}_c^h$ in line 6 ($\mathcal{P}_G^h$ in line 21) and compare the convergence rates of the eigenvalues of the POD with $\|\bar{p}_{l,k'}^{H'}\|^2_{L^2(\Omega_{1D})}$, $l = 1, .., 10$, where the coefficients $\bar{p}_{l,k'}^{H'} \in X^{H'}$ solve (3.41). If the rates do not coincide, and Q is smaller than $Q_{\max}$, we increment Q by one. The QP-INDICATOR thus enforces the adaptation of the reduction space Y_m^h and the collateral basis space W_k^h to the reference solution $p^{H\times h}$ and the nonlinear operator $A(p^{H\times h})$ by increasing the amount of information on the dynamics in the dominant direction in the spaces Y_m^h and W_k^h, if necessary. The initial value Q_0 is usually set to 1. We have $Q_{\max} = 3$, as the fact, that G is a product-like hyper-rectangular grid, prevents the applicability of Algorithm 3.3.2 to higher parameter dimensions (cf. §2.3.4).

Apart form the just stated differences and the additional computation of the snapshots $\mathcal{A}_G^h$ in line 9 and 15, and the POD for the computation of the small collateral basis $\{\kappa_k\}_{k=1}^{k_c}$ in line 19, Algorithm 3.3.2 follows the lines of Algorithm 2.3.1. Thus we use the cell indicators

$$\eta(g) := \min_{\mu\in\Xi_g} \Delta_m^k(\mu) \quad \text{and} \quad \sigma(g) := \text{diam}(g) \cdot \rho(g), \tag{3.67}$$

where $\rho(g)$ counts the number of loops in which the cell g has not been refined, since its last refinement. We mark for fixed $\theta \in (0, 1]$ in each iteration the θN_G cells g with the smallest indicators $\eta(g)$ and additionally the cells for which $\sigma(g)$ lies above a certain threshold σ_{thres}. Then all cells marked for refinement are bisected in each direction. For details see §2.3.4. We finally emphasize that for each parameter value in Ξ_G we compute the snapshots $\mathcal{P}^h(\mu)$ and $\mathcal{A}^h(\mu)$, add these snapshots to the already computed small bases $\{\phi_l\}_{l=1}^{m-1}$ and $\{\kappa_l\}_{l=1}^{k_c}$, compute the (coarse) solution $p_{m,k}^{H'}$ of (3.41) and use the a posteriori error estimator to assess if adding the current snapshots yields a good approximation. This closes the description of Algorithm 3.3.2.

Algorithm 3.3.3: ADAPTIVE-HMR-RB At first, the training sets Ξ_{G_0} and Ξ_c are formed by sampling n_Ξ or n_c parameter values from the uniform distribution over each $g \in G_0$, where $n_c > n_\Xi$. Then Algorithm 3.3.2 is called to generate the discrete manifolds Y_M^h (3.65) and W_K^h (3.66). Finally we apply a POD to determine the principal components $\{\phi_1, ..., \phi_m\}$ and $\{\kappa_1, ..., \kappa_k\}$ of Y_M^h and W_K^h, which then span the reduction space Y_m^h and the collateral basis space W_k^h. We recall that the POD spaces Y_l^{POD}, $l = 1, ..., m$, are the solutions of the optimization problem

$$Y_l^{\text{POD}} = \arg \inf_{Z_l \subset \text{span}\{Y_M^h\}} \left(\frac{1}{n_\Xi N_G} \sum_{\mu \in \Xi_G} \inf_{z_l \in Z_l} \|\mathcal{P}^h(\mu) - z_l\|^2_{L^2(\widehat{\omega})} \right), \tag{3.68}$$

and that the POD-error is defined as

$$e_m^{\text{POD}} := \left(\frac{1}{n_\Xi N_G} \sum_{\mu \in \Xi_G} \inf_{z_l \in Y_m^{\text{POD}}} \|\mathcal{P}^h(\mu) - z_l\|^2_{L^2(\widehat{\omega})} \right)^{1/2}. \tag{3.69}$$

The POD spaces W_l^{POD}, $l = 1, ..., k$, and the POD-error e_k^{POD} are defined analogously. We refer to §2.2.1 for further details. This completes the description of Algorithm 3.3.3.
A thorough study on the choice of the input parameters $m_{max}, i_{max}, n_\Xi, \sigma_{thres}$ and $N_{H'}$ has been done in §2.6 for linear PDEs. For the nonlinear case similar results are obtained in §3.6. As the spaces Y_m^h and W_k^h approximate the discrete manifolds Y_M^h and W_K^h (cf. (3.68)), we will also validate in §3.6 if they approximate the reference solution $p^{H\times h}$ and the range of the operator $A(p^{H\times h})$ with the same approximation quality.

3.4 A posteriori error estimates

The goal of this section is to derive a rigorous a posteriori error bound for the error between the reduced solution $p_{m,k}^H$ of (3.41) and a reference solution $p^{H\times h}$. To define the latter we consider the subdivision $\widehat{T} := \mathcal{T}_H \times \tau_h$ of $\widehat{\Omega}$, defined in §2.4.1, with elements $T_{i,j} := \mathcal{T}_i \times \tau_j$, $\mathcal{T}_i \in \mathcal{T}_H$ and $\tau_j \in \tau_h$, and the reference FE-space

$$V^{H\times h} := \left\{ v^{H\times h} \in C^0(\widehat{\Omega}) \mid v^{H\times h}|_{T_{i,j}} \in \mathbb{Q}_{k,l}, T_{i,j} \in \widehat{T} \right\} \subset W^{1,p}(\Omega), \tag{3.70}$$

where $\mathbb{Q}_{k,l}$ is defined as $\mathbb{Q}_{k,l} := \{\sum_j c_j v_j(x) w_j(\hat{y}) \ : \ v_j \in \mathbb{P}_k^1, w_j \in \mathbb{P}_l^1\}$ and $\mathbb{P}_k^1(\mathcal{T}_i)$ denotes the set of polynomials of order $\leq k$ over $\mathcal{T}_i$ in one variable. As $Y_m^h \subset Y^h$ we have $V_m^H \subset V^{H\times h}$ (see §2.4.1). The reference FE approximation of problem (3.1) reads:

$$\text{Find } p^{H\times h} \in V^{H\times h} : \quad \langle A(p^{H\times h}), v^{H\times h} \rangle = \langle f, v^{H\times h} \rangle \quad \forall\, v^{H\times h} \in V^{H\times h}, \tag{3.71}$$

or in short

$$\text{Find } p^{H\times h} \in V^{H\times h} : \quad \langle F(p^{H\times h}), v^{H\times h} \rangle = 0 \quad \forall\, v^{H\times h} \in V^{H\times h}, \tag{3.72}$$

where $\langle F(p^{H\times h}), v^{H\times h} \rangle = \langle A(p^{H\times h}), v^{H\times h} \rangle - \langle f, v^{H\times h} \rangle$ for all $v^{H\times h} \in V^{H\times h}$. We aim at an estimate of the type

$$\begin{aligned} &\underline{c} \left(\|F(p_{m,k}^H) - P_k^L[F(p_{m,k}^H)]\|_{W^{-1,p}(\Omega)} + \|P_k^L[F(p_{m,k}^H)]\|_{W^{-1,p}(\Omega)} \right) \\ &\quad \leq |p^{H\times h} - p_{m,k}^H|_{W^{1,p}(\Omega)} \leq \overline{c} \left(\|F(p_{m,k}^H) - P_k^L[F(p_{m,k}^H)]\|_{W^{-1,p}(\Omega)} + \|P_k^L[F(p_{m,k}^H)]\|_{W^{-1,p}(\Omega)} \right). \end{aligned} \tag{3.73}$$

However, if the considered operator A is not strongly monotone[2], (3.73) is a local result [93, 121], which means that (3.73) can only be obtained if $p^H_{m,k}$ is close enough to the reference solution $p^{H\times h}$ [121]. To assess whether the latter is fulfilled we apply the Brezzi-Rappaz-Raviart (BRR) theory [20, 23]. This has been first applied in the context of Reduced Basis Methods in [122] for the parametrized steady incompressible Navier-Stokes equations, where an affine parameter dependence of the data functions has been assumed. In [27] the results of [122] have been extended to data functions with a non-affine parameter dependence. Again a quadratically nonlinear parametrized PDE has been considered.

3.4.1 An a posteriori error bound based on the Brezzi-Rapaz-Raviart Theory

We start with defining the inf-sup stability factor and the continuity and the Lipschitz constant:

$$\beta_p := \inf_{\substack{w^{H\times h}\in V^{H\times h}\\ |w^{H\times h}|_{W^{1,p}(\Omega)}\neq 0}} \sup_{\substack{v^{H\times h}\in V^{H\times h}\\ |v^{H\times h}|_{W^{1,q}(\Omega)}\neq 0}} \frac{\langle F'(p^H_{m,k})w^{H\times h}, v^{H\times h}\rangle_{W^{-1,p}(\Omega)W^{1,q}(\Omega)}}{|w^{H\times h}|_{W^{1,p}(\Omega)}|v^{H\times h}|_{W^{1,q}(\Omega)}}, \tag{3.74}$$

$$\gamma_p := \sup_{\substack{w^{H\times h}\in V^{H\times h}\\ |w^{H\times h}|_{W^{1,p}(\Omega)}\neq 0}} \sup_{\substack{v^{H\times h}\in V^{H\times h}\\ |v^{H\times h}|_{W^{1,q}(\Omega)}\neq 0}} \frac{\langle F'(p^H_{m,k})w^{H\times h}, v^{H\times h}\rangle_{W^{-1,p}(\Omega)W^{1,q}(\Omega)}}{|w^{H\times h}|_{W^{1,p}(\Omega)}|v^{H\times h}|_{W^{1,q}(\Omega)}}, \tag{3.75}$$

$$L_p := \sup_{w^{H\times h}\in B(p^H_{m,k},R)} \frac{\|F'(w^{H\times h}) - F'(p^H_{m,k})\|_{W^{1,p}(\Omega),W^{-1,p}(\Omega)}}{|\, w^{H\times h} - p^H_{m,k}\,|_{W^{1,p}(\Omega)}}, \tag{3.76}$$

where R is supposed to be sufficiently large and the index p comes from the space $W^{1,p}(\Omega)$. Next we define a proximity indicator [27, 122]

$$\tau^k_{m,p} := \frac{2L_p}{\beta_p^2}(\|F(p^H_{m,k}) - P^L_k[F(p^H_{m,k})]\|_{W^{-1,p}(\Omega)} + \|P^L_k[F(p^H_{m,k})]\|_{W^{-1,p}(\Omega)}), \tag{3.77}$$

which will be used to validate whether $p^H_{m,k}$ is close enough to $p^{H\times h}$. We obtain the following result.

Proposition 3.11 (A rigorous a posteriori error bound)**.** *If $\tau^k_{m,p} < 1$ then there exists a unique solution $p^{H\times h} \in B(p^H_{m,k}, \frac{\beta_p}{L_p})$ of (3.71) and the error estimator*

$$\Delta^k_{m,p} := \frac{\beta_p}{L_p}(1 - \sqrt{1 - \tau^k_{m,p}}) \tag{3.78}$$

satisfies

$$|p^{H\times h} - p^H_{m,k}|_{W^{1,p}(\Omega)} \leq \Delta^k_{m,p}. \tag{3.79}$$

Proof. The proof follows the ideas in [27], which in turn uses ideas of [23,122]. To simplify notations we set for this proof $\langle\cdot,\cdot\rangle := \langle\cdot,\cdot\rangle_{W^{-1,p}(\Omega)W^{1,q}(\Omega)}$. We define a mapping $T : V^{H\times h} \to V^{H\times h}$ as

$$\langle F'(p^H_{m,k})T(w^{H\times h}), v^{H\times h}\rangle = \langle F'(p^H_{m,k})w^{H\times h}, v^{H\times h}\rangle - \langle F(w^{H\times h}), v^{H\times h}\rangle \quad \forall v^{H\times h} \in V^{H\times h}. \tag{3.80}$$

Due to the assumption $\tau^k_{m,p} < 1$, T is well-defined and $w^{H\times h}$ is a fixed point of T if and only if $w^{H\times h}$ solves (3.71). To prove the existence of a fixed point we apply the Banach fixed point

[2] An operator $A : V \to V^*$ is called strongly monotone if for all $u, v \in V$ there holds $\langle A(u) - A(v), u - v\rangle_{V^*,V} \geq \|u - v\|^2_V$.

theorem. First we show that T is a contraction on $B(p^H_{m,k}, \epsilon)$, where ϵ will be determined later on. For $w_1^{H\times h}$ and $w_2^{H\times h}$ in $B(p^H_{m,k}, \epsilon)$ we have

$$\begin{aligned}
&\left\langle F'(p^H_{m,k})(T(w_1^{H\times h}) - T(w_2^{H\times h})), v^{H\times h}\right\rangle \\
&\qquad = \left\langle F'(p^H_{m,k})(w_1^{H\times h} - w_2^{H\times h}), v^{H\times h}\right\rangle - \left\langle F(w_1^{H\times h}) - F(w_2^{H\times h}), v^{H\times h}\right\rangle \\
&\qquad = \left\langle \int_0^1 \left\{F'(p^H_{m,k}) - F'(w_2^{H\times h} + t(w_1^{H\times h} - w_2^{H\times h}))\right\}(w_1^{H\times h} - w_2^{H\times h})\, dt, v^{H\times h}\right\rangle.
\end{aligned}$$

Using (3.74), (3.76) and that $w_2^{H\times h} + t(w_1^{H\times h} - w_2^{H\times h}) \in B(p^H_{m,k}, \epsilon)$ for $t \in [0,1]$ we obtain

$$\beta_p \, |T(w_1^{H\times h}) - T(w_2^{H\times h})|_{W^{1,p}} \leq L_p \epsilon |w_1^{H\times h} - w_2^{H\times h}|_{W^{1,p}(\Omega)}.$$

Hence T is contractive for $\epsilon \in [0, \frac{\beta_p}{L_p})$. Next, we proof that T maps the ball $B(p^H_{m,k}, \epsilon)$ onto itself for certain values of ϵ. Let for that purpose $w^{H\times h}$ be in $B(p^H_{m,k}, \epsilon)$. We get

$$\begin{aligned}
&\langle F'(p^H_{m,k})(T(w^{H\times h}) - p^H_{m,k}), v^{H\times h}\rangle \\
&\quad = \left\langle F'(p^H_{m,k})(w^{H\times h} - p^H_{m,k}), v^{H\times h}\right\rangle - \left\langle F(w^{H\times h}) - F(p^H_{m,k}), v^{H\times h}\right\rangle - \left\langle F(p^H_{m,k}), v^{H\times h}\right\rangle \\
&\quad = \left\langle F'(p^H_{m,k})(w^{H\times h} - p^H_{m,k}), v^{H\times h}\right\rangle - \left\langle F(w^{H\times h}) - F(p^H_{m,k}), v^{H\times h}\right\rangle \\
&\qquad\qquad - \left\langle F(p^H_{m,k}) - P^L_k[F(p^H_{m,k})], v^{H\times h}\right\rangle - \left\langle P^L_k[F(p^H_{m,k})], v^{H\times h}\right\rangle \\
&\quad = \left\langle \int_0^1 \left\{F'(p^H_{m,k}) - F'(p^H_{m,k} + t(w^{H\times h} - p^H_{m,k}))\right\}(w^{H\times h} - p^H_{m,k})\, dt, v^{H\times h}\right\rangle \\
&\qquad\qquad - \left\langle F(p^H_{m,k}) - P^L_k[F(p^H_{m,k})], v^{H\times h}\right\rangle - \left\langle P^L_k[F(p^H_{m,k})], v^{H\times h}\right\rangle.
\end{aligned}$$

Again we employ (3.74) and (3.76) to obtain

$$\beta_p \, |T(w^{H\times h}) - p^H_{m,k}|_{W^{1,p}(\Omega)} \leq \frac{1}{2} L_p \epsilon^2 + \|F(p^H_{m,k}) - P^L_k[F(p^H_{m,k})]\|_{W^{-1,p}(\Omega)} + \|P^L_k[F(p^H_{m,k})]\|_{W^{-1,p}(\Omega)}.$$

Thus $|T(w^{H\times h}) - p^H_{m,k}|_{W^{1,p}(\Omega)}$ is bounded by ϵ if $\epsilon \in [\Delta^k_{m,p}, (\beta_p/L_p)(1 + \sqrt{1 - \tau^k_{m,p}})]$ and the assumptions of the Banach fixed point theorem are fulfilled for $\epsilon \in [\Delta^k_{m,p}, (\beta_p/L_p))$, which yields the assertion. □

We remark that $\Delta^k_{m,p}$ (3.78) only takes into account the error caused by the approximation of $F(p^H_{m,k})$ by $P^L_k[F(p^H_{m,k})]$, while the approximation $P^{L_f}_{k_f}[F'(p^H_{m,k})]$ of the Fréchet derivative $F'(p^H_{m,k})$ does not occur. However, writing down Newton's method for both $p^H_{m,k}$ and $p^{H\times h}$ it is easy to see that in general the quality of the approximation of the Fréchet derivative only affects the speed of convergence of Newton's method but not the error in the residual. It is therefore reasonable that $\Delta^k_{m,p}$ only contains the term $\|F(p^H_{m,k}) - P^L_k[F(p^H_{m,k})]\|_{W^{-1,p}(\Omega)}$ to measure the error due to the approximation of the nonlinear operator. Next, we analyze as in [27] the effectivity $\Delta^k_{m,p}/|p^{H\times h} - p^H_{m,k}|_{W^{1,p}(\Omega)}$ of the error bound (3.78).

Proposition 3.12 (Effectivity)**.** *Let us assume that*

$$\|F(p_{m,k}^H) - P_k^L[F(p_{m,k}^H)]\|_{W^{-1,p}(\Omega)} \leq c_{err}\|P_k^L[F(p_{m,k}^H)]\|_{W^{-1,p}(\Omega)} \tag{3.81}$$

for $c_{err} \in [0,1)$ *and set*

$$C_{err} := \frac{1 - c_{err}}{1 + c_{err}}.$$

If $\tau_{m,p}^k \leq \frac{1}{2}C_{err}$ *we have*

$$\Delta_{m,p}^k \leq 4C_{err}^{-1}\frac{\gamma_p}{\beta_p}\,|p^{H\times h} - p_{m,k}^H|_{W^{1,p}(\Omega)}. \tag{3.82}$$

Proof. Again we simplify notations by setting for this proof $\langle\cdot,\cdot\rangle := \langle\cdot,\cdot\rangle_{W^{-1,p}(\Omega)W^{1,q}(\Omega)}$. It is easy to see (cf. [27]) that (3.81) implies

$$\begin{aligned}\|P_k^L[F(p_{m,k}^H)]\|_{W^{-1,p}(\Omega)} + \|F(p_{m,k}^H) - P_k^L[F(p_{m,k}^H)]\|_{W^{-1,p}(\Omega)} \\ \leq C_{\mathrm{err}}^{-1}\big(\|P_k^L[F(p_{m,k}^H)]\|_{W^{-1,p}(\Omega)} - \|F(p_{m,k}^H) - P_k^L[F(p_{m,k}^H)]\|_{W^{-1,p}(\Omega)}\big).\end{aligned} \tag{3.83}$$

The following estimate differs from [27], as in [27] a quadratic nonlinear PDE in a Hilbert space is considered and the proof of the effectivity of the error bound heavily relies on these two assumptions. As $\tau_{m,p}^k \leq \frac{1}{2}C_{\mathrm{err}} \leq 1$ we can use Proposition 3.11 and get

$$\begin{aligned}&\big\langle F(p_{m,k}^H) - P_k^L[F(p_{m,k}^H)], v^{H\times h}\big\rangle + \big\langle P_k^L[F(p_{m,k}^H)], v^{H\times h}\big\rangle \\ &\quad = -\langle F'(p_{m,k}^H)(p^{H\times h} - p_{m,k}^H), v^{H\times h}\rangle \\ &\qquad + \left\langle \int_0^1 \left\{F'(p_{m,k}^H) - F'(p_{m,k}^H + t(p^{H\times h} - p_{m,k}^H))\right\}(p^{H\times h} - p_{m,k}^H)\,dt, v^{H\times h}\right\rangle.\end{aligned}$$

Employing (3.75) and (3.76) we obtain similarly to [121]

$$\begin{aligned}\|P_k^L[F(p_{m,k}^H)] + F(p_{m,k}^H) - P_k^L[F(p_{m,k}^H)]\|_{W^{-1,p}(\Omega)} \\ \leq \gamma_p\,|p^{H\times h} - p_{m,k}^H|_{W^{1,p}(\Omega)} + \frac{L_p}{2}|p^{H\times h} - p_{m,k}^H|_{W^{1,p}(\Omega)}^2\end{aligned}$$

and thus

$$\begin{aligned}\|P_k^L[F(p_{m,k}^H)]\|_{W^{-1,p}(\Omega)} - \|F(p_{m,k}^H) - P_k^L[F(p_{m,k}^H)]\|_{W^{-1,p}(\Omega)} \\ \leq \gamma_p\,|p^{H\times h} - p_{m,k}^H|_{W^{1,p}(\Omega)} + \frac{L_p}{2}|p^{H\times h} - p_{m,k}^H|_{W^{1,p}(\Omega)}^2.\end{aligned}$$

(3.83) then yields

$$\begin{aligned}\|P_k^L[F(p_{m,k}^H)]\|_{W^{-1,p}(\Omega)} + \|F(p_{m,k}^H) - P_k^L[F(p_{m,k}^H)]\|_{W^{-1,p}(\Omega)} \\ \leq C_{\mathrm{err}}^{-1}\big(\gamma_p\,|p^{H\times h} - p_{m,k}^H|_{W^{1,p}(\Omega)} + \frac{L_p}{2}|p^{H\times h} - p_{m,k}^H|_{W^{1,p}(\Omega)}^2\big).\end{aligned} \tag{3.84}$$

As $\tau_{m,p}^k \leq 1$ we have $1 - \sqrt{1-\tau_{m,p}^k} \leq \tau_{m,p}^k$ and thus obtain [27]

$$\begin{aligned}\Delta_{m,p}^k &= \frac{\beta_p}{L_p}\big(1 - \sqrt{1-\tau_{m,p}^k}\big) \leq \frac{\beta_p}{L_p}\tau_{m,p}^k \\ &= \frac{2}{\beta_p}\left(\|P_k^L[F(p_{m,k}^H)]\|_{W^{-1,p}(\Omega)} + \|F(p_{m,k}^H) - P_k^L[F(p_{m,k}^H)]\|_{W^{-1,p}(\Omega)}\right).\end{aligned} \tag{3.85}$$

Following the ideas in [27] we invoke (3.84), (3.85) and Proposition 3.11 to get

$$\begin{aligned}\frac{1}{2}C_{\mathrm{err}}\beta_p\Delta_{m,p}^k &\le \gamma_p\,|p^{H\times h}-p_{m,k}^H|_{W^{1,p}(\Omega)}+\frac{L_p}{2}|p^{H\times h}-p_{m,k}^H|_{W^{1,p}(\Omega)}^2\\ &\le \gamma_p\,|p^{H\times h}-p_{m,k}^H|_{W^{1,p}(\Omega)}+\frac{1}{2}\Delta_{m,p}^k(L_p\Delta_{m,p}^k).\end{aligned}$$

Using (3.85) again yields

$$\frac{1}{2}C_{\mathrm{err}}\beta_p\Delta_{m,p}^k \le \gamma_p\,|p^{H\times h}-p_{m,k}^H|_{W^{1,p}(\Omega)}+\frac{1}{2}\Delta_{m,p}^k\beta_p\tau_{m,p}^k,$$

and thus as $\tau_{m,p}^k \le \frac{1}{2}C_{\mathrm{err}}$

$$\Delta_{m,p}^k \le 4C_{\mathrm{err}}^{-1}\,\frac{\gamma_p}{\beta_p}\,|p^{H\times h}-p_{m,k}^H|_{W^{1,p}(\Omega)}.$$

□

Note that the terms $\|F(p_{m,k}^H)-P_k^L[F(p_{m,k}^H)]\|_{W^{-1,p}(\Omega)}$ and $\|P_k^L[F(p_{m,k}^H)]\|_{W^{-1,p}(\Omega)}$ are computable as $V^{H\times h}$ is a finite dimensional space. Alternatively, as in §2.4.2, the dual norms can be estimated by a localized residual type estimator (cf. [105]). To obtain the required interpolation estimate for the terms $|v^{H\times h}-v_m^H|_{W^{1,p}(\Omega)}$ we propose to replace $v^{H\times h}$ in the latter term by $v_{m'}^H$ with $m'>m$. As the original problem (3.1) has been stated in the space $H^1(\Omega)$ we finally derive an error bound for $|p^{H\times h}-p_{m,k}^H|_{H^1(\Omega)}$ for problems where F has to be considered as a mapping from $W^{1,p}(\Omega)$ onto $W^{-1,p}(\Omega)$ for $p>2$. As in [23] we assume that for all $z\in B(p_{m,k}^H,R):=\{z\in V^{H\times h}\,:\,|z-p_{m,k}^H|_{W^{1,p}(\Omega)}\le R\}$, $F'(z):W^{1,p}(\Omega)\to W^{-1,p}(\Omega)$ can be extended as an operator in $L(H^1(\Omega),H^{-1}(\Omega))$. In general this can be achieved by applying the Hahn-Banach theorem. Furthermore, we require that

$$0<\beta_2:=\inf_{\substack{w^{H\times h}\in V^{H\times h}\\ |w^{H\times h}|_{H^1(\Omega)}\neq 0}}\sup_{\substack{v^{H\times h}\in V^{H\times h}\\ |v^{H\times h}|_{H^1(\Omega)}\neq 0}}\frac{\langle F'(p_{m,k}^H)w^{H\times h},v^{H\times h}\rangle}{|w^{H\times h}|_{H^1(\Omega)}|v^{H\times h}|_{H^1(\Omega)}},\tag{3.86}$$

and that there exists constants γ_2 and L_2 such that

$$\langle F'(p_{m,k}^H)w^{H\times h},v^{H\times h}\rangle \le \gamma_2|w^{H\times h}|_{W^{1,p}(\Omega)}|v^{H\times h}|_{H^1(\Omega)},\tag{3.87}$$

$$\|F'(v_m^H)-F'(w_m^H)\|_{H^1(\Omega),H^{-1}(\Omega)} \le L_2\,|\,v_m^H-w_m^H\,|_{W^{1,p}(\Omega)}.\tag{3.88}$$

Following the idea of the proof of Theorem 6.4 in [23] and taking into account the additional terms due to the EPM, we obtain under the assumptions of Proposition 3.11

$$\begin{aligned}&|p^{H\times h}-p_{m,k}^H|_{H^1(\Omega)}\\ &\quad\le\frac{1}{\beta_2}\big(L_2|p^{H\times h}-p_{m,k}^H|_{H^1(\Omega)}|p^{H\times h}-p_{m,k}^H|_{W^{1,p}(\Omega)}\\ &\qquad\qquad+\|F(p_{m,k}^H)-P_k^L[F(p_{m,k}^H)]\|_{H^{-1}(\Omega)}+\|P_k^L[F(p_{m,k}^H)]\|_{H^{-1}(\Omega)}\big)\\ &\quad\le\frac{1}{\beta_2}\big(L_2|p^{H\times h}-p_{m,k}^H|_{H^1(\Omega)}\,\Delta_{m,p}^k\\ &\qquad\qquad+\|F(p_{m,k}^H)-P_k^L[F(p_{m,k}^H)]\|_{H^{-1}(\Omega)}+\|P_k^L[F(p_{m,k}^H)]\|_{H^{-1}(\Omega)}\big).\end{aligned}\tag{3.89}$$

As this bound requires the computation of the dual norms and the appearing constants both in the $W^{1,p}$- and the H^1-norm, we propose another ansatz. Due to the finite dimensionality of $V^{H\times h}$ a scaling argument yields the inverse estimate

$$|\, v^{H\times h}\,|_{W^{1,p}(\Omega)} \leq c_h |\, v^{H\times h}\,|_{H^1(\Omega)} \qquad \text{where } c_h := (H^2+h^2)^{\frac{2-p}{2p}}. \tag{3.90}$$

Based on that we define the proximity indicator

$$\tau^k_{m,2} := \frac{2L_2 c_h}{\beta_2^2}(\|F(p^H_{m,k}) - P^L_k[F(p^H_{m,k})]\|_{H^{-1}(\Omega)} + \|P^L_k[F(p^H_{m,k})]\|_{H^{-1}(\Omega)}) \tag{3.91}$$

and obtain the following result.

Proposition 3.13 (An error bound for the H^1-norm)**.** *Let $\tau^k_{m,2} < 1$ and* (3.86)*,* (3.87) *and* (3.88) *be fullfilled. Then there exists a unique solution $p^{H\times h} \in B(p^H_{m,k}, \frac{\beta_2}{L_2 c_h})$ of* (3.71)*. If we further assume that*

$$\|F(p^H_{m,k}) - P^L_k[F(p^H_{m,k})]\|_{H^{-1}(\Omega)} \leq c_{err}\|P^L_k[F(p^H_{m,k})]\|_{H^{-1}(\Omega)} \tag{3.92}$$

for $c_{err} \in [0,1)$ and $\tau^k_{m,2} \leq \frac{1}{2}C_{err}$, where $C_{err} := (1-c_{err})/(1+c_{err})$, the error estimator

$$\Delta^k_m := \frac{\beta_2}{L_2 c_h}(1-\sqrt{1-\tau^k_{m,2}}) \tag{3.93}$$

satisfies

$$\frac{C_{err}}{4}\frac{\beta_2}{\gamma_2 c_h}\Delta^k_m \leq |p^{H\times h} - p^H_{m,k}|_{H^1(\Omega)} \leq \Delta^k_m. \tag{3.94}$$

Proof. Using (3.90) the proof is completely analogous to the proofs of Proposition 3.11 and 3.12. □

As in §2.4.1 we use the Riesz representative to compute $\|P^L_k[F(p^H_{m,k})]\|_{H^{-1}(\Omega)}$ and $\|F(p^H_{m,k}) - P^L_k[F(p^H_{m,k})]\|_{H^{-1}(\Omega)}$. As assembling $\langle F(p^H_{m,k}) - P^L_k[F(p^H_{m,k})], v^{H\times h}\rangle$ requires the computation of full dimensional integrals due to the nonlinearity of F, we invoke the a posteriori error bound for the EPM derived in Proposition 3.9 to replace $F(p^H_{m,k})$ by $P^{L'}_{k'}[F(p^H_{m,k})]$. We define the Riesz representatives $\mathcal{R}^{H\times h}_m$ and $\mathcal{E}^{H\times h}_k$ as the solutions of

$$(\mathcal{R}^{H\times h}_m, v^{H\times h})_{H^1} = (P^L_k[F(p^H_{m,k})], v^{H\times h})_{H^1} \quad \forall v^{H\times h} \in V^{H\times h}, \tag{3.95}$$

and

$$(\mathcal{E}^{H\times h}_k, v^{H\times h})_{H^1} = (P^{L'}_{k'}[F(p^H_{m,k})] - P^L_k[F(p^H_{m,k})], v^{H\times h})_{H^1} \quad \forall v^{H\times h} \in V^{H\times h}, \tag{3.96}$$

respectively. Here, $(\cdot,\cdot)_{H^1}$ denotes the inner product associated with the H^1-half norm. We thus obtain

$$|\, \mathcal{R}^{H\times h}_m\,|_{H^1(\Omega)} = \|P^L_k[F(p^H_{m,k})]\|_{H^{-1}(\Omega)} \tag{3.97}$$

$$\text{and} \quad |\, \mathcal{E}^{H\times h}_k\,|_{H^1(\Omega)} = \|P^{L'}_{k'}[F(p^H_{m,k})] - P^L_k[F(p^H_{m,k})]\|_{H^{-1}(\Omega)}. \tag{3.98}$$

By doing so we maintain both reliability and effectivity of our error bound (3.93). To implement the latter, we employ the a priori bound (3.31) for the EPM to verify (3.92) without computing $\langle F(p^H_{m,k}), v^{H\times h}\rangle$ and then use the following modification of (3.83)

$$\begin{aligned}\|P^L_k[F(p^H_{m,k})]\|_{H^{-1}(\Omega)} + \|P^{L'}_{k'}[F(p^H_{m,k})] - P^L_k[F(p^H_{m,k})]\|_{H^{-1}(\Omega)} \\ \leq C^{-1}_{\text{err}}\big(\|P^L_k[F(p^H_{m,k})]\|_{H^{-1}(\Omega)} - \|F(p^H_{m,k}) - P^L_k[F(p^H_{m,k})]\|_{H^{-1}(\Omega)}\big).\end{aligned}$$

Note that due to definition of the snapshot set W_K^h (3.66), the a priori bound (3.31) for the EPM is only applicable, if W_K^h is a good approximation of the set $\{A(p^{H\times h}(\mu,\hat{y})),\, \mu\in\Xi_{train}\}$. This can be verified by comparing the convergence rates of the eigenvalues $\{\lambda_l^{\text{EPM}}\}_{l=1}^{k_{\text{POD}}}$ of the POD applied to W_K^H and the coefficients $\| \int_{\widehat{\omega}} \mathcal{I}_L[A(p_{m,k}^H)]\kappa_l\|^2_{L^2(\Omega_{1D})}$, $l=1,...,k_{\text{POD}}$. If the convergence rates do not coincide we propose to replace $\{\lambda_l^{\text{EPM}}\}_{l=1}^{k_{\text{POD}}}$ by $\| \int_{\widehat{\omega}} \mathcal{I}_L[A(p_{m,k}^H)]\kappa_l\|^2_{L^2(\Omega_{1D})}$, $l=1,...,k_{\text{POD}}$, in the a priori bound (3.31) for the EPM. This requires only the computation of $k_{\text{POD}}-k$ additional integrals in y-direction. As the behavior of the coefficients $\int_{\widehat{\omega}} \mathcal{I}_L[A(p_{m,k}^H)]\kappa_l$ strongly influences the convergence behavior of $P_k^L[A(p_{m,k}^H)]$ for increasing k we expect that (3.31) remains a reliable a priori bound when substituting $\{\lambda_l^{\text{EPM}}\}_{l=1}^{k_{\text{POD}}}$ by $\| \int_{\widehat{\omega}} \mathcal{I}_L[A(p_{m,k}^H)]\kappa_l\|^2_{L^2(\Omega_{1D})}$, $l=1,...,k_{\text{POD}}$. This is demonstrated by the numerical experiments in §3.6.

Remark 3.14. *Instead of using the Riesz representative to compute $\|P_k^L[F(p_{m,k}^H)]\|_{H^{-1}(\Omega)}$, the latter can be estimated by a localized residual type estimator (cf. [105]). However, as the Riesz representative yields the optimal estimate and exhibits the same scaling in $N_H n_h$ as localized residual type estimators, we have chosen to employ the former.*

We remark that for small inf-sup stability factors, which often occur in subsurface flow, the requirement $\tau_{m,2}^k<1$ is difficult to fulfill. In case $\tau_{m,2}^k>1$ the proximity indicator can be used as an error estimator, which yields however a bad effectivity constant due to the factor β_2^{-2}. We therefore derive additionally a less sharper error bound which is also computable for $\tau_{m,2}^k>1$.

Corollary 3.15. *Under the assumptions of Proposition 3.13 the error estimator*

$$\Delta_{m,2}^k := \frac{2}{\beta_2}\left(\|F(p_{m,k}^H)-P_k^L[F(p_{m,k}^H)]\|_{H^{-1}(\Omega)}+\|P_k^L[F(p_{m,k}^H)]\|_{H^{-1}(\Omega)}\right) \tag{3.99}$$

satisfies

$$|p^{H\times h}-p_{m,k}^H|_{H^1(\Omega)}\le \Delta_{m,2}^k. \tag{3.100}$$

If $\Delta_{m,2}^k\le\frac{2\gamma_2}{L_2}$ we obtain

$$\Delta_{m,2}^k \le 4C_{err}^{-1}\frac{\gamma_2 c_h}{\beta_2}\,|p^{H\times h}-p_{m,k}^H|_{H^1(\Omega)}. \tag{3.101}$$

Proof. (3.100) is the analogon of (3.85) for the H^1-norm. To show (3.101) we estimate as in the proof of Proposition 3.12

$$\frac{1}{2}C_{\text{err}}\beta_2\Delta_{m,2}^k \le c_h\,\gamma_2\,|p^{H\times h}-p_{m,k}^H|_{H^1(\Omega)}+\frac{L_2 c_h}{2}|p^{H\times h}-p_{m,k}^H|_{H^1(\Omega)}\Delta_{m,2}^k.$$

Inspired by [121] we use the assumption $\Delta_{m,2}^k\le\frac{2\gamma_2}{L_2}$ to obtain

$$\frac{1}{2}C_{\text{err}}\beta_2\Delta_{m,2}^k \le 2c_h\,\gamma_2\,|p^{H\times h}-p_{m,k}^H|_{H^1(\Omega)}$$

and thus the claim. □

Remark 3.16. *Apart from the additional term for the EPM the error bound $\Delta_{m,2}^k$ coincides with the bound proposed in Proposition 2.1 in the work by Verfürth [121], where $|p^{H\times h}-p_{m,k}^H|_{H^1(\Omega)}\le \min\{\frac{\beta_2}{L_2 c_h},\frac{2\gamma_2}{L_2}\}$ is assumed for the derivation of $\Delta_{m,2}^k$. Although this assumption cannot be verified, it is less strict than requiring $\tau_{m,2}^k<1$, and therefore easier to fulfill.*

Finally, we mention that in a very recent work by Dolejší, Ern and Vohralík [41] on a posteriori error estimation for possibly degenerate nonlinear advection-diffusion equations, is proposed to use an estimate for the dual norm of the residual as an error bound, and to omit the inf-sup stability factor and the Lipschitz constant. Based on that we define a third error estimator $\Delta^k_{m,res}$ as

$$\Delta^k_{m,res} := \|F(p^H_{m,k}) - P^L_k[F(p^H_{m,k})]\|_{H^{-1}(\Omega)} + \|P^L_k[F(p^H_{m,k})]\|_{H^{-1}(\Omega)}. \tag{3.102}$$

In §3.6 we will compare Δ^k_m (3.93), $\Delta^k_{m,2}$ (3.99) and $\Delta^k_{m,res}$(3.102) also for very small inf-sup stability factors.

3.4.2 Computation of the inf-sup stability factor and the Lipschitz constant

We close this section by addressing the computation of the inf-sup stability factor β_2 and the Lipschitz constant L_2. As for many problems, including the considered model problem (3.3), global bounds for the Lipschitz constant L_2 are available, we will focus on the determination of the inf-sup stability factor β_2. Inspired by the idea in [127] to employ a matrix-DEIM approximation of the jacobian for the computation of the Lipschitz constant of the considered nonlinear operator, we propose to use the EPM to approximate β_2. Precisely, we use the a posteriori error bound for the EPM derived in Proposition 3.9, to find k' such that $P^{L'}_{k'}[F'(p^H_{m,k})]$ approximates $F'(p^H_{m,k})$ up to a given tolerance and define

$$\beta_2^{\text{app}} := \inf_{\substack{w^{H\times h}\in V^{H\times h}\\ |w^{H\times h}|_{H^1(\Omega)}\neq 0}} \sup_{v^{H\times h}\in V^{H\times h}|v^{H\times h}|_{H^1(\Omega)}\neq 0} \frac{\langle P^{L'}_{k'}[F'(p^H_{m,k})]w^{H\times h}, v^{H\times h}\rangle}{|w^{H\times h}|_{H^1(\Omega)}|v^{H\times h}|_{H^1(\Omega)}}. \tag{3.103}$$

β_2^{app} equals the smallest singular value of the jacobian associated with $\langle P^{L'}_{k'}[F'(p^H_{m,k})]w^{H\times h}, v^{H\times h}\rangle$. Thus we determine the latter to compute β_2^{app}. Theorem 3.8 yields the convergence of $P^{L'}_{k'}[F'(p^H_{m,k})]$ to $F'(p^H_{m,k})$ as $k' \to K$, which implies $\beta_2^{\text{app}} \to \beta_2$ as $k' \to K$. Although we therefore expect β_2^{app} to be a very good approximation of β_2, which is demonstrated by the numerical experiments in §3.6, it is not clear that β_2^{app} is indeed a lower bound of β_2. In the RB framework the successive constraint method introduced in [65] is in wide use for the determination of a parametric lower bound for the inf-sup stability factor, which is efficiently computable in the online stage by solving a small optimization problem. However, this approach is not applicable in our context as (3.103) does not depend on one parameter value $\mu \in \mathcal{D}$ but on all "parameter values" $x \in \Omega_{1D}$ at once.

3.5 Analysis of the computational costs of the HMR-RB approach employing the EPM

This section is devoted to the comparison of the total computational costs for computing the solution $p^H_{m,k}$ of (3.41) using the HMR-RB approach and the EPM with the computation of the reference solution $p^{H\times h}$ of (3.71). We consider the same FE-spaces as used for the numerical experiments in §3.6, namely,

$$X^H = \left\{v^H \in C^0(\Omega_{1D}) : v^H|_{\mathcal{T}_i} \in \mathbb{P}^1_1(\mathcal{T}_i), \mathcal{T}_i \in \mathcal{T}_H\right\},\ Y^h = \{v^h \in C^0(\widehat{\omega}) : v^h|_{\tau_j} \in \mathbb{P}^1_1(\tau_j), \tau_j \in \tau_h\},$$

and $V^{H\times h} = \{v^{H\times h} \in C^0(\widehat{\Omega}) : v^{H\times h}|_{T_{i,j}} \in \mathbb{Q}_{1,1}, T_{i,j} \in \widehat{T}\}$. The application of the EPM allows us to decompose the computation of the discrete reduced solution $p^H_{m,k}$ in a n_h-dependent offline and

a n_h-independent online stage, where the total computational costs for $p^H_{m,k}$ comprise both offline- and online costs. Offline we construct the reduction space Y^h_m and the collateral basis space W^h_k and precompute the integrals in transverse direction occurring in (3.41). Afterwards we solve (3.41) online with Newton's method. In detail we arrive at the following total computational costs.

(i) *Offline stage: Construction of Y^h_m and W^h_k by Algorithm 3.3.3 (*Adaptive-HMR-RB*):* First, we assemble the integrals for the source term in $\mathcal{O}(\max\{N_H, n_h\})$ operations. In the adaptive refinement step we compute the set of snapshots $\mathcal{P}^h(\mu)$, $\mu \in \Xi_{train}$, by Newton's method (3.54), where the computational costs are dominated by the assembling of the jacobian, which takes $\mathcal{O}(n_{train} n_h)$ operations. As the jacobian is tridiagonal, the linear system of equations in (3.54) can be solved by a Thomas algorithm in $\mathcal{O}(n_{train} n_h)$ operations [107]. To compute the corresponding coarse reduced solutions $p^{H'}_{m,k}$ of (3.41) we have used an inexact Newton method (3.43) with a preconditioned stabilized bi-conjugate gradient (bi-cgstab) method, where the latter scaled linearly for the considered test cases in §3.6. The linear system of equations in (3.43) can be assembled in $\mathcal{O}(n_{train} N_{H'})$ operations, which equals the number of operations required to compute $p^{H'}_{m,k}$. In order to compute Δ^k_m (3.93) we apply a preconditioned conjugate gradient (pcg) method for the computation of the Riesz representatives (3.95) and (3.96) in $\mathcal{O}(n_{train} n_h N_{H'})$ operations and compute the required constants in $\mathcal{O}(n_{train} n_h N_{H'})$ operations. The latter is dominated by the determination of the inf-sup stability factor, which necessitates the assembling of the jacobian and the subsequent computation of its smallest singular value. The latter can be identified by an inverse iteration in $\mathcal{O}(n_{train} N_{H'} n_h)$ operations as the jacobian is sparse [107].

The computational costs for computing the richer collateral basis space $W^h_{k'}$ with Algorithm 3.3.1 EPM-Indicator account for $\mathcal{O}(n_h)$ operations for the application of the EIM 3.2.1, $\mathcal{O}(n_{train} n_h k)$ operations for performing the Algorithm 3.2.2 EPM, dominated by the computation of the integration error (3.28), and the costs for the POD to determine the complete collateral basis space $W_{k_{POD}}$. The computational costs of the QP-indicator mainly consist of the costs for the application of the POD to compute the reduced basis. The costs for all PODs in Algorithm 3.3.2 AdaptiveTrainExtension, including the ones to determine the coarse bases at the end of each loop over m, are dominated by the costs for the PODs applied to the discrete manifolds Y^h_M and W^h_K in Algorithm 3.3.3 Adaptive-HMR-RB to compute the reduction space Y^h_m and the collateral basis space W^h_k. The PODs in Algorithm 3.3.3 require $\mathcal{O}(n^2_{train} n_h)$ operations for the formation of the correlation matrixes and $\mathcal{O}(n^3_{train})$ operations for the solution of the eigenvalue problems. Finally, we compute the integrals in the transverse direction in (3.43), depending on the basis functions $\{\phi_l\}^m_{l=1}$ and $\{\kappa_l\}^k_{l=1}$, in $\mathcal{O}(km^2 n_h)$ operations.

(ii) *Online stage: Solution of the coupled system of nonlinear 1D PDEs* (3.41)*:* We solve (3.41) with an inexact Newton's method, applying the bi-cgstab method to solve the linear system of equations in (3.43), where the bi-cgstab method takes $\mathcal{O}(m^2 N_H)$ operations. The assembling of the jacobian in each Newton step dominates the costs for computing $p^H_{m,k}$. It requires the computation of the integrals in the dominant direction in $\mathcal{O}(LN_H)$ operations and the subsequent assembling of the matrix in $\mathcal{O}(km^2 N_H)$ operations.

As in §2.5 a threshold can be detected in the offline costs due to the mesh size independent factor n_{train}. Choosing $N_{H'}$ constant and thus independently of N_H the offline costs add up to $\mathcal{O}(n_{train} n_h)$ operations and we obtain a linear scaling of the HMR-RB approach using the EPM in $\max\{n_h, N_H\}$. The numerical experiments in §3.6 confirm the latter. The reference solution

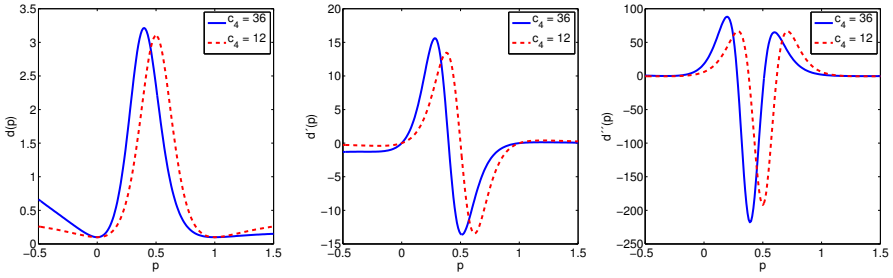

(a) d (b) d' (c) d''

Figure 3.1: The nonlinear function $d(p)$ (a) and its derivatives $d'(p)$ (b) and $d''(p)$ (c) for $c_0 = 0.1$ and $c_4 = 36$ (solid) and $c_4 = 12$ (dashed).

$p^{H\times h}$ of (3.71) is also computed by an inexact Newton method, which uses the bi-cgstab method to solve the linear system of equations, where the latter required $\mathcal{O}(N_H^{2.75})$ operations. Although the jacobian can be assembled in $\mathcal{O}(N_H n_h)$ operations, it clearly dominated the computational costs for the computation of $p^{H\times h}$ in our numerical experiments §3.6. This is due to the fact that the assembling necessitates the computation of a two-dimensional integral for each element, which is very expensive due to the required evaluations of the nonlinear operator. Based on the above analysis of the total theoretical runtimes we expect that for a sufficiently small sample size n_{train} compared to N_H and n_h, the HMR-RB approach outperforms the bilinear FEM beyond a certain mesh size. This is confirmed by the numerical experiments in §3.6.

3.6 Numerical Experiments

In this section we demonstrate the applicability of the HMR-RB approach using the EPM to nonlinear PDEs by investigating its convergence behavior and computational efficiency. Moreover we analyze the effectivity of the a posteriori error estimators derived in §3.4, including a validation of the employed a priori and a posteriori bounds for the EPM stated in Theorem 3.8 and Proposition 3.9. For this purpose we consider the model problem (3.3)

$$\text{Find } p \in H_0^1(\Omega) : \int_\Omega d(p)\nabla p \nabla v \, dxdy = \int_\Omega sv \, dxdy \quad \forall v \in H_0^1(\Omega), \tag{3.104}$$

where $s \in L^2(\Omega)$ and

$$d(p) := \frac{36}{c_4} \frac{p^2(1-p)^2}{(p^3 + \frac{12}{c_4}(1-p)^3)^2} + c_0. \tag{3.105}$$

Here, c_0 is the same constant as in (3.4) and c_4 weights the contributions of the terms p^3 and $(1-p)^3$. Furthermore we have $d(p) = \mathsf{f}'(p)$ where $\mathsf{f}(p) = \frac{p^3}{12}/(\frac{p^3}{12} + \frac{(1-p^3)}{c_4})$ has been chosen in [85] as the fractional flow function of the wetting fluid in the model for immiscible two-phase flow in porous media considered in [85]. The function $d(p)$ satisfies (3.4), where the boundedness can only be obtained locally, as $d(p)$, $d'(p)$ and $d''(p)$, depicted in Fig. 3.1, may have singularities for some choices of c_4. In the first test case we prescribe again the analytical solution of test case 1 in §2.6 to compare the convergence rates of the HMR-RB approach for linear and nonlinear problems. Also in the nonlinear case, the HMR-RB approach, no matter if the EPM is applied or not, converges exponentially fast in the model order m. However, the convergence rate is worse

than for the linear problem. In the other test case we prescribe a discontinuous source term s resulting in a solution with little spatial regularity both in the dominant and transverse direction. Still, we observe an exponential convergence rate of the HMR-RB approach using the EPM in the model order m. Both test cases have been computed employing linear FE in x- and y-direction, i.e. $X^H = \left\{v^H \in C^0(\Omega_{1D}) : v^H|_{\mathcal{T}_i} \in \mathbb{P}^1_1(\mathcal{T}_i), \mathcal{T}_i \in \mathcal{T}_H\right\}, Y^h = \left\{v^h \in C^0(\widehat{\omega}) : v^h|_{\tau_j} \in \mathbb{P}^1_1(\tau_j), \tau_j \in \tau_h\right\}$, and $V^{H\times h} = \{v^{H\times h} \in C^0(\widehat{\Omega}) : v^{H\times h}|_{T_{i,j}} \in \mathbb{Q}_{1,1}, T_{i,j} \in \widehat{T}\}$, using equidistant grids in x- and y-direction. We have only applied a simplified version of Algorithm 3.3.3 Adaptive-HMR-RB in the numerical experiments, as we have chosen the number of quadrature points employed in the parameter dependent 1D problem (3.51) a priori. However, a comparison of the performance of the HMR-RB approach using 1 or 2 quadrature points in (3.51) is provided for the second test case. Furthermore we have applied the EPM 3.2.2 with $N^{\text{int}}_{\max} = 0$ and we thus obtain $k = L$ in (3.29). We have used the a priori bound (B.4). As for $c_4 = 36$, d has a singularity near $p = -2.26$, we could not apply the global constants γ_2 and L_2 of §3.4.2. Hence we computed local approximations by evaluating d, d' and d'' in the discrete reduced solution $p^H_{m,k}$ of (3.41). Unless otherwise stated we have employed the error bound Δ^k_m (3.93) in the Algorithm 3.3.3 Adaptive-HMR-RB.

For the efficient assembling of the correlation matrix of the POD and thus the efficient computation of the collateral basis spaces W^h_k (3.66), we employed the projector $P^h : L^2(\widehat{\omega}) \to Y^h$, satisfying

$$\int_{\widehat{\omega}} P^h[\mathcal{A}^h](\mu)v^h = \int_{\widehat{\omega}} \mathcal{A}^h(\mu)v^h \quad \forall v^h \in Y^h, \ \ \mu \in \Xi_{1D}, \tag{3.106}$$

and set $\tilde{\mathcal{A}}^h_1(\mu) = P^h[\mathcal{A}^h_1](\mu)$, $\tilde{\mathcal{A}}^h_{f,1}(\mu) = P^h[\mathcal{A}^h_{f,1}](\mu)$ and $\tilde{\mathcal{A}}^h_{f,3}(\mu) = P^h[\mathcal{A}^h_{f,3}](\mu)$, where $\mathcal{A}^h_1(\mu)$, $\mathcal{A}^h_{f,1}(\mu)$ and $\mathcal{A}^h_{f,3}(\mu)$ have been defined in (3.63) and (3.64). Moreover, we define $\tilde{\mathcal{A}}^h_2(\mu)|_{\tau_j} = \frac{1}{h}\int_{\tau_j} \mathcal{A}^h_2(\mu)$ and $\tilde{\mathcal{A}}^h_{f,2}(\mu)|_{\tau_j} = \frac{1}{h}\int_{\tau_j} \mathcal{A}^h_{f,2}(\mu)$ for all $\tau_j \in \tau_h$. Note that we have $\|\tilde{\mathcal{A}}^h(\mu) - \mathcal{A}^h(\mu)\|_{L^2(\widehat{\omega})} \leq h\|\mathcal{A}^h\|_{H^1(\widehat{\omega})}$ for $\mathcal{A}(\mu) = \mathcal{A}^h_1(\mu), \mathcal{A}^h_{f,1}(\mu), \mathcal{A}^h_{f,3}(\mu)$ [114] and otherwise $\|\tilde{\mathcal{A}}^h(\mu) - \mathcal{A}^h(\mu)\|_{L^2(\widehat{\omega})} \to 0$, as $h \to 0$, as $\tilde{\mathcal{A}}^h_2(\mu)$ and $\tilde{\mathcal{A}}^h_{f,2}(\mu)$ are step functions. We designate with $W^h_{K,1}$ and $W^h_{K,2}$ the discrete operator manifolds (3.66) and with $W^H_{k,1}$ and $W^h_{k,2}$ the collateral basis spaces associated with the projected parameter dependent snapshots $\tilde{\mathcal{A}}^h_1(\mu)$ and $\tilde{\mathcal{A}}^h_2(\mu)$. Analogously $W^h_{K_f,1}$, $W^h_{K_f,2}$, and $W^h_{K_f,3}$ denote the discrete manifolds and $W^H_{k_f,1}$, $W^h_{k_f,2}$, and $W^h_{k_f,3}$ the collateral basis spaces, corresponding to the projected parameter dependent snapshots $\tilde{\mathcal{A}}^h_{f,1}(\mu)$, $\tilde{\mathcal{A}}^h_{f,2}(\mu)$, and $\tilde{\mathcal{A}}^h_{f,3}(\mu)$.

Setting $e^k_m := p^{H\times h} - p^H_{m,k}$, where $p^{H\times h}$ solves (3.71) and $p^H_{m,k}$ (3.41), we define the relative model error in the H^1-half or L^2-norm as

$$|e^k_m|^{rel}_{H^1} := |e^k_m|_{H^1}/|p^{H\times h}|_{H^1} \ \text{ and } \ \|e^k_m\|^{rel}_{L^2(\Omega)} := \|e^k_m\|_{L^2(\Omega)}/\|p^{H\times h}\|_{L^2(\Omega)}.$$

Analogous to §2.6 the relative total error $|e|^{rel}_{H^1}$ is either defined as $|e|^{rel}_{H^1} := |p - p^H_{m,k}|_{H^1}/|p|_{H^1}$ if the full solution p of (3.104) is available as in test case 1 or as $|e|^{rel}_{H^1} := |p_{fine} - p^H_{m,k}|_{H^1}/|p_{fine}|_{H^1}$, where p_{fine} denotes a very finely resolved bilinear FE solution. We distinguish between the PODs for the HMR approach and the EPM by denoting with e^{POD}_m the POD-error associated with the former and by e^k_{POD} the POD-error corresponding to the latter. We further classify the POD-error for the EPM by introducing $e^{k,1}_{\text{POD}}$ and $e^{k,2}_{\text{POD}}$, which are associated to the respective collateral basis spaces $W^h_{k,1}$ and $W^h_{k,2}$ defined at the beginning of this paragraph. Accordingly and analogous to §2.6 we set $\bar{e}^{L^2}_m := (\sum_{j=m+1}^M \|\bar{p}^H_{j,k}\|^2_{L^2(\Omega_{1D})})^{1/2}$ and $e^k_{L^2} := (\sum_{j=k+1}^K \| \int_{\widehat{\omega}} \mathcal{I}^L[A(p^H_{m,k})]\kappa_k\|^2_{L^2(\Omega_{1D})})^{1/2}$, where $M = \dim(Y^h_M)$, $K = \dim(W^h_K)$, and $\mathcal{I}^L[\cdot]$ has been defined in (3.30). We also further specify the latter by introducing $e^{k,1}_{L^2}$ and $e^{k,2}_{L^2}$, which are associated with $W^h_{k,1}$ and $W^h_{k,2}$. Furthermore

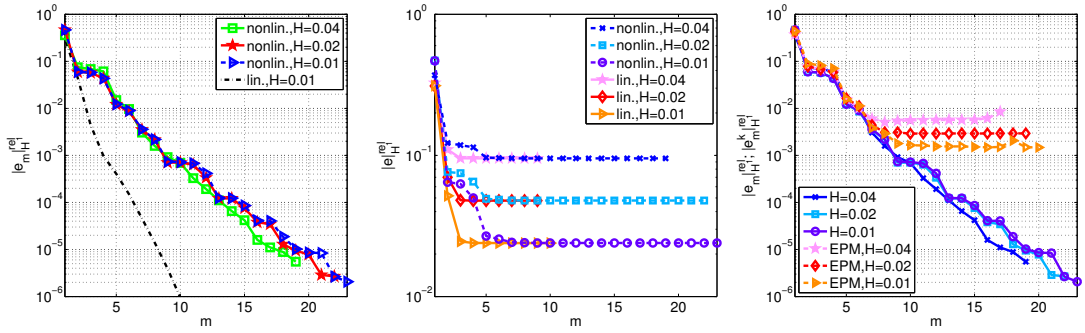

(a) $|e_m|^{rel}_{H^1}$ (b) $|e|^{rel}_{H^1}$ (c) $|e_m|^{rel}_{H^1}$ and $|e^k_m|^{rel}_{H^1}$

Figure 3.2: Test case 1: Comparison of the behavior of the relative model error $|e_m|^{rel}_{H^1(\Omega)} = |p^{H\times h} - p^H_m|_{H^1(\Omega)}/|p^{H\times h}|_{H^1(\Omega)}$ (a) and the relative total error for $|e|^{rel}_{H^1(\Omega)} = |p - p^H_m|_{H^1(\Omega)}/|p|_{H^1(\Omega)}$ (b) for the linear problem (test case 1 in §2.6) and the nonlinear problem (3.104); Comparison of the behavior of the relative model error when applying the EPM ($|e^k_m|^{rel}_{H^1(\Omega)}$) or not ($|e_m|^{rel}_{H^1(\Omega)}$) (c).

we denote with $\Delta^{k,rel}_m$, $\Delta^{k,rel}_{m,2}$ and $\Delta^{k,rel}_{m,res}$ the relative error estimators $\Delta^{k,rel}_m := \Delta^k_m/|p^{H\times h}|_{H^1}$, $\Delta^{k,rel}_{m,2} := \Delta^k_{m,2}/|p^{H\times h}|_{H^1}$ and $\Delta^{k,rel}_{m,res} := \Delta^k_{m,res}/|p^{H\times h}|_{H^1}$, where Δ^k_m, $\Delta^k_{m,2}$ and $\Delta^k_{m,res}$ have been defined in (3.93), (3.99) and (3.102), respectively. The relative proximity indicator $\tau^{k,rel}_{m,2}$ is defined as $\tau^{k,rel}_{m,2} := \tau^k_{m,2}/|p^{H\times h}|_{H^1}$, where $\tau^k_{m,2}$ has been introduced in (3.91). For the validation of the effectivity of the error bounds, we finally shorten the notation by setting $\|e_{\text{mod}}\| := \|P^L_k[F(p^H_{m,k})]\|$, $\|e_{\text{EPM}}\| := \|P^{L'}_{k'}[F(p^H_{m,k})] - P^L_k[F(p^H_{m,k})]\|$ and $\|e^{ex}_{\text{EPM}}\| := \|F(p^H_{m,k}) - P^L_k[F(p^H_{m,k})]\|$ either for the H^{-1}- or the L^2-norm. The implementation of Algorithm 3.3.3 ADAPTIVE-HMR-RB has been done in MATLAB. All computations have been performed on a computer with an Intel Core i7 (4 cores) with 2.8 GHz.

Test case 1

First, we investigate the convergence behavior of the HMR-RB approach for an analytical solution $p(x,y) = y^2(1-y)^2(0.75-y)x(2-x)\exp(\sin(2\pi x))$, which has already been considered in test case 1 in §2.6 and originally in [48,102] solving the Poisson problem. Again we choose $\Omega = (0,2)\times(0,1)$ and $c_0 = 0.1$ and $c_4 = 36$ in (3.105). We compare the convergence behavior of the relative model error $|e_m|^{rel}_{H^1(\Omega)} = |p^{H\times h} - p^H_m|_{H^1(\Omega)}/|p^{H\times h}|_{H^1(\Omega)}$ for the linear case — p^H_m solves (2.12) — with the nonlinear case, where p^H_m is the solution of the discrete reduced problem (3.12) (without using the EPM). We observe an exponential convergence rate of $|e_m|^{rel}_{H^1(\Omega)}$ also for the nonlinear problem (3.104), which is worse than the one for the Poisson problem (Fig. 3.2a). Nevertheless, also for the nonlinear case still 9 basis functions are sufficient to achieve $|e_m|^{rel}_{H^1(\Omega)} \leq 10^{-3}$ (Fig. 3.2a). Furthermore, at least for the considered mesh sizes the effects on the behavior of the relative total error $|e|^{rel}_{H^1} = |p - p^H_m|_{H^1}/|p|_{H^1(\Omega)}$ due to the deterioration of the model convergence rate are very small (Fig. 3.1b). Applying the EPM preserves the convergence rate of the model error $|e_m|^{rel}_{H^1(\Omega)}$ (Fig. 3.1c) until a so-called EPM-plateau (see [43,118] for the EIM-plateau) is reached. The model error enters an EPM-plateau if the approximation properties of the collateral basis space W^h_k prevent a further reduction of the model error, i.e. k is chosen too small compared to m, and the nonlinear operator is hence not approximated accurate enough. Our experiments showed that the tolerance

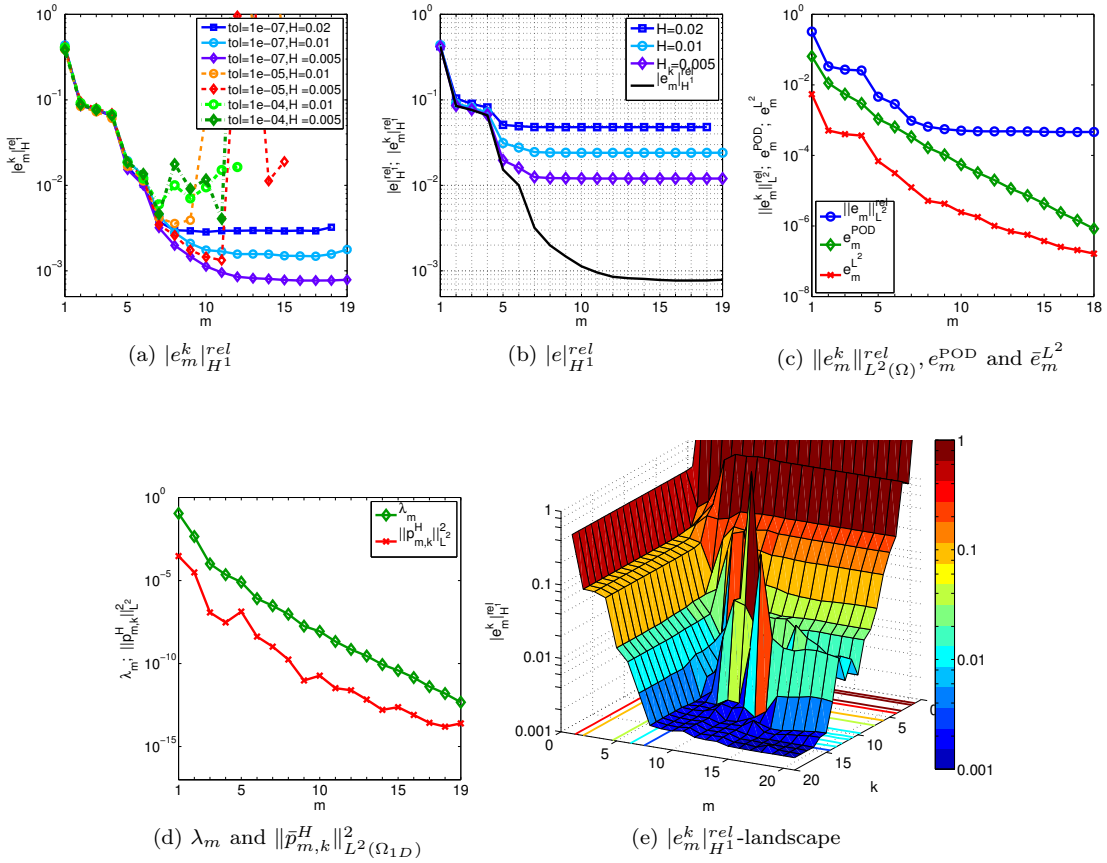

(a) $|e_m^k|_{H^1}^{rel}$ (b) $|e|_{H^1}^{rel}$ (c) $\|e_m^k\|_{L^2(\Omega)}^{rel}, e_m^{\mathrm{POD}}$ and $\bar{e}_m^{L^2}$

(d) λ_m and $\|\bar{p}_{m,k}^H\|_{L^2(\Omega_{1D})}^2$ (e) $|e_m^k|_{H^1}^{rel}$-landscape

Figure 3.3: Test case 1: Comparison of the convergence behavior of $|e_m^k|_{H^1}^{rel}$ for EPM-tolerances $\varepsilon_{\mathrm{tol}}^{\mathrm{EPM}} = 10^{-4}, 10^{-5}, 10^{-7}$ (a), and for $\varepsilon_{\mathrm{tol}}^{\mathrm{EPM}} = 10^{-7}$: $|e|_{H^1}^{rel}$ for different mesh sizes and $|e_m^k|_{H^1}^{rel}$ for $H = 0.005$ (b), $\|e_m^k\|_{L^2(\Omega)}^{rel}, e_m^{\mathrm{POD}}$ and $\bar{e}_m^{L^2}$ (c) and λ_m and $\|\bar{p}_{m,k}^H\|_{L^2(\Omega_{1D})}^2$ (d) for $H = 0.005$; Convergence behavior of $|e_m^k|_{H^1}^{rel}$ for increasing model order m and collateral basis size k for $H = 0.01$ (e); all plots $N_{H'} = 10$.

of the POD for the EPM $\varepsilon_{\mathrm{tol}}^{\mathrm{EPM}}$ should be set to $\varepsilon_{\mathrm{tol}}^{\mathrm{EPM}} = c_{tol}\varepsilon_{\mathrm{tol}}^{\mathrm{HMR}}$ with $c_{tol} \in [10^{-4}, 10^{-3}]$, to ensure that k is chosen large enough. However, even if W_k^h is spanned by all linear independent functions $\mathcal{A}^h(\mu) \in W_K^h$ (3.66), a small error cannot be avoided due to the projection of the snapshots onto the spaces of piecewise linear or piecewise constant functions and other numerical constraints. Note that the level of the EPM-plateau lowers for decreasing H and lies for all considered mesh sizes well below the total error $|e|_{H^1}^{rel}$ (Fig. 3.1b,3.1c). Hence it does not affect the latter. Finally, we remark that in all computations for the plots in Fig. 3.1 we used the exact error in the application of the Algorithms 2.3.2 Adaptive-HMR-POD or 3.3.3 Adaptive-HMR-RB (Fig. 3.1c) to assess only the influence of the nonlinearity in Fig. 3.1a and Fig. 3.1b or the application of the EPM in Fig. 3.1c.

Comparing the convergence behavior of $|e_m^k|_{H^1(\Omega)}^{rel}$ for different POD-tolerances for the EPM in Fig. 3.3a, we observe that for $\varepsilon_{\mathrm{tol}}^{\mathrm{EPM}} = 10^{-4}, 10^{-5}$ the error can even increase when entering the EPM-plateau. For $\varepsilon_{\mathrm{tol}}^{\mathrm{EPM}} = 10^{-7}$ the error stagnates in the EPM-plateau and the level of the plateau decreases uniformly for dropping mesh sizes (Fig. 3.3a). Fig. 3.3e illustrates the error convergence of $|e_m^k|_{H^1(\Omega)}^{rel}$ for a simultaneous increase of the model order m and collateral basis size k for $H = 0.01$.

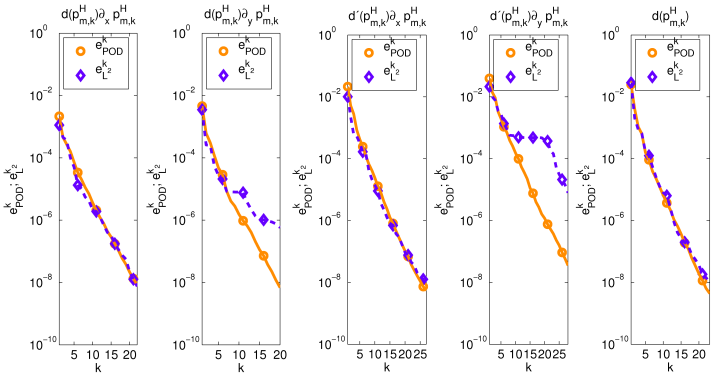

Figure 3.4: Test case 1: Comparison of e^k_{POD} and $e^k_{L^2}$ for $H = 0.005$ and $N_{H'} = 10$ for the collateral basis spaces $W^H_{k,1}$, $W^h_{k,2}$ and $W^H_{k_f,1}$, $W^h_{k_f,2}$, and $W^h_{k_f,3}$.

Again we see that for small k the scheme might even get unstable if m exceeds a certain limit, which is however not the case for higher values of k. Moreover, we observe that if the approximation of the nonlinear operator is good enough a further increase of k does not reduce $|e^k_m|^{rel}_{H^1(\Omega)}$, if m is kept fixed. Choosing $\varepsilon^{\text{EPM}}_{\text{tol}} = 10^{-7}$ and thereby ensuring that the approximation properties of W^h_k are sufficient, we finally see that for the considered mesh sizes the EPM-plateau has no effect on the relative total error $|e|^{rel}_{H^1(\Omega)}$ (Fig. 3.3b). If we compare $\|e_m\|^{rel}_{L^2(\Omega)}, e^{\text{POD}}_m$ (3.69) and $\bar{e}^{L^2}_m$ for $H = 0.005$ in Fig. 3.3c, we detect that all three quantities exhibit the same exponential convergence rate until $\|e_m\|^{rel}_{L^2(\Omega)}$ reaches the EPM-plateau. As also the convergence behavior of the eigenvalues of the POD (3.68) λ_m and of the coefficients $\|\bar{p}^H_{m,k}\|^2_{L^2(\Omega_{1D})}$ coincide (Fig. 3.3d), we conclude that for the present test case the convergence behavior of the POD transfers to the coefficients $\|\bar{p}^H_{m,k}\|^2_{L^2(\Omega_{1D})}$, $\bar{e}^{L^2}_m$ and to the model error $\|e^k_m\|^{rel}_{L^2(\Omega)}$,$|e^k_m|^{rel}_{H^1(\Omega)}$. Thus we infer that the discrete solution manifold Y^h_M (3.65) and the reference solution $p^{H\times h}$ are approximated with the same approximation accuracy by the reduction space Y^h_m. Note that due to the coincidence of the convergence rates of λ_m and $\|\bar{p}^H_{m,k}\|^2_{L^2(\Omega_{1D})}$ (Fig. 3.3d), the QP-INDICATOR introduced in §3.3.5 would not have increased the number of quadrature points used in (3.48). To assess the approximation quality of the collateral basis spaces $W^h_{k,1}$, $W^h_{k,2}$, $W^h_{k_f,1}$, $W^h_{k_f,2}$, and $W^h_{k_f,3}$ we finally compare in Fig. 3.4 the convergence rates of the respective POD-error e^k_{POD} and $e^k_{L^2}$. We observe that the rates for the approximation of $d(p^H_{m,k})\partial_x p^H_{m,k}$, $d'(p^H_{m,k})\partial_x p^H_{m,k}$ and $d(p^H_{m,k})$ coincide perfectly. The deviation for the other two could possibly be explained by the fact, that we have projected the snapshots $\mathcal{A}^h_2(y;\mu)$ (3.63) and $\mathcal{A}^h_{f,2}(y;\mu)$ (3.64) onto the space of piecewise constant functions, which yields a worse convergence behavior for decreasing h as the projection onto the space Y^h. As apart from this deviation the convergence rates coincide, we nevertheless conclude that the nonlinear operator $A(p^{H\times h})$ and its Fréchet derivative $A'(p^{H\times h})$ and the discrete operator manifolds $W^h_{K,1}$, $W^h_{K,2}$, $W^h_{K_f,1}$, $W^h_{K_f,2}$, and $W^h_{K_f,3}$ are approximated with same approximation quality.

Next, we investigate the effectivity of the a posteriori error estimators derived in §3.4. First, we remark that for the present test case we obtained the following approximate values of the inf-sup stability factor

$$\beta_2 = 0.5085 \cdot 10^{-3} \ \ (H = 0.02), \ \ \beta_2 = 0.1277 \cdot 10^{-3} \ \ (H = 0.01), \ \ \beta_2 = 0.3181 \cdot 10^{-4} \ \ (H = 0.005),$$

which indicates that $\beta_2 \sim H \cdot h$, as $H = h$. A comparison of the approximate values with the exact

m	$\varepsilon_{\text{tol}}^{\text{EPM}} = 10^{-5}$ (app)	$\varepsilon_{\text{tol}}^{\text{EPM}} = 10^{-5}$ (ex)	$\varepsilon_{\text{tol}}^{\text{EPM}} = 10^{-7}$ (app)	$\varepsilon_{\text{tol}}^{\text{EPM}} = 10^{-7}$ (ex)
1	0.000509853	0.000510013	0.000511465	0.000511595
2	0.000508364	0.000508648	0.000508366	0.000508641
3	0.000508312	0.000508587	0.000508295	0.000508561
4	0.000508484	0.000508758	0.000508476	0.000508744
5	0.000508482	0.000508785	0.000508526	0.000508827
10	0.000508419	0.000508601	0.000508515	0.000508823
15	0.000508446	0.000508749	0.000508515	0.000508823

Table 3.1: Test case 1: Comparison of the exact inf-sup stability factor (ex) with its approximate value (app) for $H = 0.02$ and different tolerances $\varepsilon_{\text{tol}}^{\text{EPM}}$ in the EPM and increasing model order m.

inf-sup stability factor in Tab. 3.1 shows that the approximation procedure proposed in §3.4.2 yields indeed a lower bound for the inf-sup stability factor and moreover a very accurate approximation. Here, we have used the MATLAB function `svds` to compute the smallest singular value of the jacobian corresponding to $\langle P_{k'}^{L'}[F'(p_{m,k}^H)], v^{H\times h}\rangle$ to determine the approximate value. For the computation of the exact inf-sup stability factor we applied the MATLAB function `svd` to the jacobian associated with $\langle F'(p_{m,k}^H), v^{H\times h}\rangle$ and took the minimum singular value. Due to the very small inf-sup stability factor neither $\tau_{m,2}^k < 1$ nor $|e_m^k|_{H^1(\Omega)} \leq \beta_2/(L_2 c_h)$ (see Fig. 3.5a and Fig. 3.5b) is fullfilled, where the latter would have allowed for an alternative rigorous derivation of $\Delta_{m,2}^k$ (see §3.4.1). Nevertheless, it can be seen in Fig. 3.5a ($\varepsilon_{\text{tol}}^{\text{EPM}} = 10^{-7}$) and Fig. 3.5b ($\varepsilon_{\text{tol}}^{\text{EPM}} = 10^{-5}$) that in contrast to $\Delta_{m,res}^{k,rel}$ (3.102), $\tau_{m,2}^{k,rel}$ (3.91) and $\Delta_{m,2}^{k,rel}$ (3.99) are reliable and efficient error bounds for $|e_m^k|_{H^1(\Omega)}$, albeit the effectivity constants are very high due to the small inf-sup stability factor. Fig. 3.5c shows the scaling of $\tau_{m,2}^{k,rel}$ for decreasing mesh sizes. We see in Fig. 3.5a-3.5c that for $\varepsilon_{\text{tol}}^{\text{EPM}} = 10^{-5}$, $\tau_{m,2}^{k,rel}$, $\Delta_{m,2}^{k,rel}$ and $\Delta_{m,res}^{k,rel}$ reproduce the convergence behavior of $|e_m^k|_{H^1(\Omega)}$ in m perfectly. For $\varepsilon_{\text{tol}}^{\text{EPM}} = 10^{-7}$ the behavior of $|e_m^k|_{H^1(\Omega)}$ until $m = 8$ ($H = 0.02, 0.01$) or $m = 10$ ($H = 0.005$) is reproduced. This can be explained by the fact that for $\varepsilon_{\text{tol}}^{\text{EPM}} = 10^{-7}$, $\|e_{\text{EPM}}^{\text{ex}}\|_{H^{-1}(\Omega)}$ lies above $\|e_{\text{EPM}}\|_{H^{-1}(\Omega)}$ (see Fig. 3.5d), as the former also takes discretization errors into account which are not included in the latter. For $\varepsilon_{\text{tol}}^{\text{EPM}} = 10^{-5}$, $\|e_{\text{EPM}}\|_{H^{-1}(\Omega)}$ and $\|e_{\text{EPM}}^{\text{ex}}\|_{H^{-1}(\Omega)}$ nearly coincide (see Fig. 3.5d). We therefore conclude that the a posteriori bound for the EPM derived in Proposition 3.9, yields a very good approximation of $\|e_{\text{EPM}}^{\text{ex}}\|_{L^2(\Omega)}$ and thus $\|e_{\text{EPM}}^{\text{ex}}\|_{H^{-1}(\Omega)}$ if the discretization error is not dominant. Here, we have set the tolerance for the POD determining the richer collateral basis space $W_{k'}^h$ to $tol_{k'}\varepsilon_{\text{tol}}^{\text{EPM}}$ with $tol_{k'} = 10^{-2}$ (§3.3.5). This yielded on average $k' - k \approx 5$ for $\varepsilon_{\text{tol}}^{\text{EPM}} = 10^{-7}$ and $k' - k \approx 8$ for $\varepsilon_{\text{tol}}^{\text{EPM}} = 10^{-5}$. To prove the effectivity of Δ_m^k and $\Delta_{m,2}^k$, we required (3.92)

$$\|e_{\text{EPM}}\|_{H^{-1}(\Omega)} \leq \|e_{\text{EPM}}^{\text{ex}}\|_{H^{-1}(\Omega)} \leq c_{\text{err}}\|e_{\text{mod}}\|_{H^{-1}(\Omega)} \quad \text{for } c_{\text{err}} \in [0,1). \tag{3.107}$$

Fig. 3.5e illustrates the convergence behavior of $\|e_{\text{EPM}}\|_{H^{-1}(\Omega)}$ and $\|e_{\text{mod}}\|_{H^{-1}(\Omega)}$ for increasing m and $H = 0.005$. We observe that even if (3.107) is violated, i.e. $c_{\text{err}} > 1$, we maintain effectivity of the error bounds (see Fig. 3.5a,3.5b and 3.5e). However, as $c_{\text{err}} > 1$ indicates that the EPM-plateau is reached (Fig. 3.5a,3.5b and 3.5e), the adherence of (3.107) is necessary to avoid the plateau. Finally, we investigate the a priori bound of the EPM derived in Theorem 3.8. As the convergence behavior of λ^k and $\| \int_{\widehat{\omega}} \mathcal{I}_L[A(p_{m,k}^H)]\kappa_k\|_{L^2(\Omega_{1D})}^2$ coincides (see Fig. 3.4) we may apply Theorem 3.8 as an error bound. Note that (3.31) is a probabilistic result and that the term $\mathcal{O}(n_{train}^{-1/4})$ does not provide an upper bound for the integration error due to the application of the Monte-Carlo method [22]. However Fig 3.5f shows that apart from some deviations due to the EPM-plateau the error $\|e_{\text{EPM}}\|_{L^2(\Omega)}$ and the POD-error $e_{\text{POD}}^k := ((e_{\text{POD}}^{k,1})^2 + (e_{\text{POD}}^{k,2})^2)^{1/2}$ have approximately the

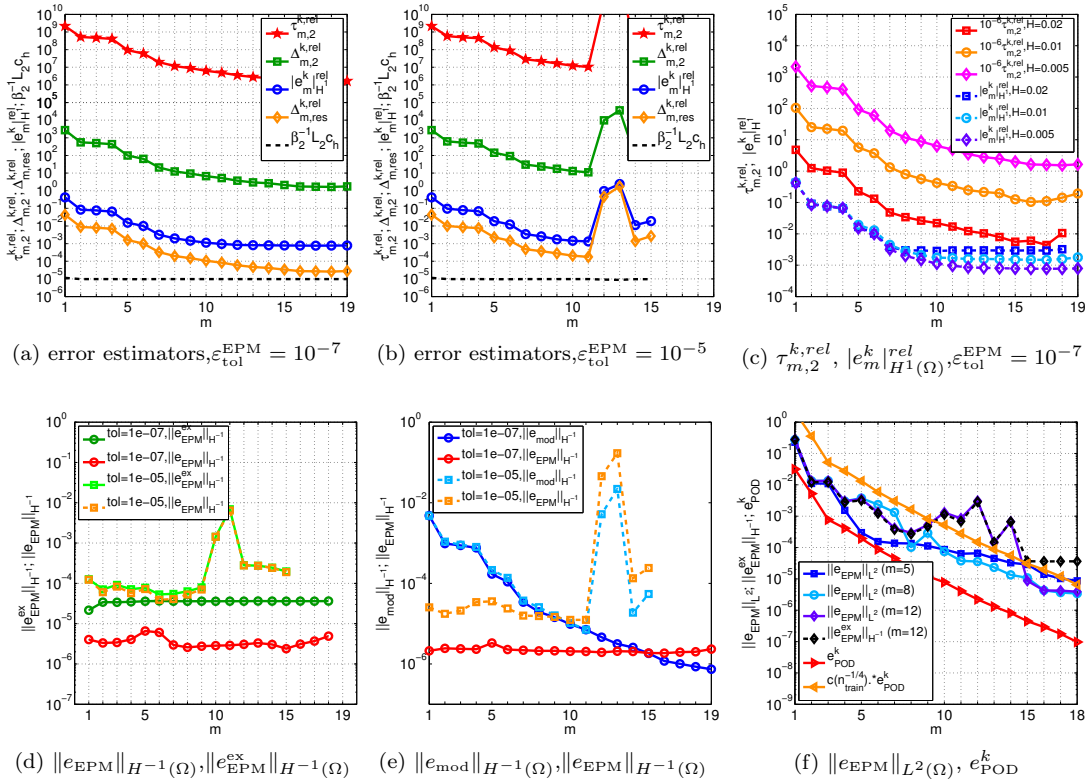

(a) error estimators, $\varepsilon_{\text{tol}}^{\text{EPM}} = 10^{-7}$ (b) error estimators, $\varepsilon_{\text{tol}}^{\text{EPM}} = 10^{-5}$ (c) $\tau_{m,2}^{k,rel}$, $|e_m^k|_{H^1(\Omega)}^{rel}$, $\varepsilon_{\text{tol}}^{\text{EPM}} = 10^{-7}$

(d) $\|e_{\text{EPM}}\|_{H^{-1}(\Omega)}$, $\|e_{\text{EPM}}^{\text{ex}}\|_{H^{-1}(\Omega)}$ (e) $\|e_{\text{mod}}\|_{H^{-1}(\Omega)}$, $\|e_{\text{EPM}}\|_{H^{-1}(\Omega)}$ (f) $\|e_{\text{EPM}}\|_{L^2(\Omega)}$, e_{POD}^k

Figure 3.5: Test case 1: Comparison of the a posteriori error estimators $\tau_{m,2}^{k,rel}$, $\Delta_{m,2}^{k,rel}$, $\Delta_{m,res}^{k,rel}$ with $|e_m^k|_{H^1(\Omega)}$ for $\varepsilon_{\text{tol}}^{\text{EPM}} = 10^{-7}$ (a) and $\varepsilon_{\text{tol}}^{\text{EPM}} = 10^{-5}$ (b) and $H = 0.005$; Comparison of $\tau_{m,2}^{k,rel}$ and $|e_m^k|_{H^1(\Omega)}$ for decreasing H and $\varepsilon_{\text{tol}}^{\text{EPM}} = 10^{-7}$ (c) and $\|e_{\text{EPM}}\|_{H^{-1}(\Omega)}$ and $\|e_{\text{EPM}}^{\text{ex}}\|_{H^{-1}(\Omega)}$ for $\varepsilon_{\text{tol}}^{\text{EPM}} = 10^{-5}, 10^{-7}$ and $H = 0.02$ (d), and $\|e_{\text{mod}}\|_{H^{-1}(\Omega)}$ and $\|e_{\text{EPM}}\|_{H^{-1}(\Omega)}$ for $\varepsilon_{\text{tol}}^{\text{EPM}} = 10^{-5}, 10^{-7}$ and $H = 0.005$ (e), and $\|e_{\text{EPM}}\|_{L^2(\Omega)}$, $\|e_{\text{EPM}}^{\text{ex}}\|_{H^{-1}(\Omega)}$, and e_{POD}^k for $\varepsilon_{\text{tol}}^{\text{EPM}} = 10^{-7}$ and $H = 0.02$ (f).

same convergence rate. The integration error can thus be estimated by the POD-error. Hence we employed the POD-error e_{POD}^k as an apriori bound in our numerical experiments and decreased the tolerance ε_{tol} in (3.38) by 10^{-1} to account for the integration error. Alternatively e_{POD}^k can be multiplied with a constant, which depends on $n_{train}^{-1/4}$ and tends to 1 for $n_{train} \to \infty$, for instance $c(n_{train}^{-1/4}) = (e_{\text{POD}}^1 + 10 n_{train}^{-1/4})/e_{\text{POD}}^1$.

Eventually, the input arguments of Algorithm 3.3.3 ADAPTIVE-HMR-RB, have been chosen as $G_0 = [0, 0.5, 1, 1.5, 2] \times [-0.5, 0.5] \times [-1, 1]$, $m_{\max} = 2$, $i_{max} = 2$, $n_\Xi = 10$, $|\Xi_c| = 50$, $\theta = 0.05$, $\sigma_{thres} = (i_{max} - 1) \cdot \lceil \text{diam}(g) \rceil + 1$ for an element $g \in G_0$ and $\varepsilon_{\text{tol}}^{\text{HMR}} = 10^{-5}$, $\varepsilon_{\text{tol}}^{\text{err}} = 10^{-9}$, $\varepsilon_{\text{tol}}^{\text{c}} = 0.1$ for all computations for this test case. The average sample size has been $n_{\text{train}} \approx 515$.

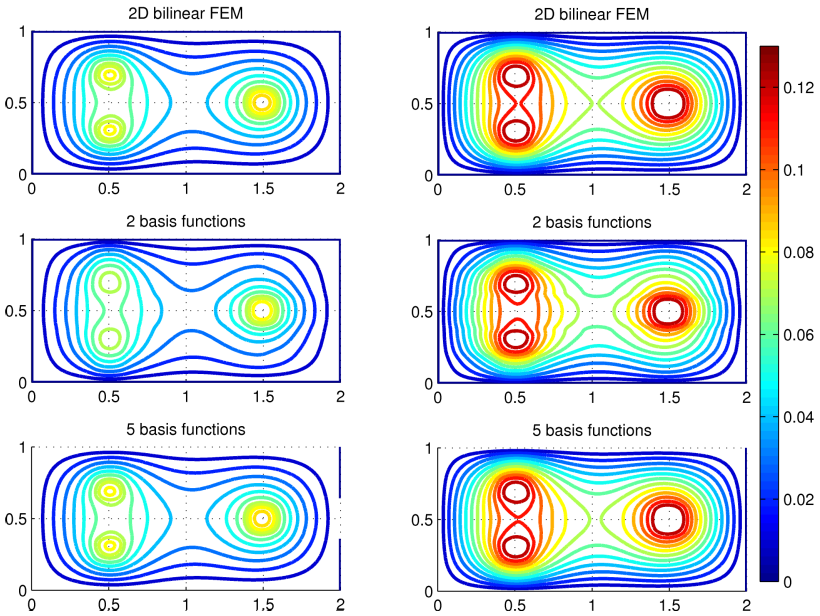

Figure 3.6: Test case 2: Comparison from top to bottom: the reference 2D bilinear FE solution $p^{H\times h}$ (3.71) and the discrete reduced solution $p^H_{m,k}$ using 2 and 5 basis functions for $c_0 = 0.15$ (left) and $c_0 = 0.075$ (right); $c_4 = 12$, $N_H = 400, n_h = 200, N_{H'} = 10$.

Test case 2

To get an idea of the performance of the HMR-RB approach when simulating subsurface flow, we investigate in this test case the convergence behavior and computational efficiency of the HMR-RB approach for the approximation of non-smooth solutions of (3.104). Furthermore we study how the diminishing of c_0 (3.4) affects the performance of our proposed method and the effectivity of the error bounds, as c_0 might approach 0 if the data functions in the Richards equation degenerate. We choose $\Omega = (0,2)\times(0,1)$ and prescribe as a source term the characteristic function $s(x,y) = \chi_{D_1\cup D_2\cup D_3}$, where $D_1 = \{(x,y)\in\Omega : 0.4\le x\le 0.6 \text{ and } 0.2\le y\le 0.36\}$, $D_2 = \{(x,y)\in\Omega : 0.4\le x\le 0.6 \text{ and } 0.64\le y\le 0.8\}$ and $D_3 = \{(x,y)\in\Omega : 1.4\le x\le 1.6 \text{ and } 0.4\le y\le 0.6\}$. Moreover, we choose $c_4 = 12$ and compare the behavior of the HMR-RB approach for $c_0 = 0.15$ and $c_0 = 0.075$. Theorem 3.1 then yields that the solution p of (3.104) is in $W^{2,q}(\Omega)$ for $q < \infty$. The reference solutions $p^{H\times h}$ (3.71) for $c_0 = 0.15$ and $c_0 = 0.075$ are depicted at the top of Fig. 3.6 for $N_H = 400$ and $n_h = 200$, where a convergence study has been done to ensure that $p^{H\times h}$ contains all essential features of the exact solution. The strengthened nonlinear effects for decreasing c_0 can nicely be observed by means of the increased range of $p^{H\times h}$ for $c_0 = 0.075$ and the much more localized peaks for $c_0 = 0.15$. Comparing the reference solutions with its HMR-RB approximations, we see that for both $c_0 = 0.15$ and $c_0 = 0.075$ already $p^H_{2,20}$ contains the three peaks and that the contour lines of $p^H_{5,20}$ and $p^{H\times h}$ coincide (Fig. 3.6).

The input arguments of Algorithm 3.3.3 Adaptive-HMR-RB have been chosen as $G_0 = [0,0.4,0.8,1.2,1.6,2]\times[0,1]\times[-1,1]$, $m_{\max} = 2$, $i_{max} = 2$, $n_\Xi = 10$, $|\Xi_c| = 50$, $\theta = 0.05$, $\sigma_{thres} = (i_{max}-1)\cdot\lceil\operatorname{diam}(g)\rceil+1$ for an element $g\in G_0$ and $\varepsilon_{\text{tol}}^{\text{HMR}} = 10^{-3}$, $\varepsilon_{\text{tol}}^{\text{EPM}} = 10^{-7}$, $\varepsilon_{\text{tol}}^{\text{err}} = 10^{-9}$ for all computations for this test case employing one quadrature point in (3.48) and thus setting $Q = 1$ in (3.46). This resulted in an average sample size of $n_{\text{train}} \approx 540$. For two quadrature points in (3.48) or $Q = 2$ in (3.46) we have chosen $G_0 = [0,0.4,0.8,1.2,1.6,2]\times[0,2]\times[-0.5,0.5]$ for

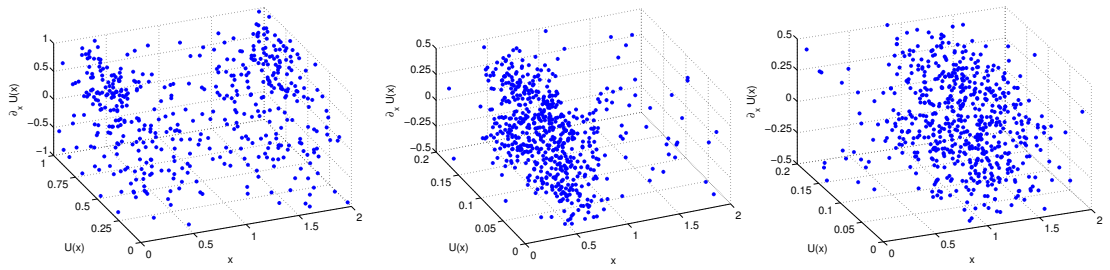

(a) 1 quad. point (b) 2 quad. points: $[x_1^q, U(x_1^q), \partial_x U(x_1^q)]$ (left), $[x_2^q, U(x_2^q), \partial_x U(x_2^q)]$ (right)

Figure 3.7: Test case 2: Plot of the adaptively refined training set generated by Algorithm 3.3.3 ADAPTIVE-HMR-RB when using 1 quadrature point in (3.48) (a) or 2 (b) for $c_0 = 0.075$, $N_H = 200$, $n_h = 100$, $N_{H'} = 10$.

$c_0 = 0.075$ and $G_0 = [0, 0.4, 0.8, 1.2, 1.6, 2] \times [0, 1] \times [-0.5, 0.5]$ for $c_0 = 0.15$, $m_{\max} = 2$, $i_{max} = 1$, $n_\Xi = 4$, $\theta = 0.01$, $\sigma_{thres} = i_{max} \cdot \lceil \mathrm{diam}(g) \rceil + 1$, $\varepsilon_{\mathrm{tol}}^{\mathrm{EPM}} = 10^{-8}$, and $\varepsilon_{\mathrm{tol}}^{\mathrm{err}} = 10^{-10}$, which yielded on average $n_{\mathrm{train}} \approx 600$. Fig. 3.7a illustrates the training set Ξ_{train} generated with Algorithm 3.3.2 ADAPTIVETRAINEXTENSION for $c_0 = 0.075$ and $Q = 1$. It can be seen that against expectations the train sample is not refined around the peaks but at the boundary of Ω_{1D}. Using two quadrature points in (3.48) we observe a refinement of the training set in the expected regions, namely around the peaks at $x = 0.5$ and $x = 1.5$ (Fig. 3.7b). This might be a reason that for the present test case the error convergence of the HMR-RB approach improves significantly, if Q is increased from 1 to 2. Analyzing the convergence behavior of $|e_m^k|_{H^1(\Omega)}^{rel}$ for $c_0 = 0.15$ (Fig. 3.8a) and $c_0 = 0.075$ (Fig. 3.8d), we detect an exponential convergence rate, which is much better for $Q = 2$. Furthermore we have observed for $Q = 1$ a much stronger increase of $|e_m^k|_{H^1(\Omega)}^{rel}$ when entering the EPM-plateau especially for coarser mesh sizes. Note that additionally $\mathcal{D}$ has been shrunk when passing from $Q = 1$ to $Q = 2$, which further improved the rates. However shrinking $\mathcal{D}$ without increasing Q had no effect. A comparison of $\|e_m\|_{L^2(\Omega)}^{rel}$ and e_m^{POD} (3.69) in Fig. 3.8b and Fig. 3.8e shows that for $Q = 2$ the convergence rates coincide till $\|e_m\|_{L^2(\Omega)}^{rel}$ approaches the EPM-plateau but clearly differ for $Q = 1$. Regarding λ_m and $\|\bar{p}_{m,k}^H\|_{L^2(\Omega_{1D})}^2$ we observe that their convergence rates significantly differ for $Q = 1$ for both $c_0 = 0.15$ (Fig. 3.8c) and $c_0 = 0.075$ (Fig. 3.8f) but coincide for $Q = 2$ for $m \leq 12$. The rise of $\|\bar{p}_{m,k}^H\|_{L^2(\Omega_{1D})}^2$ for $m > 12$ is probably caused by the EPM-plateau. Thus we conclude that for the present test case for $Q = 2$ the discrete solution manifold Y_M^h (3.65) and the reference solution $p^{H\times h}$ are approximated with the same approximation quality by the reduction space Y_m^h. Note that the QP-INDICATOR would have detected in line 6 of Algorithm 3.3.2 that an increase of Q is necessary, but would not have raised Q further in line 21 due to the coincidence of the rates of λ_m and $\|\bar{p}_{m,k}^H\|_{L^2(\Omega_{1D})}^2$ for $m \leq 10$. Comparing the convergence behavior of the HMR-RB approach with respect to a decrease of c_0, we observe only a slightly worse convergence rate of the model error and a bit stronger increase of $|e_m^k|_{H^1(\Omega)}^{rel}$ in the EPM-plateau. For $Q = 1$ the coefficients $\|\bar{p}_{m,k}^H\|_{L^2(\Omega_{1D})}^2$ stagnate at a higher level. All in all we observe only minor changes in the convergence behavior of the HMR-RB approach when decreasing c_0 from 0.15 to 0.075. Fig. 3.9a shows the error convergence of $|e_m^k|_{H^1(\Omega)}^{rel}$ for a simultaneous growth of m and k for $H = 0.01$. We see on the one hand a strong increase of the error if m exceeds k but on the other hand a nice error decay and only a small increase in the EPM-plateau if $k \geq m + 5$ is satisfied. We suppose that the worse behavior of $p_{m,k}^H$ in the EPM-plateau compared to the previous test case (compare Fig. 3.3e and Fig. 3.9a) is due to the fact that the full solution of the present test case is non-smooth. Investigating the convergence behavior of the relative total error in Fig. 3.9b demonstrates

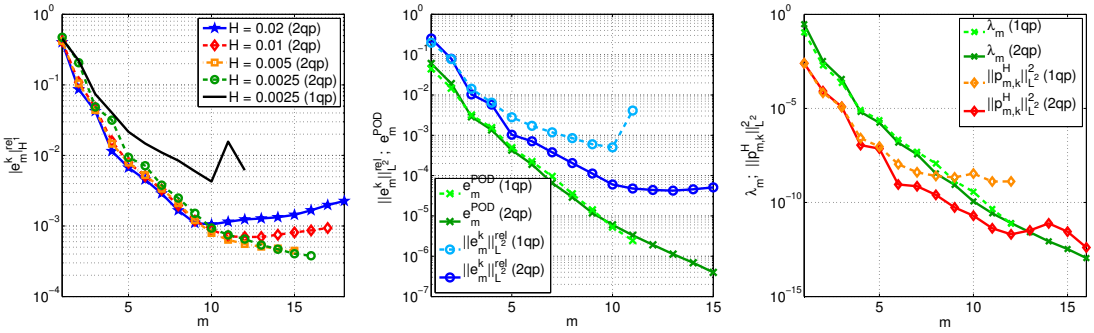

(a) $|e^k_m|^{rel}_{H^1}$ $(c_0 = 0.15)$ (b) $\|e^k_m\|^{rel}_{L^2(\Omega)}$, e^{POD}_m $(c_0 = 0.15)$ (c) $\|\bar{p}^H_{m,k}\|^2_{L^2(\Omega_{1D})}$, λ_m $(c_0 = 0.15)$

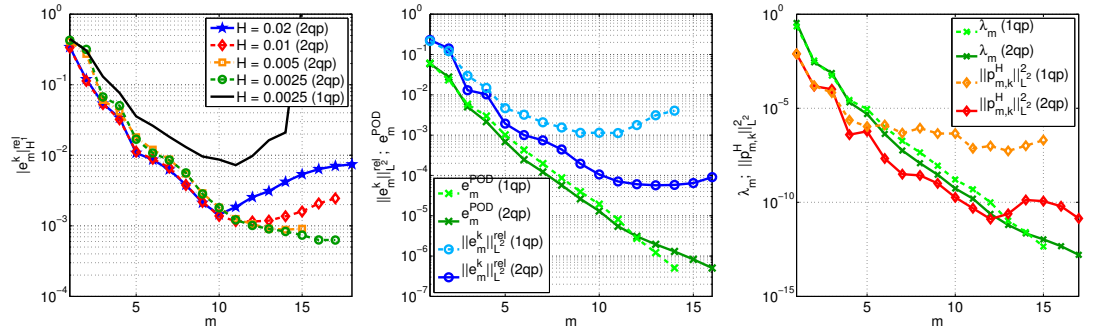

(d) $|e^k_m|^{rel}_{H^1}$ $(c_0 = 0.075)$ (e) $\|e^k_m\|^{rel}_{L^2(\Omega)}$, e^{POD}_m $(c_0 = 0.075)$ (f) $\|\bar{p}^H_{m,k}\|^2_{L^2(\Omega_{1D})}$, λ_m $(c_0 = 0.075)$

Figure 3.8: Test case 2: Comparison of the convergence behavior of $|e^k_m|^{rel}_{H^1}$ for one quadrature point (1qp) and two quadrature points (2qp) in (3.48) for $c_0 = 0.15$ (a) and $c_0 = 0.075$ (d); $|e^k_m|^{rel}_{L^2(\Omega)}$ and e^{POD}_m for $Q = 1, 2$ in (3.46) for $c_0 = 0.15$ (b) and $c_0 = 0.075$ (e) and $H = 0.0025$; $\|\bar{p}^H_{m,k}\|^2_{L^2(\Omega_{1D})}$ and λ_m for $Q = 1, 2$ in (3.46) for $c_0 = 0.15$ (c) and $c_0 = 0.075$ (f) and $H = 0.0025$. $N_{H'} = 10$ for all pictures.

that for $Q = 2$ the EPM-plateau has no effect on $|e|^{rel}_{H^1(\Omega)}$, which is unfortunately not true for $Q = 1$. Comparing the convergence rates of λ^k with $\| \int_{\widehat{\omega}} \mathcal{I}_L[A(p^H_{m,k})]\kappa_k\|^2_{L^2(\Omega_{1D})}$ for the collateral basis spaces $W^h_{k,1}$, $W^h_{k,2}$, $W^h_{k_f,1}$, $W^h_{k_f,2}$, and $W^h_{k_f,3}$ we see in Fig. 3.10 that they are comparable for $k \leq 5$ for $Q = 1$ and $k \leq 12$ for $Q = 2$, but clearly differ for higher values. This is due to the behavior of $\|\bar{p}^H_{m,k}\|^2_{L^2(\Omega_{1D})}$ (cf. Fig. 3.8c and Fig. 3.8f), which stagnate exactly for $m = 5$ $(Q = 1)$ and $m = 12$ $(Q = 2)$. However we have observed that the level of the plateau of the coefficients $\|\bar{p}^H_{m,k}\|^2_{L^2(\Omega)}$ and $\| \int_{\widehat{\omega}} \mathcal{I}_L[A(p^H_{m,k})]\kappa_k\|^2_{L^2(\Omega_{1D})}$ lowers for decreasing mesh sizes which might indicate that their stagnation is related to the EPM plateau. We hence suppose that since the solution of the present test case is non-smooth, in contrast to the previous example, the behavior of $p^H_{m,k}$ in the EPM-plateau (compare Fig. 3.3e and Fig. 3.9a) also affects the coefficients $\|\bar{p}^H_{m,k}\|^2_{L^2(\Omega)}$ and $\| \int_{\widehat{\omega}} \mathcal{I}_L[A(p^H_{m,k})]\kappa_k\|^2_{L^2(\Omega_{1D})}$.

Next, we analyze the a posteriori error bounds derived in §3.4.1. The approximate values of the inf-sup stability factor β_2 (3.86) obtained with the method proposed in §3.4.2 are indicated in Tab. 3.2 and imply that $\beta_2 \sim H \cdot h$, as $H = h$. As in the previous test case the small values of β_2 prevent that $\tau^k_{m,2} < 1$ or $|e^k_m|_{H^1(\Omega)} \leq \beta_2/(L_2 c_h)$ (see Fig. 3.11a and Fig. 3.11b) is fulfilled. In spite

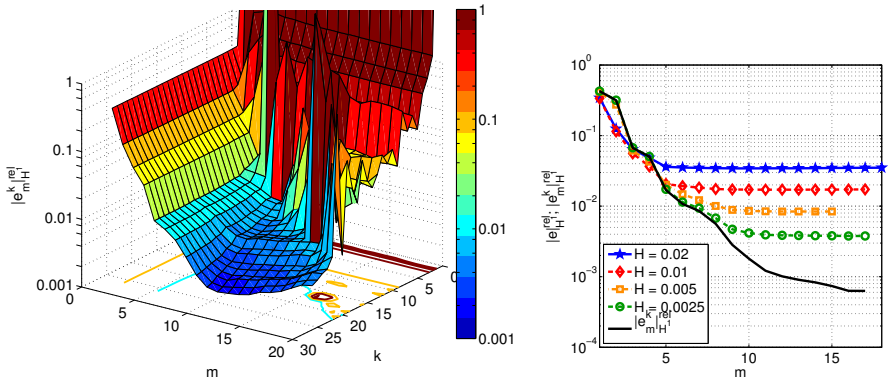

(a) $|e_m^k|_{H^1}^{rel}$ (b) $|e|_{H^1}^{rel}$

Figure 3.9: Test case 2: Convergence behavior of $|e_m^k|_{H^1}^{rel}$ for increasing m and k for $N_H = 200$, $n_h = 100$ (a) and $|e|_{H^1}^{rel}$ for decreasing mesh size (b); both pictures: $Q = 2$ in (3.46), $N_{H'} = 10$ and $c_0 = 0.075$.

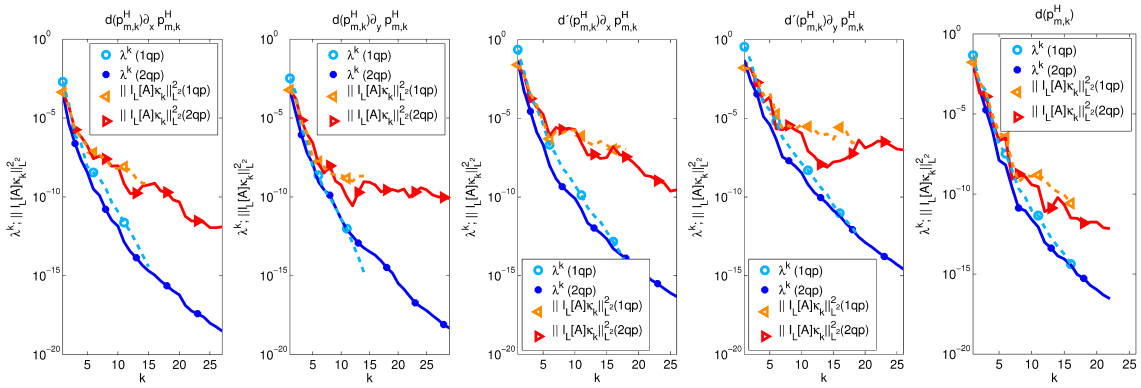

Figure 3.10: Test case 2: Comparison of λ^k and $\| \int_{\widehat{\omega}} \mathcal{I}_L[A(p_{m,k}^H)]\kappa_k\|_{L^2(\Omega_{1D})}^2$ for $Q = 1$ in (3.46) (1qp) and $Q = 2$ in (3.46) (2qp) for $H = 0.005$ and $N_{H'} = 10$ for the collateral basis spaces $W_{k,1}^H$, $W_{k,2}^h$ and $W_{k_f,1}^H$, $W_{k_f,2}^h$, and $W_{k_f,3}^h$.

of that $\tau_{m,2}^{k,rel}$ (3.91) and $\Delta_{m,2}^{k,rel}$ (3.99) are reliable error bounds for $|e_m^k|_{H^1(\Omega)}$, while $\Delta_{m,res}^{k,rel}$ (3.102) underestimates the error, albeit only slightly (Fig. 3.11a and Fig. 3.11b). Only very small differences between the error estimators for $c_0 = 0.15$ and $c_0 = 0.075$ can be detected in Fig. 3.5b. While the convergence behavior of $|e_m^k|_{H^1(\Omega)}$ in m is reproduced perfectly by $\tau_{m,2}^{k,rel}$, $\Delta_{m,2}^{k,rel}$ and $\Delta_{m,res}^{k,rel}$ for $H = 0.005$ and $H = 0.0025$ (Fig. 3.11a-3.11c), for coarser mesh sizes the error estimators are not efficient for $5 \leq m \leq 10$ (Fig. 3.11c). This is due to the fact that for $m \geq 8$ there holds $\|e_{\text{EPM}}^{\text{ex}}\|_{H^{-1}(\Omega)} \geq \|e_{\text{mod}}\|_{H^{-1}(\Omega)}$ as $\|e_{\text{EPM}}^{\text{ex}}\|_{H^{-1}(\Omega)}$ is dominated by discretization errors (Fig. 3.11d). Thus the assumption (3.92)

$$\|e_{\text{EPM}}\|_{H^{-1}(\Omega)} \leq \|e_{\text{EPM}}^{\text{ex}}\|_{H^{-1}(\Omega)} \leq c_{\text{err}}\|e_{\text{mod}}\|_{H^{-1}(\Omega)} \quad \text{with } c_{\text{err}} \in [0,1) \tag{3.108}$$

is violated, which demonstrates that for the present test case satisfying (3.92) is crucial to maintain the effectivity of the error estimators for $Q = 2$. Fig. 3.11d also shows that as in the previous test case for moderate values of k $\|e_{\text{EPM}}^{\text{ex}}\|_{H^{-1}(\Omega)}$ and $\|e_{\text{EPM}}\|_{H^{-1}(\Omega)}$ coincide perfectly, which numerically proves that also for the present test case for a nondominant discretization error the a

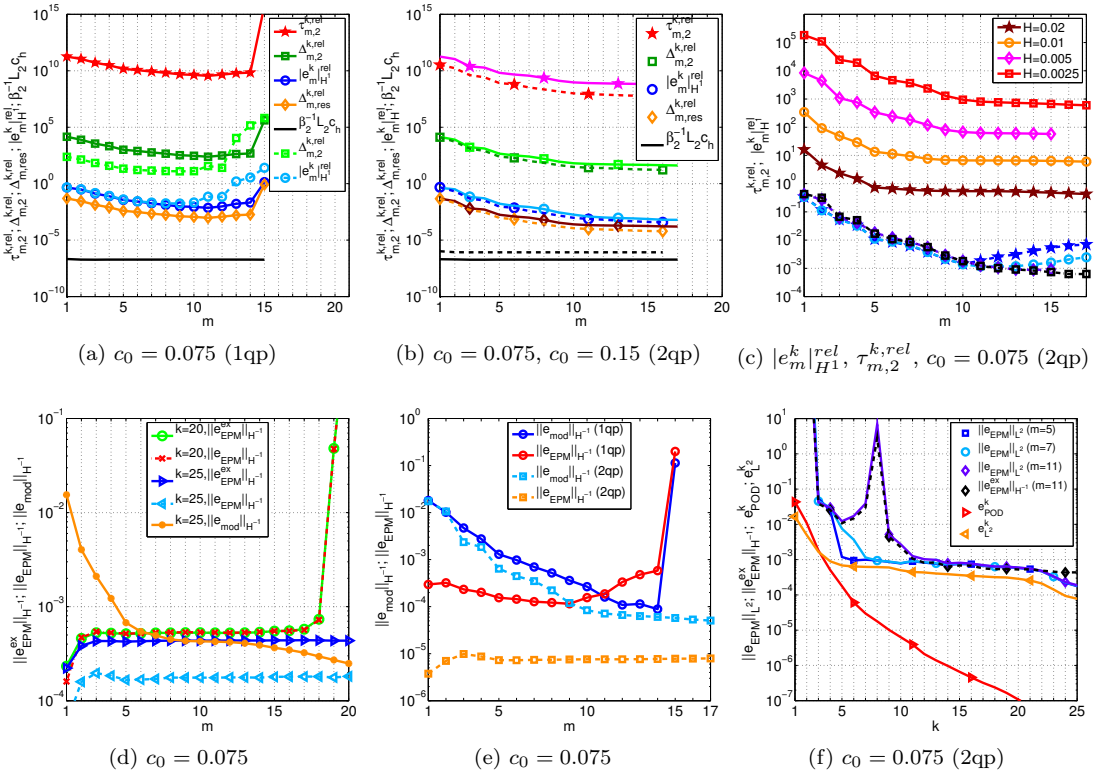

(a) $c_0 = 0.075$ (1qp) (b) $c_0 = 0.075$, $c_0 = 0.15$ (2qp) (c) $|e_m^k|_{H^1}^{rel}$, $\tau_{m,2}^{k,rel}$, $c_0 = 0.075$ (2qp)

(d) $c_0 = 0.075$ (e) $c_0 = 0.075$ (f) $c_0 = 0.075$ (2qp)

Figure 3.11: Test case 2: Comparison of the a posteriori error estimators $\tau_{m,2}^{k,rel}$, $\Delta_{m,2}^{k,rel}$, $\Delta_{m,res}^{k,rel}$ with $|e_m^k|_{H^1(\Omega)}$ for $c_0 = 0.075$, $Q = 1$ in (3.46) (1qp) and $H = 0.0025$ (solid) and $H = 0.02$ (dashed) (a) and $c_0 = 0.15$ (dashed) and $c_0 = 0.075$ (solid) and $Q = 2$ in (3.46) (2qp) and $H = 0.0025$ (b); Comparison for $c_0 = 0.075$ of $10^{-6}\tau_{m,2}^{k,rel}$ (solid) and $|e_m^k|_{H^1(\Omega)}$ (dashed) for decreasing H and $Q = 2$ (c) and $\|e_{\mathrm{EPM}}\|_{H^{-1}(\Omega)}$, $\|e_{\mathrm{EPM}}^{\mathrm{ex}}\|_{H^{-1}(\Omega)}$ and $\|e_{\mathrm{mod}}\|_{H^{-1}(\Omega)}$ for $H = 0.02$ and $Q = 2$ (d), and $\|e_{\mathrm{mod}}\|_{H^{-1}(\Omega)}$ and $\|e_{\mathrm{EPM}}\|_{H^{-1}(\Omega)}$ for $Q = 1, 2$ and $H = 0.0025$ (e), and $\|e_{\mathrm{EPM}}\|_{L^2(\Omega)}$, $\|e_{\mathrm{EPM}}^{\mathrm{ex}}\|_{H^{-1}(\Omega)}$, e_{POD}^k, and $e_{L^2}^k$ for $Q = 2$ and $H = 0.02$ (f).

posteriori bound for the EPM (3.37) results in a very good approximation of $\|e_{\mathrm{EPM}}^{\mathrm{ex}}\|_{L^2(\Omega)}$ and thus $\|e_{\mathrm{EPM}}^{\mathrm{ex}}\|_{H^{-1}(\Omega)}$. As in the previous test case we have set $\varepsilon_{\mathrm{tol}}^{\mathrm{err}} = tol_{k'}\varepsilon_{\mathrm{tol}}^{\mathrm{EPM}}$ with $tol_{k'} = 10^{-2}$ (§3.3.5), which yielded on average $k' - k \approx 8$. Note that for $Q = 1$ in (3.46) the effectivity of the error bounds is maintained even for $H = 0.02$ (Fig. 3.11a) and that $\|e_{\mathrm{EPM}}^{\mathrm{ex}}\|_{H^{-1}(\Omega)}$ and $\|e_{\mathrm{EPM}}\|_{H^{-1}(\Omega)}$ mainly coincide even for high values of k due to the higher level of the EPM-plateau. Comparing $\|e_{\mathrm{mod}}\|_{H^{-1}(\Omega)}$ and $\|e_{\mathrm{EPM}}\|_{H^{-1}(\Omega)}$ for $Q = 1, 2$ in Fig. 3.11e we observe that $\|e_{\mathrm{EPM}}\|_{H^{-1}(\Omega)}$ has improved much more than $\|e_{\mathrm{mod}}\|_{H^{-1}(\Omega)}$ due to the increase of Q. Hence increasing Q seems to significantly reduce the level of the EPM-plateau which in turn considerably improves the error behavior as has already been assessed in the analysis of Fig. 3.8. In contrast to the previous test case, also for small tolerances $\varepsilon_{\mathrm{tol}}^{\mathrm{EPM}}$ a stagnation of $\|e_{\mathrm{mod}}\|_{H^{-1}(\Omega)}$ can be observed (compare Fig. 3.5e and Fig. 3.11e). Thus we suppose that due to the worse behavior of $p_{m,k}^H$ in the EPM-plateau compared to the previous test case, the EPM-plateau affects the convergence behavior of the model error for the present example. As the convergence behavior of λ^k and $\| \int_{\widehat{\omega}} \mathcal{I}_L[A(p_{m,k}^H)]\kappa_k\|_{L^2(\Omega_{1D})}^2$ does not coincide (see Fig. 3.10), we replace, as proposed in §3.4.1, λ^k by $\| \int_{\widehat{\omega}} \mathcal{I}_L[A(p_{m,k}^H)]\kappa_k\|_{L^2(\Omega_{1D})}^2$ in the a priori bound (3.31) of Theorem 3.8. Fig. 3.11f shows that $e_{L^2}^k := ((e_{L^2}^{k,1})^2 + (e_{L^2}^{k,2})^2)^{1/2}$ captures the behavior of $\|e_{\mathrm{EPM}}^{\mathrm{ex}}\|_{L^2(\Omega)}$

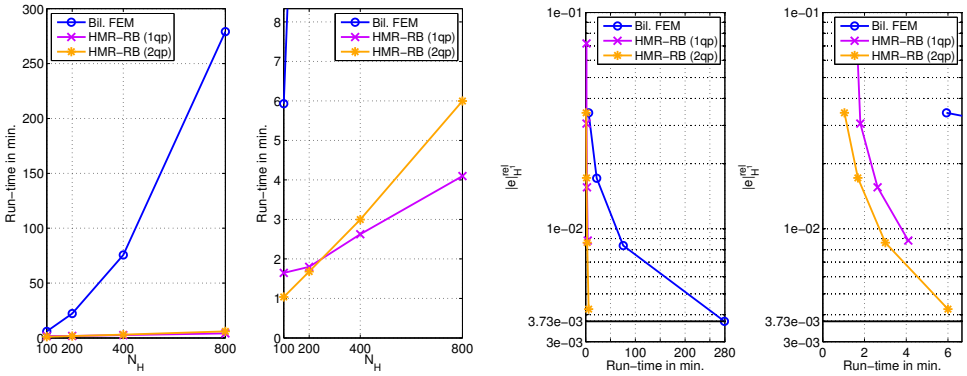

(a) Run-time [min] for increasing N_H (b) $|e|_{H^1}^{rel}$ vs. run-time [min]

Figure 3.12: Test case 2: Comparison of the total computational costs for the 2D bilinear FEM and the HMR-RB approach for $Q = 1$ in (3.46) (1qp) and $Q = 2$ in (3.46) (2qp) and $N_{H'} = 10$, $c_0 = 0.075$.

c_0	$H = 0.02$	$H = 0.01$	$H = 0.005$	$H = 0.0025$
0.15	$0.7792 \cdot 10^{-3}$	$0.1948 \cdot 10^{-3}$	$0.4871 \cdot 10^{-4}$	$0.1218 \cdot 10^{-4}$
0.075	$0.4930 \cdot 10^{-3}$	$0.1232 \cdot 10^{-3}$	$0.3080 \cdot 10^{-4}$	$0.7697 \cdot 10^{-5}$

Table 3.2: Test case 2: Approximate values of the inf-sup stability factor β_2 (3.86).

and $\|e_{\mathrm{EPM}}^{\mathrm{ex}}\|_{H^{-1}(\Omega)}$ perfectly for $k \geq m$. The deviations for $k < m$ are due to the EPM-plateau. Although the snapshots set W_K^h and $A(p^{H\times h})$ are not approximated with the same approximation quality due to the EPM-plateau (Fig. 3.10), we observe that $\|e_{\mathrm{EPM}}^{\mathrm{ex}}\|_{L^2(\Omega)}$ and $\|e_{\mathrm{EPM}}^{\mathrm{ex}}\|_{H^{-1}(\Omega)}$ coincide for $k \leq 23$. Thus, we conclude that for the present test case the modified version of the a priori bound (3.31) of Theorem 3.8, obtained by substituting λ^k by $\| \int_{\widehat{\omega}} \mathcal{I}_L[A(p_{m,k}^H)]\kappa_k\|_{L^2(\Omega_{1D})}^2$, can be applied to obtain rigorous and efficiently computable a posteriori error estimators $\Delta_m^{k,rel}$ and $\Delta_{m,2}^{k,rel}$.

Finally, we compare the total computational costs of the HMR-RB approach using the EPM to compute $p_{m,k}^H$ (3.41), including offline and online costs, with the costs of the 2D bilinear FEM for the computation of $p^{H\times h} \in V^{H\times h}$ (3.71). For the solution of the linear system of equations within Newton's method we employed in both cases a bicgstab method with the same settings. Also the tolerance for Newton's method has been chosen identically. In Fig. 3.12a we see that the bilinear FEM scales quadratically in N_H, while the HMR-RB approach with the EPM scales linearly in N_H both for $Q = 1$ and $Q = 2$ in (3.46). The theoretical computational costs derived in §3.5 are thus confirmed. In Fig. 3.12b the total computational costs of the bilinear FEM and the HMR-RB approach are plotted versus the respective relative total error $|e|_{H^1(\Omega)}^{rel}$. Due to the EPM-plateau the total error $|e|_{H^1(\Omega)}^{rel}$ for $Q = 1$ lies well above the one of the bilinear FEM for the same mesh size, while only minimal deviations can be observed for $Q = 2$. However the run-time required to achieve a certain error tolerance is very much smaller for the HMR-RB approach than for the bilinear FEM. This huge gap is due to the well-known slow performance of MATLAB for `for`-loops. The assembling of the jacobian for the bilinear FEM requires, at least to our knowledge, a `for`-loop over N_H or n_h, to compute the two-dimensional integrals for each element. In the HMR-RB approach the assembling of the jacobian requires only the computation of one-dimensional integrals in x and y-direction due to the application of the EPM, which can be computed in a fully vectorized manner

by employing the MATLAB-function `trapz`. Using another coding language as for example `C++` will therefore probably reduce this huge difference in the total computational costs but not affect the better scaling of the HMR-RB approach in N_H. Therefore also for other coding languages we expect the HMR-RB approach to outperform the 2D bilinear FEM starting from a certain mesh size.

Chapter 4

Approximation of skewed interfaces

In this chapter we address the approximation of a possibly skewed water table or similar interface with a tensor-based model reduction procedure. If we consider subsurface flow, then, depending on the permeability of the soil, the saturation profile may form a skewed interface along the water table (cf. Fig. 4.1a). Due to the fact that for a full approximation of the skewed interface the saturation profile in each point x in the dominant direction has to be included, skewed interfaces yield a bad convergence behavior of model reduction approaches based on a tensor product decomposition (Fig. 4.1b). In this chapter we propose a new ansatz to solve this problem, leading to significantly improved convergence rates. The two key ideas are the location of the interface and the subsequent removal of the interface of the solution by choosing the determined interface as the lifting function of the Dirichlet boundary conditions. This chapter is organized as follows. In Section 4.1 we first outline our approach for the location of the interface using the example of subsurface flow (Subsection 4.1.1). Afterwards, we demonstrate for linear problems how the information on the location of the information can be used to remove the interface from the model reduction procedure in Subsection 4.1.2. In Section 4.2 we exemplify this ansatz for the HMR-RB method and present an approach for the derivation of a lower-dimensional parametrized problem particularly suited for the presence of interfaces, which will be validated in Section 4.3. The capacity of the ansatz proposed in Section 4.1 to improve the convergence behavior is demonstrated in Section 4.3 for prescribed interfaces and linear problems for the HMR-RB approach in several numerical experiments, including a test case, where we do not include the exact interface but only an approximation.

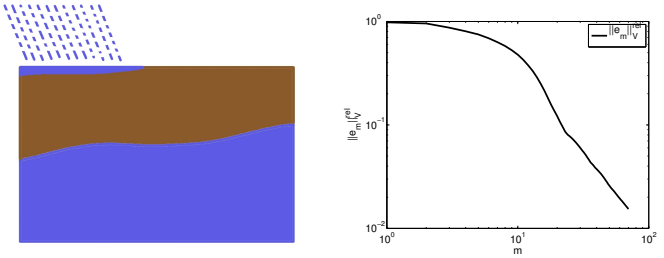

(a) Schematic saturation profile (b) relative model error

Figure 4.1: Schematic picture of subsurface flow with a skewed water table (a). Behavior of the relative model error $\|e_m\|_V^{rel}$ defined in §2.6 for the HMR-RB approach for test case 1 in §4.3 if no information on the interface is included in the model reduction process (b).

4.1 An ansatz for approximating skewed interfaces with tensor based model reduction approaches

Let $\Omega \subset \mathbb{R}^2$ denote the computational domain with Lipschitz boundary $\partial\Omega$ and $\Sigma_D \subset \partial\Omega$ the Dirichlet boundary. Ω is supposed to satisfy the assumptions of §2.1 and we assume for the sake of simplicity that $\mathcal{H}^1(\Sigma_D) > 0$, where $\mathcal{H}^1(\Sigma_D)$ denotes the one-dimensional Hausdorff-measure of Σ_D.

4.1.1 Locating the interface

We demonstrate our approach for the location of the interface using the example of saturated-unsaturated subsurface flow. For this purpose let Ω be occupied by a homogeneous soil. In the time interval $[0, T]$ we consider the Richards equation (see e.g. [13, 14, 16]) for the water saturation $s : \Omega \times [0, T] \to [0, 1]$ and the water pressure $p : \Omega \times [0, T] \to \mathbb{R}$

$$\frac{ds}{dt} - \operatorname{div}\left(Kk(s)(\nabla p + \boldsymbol{g})\right) = 0 \quad \text{in } \Omega \times [0, T]. \tag{4.1}$$

Here, k denotes the relative permeability, K the hydraulic conductivity[1], and $\boldsymbol{g}$ the gravity vector. We have normalized the porosity and the viscosity. To locate the water table, we first consider the groundwater flow equation for the piezometric head $\varphi = y + p/(\rho g)$ with a free surface. The latter is characterized by an atmospheric pressure and thus describes the location of the water table. Furthermore, ρ denotes the density of the fluid and g designates the gravity acceleration. Assuming the incompressibility of water and a flat bottom of the considered domain Ω at level $y = 0$, the piezometric head or potential can be described by the following PDE [14]

$$\begin{aligned} -K\Delta\varphi = 0 \quad & t \in [0, T] \text{ and } 0 \le y \le w(x), \\ \frac{d\varphi}{dt} - K\left[\left(\frac{d\varphi}{dx}\right)^2 + \left(\frac{d\varphi}{dy}\right)^2\right] + \frac{d\varphi}{dy}(K + N) - N = 0 \quad & t \in [0, T] \text{ and } y = w(x). \end{aligned} \tag{4.2}$$

Here, N accounts for accretion and suitable initial conditions and additional boundary conditions are prescribed. Starting from (4.2) one can derive a dimensionally reduced model for the height of the water table w by assuming a hydrostatic pressure distribution [44] or by employing an asymptotic expansion [37]. The respective PDE then reads

$$\frac{dw}{dt} - \frac{K}{2}\Delta w^2 + N = 0, \quad \text{in } \Omega_{1D} \times [0, T], \tag{4.3}$$

where Ω_{1D} denotes the computational domain in the dominant direction. Due to the structure of (4.3), solving (4.3) has the same computational complexity as solving (4.1) with the HMR-RB approach employing one basis function. It is therefore reasonable to solve (4.3) in a preprocessing step, if the so gained information accelerates the convergence of the HMR-RB approach or another employed tensor-based model reduction approach. Next, we describe how the information on the location of the water table can be exploited within the model reduction procedure.

[1] Following [14] the hydraulic conductivity describes the ability of the soil to conduct water through it under hydraulic gradients.

4.1.2 Removing the interface from the model reduction procedure

Employing the location of the water table (or a similar interface) described by the solution w of (4.3), we can define a function $\mathfrak{h} : \Omega \to \mathbb{R}$ which describes the corresponding saturation (or concentration) profile. We propose to prescribe this profile as the lifting function of the Dirichlet boundary conditions. For the sake of clarity we restrict ourselves for the rest of this chapter to linear PDEs. The ideas in the nonlinear setting are the same. We define the solution space V such that $H_0^1(\Omega) \subseteq V \subseteq H^1(\Omega)$ and consider the following full problem:

$$\text{Find } p \in V : \quad a(p, v) = f(v) - a(\mathfrak{h}, v) \quad \forall v \in V, \tag{4.4}$$

where $a(\cdot, \cdot)$ is a coercive and continuous bilinear form and $f \in V^*$, V^* denoting the dual space of V. The full solution is given as $\tilde{p} := p + \mathfrak{h}$ and lies in the space $V + \mathfrak{h}$. We define the spaces X and Y such that

$$H_0^1(\Omega_{1D}) \subseteq X \subseteq H^1(\Omega_{1D}) \text{ and } H_0^1(\widehat{\omega}) \subseteq Y \subseteq H^1(\widehat{\omega}),$$

supposing compatibility with the boundary conditions prescribed on $\partial\Omega$. We approximate p by a linear combination of tensor products

$$p_m := \sum_{l=1}^{m} \bar{p}_l(x)\phi_l(\psi(y; x)), \tag{4.5}$$

where $\bar{p}_l \in X$ and $\phi_l \in Y$, $l = 1, ..., m$ and define the reduced solution $\tilde{p}_m := p_m + \mathfrak{h}$. Depending on the chosen method p_m either fulfills a reduced problem as for instance in the Hierarchical Model Reduction (HMR) [102] or the HMR-RB approach (cf. Chapters 2 and 3) or as for example in the Proper Generalized Decomposition method (cf. [24, 77]) minimizes a variational functional.[2] We emphasize that if we assume for the solution p of the full problem (2.1) and the integral operator $(Tg)(x) := \int_{\widehat{\omega}} p(x, \hat{y})g(\hat{y})\, d\hat{y}$ an exponential convergence of the Kolmogorov n-width (cf. (2.14)), i.e. $d_n(T(L^2(\widehat{\omega})); L^2(\Omega_{1D})) = ce^{-\beta n}$, where $\widehat{\omega} = \Omega_{1D}$ and $c, \beta > 0$, it is clear that we obtain for the inclusion of the exact interface $\mathfrak{h}$ in (4.4) $d_n(\tilde{T}(L^2(\widehat{\omega})); L^2(\Omega_{1D})) = ce^{-\beta n}$, where $(\tilde{T}g)(x) := \int_{\widehat{\omega}} \tilde{p}(x, \hat{y})g(\hat{y})d\hat{y}$ and $\tilde{p}$ is the full solution of (4.4). Here, the weak form (4.4) only differs from (2.1) with respect to the Dirichlet boundary conditions. Thus both the solution p of (2.1) and the solution $\tilde{p}$ of (4.4) can be approximated by a tensor based model reduction approach with the same, possibly exponential rate, with respect to the L^2-norm (see for instance [104] for the correlation between the stated Kolmogorov n-width, Hilbert-Schmidt integral operators, and the approximation of a Hilbert-Schmidt kernel by a tensor product decomposition). Of course it depends on the applied tensor based model reduction approach if these optimal rates can be realized or not.

[2] Using the Proper Generalized Decomposition method (cf. [24, 77]), we obtain p_m by computing sequentially the pair of functions $(\bar{p}_l, \phi_l)$, $l = 1, ..., m$, as the solution of the minimization problem

$$(\bar{p}_m, \phi_m) = \underset{\bar{p} \in X, \phi \in Y}{\operatorname{argmin}} \mathcal{E}\left(\sum_{l=1}^{m-1} \bar{p}_l(x)\phi_l(\psi(y; x)) + \bar{p}(x)\phi(\psi(y; x)) \right),$$

where $\mathcal{E} : H^1(\Omega) \to \mathbb{R}$ shall be the variational functional whose minimizer $p \in V$ is the unique solution of (4.4) for symmetric bilinear forms $a(\cdot, \cdot)$.

4.2 Exemplification for the HMR-RB approach

To obtain a good approximation of solutions exhibiting a skewed interface, we have to eliminate the interface in the solutions of the lower-dimensional problem. It is therefore crucial to reproduce the balance of the relative terms in the equation of the full problem (4.4). This is difficult to realize using the approach introduced in §2.3.1 as choosing the evaluation of the unknown part of the solution in x-direction as a parameter allows too much variation in the scaling of the respective terms to counterbalance them. Thus, we present in §4.2.2 a new approach for the derivation of a lower dimensional problem based on the discretization of the full problem introduced in §2.1.3 and exemplify it for an advection-diffusion equation in §4.2.3. We also comment briefly in §4.2.2 on necessary adaptations of Algorithm 2.3.1 AdaptiveParameterRefinement and Algorithm 2.3.2 Adaptive-HMR-POD due to the exchange of the parametrized 1D problem. We begin this section by formulating the reduced problem of the HMR approach for the full problem 4.4.

4.2.1 Formulation of the reduced problem

We assume orthonormality of the set of functions $\{\phi_l\}_{l=1}^m$ with respect to the L^2-inner product on $\widehat{\omega}$ and define the reduced space

$$V_m = \left\{ v_m(x,y) = \sum_{k=1}^{m} \overline{v}_k(x)\, \phi_k(\psi(y;x)), \;\; \text{with } \overline{v}_k(x) \in X,\, x \in \Omega_{1D},\, y \in \omega_x \right\}, \tag{4.6}$$

where

$$\overline{v}_k(x) = \int_{\widehat{\omega}} v_m(x, \psi^{-1}(\hat{y};x))\, \phi_k(\hat{y})\, d\hat{y}, \qquad k = 1, ..., m.$$

By using the Galerkin projection we obtain the reduced problem:

$$\text{Find } p_m \in V_m : \quad a(p_m, v_m) = f(v_m) - a(\mathfrak{h}, v_m) \;\; \forall\, v_m \in V_m, \tag{4.7}$$

which can be rewritten as

$$\text{Find } \overline{p}_k \in X, k = 1, ..., m : \quad \sum_{k=1}^{m} a(\overline{p}_k \phi_k, \xi\phi_l) = f(\xi\phi_l) - a(\mathfrak{h}, \xi\phi_l) \;\; \forall\, \xi \in X \;\text{ and }\; l = 1, ..., m. \tag{4.8}$$

For the subdivision $\mathcal{T}_H$ of Ω_{1D} with elements $\mathcal{T}_i = (x_{i-1}, x_i)$ of width $H_i = x_i - x_{i-1}$ and maximal step size $H = \max_{\mathcal{T}_i} H_i$ defined in §2.1.3, we introduce an associated conforming Finite Element space $X^H \subset X$ with $\dim(X^H) = N_H < \infty$ and basis ξ_i^H, $i = 1, ..., N_H$. We define the discrete reduced space

$$V_m^H = \left\{ v_m^H(x,y) = \sum_{k=1}^{m} \overline{v}_k^H(x)\, \phi_k(\psi(y;x)), \;\; \text{with } \overline{v}_k^H(x) \in X^H,\, x \in \Omega_{1D},\, y \in \omega_x \right\} \tag{4.9}$$

and obtain the discrete reduced problem: Find $\overline{p}_k^H \in X^H$, $k = 1, ..., m$, such that

$$\sum_{k=1}^{m} a(\overline{p}_k^H \phi_k, \xi_i^H \phi_l) = f(\xi_i^H \phi_l) - a(\mathfrak{h}, \xi_i^H \phi_l) \;\text{ for }\; i = 1, ..., N_H \;\text{ and }\; l = 1, ..., m, \tag{4.10}$$

where the discrete reduced solution is defined as $\tilde{p}_m^H := p_m^H + \mathfrak{h}$ for $p_m^H(x,y) = \sum_{k=1}^m \overline{p}_k^H(x)\, \phi_k(\psi(y;x))$.

4.2.2 Derivation of a parametrized 1D problem in transverse direction

Using the subdivisions $\mathcal{T}_H$ of Ω_{1D} and τ_h of $\widehat{\omega}$ defined in §2.1.3 and §2.3.3 and the associated FE spaces $X^H := \{w^H \in C^0(\Omega_{1D}) : w^H|_{\mathcal{T}_i} \in \mathbb{P}^1_d(\mathcal{T}_i), \mathcal{T}_i \in \mathcal{T}_H\} \subset X$ and $Y^h := \{w^h \in C^0(\widehat{\omega}) : w^h|_{\tau_j} \in \mathbb{P}^1_s(\tau_j), \tau_j \in \tau_h\} \subset Y$ with nodal bases ξ_i^H, $i = 1, ..., N_H$ and υ_j^h, $j = 1, ..., n_h$, we obtain the reference FE approximation of the full problem (4.4): Find $\mathcal{P}_i^h \in Y^h$, $i = 1, ..., N_H$, such that

$$\sum_{i=1}^{N_H} a(\xi_i^H \mathcal{P}_i^h, \xi_k^H \upsilon_j^h) = f(\xi_k^H \upsilon_j^h) - a(\mathfrak{h}, \xi_k^H \upsilon_j^h) \quad k = 1, ..., N_H,\ j = 1, ..., n_h, \tag{4.11}$$

where $\mathcal{P}_i^h(\hat{y}) = \sum_{j=1}^{n_h} p_{i,j} \upsilon_j^h(y)$, $i = 1, ..., N_H$. We introduce as in §2.3.1 for an arbitrary integrand $t \in L^1(\widehat{\Omega})$ of an integral $I(t) := \int_{\widehat{\omega}} \int_{\Omega_{1D}} t(x, \hat{y})\, dx d\hat{y}$ the quadrature formula

$$\bar{Q}(t) := \sum_{l=1}^{\bar{Q}} \alpha_l \int_{\widehat{\omega}} \tilde{t}(x_l^q, \hat{y})\ d\hat{y}, \quad \tilde{t}(x_l^q, \hat{y}) := \lim_{\varepsilon \to 0} \frac{1}{|B_\varepsilon(x_l^q)|} \int_{B_\varepsilon(x_l^q)} t(x, \hat{y})\, dx. \tag{4.12}$$

where α_l, $l = 1, ..., \bar{Q}$ are the weights, and x_l^q, $l = 1, ..., \bar{Q}$ are the quadrature points. Replacing $I(t)$ by $\bar{Q}(t)$ in the bilinear form $a(\cdot, \cdot)$ and the linear form $f(\cdot)$, we obtain the approximations $a^{\bar{q}}(\cdot, \cdot)$ and $f^{\bar{q}}(\cdot)$. The discrete problem with quadrature then reads: Find $\mathcal{P}_i^h \in Y^h$, $i = 1, ..., N_H$, such that

$$\sum_{i=1}^{N_H} a^{\bar{q}}(\xi_i^H \mathcal{P}_i^h, \xi_k^H \upsilon_j^h) = f^{\bar{q}}(\xi_k^H \upsilon_j^h) - a^{\bar{q}}(\mathfrak{h}, \xi_k^H \upsilon_j^h) \quad k = 1, ..., N_H,\ j = 1, ..., n_h. \tag{4.13}$$

Next we parametrize (4.13) by introducing a parameter vector μ with entries $\mu_l = x_l^q$, $l = 1, ..., \bar{Q}$, in order to find the optimal locations of the quadrature points by applying RB methods (§2.3.4) and thus to find the optimal points in Ω_{1D} for solving the lower-dimensional problem in transverse direction. The parameter space $\mathcal{D}$ is defined as $\mathcal{D} := [\Omega_{1D}]^{\bar{Q}}$. As solving (4.13) is for reasons of efficiency only feasible for small values of $\bar{Q}$, the dimension of $\mathcal{D}$ is limited to $\bar{Q} \ll N_H$, and even further limited to $\bar{Q} \leq 8$, when applying Algorithm 2.3.1. The latter is due to the fact that Algorithm 2.3.1 is based on a product-like hyper-rectangular grid, which limits its applicability to small parameter dimensions (cf. §2.3.4). Therefore, we have in general $\text{supp}(\xi_i^H) \cap \text{supp}(\xi_{i'}^H) = \emptyset$ for functions $\xi_i^H, \xi_{i'}^H \in \chi^H := \{\xi_i^H : \text{supp}(\xi_i^H) \cap \mu_l \neq \emptyset,\ l = 1, ..., \bar{Q}\}$, where $\dim(\chi^H) \leq \bar{Q} \leq 8$. To introduce a coupling and an exchange of information between the respective functions we first replace the functions ξ_i^H, $i = 1, ..., N_H$, by the basis functions ξ_i^q associated with a new subdivision, which is obtained by deleting all nodes of $\mathcal{T}_H$ in the open intervals $(\lceil (x_l^q/H) \rceil H, \lfloor (x_{l+1}^q/H) \rfloor H)$, $l = 1, ..., \bar{Q}$. Here and also for the remainder of this subsection we assume that the quadrature points are sorted in ascending order and that $x_0 \geq 0$, where x_0 has been defined in the beginning of §2.1 as the left interval boundary of Ω_{1D}. $\lceil \cdot \rceil$ denotes the ceil and $\lfloor \cdot \rfloor$ the floor function. Moreover, we enhance the set of quadrature points by the points $x_{\bar{Q}+l}^q := 0.5(x_l^q + x_{l+1}^q)$, $l = 1, ..., \hat{Q}$, if $\lfloor (x_{l+1}^q/H) \rfloor - \lfloor (x_l^q/H) \rfloor \geq 2$. The weights of the quadrature α_l, $l = 1, ..., Q$ with $Q = \bar{Q} + \hat{Q}$ that we have used for the numerical tests in §4.3 are defined as

$$\alpha_l := \begin{cases} H & \text{if} \quad \lfloor \frac{x_{l-1}^q}{H} \rfloor \neq \lfloor \frac{x_l^q}{H} \rfloor \text{ and } \lfloor \frac{x_l^q}{H} \rfloor \neq \lfloor \frac{x_{l+1}^q}{H} \rfloor, \\ \frac{x_l^q + x_{l+1}^q}{2} - \lfloor \frac{x_l^q}{H} \rfloor & \text{if} \quad \lfloor \frac{x_{l-1}^q}{H} \rfloor \neq \lfloor \frac{x_l^q}{H} \rfloor, \\ \lceil \frac{x_l^q}{H} \rceil - \frac{x_l^q + x_{l-1}^q}{2} & \text{if} \quad \lfloor \frac{x_l^q}{H} \rfloor \neq \lfloor \frac{x_{l+1}^q}{H} \rfloor, \\ \frac{x_{l+1}^q - x_{l-1}^q}{2} & \text{else.} \end{cases} \tag{4.14}$$

This closes the description of the quadrature rule

$$Q(t) := \sum_{l=1}^{Q} \alpha_l \int_{\widehat{\omega}} \tilde{t}(x_l^q, \hat{y})\, d\hat{y}, \quad \tilde{t}(x_l^q, \hat{y}) := \lim_{\varepsilon \to 0} \frac{1}{|B_\varepsilon(x_l^q)|} \int_{B_\varepsilon(x_l^q)} t(x, \hat{y})\, dx. \tag{4.15}$$

Using the quadrature formula $Q(t)$ (4.15) instead of $\bar{Q}(t)$ (4.12) we obtain the following coupled system of parametrized 1D partial differential equations in the transverse direction:

$$\begin{aligned} &\text{Given any } \mu \in \mathcal{D}, \text{ find } \mathcal{P}_l^h(\mu_l) := \sum_{\substack{\xi_i^q \\ \mu_l \in \mathrm{supp}(\xi_i^q)}} \xi_i^q(\mu_l) \mathcal{P}_i^h \in Y^h, l = 1, ..., \bar{Q}, \\ &\text{such that } a^q(\mathcal{P}_l^h(\mu_l), \upsilon_j^h\, \xi_k^q; \mu) = f^q(\upsilon_j^h\, \xi_k^q; \mu) - a^q(\mathfrak{h}, \upsilon_j^h\, \xi_k^q; \mu) \text{ for } j = 1, ..., n_h,\ \xi_k^q \in \chi^q, \end{aligned} \tag{4.16}$$

where $\chi^q := \{\xi_i^q : \mathrm{supp}(\xi_i^q) \cap \mu_l \neq \emptyset,\ l = 1, ..., \bar{Q}\}$. Note that (4.16) is a coupled system of size $\leq d\bar{Q}n_h \times d\bar{Q}n_h$, where d has been defined in the beginning of this subsection as the polynomial order of the FE space X^H. We emphasize that in contrast to §2.3.1 we are solving in (4.16) for the unknown parts of the solution in the dominant direction via the coefficient functions $\mathcal{P}_i^h(\hat{y})$ and do not consider them as part of the parameter as it has been done in §2.3.1. The numerical experiments in §4.3 show that while choosing $\bar{Q} = 1$ yields a bad convergence behavior of the HMR-RB approach, due to a limited variation in the solutions of (4.16), the choice $\bar{Q} = 2$ leads to good approximation results. The fact that solving (4.16) without the artificial coupling is equivalent to solving $\bar{Q}$ coupled systems of size $dn_h \times dn_h$, which yields as just mentioned a bad convergence behavior, stresses the importance of the introduction of the artificial coupling. Finally, we emphasize that in contrast to §2.3.1 we obtain $\bar{Q}$ snapshots $\mathcal{P}^h(\mu)$ per parameter vector $\mu = (\mu_1, ..., \mu_{\bar{Q}})$ — one for each component. As a consequence one has to slightly modify Algorithm 2.3.1 AdaptiveParameterRefinement and Algorithm 2.3.2 Adaptive-HMR-POD introduced in §2.3.4. First, the error indicators $\eta(G)$ and $\sigma(G)$ in Algorithm 2.3.1 have to be computed $\bar{Q}n_{train}$ times, but in return the training set can be reduced significantly. The Mark and Refine strategies are maintained. For the application of the POD in Algorithm 2.3.2 $\mathcal{O}(\bar{Q}^2 n_{train}^2 n_h)$ operations for the assembling of the correlation matrix and $\mathcal{O}(\bar{Q}^3 n_{train}^3)$ operations for the solution of the eigenvalue problem are required. The higher costs for the computation of the snapshots $\mathcal{P}^h(\mu)$ are still dominated by the costs for the computation of the error estimator. Overall, we do not expect a significant effect on the computational costs of the HMR-RB approach by changing the parametrized 1D problem due to the trade-off between the factor $\bar{Q}$ and the smaller sample size n_{train}.

4.2.3 Example: An advection-diffusion problem

To exemplify the derivation of the coupled system of parametrized 1D partial differential equations we consider the bilinear and linear form (2.9) with associated assumptions on the data functions on a rectangular domain Ω together with non-homogeneous Dirichlet boundary conditions with lifting function $\mathfrak{h} \in H^1(\Omega)$. The spaces X and Y thus coincide with $H_0^1(\Omega_{1D})$ and $H_0^1(\widehat{\omega})$, respectively. By applying the quadrature formula defined in (4.12), we obtain the discrete problem with quadrature: Find $\mathcal{P}_i^h \in Y^h$, $i = 1, ..., N_H$, such that

$$\begin{aligned} &\sum_{i=1}^{N_H} \int_{\widehat{\omega}} \bar{\mathcal{A}}_{i,k}(y) \frac{d\mathcal{P}_i^h}{dy} \frac{d\upsilon_j^h}{dy} + \bar{\mathcal{B}}_{i,k}(y) \frac{d\mathcal{P}_i^h}{dy} \upsilon_j^h + \bar{\mathcal{C}}_{i,k}(y)\, \mathcal{P}_{i,k}^h\, \upsilon_j^h\, dy \\ &= \int_{\widehat{\omega}} \bar{\mathcal{F}}_k(y)\, \upsilon_j^h\, dy - \int_{\widehat{\omega}} \bar{\mathcal{H}}_{1,k}(y) \frac{d\upsilon_j^h}{dy} + \bar{\mathcal{H}}_{2,k}(y)\, \upsilon_j^h\, dy \quad \text{for } j = 1, ..., n_h, k = 1, ..., N_H, \end{aligned}$$

where the coefficients $\bar{\mathcal{A}}_{i,k}(y), \bar{\mathcal{B}}_{i,k}(y), \bar{\mathcal{C}}_{i,k}(y), \bar{\mathcal{F}}_k(y), \bar{\mathcal{H}}_{1,k}(y)$ and $\bar{\mathcal{H}}_{2,k}(y)$ are given by

$$\begin{aligned}
\bar{\mathcal{A}}_{i,k}(y) &= \sum_{l=1}^{\bar{Q}} \alpha_l k(x_l^q, y)\xi_i^H(x_l^q)\xi_k^H(x_l^q), \qquad \bar{\mathcal{B}}_{i,k}(y) = \sum_{l=1}^{\bar{Q}} \alpha_l b_2(x_l^q, y)\xi_i^H(x_l^q)\xi_k^H(x_l^q),\\
\bar{\mathcal{C}}_{i,k}(y) &= \sum_{l=1}^{\bar{Q}} \alpha_l k(x_l^q, y)\partial_x\xi_i^H(x_l^q)\partial_x\xi_k^H(x_l^q) + b_1(x_l^q, y)\partial_x\xi_i^H(x_l^q)\xi_k^H(x_l^q),\\
\bar{\mathcal{F}}_k(y) &= \sum_{l=1}^{\bar{Q}} \alpha_l s(x_l^q, y)\xi_k^H(x_l^q), \qquad \bar{\mathcal{H}}_{1,k}(y) = \sum_{l=1}^{\bar{Q}} \alpha_l k(x_l^q, y)\partial_y\mathfrak{h}(x_l^q, y)\xi_k^H(x_l^q),\\
\bar{\mathcal{H}}_{2,k}(y) &= \sum_{l=1}^{\bar{Q}} \alpha_l k(x_l^q, y)\partial_x\mathfrak{h}(x_l^q, y)\partial_x\xi_k^H(x_l^q) + (b_1(x_l^q, y)\partial_x\mathfrak{h}(x_l^q, y) + b_2(x_l^q, y)\partial_y\mathfrak{h}(x_l^q, y))\xi_k^H(x_l^q).
\end{aligned}$$

Here we have omitted the $\backsim$ on the integrands (cf. (4.12)) to simplify notations. Using the artificial coupling introduced in the previous subsection and the associated quadrature formula (4.15) we obtain the parametrized coupled 1D PDE in transverse direction: Given any $\mu \in \mathcal{D}$, find

$$\mathcal{P}_l^h(\mu_l) := \sum_{\substack{\xi_i^q \\ \mu_l \in \mathrm{supp}(\xi_i^q)}} \xi_i^q(\mu_l)\mathcal{P}_i^h \in Y^h, l = 1, ..., \bar{Q}, \quad \text{such that} \tag{4.18}$$

$$\begin{aligned}
&\sum_{l=1}^{\bar{Q}} \int_{\widehat{\omega}} \mathcal{A}_k^l(y;\mu)\frac{d\mathcal{P}_l^h(\mu_l)}{dy}\frac{dv_j^h}{dy} + \mathcal{B}_k^l(y;\mu)\frac{d\mathcal{P}_l^h(\mu_l)}{dy}v_j^h + \mathcal{C}_k^l(y;\mu)\frac{d\mathcal{P}_l^h(\mu_l)}{dx}v_j^h\, dy\\
&= \int_{\widehat{\omega}} \mathcal{F}_k(y;\mu)\, v_j^h\, dy - \int_{\widehat{\omega}} \mathcal{H}_{1,k}(y;\mu)\frac{dv_j^h}{dy} + \mathcal{H}_{2,k}(y;\mu)\, v_j^h\, dy \quad \text{for } j = 1, ..., n_h,
\end{aligned}$$

where the coefficients $\mathcal{A}_k^l(y;\mu), \mathcal{B}_k^l(y;\mu), \mathcal{C}_k^l(y;\mu), \mathcal{F}_k(y;\mu), \mathcal{H}_{1,k}(y;\mu)$ and $\mathcal{H}_{2,k}(y;\mu)$ are given by

$$\begin{aligned}
\mathcal{A}_k^l(y;\mu) &= \sum_{x_n^q \in (\mu_{l-1}, \mu_{l+1})} \alpha_n k(x_n^q, y)\xi_k^H(x_n^q), \qquad \mathcal{B}_k^l(y;\mu) = \sum_{x_n^q \in (\mu_{l-1}, \mu_{l+1})} \alpha_n b_2(x_n^q, y)\xi_k^H(x_n^q),\\
\mathcal{C}_k^l(y;\mu) &= \sum_{x_n^q \in (\mu_{l-1}, \mu_{l+1})} \alpha_n k(x_n^q, y)\partial_x\xi_k^H(x_n^q) + b_1(x_n^q, y)\xi_k^H(x_n^q),\\
\mathcal{F}_k(y;\mu) &= \sum_{l=1}^{Q} \alpha_l s(x_l^q, y)\xi_k^H(x_l^q), \qquad \mathcal{H}_{1,k}(y;\mu) = \sum_{l=1}^{Q} \alpha_l k(x_l^q, y)\partial_y\mathfrak{h}(x_l^q, y)\xi_k^H(x_l^q),\\
\mathcal{H}_{2,k}(y;\mu) &= \sum_{l=1}^{Q} \alpha_l k(x_l^q, y)\partial_x\mathfrak{h}(x_l^q, y)\partial_x\xi_k^H(x_l^q) + (b_1(x_l^q, y)\partial_x\mathfrak{h}(x_l^q, y) + b_2(x_l^q, y)\partial_y\mathfrak{h}(x_l^q, y))\xi_k^H(x_l^q)
\end{aligned}$$

and for notational convenience (μ_0, μ_2) and $(\mu_{\bar{Q}-1}, \mu_{\bar{Q}+1})$ stand for $[\mu_1, \mu_2)$ and $(\mu_{\bar{Q}-1}, \mu_{\bar{Q}}]$, respectively. We finally remark that $\frac{d\mathcal{P}_l^h(\mu_l)}{dx}$ has to be interpreted as

$$\frac{d\mathcal{P}_l^h(\mu_l)}{dx} = \sum_{\substack{\xi_i^q \\ \mu_l \in \mathrm{supp}(\xi_i^q)}} \frac{d\xi_i^q(\mu_l)}{dx}\mathcal{P}_i^h \in Y^h, l = 1, ..., \bar{Q}.$$

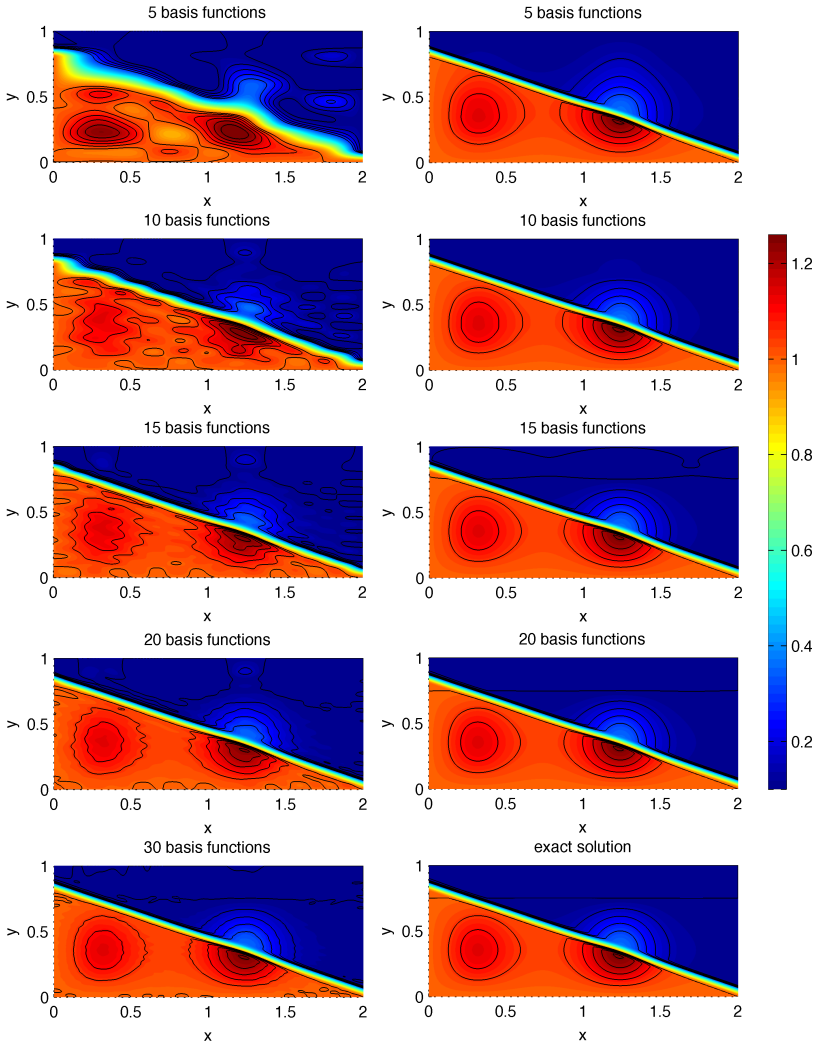

Figure 4.2: Test case 1: Comparison of the discrete reduced solution p_m^H using the lifting function g_D (4.22) (left side) for $m = 5, 10, 15, 20, 30$ (top-bottom), p_m^H using $\mathfrak{h}$ (4.20) as the lifting function (right) and $m = 5, 10, 15, 20$ with the exact solution $\tilde{p}$ (right,bottom) for $N_H = 800$, $n_h = 400$, $N_{H'} = 80$.

4.3 Numerical Experiments

In this section we demonstrate in several numerical experiments the capacity of the ansatz proposed in Subsection 4.1.2 to improve the convergence behavior for tensor based model reduction approaches using the example of the HMR-RB method. We therefore compare the convergence behavior of the model error of the HMR-RB approach in case we include information on the interface with the approximation behavior if we use an arbitrary lifting function of the Dirichlet boundary conditions. In the first test case, the full solution p of (4.4) is chosen as a multiple of the solution of test case 1 in §2.6 to have a benchmark for the convergence rate. We see a considerable improvement of the convergence behavior of the model error. An even more substantial improvement can

be observed for the second test case, where the solution exhibits more complex structures and little spatial regularity due to a discontinuous source term. While we include in test case 1 and 2 the exact interface, we use in test case 3 only an approximation of the interface as the lifting function of the Dirichlet boundary conditions and still observe a significant improvement of the convergence behavior of the HMR-RB approach. In all three test cases we have used linear FE in x- and y-direction, i.e. $X^H = \left\{v^H \in C^0(\Omega_{1D}) : v^H|_{\mathcal{T}_i} \in \mathbb{P}^1_1(\mathcal{T}_i), \mathcal{T}_i \in \mathcal{T}_H\right\}, Y^h = \left\{v^h \in C^0(\widehat{\omega}) : v^h|_{\tau_j} \in \mathbb{P}^1_1(\tau_j), \tau_j \in \tau_h\right\}$, and $V^{H\times h} = \{v^{H\times h} \in C^0(\widehat{\Omega}) : v^{H\times h}|_{T_{i,j}} \in \mathbb{Q}_{1,1}, T_{i,j} \in \hat{T}\}$. We recall that the relative model error in the V- or L^2-norm has been defined in §2.6 as $\|e_m\|^{rel}_V := \|e_m\|_V/\|p^{H\times h}\|_V$, or $\|e_m\|^{rel}_{L^2(\Omega)} := \|e_m\|_{L^2(\Omega)}/\|p^{H\times h}\|_{L^2(\Omega)}$, respectively, for $e_m = p^{H\times h} - p^H_m$. The implementations has been done in MATLAB. We performed various runs to obtain averaged error values. We did 100 runs if including $\mathfrak{h}$ both in the weak and strong formulation of 4.7 in test case 1 and also for the inclusion of $\mathfrak{h}$ in the strong form in test case 2. For all other cases we performed 50 runs. Finally, we have used equidistant grids in x- and y-direction for the computations of all three test cases and the Riesz representative based error estimator §2.4.1.

Test case 1

First, we consider a numerical example with an exact solution, where the full solution p of (4.4) is a multiple of the analytic solution of test case 1 in §2.6 to enable a comparison with the situation where no interface is present. In detail, we solve a Poisson problem on $\Omega = (0,2)\times(0,1)$ with an exact solution $\tilde{p} = p + \mathfrak{h}$, where the interface $\mathfrak{h}$ and p are given as

$$\mathfrak{h}(x,y) = \begin{cases} 1 & \text{if } y + 0.4x < 0.8, \\ 0.1 & \text{if } y + 0.4x > 0.9, \\ 0.55 + 0.45\cos(10\pi(y + 0.4x - 0.8)) & \text{if } 0.8 \le y + 0.4x \le 0.9 \end{cases}, \tag{4.20}$$

$$\text{and } p(x,y) = 5y^2(1-y)^2(0.75-y)x(2-x)\exp(\sin(2\pi x)). \tag{4.21}$$

The solution $\tilde{p}$ is displayed in the last picture of Fig. 4.2 and the skewed interface $\mathfrak{h}$ is clearly recognizable. First, we compare $\tilde{p}$ with the discrete reduced solution $\tilde{p}^H_m$, which has been computed using the lifting function

$$g_D = (-0.5x + 1)\mathfrak{h}(0,y) + 0.5x\mathfrak{h}(2,y) \tag{4.22}$$

for $m = 5, 10, 15, 20, 30$, $N_H = 800$, $n_h = 400$ and $N_{H'} = 80$ (Fig. 4.2, left), where $N_{H'}$ has been defined in §2.1.3. Whereas 15 basis functions are sufficient to obtain a good approximation of the interface $\mathfrak{h}$, we detect strong oscillations of $\tilde{p}^H_{15}$ in the other parts of the domain yielding still a bad approximation of p (4.21). These oscillations decrease for increasing m and for $m = 30$ we obtain a reasonable approximation of $\tilde{p}$. If we use $\mathfrak{h}$ as the lifting function of the Dirichlet boundary conditions to compute $\tilde{p}^H_m$ (Fig. 4.2, right) no oscillations can be detected. The contour lines of $\tilde{p}^H_{20}$ match perfectly with the ones of $\tilde{p}$ and already for $m = 10$ and 15 only small deviations can be observed. All in all we see a much better qualitative convergence behavior for the solution of (4.10).

To analyze the capacity of the proposed method to improve the convergence behavior also from a quantitative viewpoint, we compare the convergence behavior of the relative model error $\|e_m\|^{rel}_V$ for increasing model order m. Using g_D requires more than 70 basis functions to obtain $\|e_m\|^{rel}_V \le 0.01$ for $H \le 0.00625$ (Fig. 4.3a), which can be attained for $m = 16$ if choosing $\mathfrak{h}$ (Fig. 4.3b). However we see in Fig. 4.3b that the convergence rate has only improved slightly and that the improvement of the convergence behavior can be mainly ascribed to a better relative error already for $m = 1$ of the solution of (4.10). We have thus recomputed the HMR-RB approximation, employing a reconstruction of the derivative of the interface in the dominant direction, for the

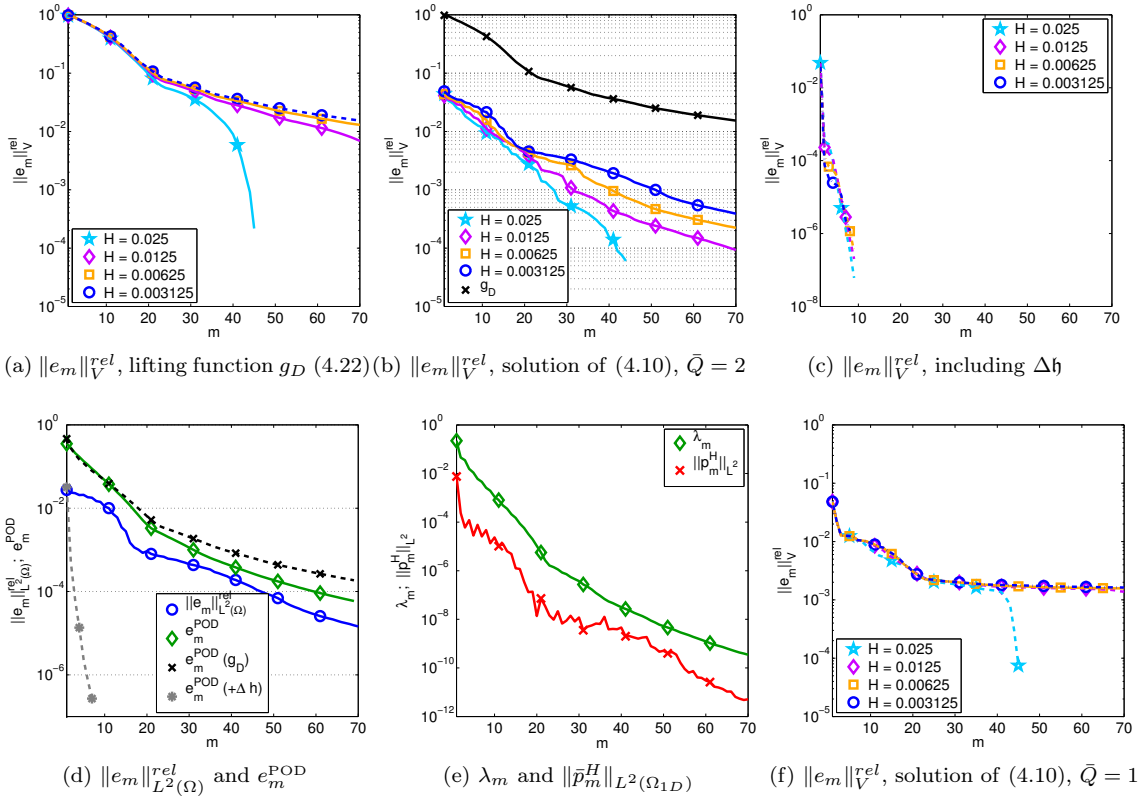

(a) $\|e_m\|_V^{rel}$, lifting function g_D (4.22) (b) $\|e_m\|_V^{rel}$, solution of (4.10), $\bar{Q} = 2$ (c) $\|e_m\|_V^{rel}$, including $\Delta\mathfrak{h}$

(d) $\|e_m\|_{L^2(\Omega)}^{rel}$ and e_m^{POD} (e) λ_m and $\|\bar{p}_m^H\|_{L^2(\Omega_{1D})}$ (f) $\|e_m\|_V^{rel}$, solution of (4.10), $\bar{Q} = 1$

Figure 4.3: Test case 1: Comparison of the model error convergence of $\|e_m\|_V^{rel}$, if using the lifting function g_D (4.22) (a), including $\mathfrak{h}$ in the strong formulation of (4.7) (c) or in the weak form of (4.7) and choosing $\bar{Q} = 2$ in (4.16) (b) or $\bar{Q} = 1$ (f); comparison of $\|e_m\|_{L^2(\Omega)}^{rel}$ and e_m^{POD} for the solution $\tilde{p}_m^H$ of (4.10) with e_m^{POD} if including $\Delta\mathfrak{h}$ in strong form ($+\Delta h$) or using g_D (g_D) (d) and λ_m and $\|\bar{p}_m^H\|_{L^2(\Omega_{1D})}$ for the solution of (4.10) (e); all computations: $N_{H'} = 10$.

derivation of the parameterized lower dimensional system (4.16). This reconstruction mimics the behavior of the derivative in two space dimensions. One example for such a reconstruction is the Riesz representative $\mathcal{R}^{H\times h}$, defined as

$$\int_{\widehat{\Omega}} \mathcal{R}^{H\times h} v^{H\times h} = a(\mathfrak{h}, v^{H\times h}). \tag{4.23}$$

Note that prescribing $\mathcal{R}^{H\times h}$ is equivalent to adding $\Delta\mathfrak{h}$ to the source and sink term directly in the strong formulation of (4.7), if $\mathfrak{h}$ is sufficiently regular. By doing so we obtained the expected fast exponential convergence rate of $\|e_m\|_V^{rel}$ (Fig. 4.3c), already observed in test case 1 in §2.6 (Fig. 2.2). As the convergence rates of $\|e_m\|_{L^2(\Omega)}^{rel}$ and e_m^{POD} and also λ_m and $\|\bar{p}_m^H\|_{L^2(\Omega_{1D})}$ for the solution of (4.10) coincide to a great extend (Fig. 4.3d and Fig. 4.3e), we conclude that already the discrete solution manifold Y_M^h — defined in (2.33) — used for the computation of the reduction space Y_m^h and thus the discrete reduced solution $\tilde{p}_m^H$ of (4.10) can be badly approximated by a m-dimensional subspace. Hence although the reference solution $p^{H\times h}$ of (4.11) could be approximated exponentially fast (Fig. 4.3c), this approximation quality cannot be realized due to a deficient construction of Y_M^h. We further infer that the equivalence of including $\mathfrak{h}$ in the strong or weak

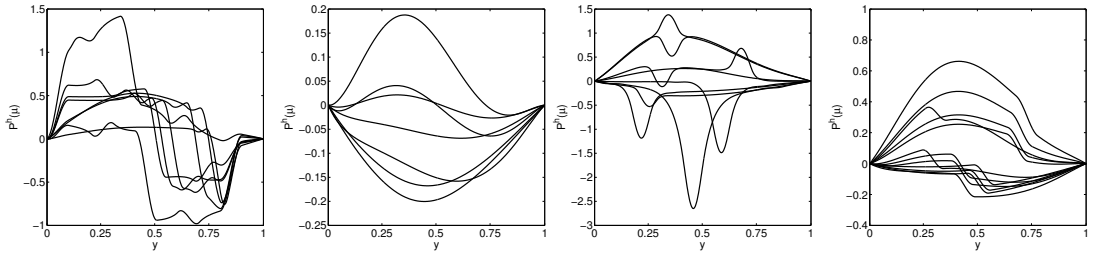

(a) lift. funct. g_D (4.22) (b) incl. $\Delta\mathfrak{h}$ (c) (4.16), $\bar{Q} = 2$ (d) (4.16), $\bar{Q} = 1$

Figure 4.4: Test case 1: Typical snapshots of the discrete solution manifold Y_M^h (2.33) if the lifting function g_D (4.22) is used and therefore no information on the interface is included in the model reduction preocedure (a), if $\Delta\mathfrak{h}$ is added in the strong formulation of (4.7) (b), (4.16) is solved with $\bar{Q} = 2$ (c) and $\bar{Q} = 1$ (d).

formulation of (4.7) cannot be reproduced properly by the lower-dimensional problems, because otherwise the convergence rates of e_m^{POD} would be the same for both cases. This statement can be confirmed by comparing the discrete solution manifold Y_M^h for the different cases. If using g_D as the lifting function the snapshots $\mathcal{P}^h(\mu)$ contain all the sharp interface, have seldom the right slope in the other part of $\widehat{\omega}$ and exhibit often strong oscillations (Fig. 4.4a), explaining both the qualitative and quantitative convergence behavior obtained in this case. If we add $\Delta\mathfrak{h}$ in the strong formulation of the PDE we see in Fig. 4.4b that the snapshots $\mathcal{P}^h(\mu)$ resemble evaluations of p (4.21). In contrast the snapshots of (4.16) for $\bar{Q} = 2$ are either located peaks or additionally contain small peaks at the location of the interface (Fig. 4.4c), showing that the interface $\mathfrak{h}$ has not been removed completely from the snapshots $\mathcal{P}^h(\mu)$ as it has been possible in the case of adding $\Delta\mathfrak{h}$ (Fig. 4.4b). This confirms the assertion that the equivalence of including $\mathfrak{h}$ in the strong or weak formulation of (4.7) cannot be reproduced properly with the approach for the derivation of the parametrized 1D problem proposed in §4.2.2. Nevertheless, we emphasize that a significant improvement of the convergence behavior has been achieved (Fig. 4.3b) for 2 quadrature points which is not possible if following the ansatz of §2.3.1. Finally, we remark that for $\bar{Q} = 1$ we observe for $m \geq 20$ a stagnation of $\|e_m\|_V^{rel}$ (Fig. 4.3f). This can be ascribed to the fact that although the snapshots $\mathcal{P}^h(\mu) \in Y_M^h$ in Fig. 4.4d show a certain similarity to the snapshots in Fig. 4.4b, they all contain different slopes of the interface, which are not present in p (4.21), prohibiting a convergence to the reference solution.

Test case 2

In this test case we consider a problem in which the solution exhibits more complex features than in the previous example due to a discontinuous source term. In detail, we solve a Poisson problem on $\Omega = (0, 2) \times (0, 1.1)$ with a concentration profile $\mathfrak{h}$ and a source term s defined as

$$\mathfrak{h}(x, y) = \begin{cases} 1 & \text{if } y + 0.4x < 0.8, \\ 0.1 & \text{if } y + 0.4x > 0.9, \\ 0.55 + 0.45\cos(10\pi(y + 0.4x - 0.8)) & \text{if } 0.8 \leq y + 0.4x \leq 0.9. \end{cases} \tag{4.24}$$

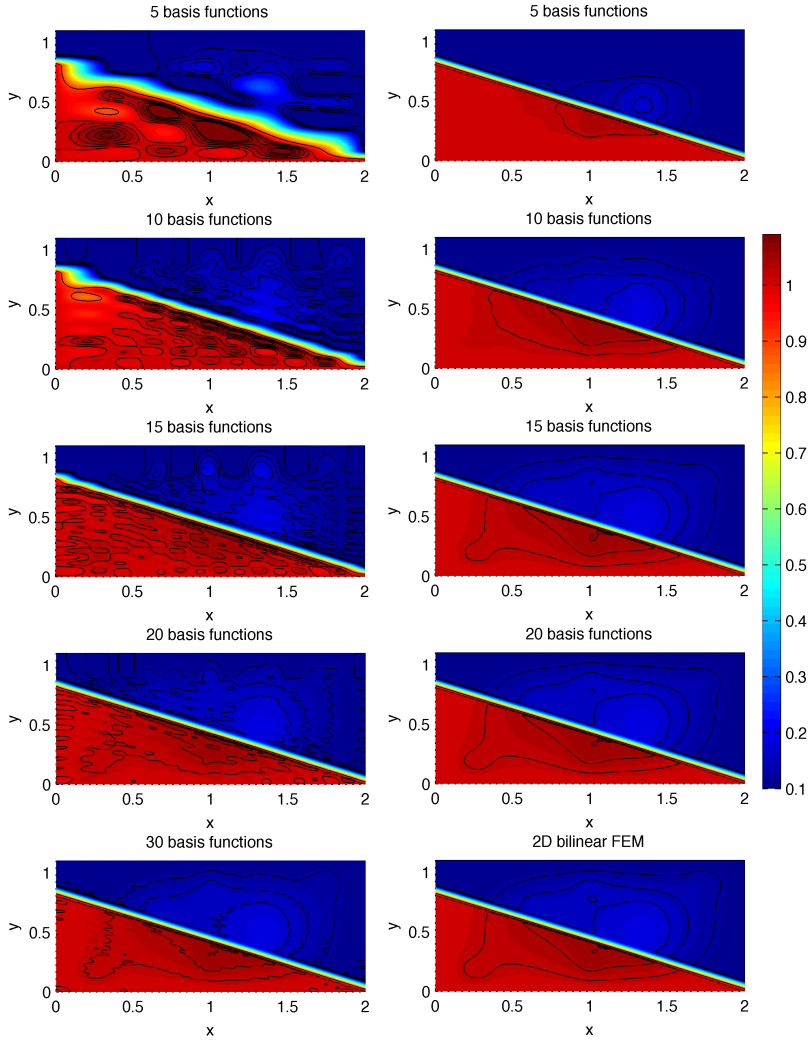

Figure 4.5: Test case 2: Comparison of the discrete reduced solution p_m^H using the lifting function g_D (4.26) (left side) for $m = 5, 10, 15, 20, 30$ (top-bottom), p_m^H using $\mathfrak{h}$ (4.24) as the lifting function (right) and $m = 5, 10, 15, 20$ with the reference solution $\tilde{p}^{H\times h}$ (right,bottom) for $N_H = 800$, $n_h = 440$, $N_{H'} = 80$.

and

$$s(x,y) = -\Delta\mathfrak{h} + \begin{cases} 2.25 & \text{if } 0.15 \le x \le 0.35, \;\; 0.05 \le y \le 0.25, \\ 2.25 & \text{if } 0.55 \le x \le 0.75, \;\; 0.6 \le y \le 0.8, \\ 4 & \text{if } 0.95 \le x \le 1.05, \;\; 0.15 \le y \le 0.35 \text{ and } 0.75 \le y \le 0.95, \\ 4 & \text{if } 1.25 \le x \le 1.45, \;\; 0.35 \le y < 0.55, \\ 2 & \text{if } 1.25 \le x \le 1.45, \;\; 0.55 \le y \le 0.75, \\ 2.25 & \text{if } 1.65 \le x \le 1.85, \;\; 0.85 \le y \le 1.05, \end{cases} \tag{4.25}$$

We prescribe non-homogeneous Dirichlet boundary conditions on the whole $\partial\Omega$, where the respective

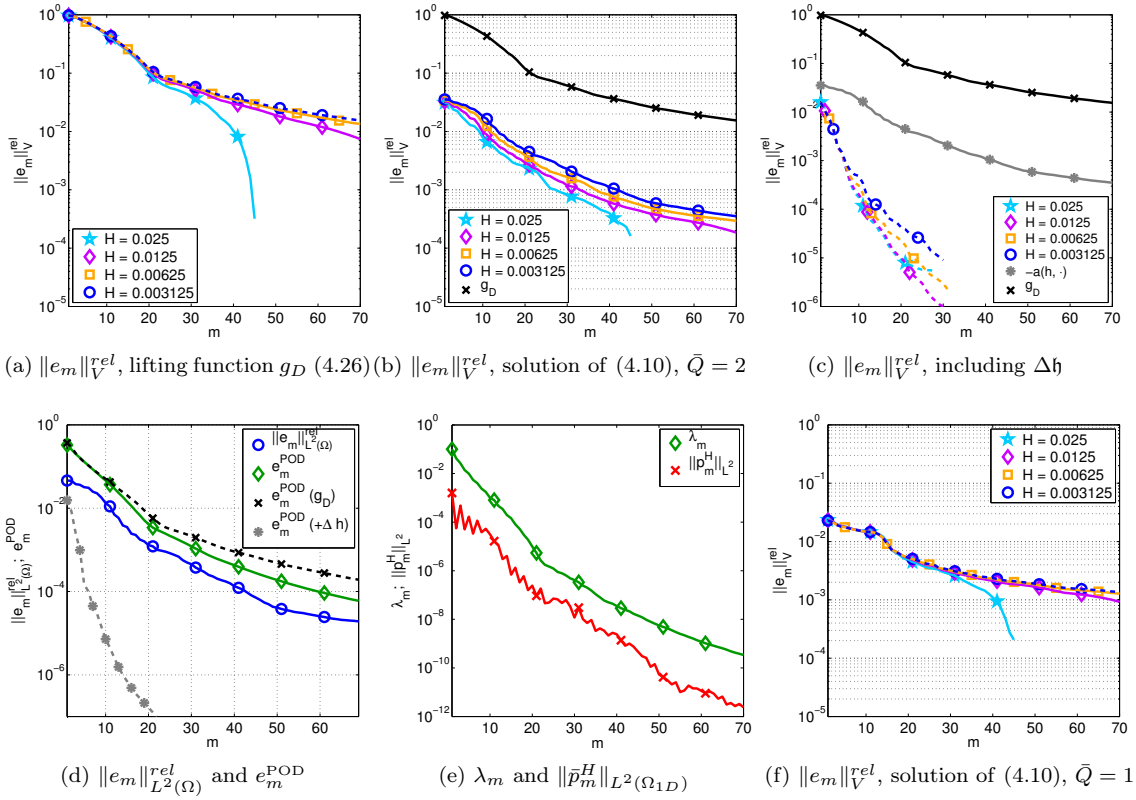

(a) $\|e_m\|_V^{rel}$, lifting function g_D (4.26) (b) $\|e_m\|_V^{rel}$, solution of (4.10), $\bar{Q} = 2$ (c) $\|e_m\|_V^{rel}$, including $\Delta\mathfrak{h}$

(d) $\|e_m\|_{L^2(\Omega)}^{rel}$ and e_m^{POD} (e) λ_m and $\|\bar{p}_m^H\|_{L^2(\Omega_{1D})}$ (f) $\|e_m\|_V^{rel}$, solution of (4.10), $\bar{Q} = 1$

Figure 4.6: Test case 2: Comparison of the model error convergence of $\|e_m\|_V^{rel}$, if using the lifting function g_D (4.26) (a), including $\mathfrak{h}$ in the strong formulation of (4.7) (c) or in the weak form of (4.7) and choosing $\bar{Q} = 2$ in (4.16) (b) or $\bar{Q} = 1$ (f); comparison of $\|e_m\|_{L^2(\Omega)}^{rel}$ and e_m^{POD} for the solution $\tilde{p}_m^H$ of (4.10) with e_m^{POD} if including $\Delta\mathfrak{h}$ in strong form ($+\Delta h$) or using g_D (g_D) (d) and λ_m and $\|\bar{p}_m^H\|_{L^2(\Omega_{1D})}$ for the solution of (4.10) (e); all computations: $N_{H'} = 10$.

boundary values are obtained by evaluating $\mathfrak{h}$ on $\partial\Omega$. The reference solution $\tilde{p}^{H\times h}$ for $N_H = 800$, $n_h = 440$ is depicted in the last picture of Fig. 4.5 and contains apart from the skewed interface $\mathfrak{h}$ also a part $p^{H\times h}$ induced by the source term. We have done a convergence study to ensure that $\tilde{p}^{H\times h}$ contains all essential features of the exact solution. Comparing $\tilde{p}^{H\times h}$ with the discrete reduced solution $\tilde{p}_m^H$, computed using the lifting function

$$g_D = (-0.5x + 1)\mathfrak{h}(0, y) + 0.5x\mathfrak{h}(2, y) \tag{4.26}$$

for $m = 5, 10, 15, 20, 30$, $N_H = 800$, $n_h = 440$ and $N_{H'} = 80$ (Fig. 4.5, left), we observe that 30 basis functions are required to obtain an acceptable approximation of $\tilde{p}^{H\times h}$. The oscillations are even stronger than in the previous example and result in a very slow approximation of $p^{H\times h}$. Note that even for $m = 15$ no resemblance between the contour lines of $\tilde{p}_{15}^H$ and $\tilde{p}^{H\times h}$ can be detected. In contrast already $\tilde{p}_{15}^H$ — the solution of (4.10) for $m = 15$ — contains all essential features of the solution including the two small peaks around $x = 1$ and we see a very good visual agreement of $\tilde{p}_{20}^H$ and $\tilde{p}^{H\times h}$. Altogether we observe a very much better qualitative convergence behavior, when choosing $\mathfrak{h}$ as the lifting function, where the gap is even greater than in the previous test case.

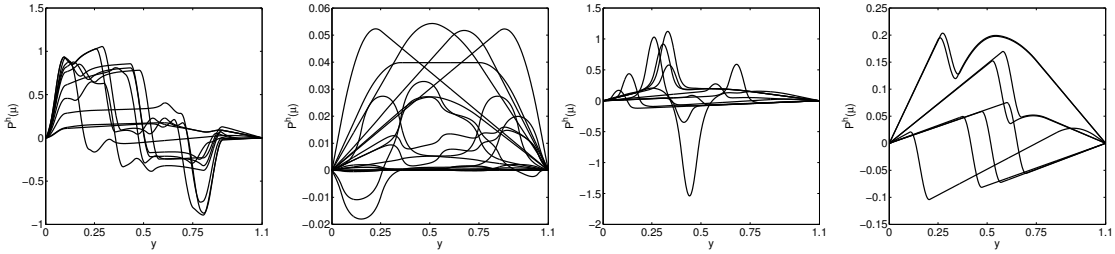

(a) lift. func. g_D (4.26) (b) incl. $\Delta\mathfrak{h}$ (c) (4.16), $\bar{Q} = 2$ (d) (4.16), $\bar{Q} = 1$

Figure 4.7: Test case 2: Typical snapshots of the discrete solution manifold Y_M^h (2.33) if the lifting function g_D (4.26) is used and therefore no information on the interface is included in the model reduction procedure (a), if $\Delta\mathfrak{h}$ is added in the strong formulation of (4.7) (b), (4.16) is solved with $\bar{Q} = 2$ (c) and $\bar{Q} = 1$ (d).

Studying the convergence behavior of $\|e_m\|_V^{rel}$ we observe a bigger improvement of the convergence behavior for $m \leq 60$ for $H = 0.003125$, if including $\mathfrak{h}$, in comparison to the previous example (Fig. 4.6a, Fig. 4.6b, Fig. 4.3b). For $m > 60$ the convergence behavior is comparable. Adding $\Delta\mathfrak{h}$ directly to the source term s in the strong formulation of (4.7) yields an exponential convergence rate of $\|e_m\|_V^{rel}$ (Fig. 4.6c). The behavior of $\|e_m\|_V^{rel}$ in both cases — either including $\mathfrak{h}$ in the weak (Fig. 4.6b) or in the strong formulation (Fig. 4.6c) — demonstrates the capacity of the ansatz proposed in §4.1 to improve the convergence behavior for the HMR-RB approach. As however the convergence rates of e_m^{POD} and $\|e_m\|_{L^2(\Omega)}^{rel}$ and λ_m and $\|\bar{p}_m\|_{L^2(\Omega_{1D})}$, respectively, for the solution of (4.10) are roughly the same (Fig. 4.6d, 4.6e) and differ from the ones obtained if including $\Delta\mathfrak{h}$ in the strong formulation of (4.7), we conclude that also for this test case the equivalence of including $\mathfrak{h}$ in the strong or weak formulation of (4.7) cannot be reproduced by the parametrized 1D problem, prohibiting an exponentially fast approximation of the reference solution $\tilde{p}^{H\times h}$ of (4.11) by $\tilde{p}_m^H$ — the solution of (4.10). Finally, we observe again a significant deterioration of the convergence rate of $\|e_m\|_V^{rel}$ for the solution of (4.10) for one quadrature point in comparison to $\bar{Q} = 2$ (Fig. 4.6f).

In Fig. 4.7 some exemplary snapshots $\mathcal{P}^h(\mu)$ are depicted in order to help to explain the convergence behavior observed in Fig. 4.6. In case we add $\Delta\mathfrak{h}$, the snapshots look like the profile of $p^{H\times h}$ in the transverse direction (Fig.4.7b), whereas the solutions of (4.16) for $\bar{Q} = 2$ additionally exhibit a peak around the interface (Fig.4.7c). If we use g_D as the lifting function, the snapshots $\mathcal{P}^h(\mu)$ feature very strong oscillations but barely resemble the slope of $p^{H\times h}$ (Fig.4.7a). Also the snapshots for $\bar{Q} = 1$ in (4.16) contain only few information on the profile of $p^{H\times h}$ in the transverse direction (Fig.4.7d), indicating that the artificial coupling introduced in §4.2.2 is necessary to obtain a good approximation behavior of the HMR-RB approach.

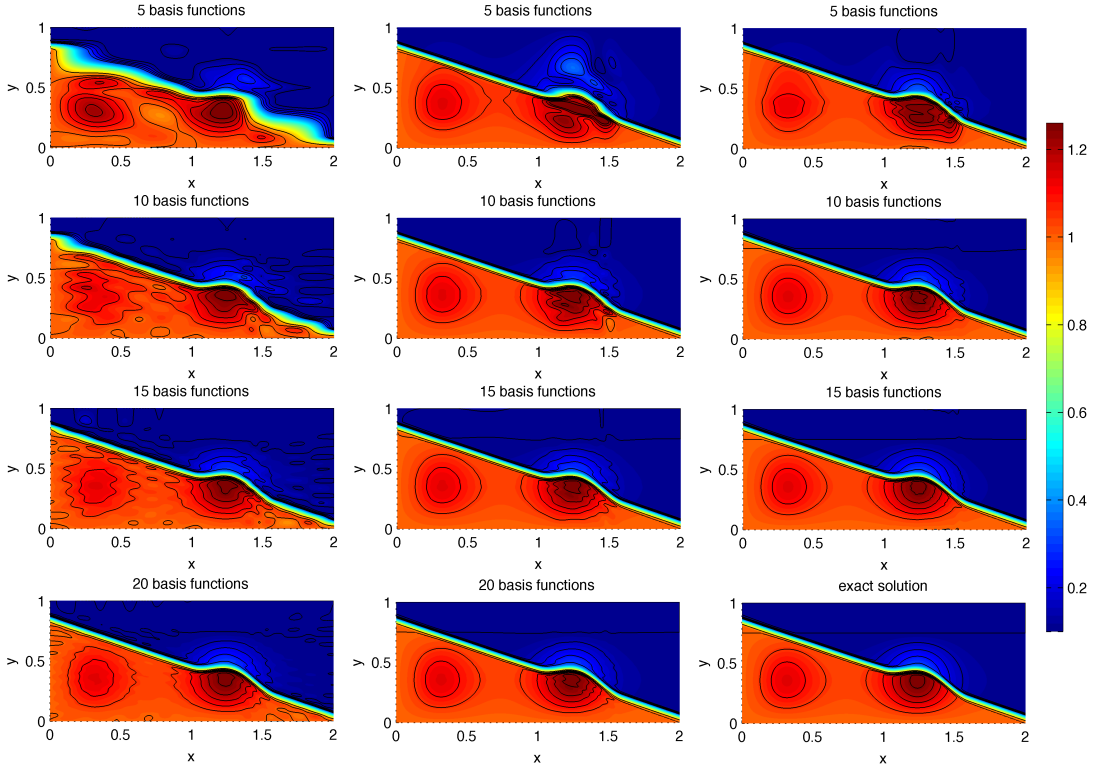

Figure 4.8: Test case 3: Comparison of the discrete reduced solution $\tilde{p}_m^H$ using the lifting function g_D (left side) for $m = 5, 10, 15, 20$ (top-bottom), $\tilde{p}_m^H$ using $\bar{\mathfrak{h}}$ (4.29) as the lifting function in (4.10) and $m = 5, 10, 15, 20$ (middle), $\tilde{p}_m^H$ if including $\Delta\bar{\mathfrak{h}}$ in the strong formulation of (4.7) for $m = 5, 10, 15$ (right) with the exact solution $\tilde{p}$ (right, bottom) for $N_H = 800$, $n_h = 400$, $N_{H'} = 80$.

Test case 3

Finally, we consider a test case in which we do not include the exact interface $\mathfrak{h}$ but only an approximation $\bar{\mathfrak{h}}$ as we usually cannot expect to be able to determine the exact interface but rather only an approximation. We solve a Poisson problem on $\Omega = (0, 2) \times (0, 1)$, where we choose the exact solution $\tilde{p} = p + \mathfrak{h}$ where

$$\mathfrak{h}(x, y) = \begin{cases} 1 & \text{if } y + 0.4x - \mathfrak{j}(x) < 0.8, \\ 0.1 & \text{if } y + 0.4x - \mathfrak{j}(x) > 0.9, \\ 0.55 + 0.45\cos(10\pi(y + 0.4x - 0.8 - \mathfrak{j}(x))) & \text{if } 0.8 \le y + 0.4x - \mathfrak{j}(x) \le 0.9 \end{cases} \tag{4.27}$$

$$\text{for } \mathfrak{j}(x) = \begin{cases} 0.1\sin^2(\frac{5\pi}{3}(x-1)) & \text{if } 1 \le x \le 1.6, \\ 0 & \text{else,} \end{cases}$$

$$\text{and } p(x, y) = 5y^2(1-y)^2(0.75-y)x(2-x)\exp(\sin(2\pi x)), \tag{4.28}$$

which is the same choice of p as in test case 1. The exact solution $\tilde{p}$ is depicted in the last picture of Fig. 4.8 and it can be seen that $\mathfrak{h}$ is curved between $x = 1$ and $x = 1.6$. In Fig. 4.8 on the left we see the discrete reduced solution $\tilde{p}_m^H$, computed with the same lifting function $g_D =$

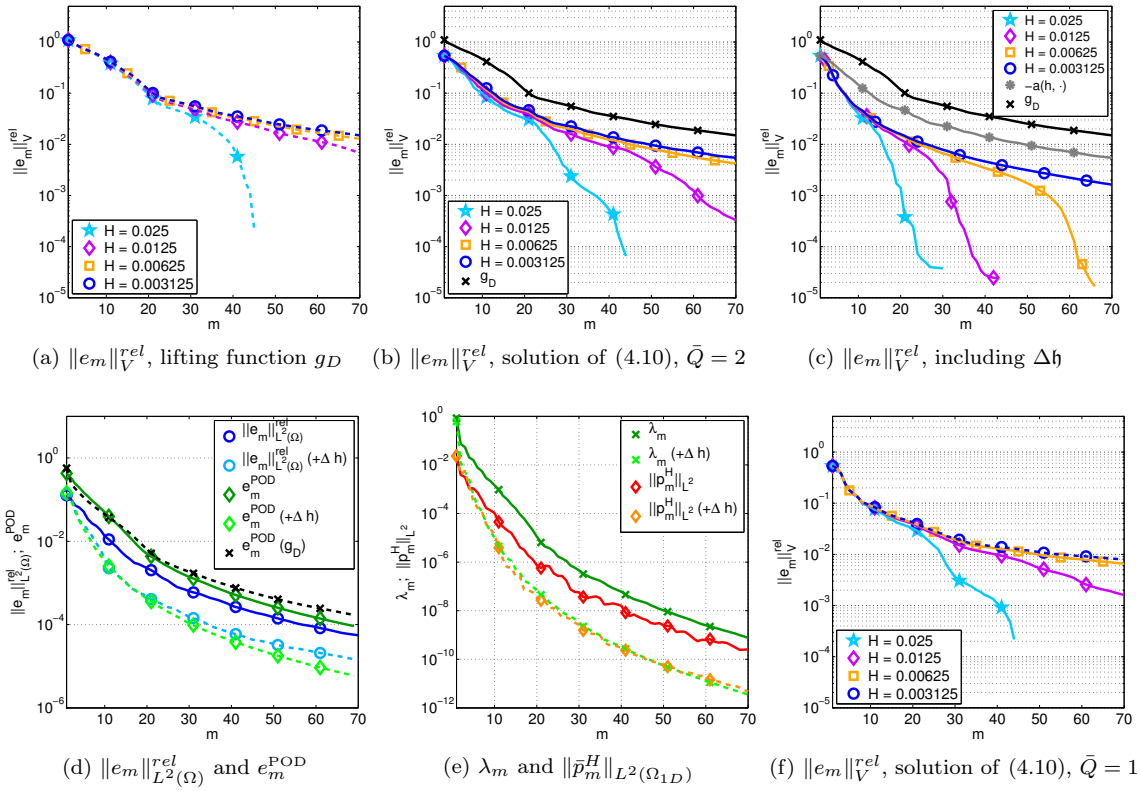

(a) $\|e_m\|_V^{rel}$, lifting function g_D (b) $\|e_m\|_V^{rel}$, solution of (4.10), $\bar{Q} = 2$ (c) $\|e_m\|_V^{rel}$, including $\Delta\mathfrak{h}$

(d) $\|e_m\|_{L^2(\Omega)}^{rel}$ and e_m^{POD} (e) λ_m and $\|\tilde{p}_m^H\|_{L^2(\Omega_{1D})}$ (f) $\|e_m\|_V^{rel}$, solution of (4.10), $\bar{Q} = 1$

Figure 4.9: Test case 3: Comparison of the model error convergence of $\|e_m\|_V^{rel}$, if using the lifting function g_D (4.26) (a), including $\mathfrak{h}$ in the strong form of (4.7) (c) or in the weak form of (4.7) and choosing $\bar{Q} = 2$ in (4.16) (b) or $\bar{Q} = 1$ (f); comparison of $\|e_m\|_{L^2(\Omega)}^{rel}$ and e_m^{POD} for the solution $\tilde{p}_m^H$ of (4.10) with e_m^{POD} if including $\Delta\mathfrak{h}$ in strong form ($+\Delta h$) or using g_D (g_D) (d) and λ_m and $\|\tilde{p}_m^H\|_{L^2(\Omega_{1D})}$ for the solution of (4.10) (e); all computations: $N_{H'} = 10$.

$(-0.5x + 1)\mathfrak{h}(0, y) + 0.5x\mathfrak{h}(2, y)$ as in test case 2 for $m = 5, 10, 15, 20$, $N_H = 800$, $n_h = 400$ and $N_{H'} = 80$ and observe a qualitative convergence behavior very similar to the one in test case 1 (Fig. 4.2, left). Next, we compare the exact solution $\tilde{p}$ with the discrete reduced solution $\tilde{p}_m^H$, which has been computed using the approximating interface

$$\bar{\mathfrak{h}}(x, y) = \begin{cases} 1 & \text{if } y + 0.4x < 0.8, \\ 0.1 & \text{if } y + 0.4x > 0.9, \\ 0.55 + 0.45\cos(10\pi(y + 0.4x - 0.8)) & \text{if } 0.8 \le y + 0.4x \le 0.9 \end{cases} \tag{4.29}$$

for $m = 5, 10, 15, 20$, $N_H = 800$, $n_h = 400$ and $N_{H'} = 80$ (Fig. 4.8, middle). We observe that the bending of the actual interface $\mathfrak{h}$, which is not included in the approximation $\bar{\mathfrak{h}}$, causes oscillations in the interval $[0.9, 1.6] \subset \Omega_{1D}$ yielding a slower approximation behavior of $\tilde{p}_m^H$ than in test case 1 (Fig. 4.2, right). Eventually, 20 basis functions are required to obtain a good approximation of $\tilde{p}$. Overall we still observe a significant improvement of the qualitative convergence behavior if including an approximation of the interface, but, as expected, the gain is not as big as if including the exact interface. If we add $\Delta\bar{\mathfrak{h}}$ in the strong formulation of (4.7) and compute the associated discrete reduced solution for $m = 5, 10, 15$, $N_H = 800$, $n_h = 400$ and $N_{H'} = 80$ (Fig. 4.8, right), we detect only few oscillations and see already for $\tilde{p}_{15}^H$ a good visual agreement with the exact solution $\tilde{p}$.

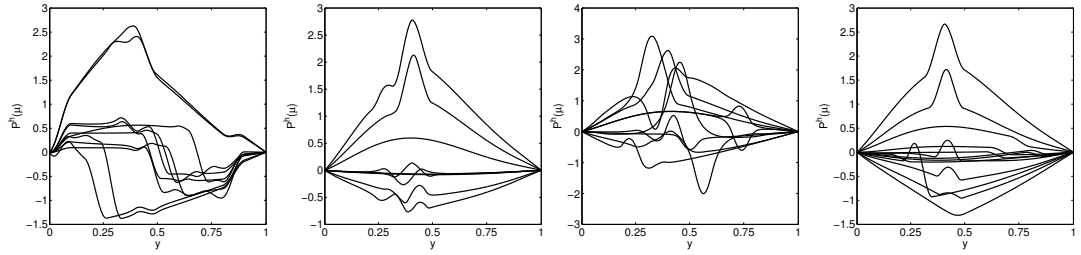

(a) lift. func. g_D (4.26) (b) incl. $\Delta\mathfrak{h}$ (c) (4.16), $\bar{Q} = 2$ (d) (4.16), $\bar{Q} = 1$

Figure 4.10: Test case 3: Typical snapshots of the discrete solution manifold Y_M^h (2.33) if the lifting function g_D (4.26) is used and therefore no information on the interface is included in the model reduction preocedure (a), if $\Delta\mathfrak{h}$ is added in the strong formulation of (4.7) (b), (4.16) is solved with $\bar{Q} = 2$ (c) and $\bar{Q} = 1$ (d).

Analyzing the convergence behavior of the relative model error $\|e_m\|_V^{rel}$, we see in Fig. 4.9b that on the one hand solving (4.10) with the approximating interface $\mathfrak{h}$ enhances the convergence behavior but on the other hand the improvement is much smaller than in the two previous examples. Including $\Delta\mathfrak{h}$ in the strong formulation of (4.7) further improves both the convergence behavior and rate of $\|e_m\|_V^{rel}$ (Fig. 4.9c) and e_m^{POD} (Fig. 4.9d) but not to the same extend as in the test cases 1 and 2. This supports the findings gained for the qualitative convergence behavior. As the convergence rate of e_m^{POD} is better than the one of $\|e_m\|_{L^2(\Omega)}^{rel}$ if we include $\Delta\mathfrak{h}$, the convergence behavior of the model error may perhaps be further improved for instance by increasing the sample size. Finally, we state that the convergence behavior of $\|e_m\|_V^{rel}$ for choosing $\bar{Q} = 1$ in (4.16) is only slightly worse than the one for $\bar{Q} = 2$. This can be explained by the fact that the snapshots of (4.16) for $\bar{Q} = 1$ (Fig. 4.10d) resemble very much both the snapshots of (4.16) for $\bar{Q} = 2$ (Fig. 4.10c) and the snapshots $\mathcal{P}^h(\mu)$ if including $\Delta\mathfrak{h}$ (Fig. 4.10b). Also for this test case the snapshots computed using the lifting function g_D contain hardly any information on the profile of p (Fig. 4.10a), prohibiting a fast convergence to the exact solution.

We conclude the numerical experiments with some remarks on the reconstruction procedure. As computing $\mathcal{R}^{H\times h}$ with (4.23) is as expensive as solving the reference solution, this strategy is not feasible from a computationally viewpoint. We therefore propose to use an ansatz, which has some similarities with an oversampling strategy (see e.g. [1,58,90] and references therein), that is employed in the field of Multiscale Methods. Precisely, when deriving the parametrized dimensionally reduced problem (4.16) for a parameter value $\mu \in \Xi_{train}$, we first solve

$$\int_{B(\mu,R)\times\widehat{\omega}} \mathcal{R}_\mu^{H\times h} v^{H\times h} = a(\nabla\mathfrak{h}, v^{H\times h})_{B(\mu,R)\times\widehat{\omega}}. \tag{4.30}$$

Here, $B(\mu, R)$ denotes the ball of radius R around μ. $\mathcal{R}_\mu^{H\times h}(\mu,\cdot)$ can then be added to the source term in the parametrized dimensionally reduced problem (4.16). Studying such type of reconstructions is a task for future research.

Chapter 5

Conclusion and Perspectives

Conclusion

In this thesis we have introduced a dimensional reduction approach which uses a highly nonlinear approximation based on Reduced Basis (RB) methods to determine the reduction space Y_m in the Hierarchical Model Reduction (HMR) framework. Starting from the full problem, initially a parametrized lower dimensional problem in the transverse direction has been derived. Here, the parametrization enabled us to include the unknown behavior of the full solution in the dominant direction in Y_m. The generation of snapshots is based on a reliable and efficient a posteriori error estimator combined with an adaptive training set extension. Finally, a proper orthogonal decomposition (POD) is applied to the set of snapshots to select the principal components, which form the reduction space Y_m. Numerical experiments show a fast convergence of the Hierarchical Model Reduction-Reduced Basis (HMR-RB) approximation to the full solution and demonstrate the computational efficiency of the proposed method.

To approach the long-term goal of our ongoing research, namely the treatment of saturated-unsaturated subsurface flow, modeled by Richards' equation, we first introduced the HMR-RB approach for linear partial differential equations (PDEs) and subsequently adapted the concept to nonlinear PDEs. Finally, we addressed the approximation of a skewed water table.
In the linear setting the numerical experiments demonstrate that the set of solution snapshots and the reference solution are approximated by the reduction space Y_m with the same accuracy for the purely diffusive problems. For problems with a dominant advective term a comparable approximation rate can be achieved by using quadrature rules of higher accuracy when deriving the parametrized problem. Thus, we conclude that the proposed ansatz for the derivation of the parametrized 1D problems is able to transfer the essential transverse features of the solution to the solution manifold. Furthermore, numerical experiments demonstrate that the new approach converges exponentially fast with respect to the model order m for problems with smooth solutions as well as for a test case where the source term is only continuous. Even for a test case where the source term does not allow a tensor product decomposition and only a polynomial convergence rate in m is achieved, very few basis functions suffice to balance the model and the discretization errors. Our new approach shows faster convergence with respect to the model order than the classical HMR ansatz using trigonometric polynomials in all test cases. An analysis of the computational costs shows that the HMR-RB approach scales linearly in the number of degrees of freedom used for the computations in the dominant direction, whereas the corresponding finite element reference approximation exhibits at best a quadratic scaling. Finally, we demonstrated that the new approach

is indeed particularly beneficial for problems that exhibit a main stream and hence a dominant spatial direction.
To conduct a dimensional reduction also for nonlinear PDEs we expanded the nonlinear operator in a orthonormal (collateral) basis in the transverse direction. Also for the construction of the collateral basis space W_k we used a highly nonlinear approximation. A manifold of parametrized lower dimensional operator evaluations has been generated by using the solutions of the parametrized dimensionally reduced problem and the corresponding parametrization. In this way we included information on the evaluation of the nonlinear operator in the unknown full solution in the dominant direction in W_k. Operator and solution snapshot sets have been simultaneously generated with an adaptive training set extension, and by applying a POD to the former the collateral basis space is constructed. The coefficients of the operator approximation have been computed with the newly introduced Empirical Projection Method (EPM), which is an adaptive integration algorithm based on the Empirical Interpolation Method [12]. While for the basis selection with the greedy algorithm and the POD several convergence results are already proven, to the best of our knowledge no result that could have been employed, has been proven until now for the approximation of a nonlinear operator. This gap has been closed by the introduction of the Empirical Projection Method and the proven rigorous a priori and a posteriori error bounds. We used these bounds to derive a rigourous and effective error estimator based on the Brezzi-Rappaz-Raviart theory, which is employed for the construction of the snapshot sets. Here, we extended the results on the effectivity of the error estimator in [27] from quadratically nonlinear PDEs to general nonlinear PDEs. The numerical experiments for the nonlinear diffusion equation show that the reference solution and the set of solution snapshots are approximated by the reduction space Y_m with the same approximation quality. Here, a quadrature formula of higher accuracy had to be employed for a test case with a non-smooth solution. The evaluation of the nonlinear operator in the reference solution and the set of operator snapshots are approximated by the collateral basis space W_k with the same spproximation accuracy for a problem with an analytic solution and a comparable quality for a problem with a non-smooth solution. Hence, we conclude that by employing the suggested ansatz for the generation of the solution and the operator manifold we are able to transfer the relevant transverse dynamics of the reference solution and the operator evaluation to the respective manifolds. Furthermore, the numerical experiments demonstrate an exponential convergence behavior of the HMR-RB approach both for a problem with an analytical solution and a test case with a non-smooth solution also for small ellipticity constants. The applicability of the theoretical results including the bounds for the EPM is demonstrated, too. Run-time experiments show a linear scaling of the HMR-RB approach in the number of degrees of freedom used for the computations in the dominant direction, while the respective finite element reference approximation scales quadratically. This demonstrates the computational efficiency of the proposed method also in the nonlinear setting.
Finally, we have suggested a new ansatz for the approximation of a possibly skewed water table and similar interfaces with tensor-based model reduction approaches. First, we compute the height of the water table by solving the dimensionally reduced problem which is derived by employing the Dupuit assumption. By choosing the obtained saturation profile as the lifting function of the Dirichlet boundary conditions, we remove the part of the full solution which can be badly approximated by a tensor-based model reduction approach, and thus prevents a fast convergence of the latter. For other applications one can proceed in the same manner, if a dimensionally reduced problem which locates the interface can be derived. Exemplifying the proposed ansatz for the HMR-RB approach we derived a coupled parametrized lower dimensional problem starting from the reference finite element approximation, where the parameter vector coincides with the quadrature points. We solve for the unknown parts of the solution in the dominant direction via the coupling. For prescribed interfaces the numerical experiments demonstrate that the convergence behavior improves considerably also if we can locate the interface only approximately. The validation of the

proposed derivation of the parametrized coupled 1D problem shows that the 1D problems do not reproduce properly the equivalence of including the interface in the strong or the weak formulation of the PDE. Here, we have obtained a worse approximation behavior for the inclusion in the weak form. A possible ansatz to solve this problem is to use a reconstruction of the derivative of the interface in the dominant direction which mimics its behavior in two space dimensions. Using the Riesz representative of the lifting function is one example for such a reconstruction. The numerical experiments demonstrated that by employing this reconstruction the features of the full solution apart the interface can be approximated exponentially fast if these features allow for such a rate. Finally, the numerical tests show that the features of the full solution apart the water table (interface) are approximated very slowly if no information on the interface is included. We therefore expect the proposed ansatz to be also beneficial when applied within the context of subsurface flow.

Perspectives

The dimensional reduction approach introduced in this thesis and its generalization to nonlinear PDEs offers several starting points for future research. Having the application of the HMR-RB approach to the Richards equation in mind, we plan to extend our proposed method to time-dependent problems. Here, existing methodologies from the field of RB methods (see e.g. [63] and references therein) can be used. Another issue is the treatment of degenerate equations, including the derivation of reliable a posteriori error bounds. The study of the behavior of the HMR-RB approach for decreasing ellipticity constants in Section 3.6 can be seen as a first step in that direction. As the considered computational domains in applications within the field of subsurface flow typically have a great horizontal extension, we plan to derive a local HMR-RB approach by integrating our proposed method in the domain decomposition framework introduced in [102]. Here, considering different sets of basis functions in different parts of the domain will hopefully allow us to efficiently deal also with large computational domains. Finally, proving convergence of the proposed method and deriving convergence rates is another task for future investigation. Here, the techniques employed for the proof of the a priori bound of the Empirical Projection Method give a hint how to proceed.

Appendices

Appendix A

Appendix to Chapter 1

A.1 Exemplification of the HMR-RB approach for an advection-diffusion-reaction problem on a domain with a curved boundary

We consider an advection-diffusion-reaction problem. Let $\Omega \subset \mathbb{R}^2$ be the computational domain with Lipschitz boundary $\partial\Omega$ and outer normal ν. Let Σ_R, $\Sigma_D \subset \partial\Omega$ be two relatively open, pairwise disjoint one-dimensional Lipschitz manifolds, such that $\partial\Omega = \Sigma_R \cup \Sigma_D$. Here Σ_R is the Robin and Σ_D is the Dirichlet boundary. We assume for the sake of simplicity $\mathcal{H}^1(\Sigma_D) > 0$, where $\mathcal{H}^1(\Sigma_D)$ denotes the one-dimensional Hausdorff-measure of Σ_D. Furthermore we assume homogeneous Dirichlet boundary conditions and refer to Chapter 4 for the treatment of non-homogeneous Dirichlet boundary conditions. We consider the following problem for $p : \Omega \to \mathbb{R}$

$$\begin{aligned} -\nabla \cdot (k \nabla p - \mathbf{b}\, p) + dp &= s && \text{in } \Omega, \\ p &= 0 && \text{on } \Sigma_D, \\ -(k \nabla p - \mathbf{b}\, p) \cdot \nu &= g_R(p) && \text{on } \Sigma_R. \end{aligned} \tag{A.1}$$

To guarantee well-posedness of the problem in the weak form (see below), we assume $k \in L^\infty(\Omega)$ with $0 < c_0 \leq k \leq c_1$ for constants $c_0, c_1 \in \mathbb{R}^+$, $\mathbf{b} \in [W^{1,\infty}(\Omega)]^2$, $d \in L^\infty(\Omega)$, $s \in L^2(\Omega)$ and $d + 1/2\nabla \cdot \mathbf{b} \geq 0$ and $\mathbf{b} \cdot \nu \leq 0$ on Σ_R. The Robin boundary conditions are assumed to be affine in p, i.e.

$$g_R(p) = g_{R,1}\, p - g_{R,2}$$

where $g_{R,1} \in L^\infty(\Sigma_R)$ and $g_{R,2} \in L^2(\Sigma_R)$. Let furthermore be $V = \{v \in H^1(\Omega) \mid v = 0 \text{ on } \Sigma_D\}$. Then we define for $v, w \in V$ the bilinear form

$$a(w, v) := \int_\Omega k \nabla w \nabla v - \int_\Omega \mathbf{b}\, w \nabla v + \int_\Omega d\, w\, v + \int_{\Sigma_R} g_{R,1}\, w\, v, \tag{A.2}$$

and the linear form

$$f(v) := \int_\Omega s\, v + \int_{\Sigma_R} g_{R,2}\, v. \tag{A.3}$$

Thus the corresponding weak formulation of (A.1) reads:

$$\text{Find } p \in V \text{ such that } a(p, v) = f(v) \quad \forall\, v \in V. \tag{A.4}$$

A.1.1 Formulation of the reduced problem in the Hierarchical Model Reduction framework

The reduced problem reads: Find $p_m \in V_m$ such that for all $v_m \in V_m$ there holds

$$\int_\Omega k\,\nabla p_m\,\nabla v_m - \int_\Omega \mathbf{b}\,p_m\,\nabla v_m + \int_\Omega d\,p_m\,v_m + \int_{\Sigma_R} g_{R,1}\,p_m\,v_m = \int_\Omega s\,v_m + \int_{\Sigma_R} g_{R,2}\,v_m.$$

We rewrite p_m as $p_m(x,y) = \sum_{l=1}^m \overline{p}_l(x)\,\phi_l(\psi_x(y))$ and choose the test functions $v_k(x,y) = \xi(x)\,\phi_k(\psi_x(y))$, $k = 1, ..., m$, for an arbitrary $\xi(x) \in X$. Then we use the gradient expansion

$$\nabla\left(\xi(x)\phi_k(\psi(y;x))\right) = \phi_k(\psi(y;x))\begin{pmatrix}\frac{d\xi(x)}{dx}\\ 0\end{pmatrix} + \xi(x)\phi_k'(\psi(y;x))\begin{pmatrix}\mathcal{D}_1(z)\\ \mathcal{D}_2(z)\end{pmatrix}$$

for $k = 1, ..., m$, and $\xi \in X$, where $\phi_k'(\psi(y;x))$ means $d\phi_k(\psi(y;x))/d\hat{y}$ at the point $\psi(y;x)$. After transforming Ω into $\widehat{\Omega}$ via Ψ, we get the following problem for the coefficient functions:

$$\sum_{l=1}^m \int_{\Omega_{1D}} A_{lk}(x)\frac{d\overline{p}_l(x)}{dx}\frac{d\xi(x)}{dx} + B_{1,lk}(x)\frac{d\overline{p}_l(x)}{dx}\xi(x) + B_{2,lk}(x)\overline{p}_l(x)\frac{d\xi(x)}{dx} + D_{lk}(x)\overline{p}_l(x)\xi(x)dx$$
$$+ G_{lk}(x_0)\,p_l(x_0)\xi(x_0) = \int_{\Omega_{1D}} F_k(x)\,\xi(x) + G_k(x_0), \tag{A.5}$$

with

$$\begin{aligned}
A_{lk}(x) &= \int_{\hat{\gamma}} k(x,\psi^{-1}(\hat{y};x))\phi_l(\hat{y})\phi_k(\hat{y})|\mathcal{D}_2^{-1}(x,\psi^{-1}(\hat{y};x))|\,d\hat{y},\\
B_{1,lk}(x) &= \int_{\hat{\gamma}} k(x,\psi^{-1}(\hat{y};x))\phi_l(\hat{y})\phi_k'(\hat{y})\,\mathcal{D}_1(x,\psi^{-1}(\hat{y};x))|\mathcal{D}_2^{-1}(x,\psi^{-1}(\hat{y};x))|\,d\hat{y},\\
B_{2,lk}(x) &= \int_{\hat{\gamma}} \Big[k(x,\psi^{-1}(\hat{y};x))\phi_l'(\hat{y})\phi_k(\hat{y})\,\mathcal{D}_1(x,\psi^{-1}(\hat{y};x))\\
&\qquad -b_1(x,\psi^{-1}(\hat{y};x))\phi_l(\hat{y})\phi_k(\hat{y})\Big]|\mathcal{D}_2^{-1}(x,\psi^{-1}(\hat{y};x))|\,d\hat{y},\\
D_{lk}(x) &= \int_{\hat{\gamma}} \Big[k(x,\psi^{-1}(\hat{y};x))\phi_l'(\hat{y})\phi_k'(\hat{y})\left\{\left[\mathcal{D}_1(x,\psi^{-1}(\hat{y};x))\right]^2 + \left[\mathcal{D}_2(x,\psi^{-1}(\hat{y};x))\right]^2\right\}\\
&\qquad -\mathbf{b}(x,\psi^{-1}(\hat{y};x))\phi_l(\hat{y})\phi_k'(\hat{y})\cdot\begin{pmatrix}\mathcal{D}_1(x,\psi^{-1}(\hat{y};x))\\ \mathcal{D}_2(x,\psi^{-1}(\hat{y};x))\end{pmatrix}\\
&\qquad +d(x,\psi^{-1}(\hat{y};x))\phi_l(\hat{y})\phi_k(\hat{y})\Big]|\mathcal{D}_2^{-1}(x,\psi^{-1}(\hat{y};x))|\,d\hat{y}\\
&\qquad +g_{R,1}(x,\psi_x^{-1}(y_0))\phi_l(y_0)\phi_k(y_0)|\mathcal{D}_2^{-1}(x,\psi_x^{-1}(y_0))|,\\
G_{lk}(x_0) &= \int_{\hat{\gamma}} g_{R,1}(x_0,\psi_{x_0}^{-1}(\hat{y}))\phi_l(\hat{y})\phi_k(\hat{y})|\mathcal{D}_2^{-1}(x_0,\psi_{x_0}^{-1}(\hat{y}))|\,d\hat{y},\\
F_k(x) &= \int_{\hat{\gamma}} \Big[s(x,\psi^{-1}(\hat{y};x))\,\phi_k(\hat{y})\Big]|\mathcal{D}_2^{-1}(x,\psi^{-1}(\hat{y};x))|\,d\hat{y}\\
&\qquad +g_{R,2}(x,\psi_x^{-1}(y_0))\phi_k(y_0)|\mathcal{D}_2^{-1}(x,\psi_x^{-1}(y_0))|,\\
G_k(x_0) &= \int_{\hat{\gamma}} g_{R,2}(x_0,\psi_{x_0}^{-1}(\hat{y}))\phi_k(\hat{y})|\mathcal{D}_2^{-1}(x_0,\psi_{x_0}^{-1}(\hat{y}))|\,d\hat{y}.
\end{aligned}$$

We emphasize that due to the transformation Ψ the coupled system (A.5) contains additional advective and reactive terms.

A.1.2 Derivation of the parameter dependent one-dimensional problem in the HMR-RB approach

We assume that

$$p(x,\hat{y}) \approx U(x)\cdot\mathcal{P}(\hat{y}), \tag{A.6}$$

for an unknown function $U(x)$. Inserting (A.6) into (A.4) and applying the quadrature formula defined in (2.26), yields the reduced problem with quadrature: Given any $U\in X$, find $\mathcal{P}\in Y$ such that:

$$\int_{\hat{\gamma}} A(\hat{y})\,\partial_{\hat{y}}\,\mathcal{P}(\hat{y})\,\partial_{\hat{y}}\,v(\hat{y}) + B_1(\hat{y})\,\partial_{\hat{y}}\,\mathcal{P}(\hat{y})\,v(\hat{y}) + B_2(\hat{y})\,\mathcal{P}(\hat{y})\,\partial_{\hat{y}}\,v(\hat{y}) + D(\hat{y})\,\mathcal{P}(\hat{y})\,v(\hat{y})\,d\hat{y}$$
$$+ G_1(y_0)\mathcal{P}(y_0)v(y_0) = \int_{\hat{\gamma}} F(\hat{y})\,v(\hat{y})\,d\hat{y} + G_2(y_0)\,v(y_0),$$

where

$$A(\hat{y}) = \sum_{l=1}^{Q}\alpha_l\,k(x_l^q,\psi^{-1}(\hat{y};x_l^q))\,(U(x_l^q))^2\,[\mathcal{D}_1^2(x_l^q,\psi^{-1}(\hat{y};x_l^q))$$
$$+\mathcal{D}_2^2(x_l^q,\psi^{-1}(\hat{y};x_l^q))]\,|\mathcal{D}_2^{-1}(x_l^q,\psi^{-1}(\hat{y};x_l^q))|,$$

$$B_1(\hat{y}) = \sum_{l=1}^{Q}\alpha_l\,k(x_l^q,\psi^{-1}(\hat{y};x_l^q))\,\partial_x U(x_l^q)\,U(x_l^q)\,\mathcal{D}_1(x_l^q,\psi^{-1}(\hat{y};x_l^q))\,|\mathcal{D}_2^{-1}(x_l^q,\psi^{-1}(\hat{y};x_l^q))|$$

$$B_2(\hat{y}) = \sum_{l=1}^{Q}\alpha_l\,k(x_l^q,\psi^{-1}(\hat{y};x_l^q))\,\partial_x U(x_l^q)\,U(x_l^q)\,\mathcal{D}_1(x_l^q,\psi^{-1}(\hat{y};x_l^q))$$
$$-\mathbf{b}(x_l^q,\psi^{-1}(\hat{y};x_l^q))\,(U(x_l^q))^2\cdot\begin{pmatrix}\mathcal{D}_1(x_l^q,\psi^{-1}(\hat{y};x_l^q))\\ \mathcal{D}_2(x_l^q,\psi^{-1}(\hat{y};x_l^q))\end{pmatrix}\,|\mathcal{D}_2^{-1}(x_l^q,\psi^{-1}(\hat{y};x_l^q))|$$

$$D(\hat{y}) = \sum_{l=1}^{Q}\alpha_l\,\Big\{\Big[k(x_l^q,\psi^{-1}(\hat{y};x_l^q))(\partial_x U(x_l^q))^2 - b_1(x_l^q,\psi^{-1}(\hat{y};x_l^q))\,\partial_x U(x_l^q)\,U(x_l^q)$$
$$+d(x_l^q,\psi^{-1}(\hat{y};x_l^q))(U(x_l^q))^2\Big]\cdot|\mathcal{D}_2^{-1}(x_l^q,\psi^{-1}(\hat{y};x_l^q))|\Big\}$$
$$+g_{R,1}(x_0,\psi^{-1}(\hat{y};x_0))\,(U(x_0))^2\,|\mathcal{D}_2^{-1}(x_0,\psi^{-1}(\hat{y};x_0))|,$$

$$G_1(y_0) = \sum_{l=1}^{Q}\alpha_l g_{R,1}(x_l^q,\psi^{-1}(y_0;x_l^q))\,(U(x_l^q))^2\,|\mathcal{D}_2^{-1}(x_l^q,\psi^{-1}(y_0;x_l^q))|,$$

$$F(\hat{y}) = \sum_{l=1}^{Q}\alpha_l\,\Big\{s(x_l^q,\psi^{-1}(\hat{y};x_l^q))\,U(x_l^q)|\mathcal{D}_2^{-1}(x_l^q,\psi^{-1}(\hat{y};x_l^q))|\Big\}$$
$$+g_{R,2}(x_0,\psi^{-1}(\hat{y};x_0))\,U(x_0)\,|\mathcal{D}_2^{-1}(x_0,\psi^{-1}(\hat{y};x_0))|,$$

$$G_2(y_0) = \sum_{l=1}^{Q}\alpha_l g_{R,2}(x_l^q,\psi^{-1}(y_0;x_l^q))\,U(x_l^q)\,|\mathcal{D}_2^{-1}(x_l^q,\psi^{-1}(y_0;x_l^q))|.$$

Note that also for the 1D problem the advection and reaction is reinforced due to the transformation Ψ. Assuming that $x_0, x_1 \notin \{x_l^q\}_{l=1}^Q$ the parameter μ and the parameter space $\mathcal{D}$ read as $\mu = (x_l^q, U(x_l^q), \partial_x U(x_l^q), U(x_0))$, $l = 1,...,Q$, and $\mathcal{D} := [\Omega_{1D}\times I_0\times I_1]^Q\times I_0$. We shorten notations by setting $\mu = ([\mu_{l,1},\mu_{l,2},\mu_{l,3}]_{l=1}^Q,\mu_b)$ where $\mu_{l,1}$ replaces x_l^q, $\mu_{l,2}$ replaces $U(x_l^q)$, $\mu_{l,3}$ replaces $\partial_x U(x_l^q)$

and μ_b stands for $U(x_0)$. We obtain the parametrized 1D PDE in transverse direction:

$$\int_{\hat{\gamma}} A(\hat{y})\,\partial_{\hat{y}}\,\mathcal{P}(\hat{y})\,\partial_{\hat{y}}\,v(\hat{y}) + B_1(\hat{y})\,\partial_{\hat{y}}\,\mathcal{P}(\hat{y})\,v(\hat{y}) + B_2(\hat{y})\,\mathcal{P}(\hat{y})\,\partial_{\hat{y}}\,v(\hat{y}) + D(\hat{y})\,\mathcal{P}(\hat{y})\,v(\hat{y})\,d\hat{y}$$
$$+ G_1(y_0)\mathcal{P}(y_0)v(y_0) = \int_{\hat{\gamma}} F(\hat{y})\,v(\hat{y})\,d\hat{y} + G_2(y_0)\,v(y_0),$$

where

$$\begin{aligned}
A(\hat{y}) &= \sum_{l=1}^{Q} \alpha_l\, k(\mu_{l,1}, \psi^{-1}(\hat{y};\mu_{l,1}))\,\mu_{l,2}^2\,[\mathcal{D}_1^2(\mu_{l,1}, \psi^{-1}(\hat{y};\mu_{l,1}))\\
&\qquad + \mathcal{D}_2^2(\mu_{l,1}, \psi^{-1}(\hat{y};\mu_{l,1}))]\,|\mathcal{D}_2^{-1}(\mu_{l,1}, \psi^{-1}(\hat{y};\mu_{l,1}))|,\\
B_1(\hat{y}) &= \sum_{l=1}^{Q} \alpha_l\, k(\mu_{l,1}, \psi^{-1}(\hat{y};\mu_{l,1}))\,\mu_{l,3}\,\mu_{l,2}\,\mathcal{D}_1(\mu_{l,1}, \psi^{-1}(\hat{y};\mu_{l,1}))\,|\mathcal{D}_2^{-1}(\mu_{l,1}, \psi^{-1}(\hat{y};\mu_{l,1}))|\\
B_2(\hat{y}) &= \sum_{l=1}^{Q} \alpha_l\, k(\mu_{l,1}, \psi^{-1}(\hat{y};\mu_{l,1}))\,\mu_{l,3}\,\mu_{l,2}\,\mathcal{D}_1(\mu_{l,1}, \psi^{-1}(\hat{y};\mu_{l,1}))\\
&\qquad - \mathbf{b}(\mu_{l,1}, \psi^{-1}(\hat{y};\mu_{l,1}))\,\mu_{l,2}^2 \cdot \begin{pmatrix}\mathcal{D}_1(\mu_{l,1}, \psi^{-1}(\hat{y};\mu_{l,1}))\\ \mathcal{D}_2(\mu_{l,1}, \psi^{-1}(\hat{y};\mu_{l,1}))\end{pmatrix}\,|\mathcal{D}_2^{-1}(\mu_{l,1}, \psi^{-1}(\hat{y};\mu_{l,1}))|\\
D(\hat{y}) &= \sum_{l=1}^{Q} \alpha_l \Big\{ \Big[k(\mu_{l,1}, \psi^{-1}(\hat{y};\mu_{l,1}))\mu_{l,3}^2 - b_1(\mu_{l,1}, \psi^{-1}(\hat{y};\mu_{l,1}))\,\mu_{l,3}\,\mu_{l,2}\\
&\qquad + d(\mu_{l,1}, \psi^{-1}(\hat{y};\mu_{l,1}))\mu_{l,2}^2\Big] \cdot |\mathcal{D}_2^{-1}(\mu_{l,1}, \psi^{-1}(\hat{y};\mu_{l,1}))|\Big\}\\
&\qquad + g_{R,1}(x_0, \psi^{-1}(\hat{y};x_0))\,\mu_b^2\,|\mathcal{D}_2^{-1}(x_0, \psi^{-1}(\hat{y};x_0))|,\\
G_1(y_0) &= \sum_{l=1}^{Q} \alpha_l g_{R,1}(\mu_{l,1}, \psi^{-1}(y_0;\mu_{l,1}))\,\mu_{l,2}^2\,|\mathcal{D}_2^{-1}(\mu_{l,1}, \psi^{-1}(y_0;\mu_{l,1}))|,\\
F(\hat{y}) &= \sum_{l=1}^{Q} \alpha_l \Big\{ s(\mu_{l,1}, \psi^{-1}(\hat{y};\mu_{l,1}))\,\mu_{l,2}|\mathcal{D}_2^{-1}(\mu_{l,1}, \psi^{-1}(\hat{y};\mu_{l,1}))|\Big\}\\
&\qquad + g_{R,2}(x_0, \psi^{-1}(\hat{y};x_0))\,\mu_b\,|\mathcal{D}_2^{-1}(x_0, \psi^{-1}(\hat{y};x_0))|,\\
G_2(y_0) &= \sum_{l=1}^{Q} \alpha_l g_{R,2}(\mu_{l,1}, \psi^{-1}(y_0;\mu_{l,1}))\,\mu_{l,2}\,|\mathcal{D}_2^{-1}(\mu_{l,1}, \psi^{-1}(y_0;\mu_{l,1}))|.
\end{aligned}$$

A.2 Alternative proof of Proposition 2.6

In this section we present an alternative proof of Proposition 2.6 yielding slightly different constants in the estimate (2.51). Due to $\|p - p_m^H\|_V = \|p_0 - p_0^{mH}\|_V$ it is sufficient to derive an estimate for the latter. We set $W = (L^2(\Omega))^2$ and denote by V^* and W^* the dual spaces of V and W. The corresponding dual pairings are designated $\langle\,.\,,\,.\,\rangle_V$ and $\langle\,.\,,\,.\,\rangle_W$ and we identify W^* with W. We denote the conjugate of a functional $\mathfrak{L} \in V^*$ or W^* as $\mathfrak{L}^*$ and recall its definition $\mathfrak{L}^*(v^*) := \sup_{v\in V}\{\langle v^*, v\rangle_V - \mathfrak{L}(v)\}$ for $\mathfrak{L} \in V^*$ (cf. [47]). Next we define the primal and the corresponding dual problem (cf. [47]).

Definition A.1 (Primal problem $\mathfrak{P}$)**.** *Find $p_0 \in V$ such that*

$$\mathfrak{J}(p_0, \nabla p_0) = \inf_{v \in V} \mathfrak{J}(v, \nabla v), \tag{A.7}$$

where

$$\begin{aligned} \mathfrak{J}(v, \nabla v) &:= \mathfrak{F}(v) + \mathfrak{G}(\nabla v), \quad \textit{with} \\ \mathfrak{F}(v) &:= \begin{cases} -\int_\Omega s\, v \;\, dx\, dy - \int_{\Sigma_N} g_N\, v \;\, dx\, dy & \textit{if } v \in V, \\ +\infty & \textit{otherwise}, \end{cases} \\ \textit{and} \qquad \mathfrak{G}(\nabla v) &:= \frac{1}{2}\int_\Omega k\, |\, \nabla v\, |^2 \, dx\, dy + \int_\Omega k\, \nabla g_D\, \nabla v \;\, dx\, dy. \end{aligned} \tag{A.8}$$

Definition A.2 (Dual problem $\mathfrak{P}^*$)**.** *Find $q^* \in W^*$ such that*

$$-\mathfrak{J}^*(-\operatorname{div} q^*, -q^*) = \sup_{y^* \in W^*} -\mathfrak{J}^*(-\operatorname{div} y^*, -y^*), \tag{A.9}$$

where

$$\mathfrak{J}^*(-\operatorname{div} y^*, -y^*) = \mathfrak{F}^*(-\operatorname{div} y^*) + \mathfrak{G}^*(-y^*), \quad \textit{with} \tag{A.10}$$

$$\mathfrak{F}^*(-\operatorname{div} y^*) = \begin{cases} 0 & \textit{if } y^* \in \mathfrak{Q}_c^*, \\ +\infty & \textit{otherwise}, \end{cases} \tag{A.11}$$

$$\mathfrak{G}^*(-y^*) = \int_\Omega \frac{1}{2} k^{-1} |\, y^*\, |^2 + \nabla g_D \cdot y^* + \frac{1}{2} k\, \nabla g_D \cdot \nabla g_D \, dx\, dy, \tag{A.12}$$

and $\mathfrak{Q}_c^* := \left\{ y^* \in W^* \,:\, \int_\Omega \nabla v \cdot y^* + f v \, dx\, dy + \int_{\Sigma_N} g_N v \, dx\, dy = 0 \quad \forall v \in V \right\}$.

The following existence theorem is well known in the context of duality theory.

Theorem A.3. *Let the functionals $\mathfrak{J}(v, \nabla v), \mathfrak{F}(v)$ and $\mathfrak{G}(v)$ be given as in (A.8). Then there exists a minimizer p_0 to the primal Problem $\mathfrak{P}$ and a maximizer q^* to the dual problem $\mathfrak{P}^*$. Futhermore there holds*

$$\mathfrak{J}(p_0, \nabla p_0) = -\mathfrak{J}^*(-\operatorname{div} q^*, -q^*) \tag{A.13}$$

and

$$(i)\;\; \mathfrak{F}(p_0) + \mathfrak{F}^*(-\operatorname{div} q^*) - \langle -\operatorname{div} q^*, p_0 \rangle_V = 0, \;\; \textit{and} \;\; (ii)\;\; \mathfrak{G}(\nabla p_0) + \mathfrak{G}^*(-q^*) + \langle q^*, \nabla p_0 \rangle_W = 0. \tag{A.14}$$

Proof. See for instance [47, 109]. □

For an arbitrary function in $v \in V$ we define $\mathfrak{e} := p_0 - v$ and the function $\mathfrak{g} : \mathbb{R}^2 \to \mathbb{R}$, $\mathfrak{g}(\nabla v) = \frac{1}{2}\, k\, |\nabla v|^2 + \nabla g_D \nabla v$. It is easy to prove that

$$\frac{1}{2}\, \|\mathfrak{e}\|_V^2 \le \mathfrak{J}(v, \nabla v) - \mathfrak{J}(p_0, \nabla p_0) \quad \forall v \in V, \tag{A.15}$$

that $\mathfrak{G}^*$ is Gâteaux differentiable, and that it fulfills the following estimates

$$\|\mathfrak{G}^{*\prime}(y^*) - \mathfrak{G}^{*\prime}(z^*)\|_W \le \frac{1}{c_3} \|y^* - z^*\|_W, \tag{A.16}$$

$$\langle y^* - z^*, \mathfrak{G}^{*\prime}(y^*) - \mathfrak{G}^{*\prime}(z^*) \rangle_W \le \frac{1}{c_3} \|y^* - z^*\|_W^2. \tag{A.17}$$

Therefore we can apply the theory developed in [109] and obtain the following result.

Proposition A.4. *Let the functionals $\mathfrak{J}(v, \nabla v), \mathfrak{F}(v)$ and $\mathfrak{G}(v)$ be given as in (A.8). Then there holds the following estimate*

$$\frac{1}{4}\|\mathfrak{e}\|_V^2 \leq M_D(y^*, \nabla v) + M_R(y^*) \qquad \forall y^* \in W^*, \tag{A.18}$$

where

$$M_D(y^*, \nabla v) = \frac{1}{2}\left[\int_\Omega \left(\mathfrak{g}(\nabla v) + \mathfrak{g}^*(-y^*) + y^* \cdot \nabla v\right) dx\, dy + \frac{c_3}{4}\int_\Omega \left(\mathfrak{g}^{*\prime}(-y^*) - \nabla v\right)^2 dx\, dy\right], \tag{A.19}$$

$$M_R(y^*) = \frac{c_p^2}{c_3}\|r(y^*)\|_{V^*}^2, \tag{A.20}$$

and

$$\|r(y^*)\|_{V^*} := \sup_{\substack{w \in V \\ w \neq 0}} \frac{\left|\int_\Omega sw + y^* \nabla w\, dx\, dy + \int_{\Sigma_N} g_N w\, dx\, dy\right|}{\|\nabla w\|_{L^2(\Omega)}}. \tag{A.21}$$

c_p is the constant in the Poincaré inequality.

Proof. See [109]. □

The first term $M_D(y^*, \nabla v)$ is equal to zero if and only if

$$\nabla v = \mathfrak{g}^{*\prime}(-y^*), \tag{A.22}$$

which is equivalent to

$$y^* = -\mathfrak{g}'(\nabla v). \tag{A.23}$$

Choosing $v = p_0^{mH}$ and $y^* = -\mathfrak{g}'(\nabla p_0^{mH}) = -k\,\nabla p_0^{mH} - k\nabla g_D$ completes the proof of the following proposition, which is the analogue of Proposition 2.6.

Proposition A.5. *Let $p \in V$ be the solution of the full problem (2.1) and $p_m^H \in V_m^H$ the solution of the discrete reduced problem (2.12). Then we have*

$$\|p - p_m^H\|_V \leq \frac{2c_p}{\sqrt{c_3}} \sup_{\substack{w \in V \\ w \neq 0}} \frac{\left|\int_\Omega sw - k\nabla p_m^H \nabla w + \int_{\Sigma_N} g_N w\right|}{\|\nabla w\|_{L^2(\Omega)}}, \tag{A.24}$$

where c_p is the Poincaré constant and c_3 the coercivity constant of the diffusion coefficient k.

A.3 Definition of the source term s of test case 2

The source term s used in test case 2 and depicted in Fig. 2.4 is defined as follows.

$$s(x, y) := 1.5e^{-5x} \cdot \sin(\pi y) + \sum_{i=1}^{5} s_{x,i}(x) \cdot s_{y,i}(y) \tag{A.25}$$

with

$$s_{x,1}(x) := \begin{cases} -800x^2 + 120x - 2.5 & \text{for } 0.025 \le x \le 0.125, \\ -800x^2 + 1000x - 310.5 & \text{for } 0.575 \le x \le 0.675, \\ 0 & \text{else,} \end{cases}$$

$$s_{x,2}(x) := \begin{cases} -400x^2 + 140x - 11.25 & \text{for } 0.125 \le x \le 0.225, \\ -800x^2 + 1160x - 418.5 & \text{for } 0.675 \le x \le 0.775, \\ 0 & \text{else,} \end{cases}$$

$$s_{x,3}(x) := \begin{cases} -560x^2 + 308x - 40.95 & \text{for } 0.225 \le x \le 0.325, \\ -800x^2 + 1320x - 542.5 & \text{for } 0.775 \le x \le 0.875, \\ 0 & \text{else,} \end{cases}$$

$$s_{x,4}(x) := \begin{cases} -400x^2 + 300x - 55.25 & \text{for } 0.325 \le x \le 0.425, \\ -800x^2 + 1480x - 682.5 & \text{for } 0.875 \le x \le 0.975, \\ 0 & \text{else,} \end{cases}$$

$$s_{x,5}(x) := \begin{cases} -800x^2 + 760x - 178.5 & \text{for } 0.425 \le x \le 0.525, \\ -800x^2 + 1640x - 838.5 & \text{for } 0.975 \le x \le 1.075, \\ 0 & \text{else,} \end{cases}$$

$$s_{y,1}(y) := -100y^2 + 30y - 1.25 \quad \text{for } 0.05 \le y \le 0.25,$$

$$s_{y,2}(y) := -200y^2 + 280y - 96 \quad \text{for } 0.6 \le y \le 0.8,$$

$$s_{y,3}(y) := \begin{cases} -140y^2 + 70y - 7.35 & \\ \quad \text{for } 0.15 \le y \le 0.35, & \\ -140y^2 + 238y - 99.75 & \\ \quad \text{for } 0.75 \le y \le 0.95, & \\ 0 \text{ else,} & \end{cases}$$

$$s_{y,4}(y) := \begin{cases} -200y^2 + 180y - 38.5 & \\ \quad \text{for } 0.35 \le y \le 0.55, & \\ -100y^2 + 130y - 41.25 & \\ \quad \text{for } 0.55 \le y \le 0.75, & \\ 0 \text{ else,} & \end{cases}$$

$$s_{y,5}(y) := -100y^2 + 190y - 89.25 \quad \text{for } 0.85 \le y \le 1.05.$$

Appendix B

Appendix to Chapter 3

B.1 Convergence of the EPM in the discrete setting

For the sake of completeness in Algorithm B.1.1 DEIM a continuous version of the Discrete Empirical Interpolation Method [31] is described. Here, we use the same notation as in §3.2.

Algorithm B.1.1: Discrete Empirical Interpolation Method

DEIM(W_k,$\widehat{\omega}$)

Set

$$t_1 := \arg \operatorname*{ess\,sup}_{y \in \widehat{\omega}} |\kappa_1(\hat{y})|, \quad \text{and} \quad \zeta_1 = \kappa_1.$$

for $l = 1, \ldots, k$ **do**

Solve for the coefficients σ_j^{l-1}:

$$\sum_{j=1}^{l-1} \sigma_j^{l-1} \zeta_j(t_i) = \kappa_l(t_i), \;\; i = 1, ..., l-1.$$

Compute the residual

$$r_l(\hat{y}) := \kappa_l(\hat{y}) - \sum_{j=1}^{l-1} \sigma_j^{l-1} \zeta_j(\hat{y}).$$

Set

$$t_l = \arg \operatorname*{ess\,sup}_{y \in \widehat{\omega}} |r_l(\hat{y})|, \quad \text{and} \quad \zeta_l = \kappa_l, \quad 1 \leq i, j \leq l.$$

end

return T_k

Next we prove convergence of the EPM 3.2.2 in the discrete setting. The main ingredients are again the usage of the POD error (2.22) and a special case of

Lemma B.1 (Lebegue's lemma [39])**.** *If P is a projector of V onto $W \subset V$, then we have*

$$\|f - P[f]\| \leq (1 + \|P\|)\|f - f^*\|,$$

where f^* denotes the best approximation of f in W with respect to the considered norm.

For the L^∞-norm the operator norm of $\mathcal{I}_L$ coincides with the 'Lebesgue constant' [12,80,107], which is defined as

$$\Lambda_k^I := \operatorname*{ess\,sup}_{\hat{y}\in I} \sum_{l=1}^{k} |\vartheta_l^I(\hat{y})|. \tag{B.1}$$

As the operator norm of $\mathcal{I}_L$ can in general not be bounded in the L^2-norm we prove convergence only in the discrete setting employing the inverse estimate between the L^∞- and L^2-norm. To define a discrete approximation of u, we use the partition $\widehat{T} := \mathcal{T}_H \times \tau_h$ of $\widehat{\Omega}$ and the bilinear FE-space

$$V^{H\times h} := \left\{ v^{H\times h} \in C^0(\widehat{\Omega}) \mid v^{H\times h}|_{T_{i,j}} \in \mathbb{Q}_{1,1}, T_{i,j} \in \widehat{T} \right\} \subset H_0^1(\widehat{\Omega}),$$

introduced in §2.4.1. We introduce the projector $P^{H\times h} : L^2(\widehat{\Omega}) \to V^{H\times h}$ satisfying

$$\int_\Omega P^{H\times h}[u] v^{H\times h} = \int_\Omega u v^{H\times h} \quad \forall v^{H\times h} \in V^{H\times h}, \tag{B.2}$$

and set $u^{H\times h} := P^{H\times h}[u]$. For $u \in H^1(\Omega)$ we have $\|u - u^{H\times h}\|_{L^2(\Omega)} \leq (h^2 + H^2)^{1/2} \|u\|_{H^1(\Omega)}$ [114]. We obtain the following result.

Proposition B.2 (Convergence of the EPM in the discrete setting)**.** *We assume that $u \in H^1(\Omega)$. Let $W_K^h := \{u^{H\times h}(\mu, \hat{y}),\, \mu \in \Xi_{1D}\}$ be a set of snapshots of the function $u^{H\times h}$, where $\Xi_{1D} \subset \Omega_{1D}$ is a finite dimensional train sample of size $|\Xi_{1D}| = n$ and the parameter values $\mu \in \Xi_{1D}$ are sampled from the uniform distribution over Ω_{1D}. The collateral basis space $W_k^h = \operatorname{span}\{\kappa_1^h, ..., \kappa_k^h\}$ is determined by a POD and can thus be defined as*

$$W_k^h = \arg \inf_{\substack{\tilde{W}_k^h \subset \operatorname{span}\{W_K^h\} \\ \dim(\tilde{W}_k^h) = k}} \left(\frac{1}{n} \sum_{\mu\in\Xi_{1D}} \inf_{\tilde{w}_k^h \in \tilde{W}_k^h} \|u^{H\times h}(\mu, \cdot) - \tilde{w}_k^h\|_{L^2(\widehat{\omega})}^2 \right). \tag{B.3}$$

Finally, $\{\lambda_l^n\}_{l=1}^{d(n)}$ denotes the set of eigenvalues of the correlation matrix eigenvalue problem that is equivalent to the optimization problem (B.3)*. Then we have for each interval $I \in \mathfrak{I}$*

$$\begin{aligned} &\left(\tfrac{1}{n} \textstyle\sum_{\mu\in\Xi_{1D}} \| \int_{\widehat{\omega}} \sum_{l=1}^{k} (u^{H\times h}(\mu, \hat{y}) - \mathcal{I}_L[u^{H\times h}](\mu, \hat{y})) \kappa_l^h(\hat{y})\, d\hat{y}\, \kappa_l^h \|_{L^2(I)}^2 \right)^{1/2} \\ &\qquad \leq \sqrt{k} \left(1 + \left(\textstyle\sum_{I\in\mathfrak{I}} (\Lambda_k^I)^2\right)^{1/2} h^{-1}\right) \left(\sum_{l=k+1}^{d(n)} \lambda_l^n \right)^{1/2}. \end{aligned} \tag{B.4}$$

Proof. Let I be an arbitrary interval in $\mathfrak{I}$. $\int_{\widehat{\omega}} \kappa_i^h \kappa_j^h = \delta_{ij}$ and some simple transformations and estimates yield

$$\begin{aligned} &\frac{1}{n} \sum_{\mu\in\Xi_{1D}} \| \int_{\widehat{\omega}} \sum_{l=1}^{k} (u^{H\times h}(\mu, \hat{y}) - \mathcal{I}_L[u^{H\times h}](\mu, \hat{y})) \kappa_l^h(\hat{y})\, d\hat{y}\, \kappa_l^h \|_{L^2(I)}^2 \\ &\qquad \leq \frac{1}{n} \sum_{\mu\in\Xi_{1D}} \sum_{l=1}^{k} \left(\int_{\widehat{\omega}} (u^{H\times h}(\mu, \hat{y}) - \mathcal{I}_L[u^{H\times h}](\mu, \hat{y})) \kappa_l^h(\hat{y})\, d\hat{y} \right)^2 \\ &\qquad \leq \frac{1}{n} \sum_{\mu\in\Xi_{1D}} k \|u^{H\times h}(\mu, \cdot) - \mathcal{I}_L[u^{H\times h}](\mu, \cdot)\|_{L^2(\widehat{\omega})}^2. \end{aligned} \tag{B.5}$$

For each $\mu \in \Xi_{1D}$ we can further estimate:

$$\begin{aligned}&\|u^{H\times h}(\mu,\cdot) - \mathcal{I}_L[u^{H\times h}](\mu,\cdot)\|_{L^2(\widehat{\omega})}\\ &\leq \underbrace{\|u^{H\times h}(\mu,\cdot) - \mathcal{I}_L[P_k[u^{H\times h}]](\mu,\cdot)\|_{L^2(\widehat{\omega})}}_{(i)} + \underbrace{\|\mathcal{I}_L[P_k[u^{H\times h}]](\mu,\cdot) - \mathcal{I}_L[u^{H\times h}](\mu,\cdot)\|_{L^2(\widehat{\omega})}}_{(ii)},\end{aligned}$$

where $P_k[u^{H\times h}]$ is defined analogous to (3.26). Exploiting that the EIM is exact on the space $W_k^h|_I$ (Lemma 3.6) we obtain for (i):

$$\begin{aligned}\|u^{H\times h}(\mu,\cdot) - \mathcal{I}_L[P_k[u^{H\times h}]](\mu,\cdot)\|^2_{L^2(\widehat{\omega})} &= \sum_{I\in\mathfrak{I}} \|u^{H\times h}(\mu,\cdot) - \mathcal{I}_L[P_k[u^{H\times h}]](\mu,\cdot)\|^2_{L^2(I)}\\ &= \sum_{I\in\mathfrak{I}} \|u^{H\times h}(\mu,\cdot) - P_k[u^{H\times h}](\mu,\cdot)\|^2_{L^2(I)}\\ &= \|u^{H\times h}(\mu,\cdot) - P_k[u^{H\times h}](\mu,\cdot)\|^2_{L^2(\widehat{\omega})}.\end{aligned} \tag{B.6}$$

Using the definition of the Lebesgue constant (B.1) we get for (ii):

$$\begin{aligned}\|\mathcal{I}_L[P_k[u^{H\times h}]](\mu,\cdot) - \mathcal{I}_L[u^{H\times h}](\mu,\cdot)\|^2_{L^2(\widehat{\omega})} &= \sum_{I\in\mathfrak{I}} \|\mathcal{I}_L[P_k[u^{H\times h}]](\mu,\cdot) - \mathcal{I}_L[u^{H\times h}](\mu,\cdot)\|^2_{L^2(I)}\\ &\leq \sum_{I\in\mathfrak{I}} (\Lambda_k^I)^2 \|P_k[u^{H\times h}](\mu,\cdot) - u^{H\times h}(\mu,\cdot)\|^2_{L^\infty(\widehat{\omega})}.\end{aligned} \tag{B.7}$$

The estimates (B.6) and (B.7) and the inverse estimate $\|v^h\|_{L^\infty(\widehat{\omega})} \leq h^{-1}\|v^h\|_{L^\infty(\widehat{\omega})}$, which holds for all $v^h \in Y^h$, yield

$$\begin{aligned}&\|u^{H\times h}(\mu,\cdot) - \mathcal{I}_L[u^{H\times h}](\mu,\cdot)\|_{L^2(\widehat{\omega})}\\ &\leq \|u^{H\times h}(\mu,\cdot) - \mathcal{I}_L[P_k[u^{H\times h}]](\mu,\cdot)\|_{L^2(\widehat{\omega})} + \|\mathcal{I}_L[P_k[u^{H\times h}]](\mu,\cdot) - \mathcal{I}_L[u^{H\times h}](\mu,\cdot)\|_{L^2(\widehat{\omega})}\\ &\leq \|u^{H\times h}(\mu,\cdot) - P_k[u^{H\times h}](\mu,\cdot)\|_{L^2(\widehat{\omega})} + \left(\sum_{I\in\mathfrak{I}} (\Lambda_k^I)^2\right)^{1/2} \|P_k[u^{H\times h}](\mu,\cdot) - u^{H\times h}(\mu,\cdot)\|_{L^\infty(\widehat{\omega})}\\ &\leq (1 + \left(\sum_{I\in\mathfrak{I}} (\Lambda_k^I)^2\right)^{1/2} h^{-1})\|u^{H\times h}(\mu,\cdot) - P_k[u^{H\times h}](\mu,\cdot)\|_{L^2(\widehat{\omega})}.\end{aligned} \tag{B.8}$$

Note that (B.8) is a special case of Lebesgue's lemma B.1. The estimates (B.5) and (B.8) together with the definition of the POD-error (2.22) yield

$$\begin{aligned}&\frac{1}{n}\sum_{\mu\in\Xi_{1D}} \| \int_{\widehat{\omega}} \sum_{l=1}^{k} (u^{H\times h}(\mu,\hat{y}) - \mathcal{I}_L[u^{H\times h}](\mu,\hat{y}))\kappa_l^h(\hat{y})\, d\hat{y}\, \kappa_l^h\|^2_{L^2(I)}\\ &\qquad\leq \frac{1}{n}\sum_{\mu\in\Xi_{1D}} k(1 + \left(\sum_{I\in\mathfrak{I}} (\Lambda_k^I)^2\right)^{1/2} h^{-1})^2 \|u^{H\times h}(\mu,\cdot) - P_k[u^{H\times h}](\mu,\cdot)\|^2_{L^2(\widehat{\omega})}\\ &\qquad\leq k(1 + \left(\sum_{I\in\mathfrak{I}} (\Lambda_k^I)^2\right)^{1/2} h^{-1})^2 \left(\sum_{l=k+1}^{d(n)} \lambda_l^n\right)\end{aligned}$$

and thus the claim. □

Regarding the behavior of the Lebesgue constant it has been shown in [12] that $\Lambda_k^I \leq 2^k - 1$. Although this bound can be actually reached [80], $\Lambda_k^I \leq 2^k - 1$ is a very pessimistic result and in numerical experiments a very moderate behavior is observed (cf. [43, 80, 87]). Note that (B.4) only yields convergence of the EPM if the POD-error converges faster than $(\sqrt{k}(1 + \left(\sum_{I \in \mathfrak{I}} (\Lambda_k^I)^2\right)^{1/2} h^{-1}))^{-1}$.

Bibliography

[1] A. Abdulle, W. E, B. Engquist, and E. Vanden-Eijnden, *The heterogeneous multiscale method*, Acta Numer., 21 (2012), pp. 1–87. 105

[2] M. Ainsworth, *A posteriori error estimation for fully discrete hierarchic models of elliptic boundary value problems on thin domains*, Numer. Math., 80 (1998), pp. 325–362. 3

[3] G. Akrivis, C. Makridakis, and R. H. Nochetto, *A posteriori error estimates for the Crank-Nicolson method for parabolic equations*, Math. Comp., 75 (2006), pp. 511–531. 23

[4] H. W. Alt, *Linear functional analysis. An application oriented introduction. (Lineare Funktionalanalysis. Eine anwendungsorientierte Einführung.) 6th revised ed.*, Berlin: Springer, 2012. 47, 56

[5] A Ammar, F Chinesta, P Diez, and A Huerta, *An error estimator for separated representations of highly multidimensional models*, Computer Methods in Applied Mechanics and Engineering, 199 (2010), pp. 1872–1880. 4

[6] A. Ammar, B. Mokdad, F. Chinesta, and R. Keunings, *A new family of solvers for some classes of multidimensional partial differential equations encountered in kinetic theory modeling of complex fluids*, Journal of Non-Newtonian Fluid Mechanics, 139 (2006), pp. 153–176. 4

[7] ——, *A new family of solvers for some classes of multidimensional partial differential equations encountered in kinetic theory modelling of complex fluids: Part ii: Transient simulation using space-time separated representations*, Journal of Non-Newtonian Fluid Mechanics, 144 (2007), pp. 98–121. 4

[8] E. Audusse, *A multilayer Saint-Venant model: derivation and numerical validation*, Discrete Contin. Dyn. Syst. Ser. B, 5 (2005), pp. 189–214. 4

[9] E. Audusse, M. O. Bristeau, and A. Decoene, *Numerical simulations of 3D free surface flows by a multilayer Saint-Venant model*, Internat. J. Numer. Methods Fluids, 56 (2008), pp. 331–350. 4

[10] E. Audusse, M.-O. Bristeau, B. Perthame, and J. Sainte-Marie, *A multilayer Saint-Venant system with mass exchanges for shallow water flows. Derivation and numerical validation*, ESAIM Math. Model. Numer. Anal., 45 (2011), pp. 169–200. 4

[11] I. Babuška and C. Schwab, *A posteriori error estimation for hierarchic models of elliptic boundary value problems on thin domains*, SIAM J. Numer. Anal., 33 (1996), pp. 221–246. 3

[12] M. Barrault, Y. Maday, N.C. Nguyen, and A.T. Patera, *An 'empirical interpolation' method: application to efficient reduced-basis discretization of partial differential equations*, C. R. Math. Acad. Sci. Paris Series I, 339 (2004), pp. 667–672. 2, 45, 51, 52, 53, 108, 122, 124

[13] P. Bastian, H. Berninger, A. Dedner, C. Engwer, P. Henning, R. Kornhuber, D. Kröner, M. Ohlberger, O. Sander, G. Schiffler, N. Shokina, and K. Smetana, *Adaptive modelling of coupled hydrological processes with application in water management.* Günther, Michael (ed.) et al., Progress in industrial mathematics at ECMI 2010. Proceedings of the 16th European conference on mathematics for industry, Wuppertal, Germany, July 26–30, 2010. Berlin: Springer. Mathematics in Industry 17, (2012), pp. 561–567. 90

[14] J. Bear, *Dynamics of fluids in porous media*, Dover Publications, New York, 1988. 90

[15] B. J. Bellhouse, F. H. Bellhouse, C. M. Curl, T. I. MacMillan, A. J. Gunning, E. H. Spratt, S. B. MacMurray, and J. M. Nelems, *A high efficiency membrane oxygenator and pulsatile pumping system and its applications to animal trials*, Trans. Amer. Soc. Artif. Int. Organs, 19 (1973), pp. 72–79. 35

[16] H. Berninger, M. Ohlberger, O. Sander, and K. Smetana, *Unsaturated subsurface flow with surface water and nonlinear in- and outflow conditions*, arXiv Preprint (submitted), Number 1301.2488, http://arxiv.org/abs/1301.2488, (2013). 45, 90

[17] P. Binev, A. Cohen, W. Dahmen, R. DeVore, G. Petrova, and P. Wojtaszczyk, *Convergence rates for greedy algorithms in reduced basis methods*, SIAM J. Math. Anal., 43 (2011), pp. 1457–1472. 1, 12, 13, 15

[18] F. Blanc, O. Gipouloux, G. Panasenko, and A. M. Zine, *Asymptotic analysis and partial asymptotic decomposition of domain for Stokes equation in tube structure*, Math. Models Methods Appl. Sci., 9 (1999), pp. 1351–1378. 3

[19] S. C. Brenner and L. R. Scott, *The mathematical theory of finite element methods*, vol. 15 of Texts in Applied Mathematics, Springer-Verlag, New York, 1994. 20

[20] F. Brezzi, J. Rappaz, and P.-A. Raviart, *Finite-dimensional approximation of nonlinear problems. I. Branches of nonsingular solutions*, Numer. Math., 36 (1980), pp. 1–25. 5, 45, 67

[21] A. Buffa, Y. Maday, A. T. Patera, C. Prud'homme, and G. Turinici, *A priori convergence of the greedy algorithm for the parametrized reduced basis method*, ESAIM Math. Model. Numer. Anal., 46 (2012), pp. 595–603. 1, 12, 13, 15

[22] R. E. Caflisch, *Monte Carlo and quasi-Monte Carlo methods*, in Acta numerica, 1998, vol. 7 of Acta Numer., Cambridge Univ. Press, Cambridge, 1998, pp. 1–49. 56, 57, 80

[23] G. Caloz and J. Rappaz, *Numerical analysis for nonlinear and bifurcation problems*, in Handbook of numerical analysis, Vol. V, North-Holland, Amsterdam, 1997, pp. 487–637. 5, 45, 47, 67, 70

[24] E. Cancès, V. Ehrlacher, and T. Lelièvre, *Convergence of a greedy algorithm for high-dimensional convex nonlinear problems.*, Math. Models Methods Appl. Sci., 21 (2011), pp. 2433–2467. 4, 30, 91

[25] C. Canuto, M. Y. Hussaini, A. Quarteroni, and T. A. Zang, *Spectral methods. Fundamentals in single domains.*, Springer, Berlin, 2006. 29

[26] C. Canuto, Y. Maday, and A. Quarteroni, *Analysis of the combined finite element and Fourier interpolation*, Numer. Math., 39 (1982), pp. 205–220. 3, 29, 40

[27] C. Canuto, T. Tonn, and K. Urban, *A posteriori error analysis of the reduced basis method for nonaffine parametrized nonlinear PDEs*, SIAM J. Numer. Anal., 47 (2009), pp. 2001–2022. 5, 45, 60, 67, 68, 69, 70, 108

[28] K. Carlberg, *Model reduction of nonlinear mechanical systems via optimal projection and tensor approximation*, PhD thesis, Stanford University, 2011. 55

[29] K. Carlberg, C. Bou-Mosleh, and C. Farhat, *Efficient non linear model reduction via a least-squares Petrov-Galerkin projection and compressive tensor approximations.*, Int. J. Numer. Methods Eng., 86 (2011), pp. 155–181. 55

[30] K. Carlberg, C. Farhat, J. Cortial, and D. Amsallem, *The GNAT method for nonlinear model reduction: effective implementation and application to computational fluid dynamics and turbulent flows*, Journal of Computational Physics, in press, (2013). 55, 59

[31] S. Chaturantabut and D. C. Sorensen, *Nonlinear model reduction via discrete empirical interpolation*, SIAM J. Sci. Comp., 32 (2010), pp. 2737–2764. 11, 54, 55, 57, 121

[32] ——, *A state space error estimate for POD-DEIM nonlinear model reduction*, SIAM J. Numer. Anal., 50 (2012), pp. 46–63. 55

[33] F. Chinesta and E. Ammar, A.and Cueto, *Recent advances and new challenges in the use of the proper generalized decomposition for solving multidimensional models*, Arch. Comput. Methods Eng., 17 (2010), pp. 327–350. 4

[34] F. Chinesta, P. Ladeveze, and E. Cueto, *A short review on model order reduction based on proper generalized decomposition*, Archives of Computational Methods in Engineering, 18 (2011), pp. 395–404. 4

[35] M. Chipot, *Elements of nonlinear analysis*, Birkhäuser Verlag, Basel, 2000. 47

[36] P. G. Ciarlet, *Plates and junctions in elastic multi-structures: An asymptotic analysis*, vol. 14, Masson, Paris, 1990. 3

[37] G. Dagan, *Second-order theory of shallow free-surface flow in porous media.*, Q. J. Mech. Appl. Math., 20 (1967), pp. 517–526. 3, 90

[38] R. DeVore, *Nonlinear approximation*, in Acta numerica, 1998, vol. 7 of Acta Numer., Cambridge Univ. Press, Cambridge, 1998, pp. 51–150. 1

[39] R. DeVore and G. G. Lorentz, *Constructive approximation*, vol. 303 of Grundlehren der Mathematischen Wissenschaften [Fundamental Principles of Mathematical Sciences], Springer-Verlag, Berlin, 1993. 121

[40] R. DeVore, G. Petrova, and P. Wojtaszczyk, *Greedy algorithms for reduced bases in banach spaces*, Constructive Approximation, (2013), pp. 1–12. 1, 12, 13, 14, 15

[41] V. Dolejší, A. Ern, and M. Vohralík, *A framework for robust a posteriori error control in unsteady nonlinear advection-diffusion problems*, SIAM J. Numer. Anal., to appear (2013). 46, 73

[42] M. Drohmann, *Reduced basis model reduction for nonlinear evolution equations*, PhD thesis, Universität Münster, 2012. 11, 55

[43] M. Drohmann, B. Haasdonk, and M. Ohlberger, *Reduced basis approximation for nonlinear parametrized evolution equations based on empirical operator interpolation*, SIAM J. Sci. Comput., 34 (2012), pp. A937–A969. 54, 55, 57, 59, 77, 124

[44] J. Dupuit, *Études Théoriques et Pratiques sur le Mouvement des Eaux dans les Canaux Découverts et à Travers les Terrains Permeables*, Dunod, Paris, 2nd ed., 1863. 3, 90

[45] J. L. Eftang, M. A. Grepl, and A. T. Patera, *A posteriori error bounds for the empirical interpolation method*, C. R. Acad. Sci. Paris, Ser. I 348, (2010), pp. 575–579. 57

[46] J. L. Eftang, A. T. Patera, and E. M. Rønquist, *An "hp" certified reduced basis method for parametrized elliptic partial differential equations*, SIAM J. Sci. Comput., 32 (2010), pp. 3170–3200. 1, 19, 21

[47] I. Ekeland and R. Temam, *Convex analysis and variational problems*, North-Holland, Amsterdam, 1976. Translated from the French, Studies in Mathematics and its Applications, Vol. 1. 116, 117

[48] A. Ern, S. Perotto, and A. Veneziani, *Hierarchical model reduction for advection-diffusion-reaction problems*, in Numerical Mathematics and Advanced Applications, Karl Kunisch, Günther Of, and Olaf Steinbach, eds., Springer Berlin Heidelberg, 2008, pp. 703–710. 1, 3, 8, 9, 27, 29, 40, 46, 77

[49] L. C. Evans, *Partial differential equations*, vol. 19 of Graduate Studies in Mathematics, American Mathematical Society, Providence, RI, 1998. 48, 50, 51

[50] R. Everson and L. Sirovich, *Karhunen–loeve procedure for gappy data*, Journal of the Optical Society of America A, 12 (1995), pp. 1657–1664. 55

[51] A. Falcó and A. Nouy, *Proper generalized decomposition for nonlinear convex problems in tensor Banach spaces*, Numer. Math., 121 (2012), pp. 503–530. 4

[52] E. D. Fernández-Nieto, E. H. Koné, T. Morales de Luna, and R. Bürger, *A multilayer shallow water system for polydisperse sedimentation*, Journal of Computational Physics, 238 (2013), pp. 281–314. 4

[53] L. E. Figueroa and E. Süli, *Greedy approximation of high-dimensional Ornstein–Uhlenbeck operators*, Foundations of Computational Mathematics, 12 (2012), pp. 573–623. 4

[54] F. Fontvieille, G. P. Panasenko, and J. Pousin, *F.E.M. implementation for the asymptotic partial decomposition*, Appl. Anal., 86 (2007), pp. 519–536. 3

[55] L. Formaggia, J. F. Gerbeau, F. Nobile, and A. Quarteroni, *On the coupling of 3D and 1D Navier-Stokes equations for flow problems in compliant vessels*, Comput. Methods Appl. Mech. Engrg., 191 (2001), pp. 561–582. 4

[56] L. Formaggia, F. Nobile, A. Quarteroni, and A. Veneziani, *Multiscale modelling of the circulatory system: a preliminary analysis.*, Comput. Vis. Sci., 2 (1999), pp. 75–83. 4

[57] K. O. Friedrichs, *On the derivation of the shallow water theory, appendix to: "The formulation of breakers and bores" by J. J. Stoker*, Comm. Pure Appl. Math., 1 (1948), pp. 1–87. 3

[58] A. Gloria, *An analytical framework for numerical homogenization. II. Windowing and oversampling*, Multiscale Model. Simul., 7 (2008), pp. 274–293. 105

[59] M. A. Grepl, Y. Maday, N. C. Nguyen, and A. T. Patera, *Efficient reduced-basis treatment of nonaffine and nonlinear partial differential equations*, M2AN Math. Model. Numer. Anal., 41 (2007), pp. 575–605. 52, 54

[60] M. D. Gunzburger, *Perspectives in flow control and optimization*, vol. 5 of Advances in Design and Control, Society for Industrial and Applied Mathematics (SIAM), Philadelphia, PA, 2003. 11

[61] B. Haasdonk, M. Dihlmann, and M. Ohlberger, *A training set and multiple bases generation approach for parameterized model reduction based on adaptive grids in parameter space*, Math. Comput. Model. Dyn. Syst., 17 (2011), pp. 423–442. 1, 15, 18, 19, 63, 64

[62] B. Haasdonk and M. Ohlberger, *Adaptive basis enrichment for the reduced basis method applied to finite volume schemes*, in Finite volumes for complex applications V, ISTE, London, 2008, pp. 471–478. 1, 15, 18, 19, 63, 64

[63] ——, *Reduced basis method for finite volume approximations of parametrized linear evolution equations*, M2AN Math. Model. Numer. Anal., 42 (2008), pp. 277–302. 109

[64] P. Holmes, J. L. Lumley, G. Berkooz, and C. W. Rowley, *Turbulence, coherent structures, dynamical systems and symmetry*, Cambridge Monographs on Mechanics, Cambridge University Press, Cambridge, second ed., 2012. 11

[65] D. B. P. Huynh, G. Rozza, S. Sen, and A. T. Patera, *A successive constraint linear optimization method for lower bounds of parametric coercivity and inf-sup stability constants*, C. R. Math. Acad. Sci. Paris, 345 (2007), pp. 473–478. 73

[66] R. S. Johnson, *A modern introduction to the mathematical theory of water waves*, Cambridge Texts in Applied Mathematics, Cambridge University Press, Cambridge, 1997. 3

[67] I. T. Jolliffe, *Principal component analysis*, Springer Series in Statistics, Springer-Verlag, New York, second ed., 2002. 11

[68] N. Jung, *Error Estimation for Parametric Model Order Reduction and its Application*, PhD thesis, Technische Universität München, 2011. 59

[69] M. Kahlbacher and S. Volkwein, *Galerkin proper orthogonal decomposition methods for parameter dependent elliptic systems*, Discuss. Math. Differ. Incl. Control Optim., 27 (2007), pp. 95–117. 1, 11, 12

[70] K. Karhunen, *Zur Spektraltheorie stochastischer Prozesse*, Ann. Acad. Sci. Fennicae. Ser. A. I. Math.-Phys., 37 (1946). 11

[71] S. Karlin and W. J. Studden, *Tchebycheff systems: With applications in analysis and statistics*, Pure and Applied Mathematics, Vol. XV, Interscience Publishers John Wiley & Sons, New York-London-Sydney, 1966. 52

[72] K. Kunisch and S. Volkwein, *Galerkin proper orthogonal decomposition methods for parabolic problems*, Numerische Mathematik, 90 (2001), pp. 117–148. 55

[73] ——, *Galerkin proper orthogonal decomposition methods for a general equation in fluid dynamics*, SIAM J. Numer. Anal., 40 (2002), pp. 492–515. 55, 57

[74] O. A. Ladyzhenskaya and N. N. Ural'tseva, *Linear and quasilinear elliptic equations.*, Mathematics in Science and Engineering. 46. New York-London: Academic Press. XVIII, 1968. 62

[75] O. Lass and S. Volkwein, *POD galerkin schemes for nonlinear elliptic-parabolic systems*, to appear in SIAM J. Sci. Comp., (2013). 11

[76] T. Lassila, A. Manzoni, A. Quarteroni, and G. Rozza, *Generalized reduced basis methods and n-width estimates for the approximation of the solution manifold of parametric pdes*, in Analysis and Numerics of Partial Differential Equations, Springer, 2013, pp. 307–329. 14

[77] C. Le Bris, T. Lelièvre, and Y. Maday, *Results and questions on a nonlinear approximation approach for solving high-dimensional partial differential equations*, Constr. Approx., 30 (2009), pp. 621–651. 4, 91

[78] M. Loève, *Probability theory*, D. Van Nostrand Company, Inc., Toronto-New York-London, 1955. 11

[79] J. Ma, V. Rokhlin, and S. Wandzura, *Generalized Gaussian quadrature rules for systems of arbitrary functions*, SIAM J. Numer. Anal., 33 (1996), pp. 971–996. 52

[80] Y. Maday, N. C. Cuong Nguyen, A. T. Patera, and G. S. H. Pau, *A general multipurpose interpolation procedure: the magic points*, Commun. Pure Appl. Anal., 8 (2009), pp. 383–404. 52, 53, 54, 122, 124

[81] Y. Maday, A. T. Patera, and G. Turinici, *A priori convergence theory for reduced-basis approximations of single-parameter elliptic partial differential equations.*, J. Sci. Comput., 17 (2002), pp. 437–446. 12

[82] ——, *Global a priori convergence theory for reduced-basis approximations of single-parameter symmetric coercive elliptic partial differential equations*, C. R. Math. Acad. Sci. Paris, 335 (2002), pp. 289–294. 12

[83] Y. Maday and B. Stamm, *Locally adaptive greedy approximations for anisotropic parameter reduced basis spaces*, arXiv Preprint (submitted), Number 1204.3846, http://arxiv.org/abs/1204.3846, (2012). 19

[84] L. Mauri, S. Perotto, and A. Veneziani, *Adaptive geometrical multiscale modeling for hydrodynamic problems*, in Numerical Mathematics and Advanced Applications 2011, Andrea Cangiani, Ruslan L. Davidchack, Emmanuil Georgoulis, Alexander N. Gorban, Jeremy Levesley, and Michael V. Tretyakov, eds., Springer Berlin Heidelberg, 2013, pp. 723–730. 4

[85] A. Michel, *A finite volume scheme for two-phase immiscible flow in porous media*, SIAM J. Numer. Anal., 41 (2003), pp. 1301–1317 (electronic). 75

[86] E. Miglio, S. Perotto, and F. Saleri, *Model coupling techniques for free-surface flow problems: Part I*, Nonlinear Analysis, 63 (2005), pp. e1885–e1896. 4

[87] N. C. Nguyen, A. T. Patera, and J. Peraire, *A 'best points' interpolation method for efficient approximation of parametrized functions*, Internat. J. Numer. Methods Engrg., 73 (2008), pp. 521–543. 53, 124

[88] A. Nouy, *A generalized spectral decomposition technique to solve a class of linear stochastic partial differential equations*, Comput. Methods Appl. Mech. Engrg., 196 (2007), pp. 4521–4537. 4

[89] ——, *A priori model reduction through proper generalized decomposition for solving time-dependent partial differential equations*, Computer Methods in Applied Mechanics and Engineering, 199 (2010), pp. 1603–1626. 4

[90] M. Ohlberger, *A posteriori error estimates for the heterogeneous multiscale finite element method for elliptic homogenization problems*, Multiscale Model. Simul., 4 (2005), pp. 88–114 (electronic). 105

[91] M. Ohlberger and K. Smetana, *A new problem adapted hierarchical model reduction technique based on reduced basis methods and dimensional splitting*, Preprint 03/10, FB 10, University Muenster, December 2010. 2

[92] ——, *A new hierarchical model reduction-reduced basis technique for advection-diffusion-reaction problems*, in Proceedings of the V International Conference on Adaptive Modeling and Simulation (ADMOS 2011) held in Paris, France, 6-8 June 2011, D. Aubry, P. Díez, B. Tie, and N. Parés, eds., Barcelona, 2011, International Center for Numerical Methods in Engineering (CIMNE), pp. 343–354. 2

[93] C. Ortner, *A posteriori existence in numerical computations*, SIAM J. Numer. Anal., 47 (2009), pp. 2550–2577. 67

[94] G. P. Panasenko, *Method of asymptotic partial decomposition of domain*, Math. Models Methods Appl. Sci., 8 (1998), pp. 139–156. 3

[95] G. P. Panasenko, *Asymptotic expansion of the solution of Navier-Stokes equation in tube structure and partial asymptotic decomposition of the domain*, Appl. Anal., 76 (2000), pp. 363–381. 3

[96] G. P. Panasenko and M.-C. Viallon, *The finite volume implementation of the partial asymptotic domain decomposition*, Appl. Anal., 87 (2008), pp. 1397–1424. 3

[97] A. T. Patera and G. Rozza, *Reduced basis approximation and a posteriori error estimation for parametrized partial differential equations*, Version 1.0, Copyright MIT 2006, to appear in (tentative rubric) MIT Pappalardo Graduate Monographs in Mechanical Engineering, 2006. 11, 20, 21, 26

[98] K. Pearson, *On lines and planes of closest fit to systems of points in space.*, Phil. Mag., 2 (1901), pp. 559–572. 11

[99] B. Peherstorfer, D. Butnaru, K. Willcox, and H-J. Bungartz, *Localized discrete empirical interpolation method*, Technical Report TR-13-1, MIT Aerospace Computational Design Laboratory, 2013.

[100] S. Perotto, *Hierachical model (hi-mod) reduction in non-rectilinear domains*, MOX-Report 52/2012, MOX, Dipartimento di Matematica "F. Brioschi" Politecnico di Milano, 2012. 1, 3

[101] S. Perotto, A. Ern, and A. Veneziani, *Hierarchical local model reduction for elliptic problems I: a domain decomposition approach*, MOX-Report 15/2009, MOX, Dipartimento di Matematica "F. Brioschi" Politecnico di Milano, 2009. 27, 29

[102] ——, *Hierarchical local model reduction for elliptic problems: a domain decomposition approach*, Multiscale Model. Simul., 8 (2010), pp. 1102–1127. 1, 3, 4, 7, 8, 9, 27, 29, 35, 40, 46, 47, 77, 91, 109

[103] S. Perotto and A. Zilio, *Hierarchical model reduction: Three different approaches*, in Numerical Mathematics and Advanced Applications 2011, Andrea Cangiani, Ruslan L. Davidchack, Emmanuil Georgoulis, Alexander N. Gorban, Jeremy Levesley, and Michael V. Tretyakov, eds., Springer Berlin Heidelberg, 2013, pp. 851–859. 1, 3

[104] A. Pinkus, *n-widths in approximation theory*, vol. 7 of Ergebnisse der Mathematik und ihrer Grenzgebiete (3), Springer-Verlag, Berlin, 1985. 1, 11, 14, 15, 91

[105] J. Pousin and J. Rappaz, *Consistency, stability, a priori and a posteriori errors for Petrov-Galerkin methods applied to nonlinear problems*, Numer. Math., 69 (1994), pp. 213–231. 50, 70, 72

[106] A. Quarteroni, G. Rozza, and A. Manzoni, *Certified reduced basis approximation for parametrized partial differential equations and applications*, J. Math. Ind., 1, Art. 3 (2011). 11

[107] A. Quarteroni, R. Sacco, and F. Saleri, *Numerical mathematics*, vol. 37 of Texts in Applied Mathematics, Springer-Verlag, New York, 2000. 16, 26, 56, 60, 74, 122

[108] A. Quarteroni and A. Veneziani, *Analysis of a geometrical multiscale model based on the coupling of ODEs and PDEs for blood flow simulations*, Multiscale Model. Simul., 1 (2003), pp. 173–195 (electronic). 4

[109] S. I. Repin, *A posteriori error estimation for variational problems with uniformly convex functionals*, Math. Comp., 69 (2000), pp. 481–500. 117, 118

[110] G. Rozza, D.B.P. Huynh, and A.T. Patera, *Reduced basis approximation and a posteriori error estimation for affinely parametrized elliptic coercive partial differential equations: application to transport and continuum mechanics*, Arch. Comput. Meth. Eng., 15 (2008), pp. 229–275. 11, 12, 13, 20, 21, 26

[111] M. Růžička, *Nonlinear functional analysis. An introduction. (Nichtlineare Funktionalanalysis. Eine Einführung.)*, Springer, Berlin, 2004. 48

[112] J. Sainte-Marie, *Vertically averaged models for the free surface non-hydrostatic Euler system: derivation and kinetic interpretation*, Math. Models Methods Appl. Sci., 21 (2011), pp. 459–490. 4

[113] R. Schaback and H. Wendland, *Numerical mathematics. (Numerische Mathematik.) 5th completely new revised ed.*, Springer, Berlin, 2005. 49

[114] L. R. Scott and S. Zhang, *Finite element interpolation of nonsmooth functions satisfying boundary conditions*, Math. Comp., 54 (1990), pp. 483–493. 76, 122

[115] L. Sirovich, *Turbulence and the dynamics of coherent structures. I. Coherent structures*, Quart. Appl. Math., 45 (1987), pp. 561–571. 11, 12

[116] J. J. Stoker, *Water waves*, Wiley Classics Library, John Wiley & Sons Inc., New York, 1992. The mathematical theory with applications, Reprint of the 1957 original, A Wiley-Interscience Publication. 3

[117] V. N. Temlyakov, *Greedy approximation*, Acta Numer., 17 (2008), pp. 235–409. 13

[118] T. Tonn, *Reduced-Basis Method (RBM) for Non-Affine Elliptic Parametrized PDEs*, PhD thesis, Universität Ulm, 2011. 52, 77

[119] K. Urban and B. Wieland, *Affine decompositions of parametric stochastic processes for application within reduced basis methods*, in accepted for publication in Proceedings MATHMOD 2012, 7th Vienna International Conference on Mathematical Modelling, 2012. 54, 57

[120] S. A. Urquiza, P. J. Blanco, M. J. Vénere, and R. A. Feijóo, *Multidimensional modelling for the carotid artery blood flow*, Comput. Methods Appl. Mech. Engrg., 195 (2006), pp. 4002–4017. 4

[121] R. Verfürth, *A posteriori error estimates for nonlinear problems. Finite element discretizations of elliptic equations*, Math. Comp., 62 (1994), pp. 445–475. 45, 67, 69, 72

[122] K. Veroy and A. T. Patera, *Certified real-time solution of the parametrized steady incompressible Navier-Stokes equations: rigorous reduced-basis a posteriori error bounds*, Internat. J. Numer. Methods Fluids, 47 (2005), pp. 773–788. 67

[123] K. Veroy, C. Prud'homme, D. V. Rovas, and A. T. Patera, *A posteriori error bounds for reduced-basis approximation of parametrized noncoercive and nonlinear elliptic partial differential equations*, in Proceedings of the 16th AIAA Computational Fluid Dynamics Conference, vol. 3847, 2003. 12

[124] M. Vogelius and I. Babuška, *On a dimensional reduction method. I. The optimal selection of basis functions*, Math. Comp., 37 (1981), pp. 31–46. 1, 3

[125] ——, *On a dimensional reduction method. II. Some approximation-theoretic results*, Math. Comp., 37 (1981), pp. 47–68. 1, 3

[126] ——, *On a dimensional reduction method. III. A posteriori error estimation and an adaptive approach*, Math. Comp., 37 (1981), pp. 361–384. 1, 3

[127] D. Wirtz, D. C. Sorensen, and B. Haasdonk, *A-posteriori error estimation for DEIM reduced nonlinear dynamical systems*, tech. report, SimTech Preprint, University Stuttgart, http://www.agh.ians.uni-stuttgart.de/publications/2012/WSH12, 2012. 46, 57, 73

[128] N. Yarvin and V. Rokhlin, *Generalized Gaussian quadratures and singular value decompositions of integral operators*, SIAM J. Sci. Comput., 20 (1998), pp. 699–718 (electronic). 52